Neuromuscular modularity and behavioral correlates of motor control and learning

by

Simon Alexander Overduin

B.Sc., Biology and Psychology
Wilfrid Laurier University, 2000

Submitted to the Department of Brain and Cognitive Sciences
in Partial Fulfillment of the requirements for the Degree of

Doctor of Philosophy in Neuroscience

at the

Massachusetts Institute of Technology

February 2006

Signature of Author . . . . . .
Simon Overduin, B.Sc.
Department of Brain and Cognitive Sciences
December 8, 2005

Certified by . . . . . .
Emilio Bizzi, M.D.
Institute Professor and Eugene McDermott Professor
Thesis Supervisor

Accepted by . . . . . .
Earl Miller, Ph.D.
Picower Professor of Neuroscience
Chairman, Department Graduate Committee

Neuromuscular modularity and behavioral correlates of motor control and learning

by
Simon Alexander Overduin

Submitted to the Department of Brain and Cognitive Sciences on December 1, 2005,
in partial fulfillment of the requirements for the degree of
Doctor of Philosophy in Neuroscience

Abstract

I studied organizational principles that may subserve the control and learning of forelimb movements. Among these principles, I focused on muscular coordination patterns, motor cortical excitability, and sensorimotor interactions.

I found that muscle activity in grasping and reaching behaviors could be reconstructed by linear combinations of a small number of time-varying muscle synergies, each fit with coefficients unique to the behavior. However, the generalization of these synergies between behavioral conditions was limited, in part by the sensitivity of the extraction algorithm to stereotyped muscular relations within contrasted conditions. In reaching studies designed to assist or resist different movement directions, I found a gradual change in the structure, as well as recruitment, of synergies. When a perturbation was targeted to the activity within a single muscle, I found a transient, relative suppression of this muscle in response to descending motor commands.

In other motor cortical microstimulation experiments, I confirmed that long-train microstimulation is able to evoke complex, convergent movements. Even during highly-trained reaching movements, I found that there was relatively little invariance of the muscular patterns in relation to kinematic variables coding for the hand's displacement and velocity. In two studies examining the kinematic consequences of modulating cortical excitability, I either infused tissue plasminogen activator into monkey cortex or applied transcranial magnetic stimulation to human cortex, either while or before each adapted to a clockwise force field. In both cases basal motor performance was spared, but each manipulation appeared to be associated with disruptions of subjects' ability to retain, improve, or recall recent adaptations.

Among other human studies, I investigated the interaction of dynamic adaptation and sequence learning, and found that simultaneous acquisition of a force field and a sequence does not impair performance on either but may have enabled subjects to tune in to, and chunk, their movements. I found that motor consolidation may be dependent on the more effortful learning enabled by catch-trial interruptions of practice on a novel condition. Finally, I used functional imaging and manual cutaneous stimulation to show that the hemodynamic response was biased according to receptor density but generally non-somatotopic and distributed throughout sensorimotor cortex.

Thesis supervisor: Emilio Bizzi
Title: Institute Professor

ACKNOWLEDGMENTS

As in the thesis that follows, I begin with the monkeys. The nonhuman primate data presented here (Studies 1-6) were collected from Carlo, Steffi, and in particular, Lucia. As for humans, the monkey electrophysiology work in Studies 1, 2 and 3 would not have been possible except for my collaboration with Andrea d'Avella and (in Study 3) with Jinsook Roh. Much of the additional work on monkey cybernetic glove development, not discussed here, was done by Farah Zaheer and Allison Glinka. An additional experiment on rats that refined our implantation techniques was done together with Matthew Tresch. The monkey electrophysiology work in Study 4 was done in collaboration with Andrea d'Avella, Andrew Richardson, and Glenda Lassi. For the further monkey work reported in Studies 5 and 6, I again thank Andrew. Additional work on cortical data analysis, not reported here, was done together with Jeffrey Moore. The monkey pharmacological investigation (Study 7) was done together with Andrew, Amanda Mower, and Mriganka Sur. The human psychophysics research in Studies 8-10 was conducted in collaboration with Daniel Press, Andrew Richardson, and (in Study 8) Antoni Valero and Camillo Padoa-Schioppa. Additional thanks go to Martin Ramos Rizo-Patron for engineering assistance and to Christi Winiarz for data collection (Study 9). For the human imaging work in Studies 11 and 12, I collaborated with Philip Servos, and also thank Joe Gati, Andrea Santi, and Nancy Kanwisher for technical assistance.

I would also like to acknowledge the administrative support of Charlotte Potak, and the technical assistance of Margo Cantor, Sylvester Szczepanowski, and Steve Marchetti. Additional thanks go to Vincent Cheung, Max Berniker, and Philippe Saltiel for helpful discussions, and likewise to my committee members Chris Moore, Earl Miller, and Lee Miller. I am particularly indebted the support and wisdom of my supervisor, Emilio Bizzi. Among my collaborators mentioned above, Andrea and Andrew have also been key sources of guidance and friendship. Finally, personal thanks go to my colleagues and former roommates Nathan Wilson and Florian Wolf for their inspiration, to Rahmat Muhammad for her patient encouragement and help with the text of this thesis, and to my family—especially my parents Jan and Margaret—for their constant support.

Concerning funding: the monkey projects (Studies 1-7) were supported by a National Institute of Neurological Disorders and Stroke grant (NINDS NS044393) and a National Institutes of Health grant (NIH MH48185) to Emilio Bizzi. The human psychophysics projects (Studies 8-10) were supported by an NIH grant (NIH K23-MH65434) to Dan Press. The human imaging experiments (Studies 11-12) were supported by grants from the Natural Sciences and Engineering Research Council of Canada (NSERC 194188-01), the Canada Research Chairs program (CRC 950-201040), and the Ontario Premier's Research Excellence Award program (PREA 98-1-0006) to Philip Servos. My own scholarship was supported in part by NSERC PGS-A and PGS-B postgraduate awards, and a Schoemaker Award.

CONTENTS

FIGURES

TABLES

ABBREVIATIONS

abd.	abductor
add.	adductor
ANOVA	analysis of variance
BDNF	brain derived neurotropic factor
BOLD	blood-oxygenation level dependent
CS	central sulcus
D1	digit 1 (thumb)
D2	digit 2 (index finger)
D4	digit 4 (ring finger)
digit.	digitorum
EMG	electromyography
EPI	echo planar imaging
ext.	extensor
FA	flip angle
FDI	first dorsal interosseus
fl.	flexor
fMRI	functional MRI
FOV	field of view
ICA	independent components analysis
IU	international units
LED	light-emitting diode
LI	learning index
LLE	locally linear embedding
L-LTP	late phase of LTP
LTP	long term potentiation
MDS	multidimensional scaling
MEP	motor-evoked potential
MI	primary motor cortex
MRI	magnetic resonance imaging
MT	motor threshold
NMDA	N-methyl-D-aspartate
NMF	non-negative matrix factorization
NR1	NMDA receptor 1 subunit
opp.	opponens
PCA	principal components analysis
PET	positron emission tomography
PoCG	postcentral gyrus
PoCS	postcentral sulcus
R-ICMS	repetitive intracortical microstimulation
RMS	root-mean-square
ROI	region of interest
rTMS	repetitive TMS
SD	standard deviation
SEM	standard error of the mean
SI	primary somatosensory cortex
SII	secondary somatosensory cortex
SMA	supplementary motor area
SME	sensorimotor efficiency
SRTT	serial reaction time task
TE	echo time
TI	inversion time
TMS	transcranial magnetic stimulation
tPA	tissue plasminogen activator
TR	repetition time

FOREWORD

This thesis is composed of 12 Studies. The Abstract and Conclusion binding these Studies give an overview of the scientific methods and findings of the thesis. The content of the twelve chapters (the outer ring of the figure below) can be described according to several underlying dimensions. First, the initial studies focus on monkey models, while later studies move to human experiments. Second, I have focused on movements of the whole arm or the hand, or the central encoding of these body parts. Third, the methods I used could be defined as ones primarily suitable for correlating motor variables to normal behavior, while others have explicitly interfered with the motor system in order to observe its function at a causal level. Fourth, the studies may be divided into those concerned primarily with motor control or with learning. Finally, the involvement of sensory feedback, rather than strictly motor processing, becomes more of a concern in the later chapters. Most chapters can be uniquely identified by their relation, in whole or in part, to these dimensions.

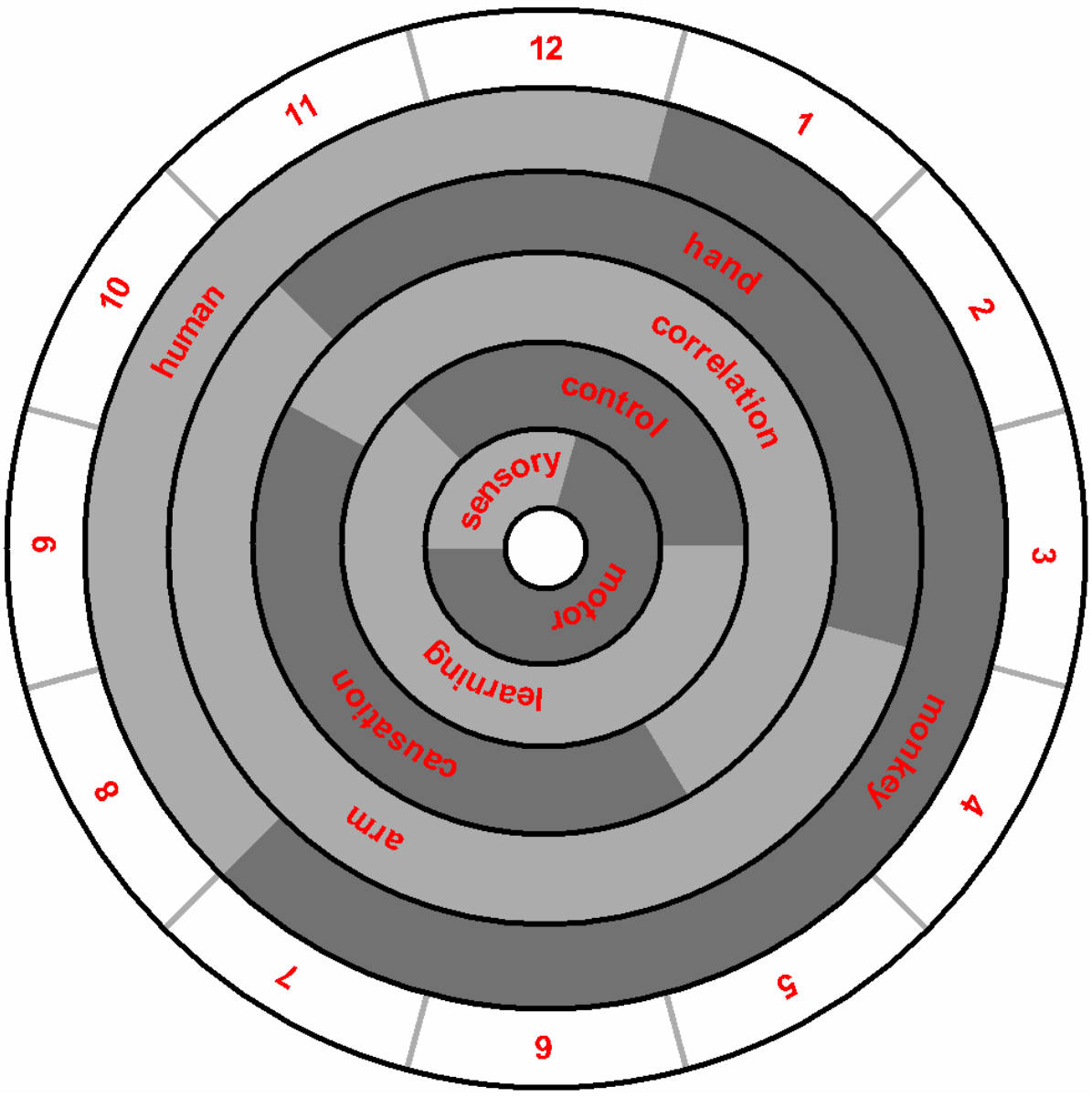

STUDIES

1 Muscle Synergy Modulation in the Control of Grasping

I tested a muscle synergy model capturing both non-negative and time-varying properties of muscle contraction and coordination in a nonhuman primate model. I recorded electromyographic (EMG) activity from 18 chronic intramuscular electrodes implanted in arm and hand muscles of two rhesus macaque monkeys, including 12 muscles implanted in both monkeys that spanned extrinsic flexor and extensor and intrinsic hand muscles. Each animal was presented with a set of 11 or 13 novel plastic cubes, spheres, or cylinders after having been trained extensively to perform a reach-to-grasp and transport behavior using its left hand to bring a canonical sphere from one side of its workspace to the other. The analysis here focused on 40 trials performed with each object and the same (rightward) direction of transport. After averaging these trials together, I found that three time-varying muscle synergies were able to account for 79% of the EMG variance recorded from each monkey. Three synergies appeared to be an appropriate number given that fewer than three was not able to explain as much of the variance as were 18 single-muscle "synergies" similarly extracted from the data, while more than three synergies were only associated with small increases in EMG variance-explained. In reconstructing each monkey's data as a linear summation of these three synergies, each given an optimal weight and onset time, I found that one synergy in each monkey scaled with object mass. Object shape was not reflected in the synergy coefficients, except perhaps in interaction with object scale. The timing coefficients fit to the synergies showed relatively little modulation, but did indicate a consistent temporal ordering of the synergies. Detailed biomechanical interpretation of the synergies' function was precluded by substantial differences between the two monkeys' synergy sets, only one synergy of which appeared to be significantly correlated and also to display similar coefficient modulation for objects shared by the two monkeys. These between-subject differences were evident in the EMG data prior to extraction, and may have been related to differences in electrode placement or quality, or motor strategies used by the monkeys.

1.1 INTRODUCTION

1.1.1 Muscle synergies as a motor control solution

The following three chapters concern the manner in which the primate central nervous system controls the movements of the hand. Movement control is an amazing feat that requires the nervous system to monitor and control a multitude of motor units and external variables (Bernstein, 1967). The large degree of redundancy in the design of the hand provides great flexibility for grasping a variety of objects and otherwise interacting with the environment, but makes the control and learning problems particularly complex. The sensorimotor system is faced with an ill-posed problem: a movement can only be accomplished by selecting an appropriate combination of muscle activations and joint rotations from an enormous array of possible combinations of these degrees of freedom.

In studying sensory systems, investigators have dealt with another ill-posed problem: that of recognizing objects from ambiguous arrays of stimuli. In this domain, researchers have proposed to bind low-level stimuli into invariant features and thence into perceived objects in a hierarchical fashion (Marr, 1982). In the visual system, for example, objects are identified by their possession of features such as edges and constant surface texture. A similarly heuristic solution to the problem of movement selection has been the idea of muscle primitives or synergies (Sherrington, 1906), i.e. invariant patterns of muscle activity that form the modular building blocks of more complex motor plans. By activating muscles as "synergies," the nervous system would effectively reduce the degrees of freedom available.

Despite the long history of this idea, actual evidence for muscle synergies and their central coding has been slow in coming. In lower vertebrates, controlled movements elicited by cutaneous or spinal stimulation have been shown to possess synergistic patterns of muscle recruitment (Tresch et al., 1999; Saltiel et al., 2001). A modular organization has more recently been extended to natural behaviors of the frog such as swimming, jumping, walking, and defensive movements (d'Avella et al., 2003)—consistent with Gibson's (1979) prescription to use ecologically natural stimuli in order to understand perception (e.g. Rieke et al., 1995; Reinagel & Reid, 2000). In mammals, the hindlimb muscle activity of cats has similarly been shown to readily decompose into muscle synergies (Ting & Macpherson, 2005), albeit in a postural rather than movement control paradigm.

The present investigation derives from those studies and extends the synergy hypothesis to a considerably more complex system, the monkey forelimb. In this study, I observed patterns of EMG activity during a variety of natural grasping movements of the hand as it interacted with a variety of plastic objects. The optimization procedure of d'Avella et al. (2003) was then applied to test the degree to which EMG patterns are generated by combinations of synergies (depicted schematically in Figure 1-1) rather than by independently-controlled muscles. According to the model, each synergy participates in the data reconstruction with a particular amplitude and timing coefficient specific to a given behavior and synergy. These scalar coefficients are assumed to reflected flexible, centrally-driven commands. The synergy structures themselves are assumed—for now—to be encoded in a fixed manner within the nervous system.

1.1.2 Grasping behaviors of the primate

The wide variety of grasp postures and manipulatory movements available to the primate hand allows flexible handling of various object shapes and sizes (Napier, 1956). While study of these behaviors is complicated by the kinematic ambit of the primate hand (compare the two-dimensional reaching task introduced in Chapter 4), such movements allowed me to investigate the parametric modulation of muscle synergies as a function of object properties (mass, size, shape, and location) and task demands.

Several earlier studies of grasp control in humans (e.g. Santello & Soechting, 1997/1998; Mason et al., 2001) and monkeys (Roy et al., 2002) have focused on kinematic variables (like grasp aperture) and their dependence on object parameters. For instance, the kinematics of prehension movements were investigated by Roy et al. (2002) in macaques trained to grasp cylinders of variable size and location. Less

regard has been given to the neurophysiological control underlying the grasping behaviors. Investigators have studied forelimb EMG activation in rhesus monkeys trained to reach for, grasp, and pull with a small, controlled force on a set of six (Brochier et al., 2004) or sixteen (Mason et al., 2004) different objects. Using a similar design to study visual and haptic interactions in the anterior intraparietal cortex, Murata et al. (1996, 2000) had monkeys pull or hold objects of variable size, shape, or orientation.

Here my interest in invariant and generalizable patterns of muscular activation led me to maximize such patterns by including a variety of object and task conditions. My set of grasping tasks is distinguished principally by: 1) the systematic and relatively independent variation of behavioral dimensions including task and object properties; and 2) the relatively controlled manner in which at least some of the object sets were introduced to the monkey, allowing me to address issues of motor generalization and adaptation.

In particular, to explore the space of manual behaviors I presented the monkey with a rich set of objects in which I have systematically varied object parameters (*shape*, *size*, and *mass*), and with these objects I required the monkey to perform various *tasks*: transportation, isometric pulling, or exploratory rotation. Object *location* was a further variable of interest, though it was expected to modulate the basic reaching component in these behaviors rather than the finer grasping movements that were of greater interest given my relatively distal sampling of muscles. In this chapter I focus on synergy modulation with object size and shape. In Chapter 2 I consider the monkeys' generalization to novel object shapes or sizes, and also to different object locations. In Chapter 3 I describe the monkey's generalization to multiple tasks performed with the same object.

1.2 METHODS

1.2.1 Subjects

I collected EMG and behavioral data from two rhesus macaques (*Macaca mulatta*) while they performed object transport behaviors. In the text that follows I refer to these monkeys as G0 and G1 (7- and 8-year old female monkeys, respectively). Cortical data was recorded separately (monkey G0) or simultaneously (G1) but is not presented here. All procedures were approved by the MIT Committee on Animal Care.

1.2.2 Paradigm

Transportation task Each animal was trained to perform a variety of grasping behaviors, using the left hand (which I found to be non-dominant for such behaviors; see Discussion). During the recordings presented here the monkey was head-fixed by means of an implanted cranial post, but still able to see the task tray in front of it. (I do not consider the effect of this head-posting, or postural factors in general, on the monkeys' EMG patterns.) As depicted in Figure 1-2, the task involved a reach-to-grasp and a transportation movement. Each monkey was trained to use its hand: 1) to press a start button located on the left side of its workspace;

then 2) within 1.0 s to reach for and remove a clearly visible object in one of two 2-cm-deep, 7-cm-wide cylindrical (monkey G0) or conical (G1) wells fixed on the tray; and finally 3) to release it in the opposing tray location 20 cm away (where it had to remain stably for at least 0.1 s, without bouncing out) following either a "leftward" or a "rightward" transport of 1.0 s or less. During the transport the monkey's hand had to clear a plastic barrier 3-4 cm high that divided the left and right halves of the tray. (The monkey's right hand was not able to participate in the task given another plastic barrier.) After receiving its reward (~0.3 ml water or apple juice delivered automatically via a drinking spout) the monkey was able to initiate a new trial at will. After every 10 successful trials, I removed the object and replaced it with another (or, during training, with the same, canonical sphere). Within such blocks, objects were presented for as many trials as were required to achieve 10 successful transport behaviors. The selection of objects across blocks was random except for the restriction that the same object would not be presented for two or more blocks in a row within a given day. These task requirements were imposed by a software acquisition and control suite written in LabVIEW (National Instruments).

Objects Although the transportation task was relatively stereotyped, I attempted to explore a wide space of reach-to-grasp behaviors by presenting the monkeys with a rich set of objects. Among these objects I systematically varied object parameters, in particular, shape and size. The 24 objects used in this chapter and the next, displayed schematically in Figure 1-3, were custom-designed three-dimensional shapes fashioned out of Delrin plastic and weighing between 0.1 g and 215 g. The density of these objects was constant at 1.4 g/cm^3, and no attempt was made to equalize the mass of the objects within this set. The canonical object used in training was a sphere of intermediate size (33.5 g and 3.6 cm in diameter). The remaining objects included four other spheres of regularly-varying radius (denoted *s0x*; range 1.1 to 4.6 cm), five cubes of regularly-varying width (*c0x*; range 1.5-3.6 cm), and twelve cylinders that spanned three dimensions (height *h0x,* 0.6-6.4 cm; width *w0x*, 1.3-3.8 cm; and "arc" or concavity *a0x*, 1.3-3.2 cm) but were united by one prototypical cylinder (*h05½/w06/a06*). (The number in the object code denotes the relative magnitude of the variable dimension according to a linear scale, e.g. cube width incremented by 0.5 cm.) These objects had not previously been experienced by the monkeys, with the exception of the training object (*s08*), and spheres *s05-s10* and cubes *c03-c06* which had been handled by monkey G0 on each of 18 and 2 days, respectively, prior to the recordings described here. Also, monkey G1 had previously experienced the cube of size *c05* and the prototypical cylinder in a separate study, described in Chapter 3. Both of these prior recordings were completed two months prior to the beginning of the recordings presented here. Over the course of the recordings presented here and in Chapter 2, monkeys G0 and G1 experienced the same objects, except that monkey G0 received six spheres of sizes *s05-s10*, while monkey G1 received spheres of sizes *s03-s08*.

Object sets Although the two monkeys handled a nearly identical range of objects, they differed in the order in which these objects were presented. In this chapter I describe only the first of two sets of objects experienced by each monkey. In Chapter 2 I look at each monkey's generalization to the second set of objects. Monkey G0 was presented with the entire set of spheres and cubes in a pseudorandomly interleaved

fashion over five sessions spanning 10 days, and then was presented with the cylinder set. In contrast, I initially presented monkey G1 with a subset of the objects in each shape category (spheres *s04*, *s06*, *s08*; cubes *c03*, *c05*, *c07*; and the prototypical cylinder as well as cylinders of height *h01* and *h03*, width *w02* and *w04*, and curvature *a02* and *a04*), over nine sessions spanning 19 days. The monkey was then presented with the remaining objects (see Chapter 2), again pseudorandomly interleaved. The greater number of days of recording conducted on monkey G1 allowed me to collect more trials per object, although here I consider only the same, minimum number of trials performed by each monkey with each of the 24 objects and in each of the two directions of movement (see Analysis, below). For both monkeys and all object conditions I sampled trials from the entire span of days in which the monkey experienced the object.

1.2.3 Recording/Stimulation

Event markers Basic and indirect kinematic information was collected in the form of event times. The trial start time was indicated by the digital state of the start button (after custom "debouncing" of this record), a signal that I recorded digitally with monkey G0 and with greater, analog precision with monkey G1. Trial end time was determined by the software once the trial success conditions had or had not been met, and was logged more precisely in the case of monkey G1 as the digital state of the liquid dispenser solenoid control channel. For monkey G1, the data acquisition board (National Instruments) also recorded the digital signals from photosensors (Omron) mounted orthogonally and at staggered heights in each of the two conical object wells located on the tray in front of the monkey. For monkey G0, lowpass-filtered analog pressure sensor signals were used in place of photosensors, but were found not to be reliably sensitive to the presence of objects less massive than 5 g (hence in the 24-object set I substituted two large spheres for the two smallest spheres handled by monkey G1). These records provided information on times of object removal and object deposit in the target well. In particular, I used the event marker corresponding to the object's removal from the well to divide each trial into an initial *reach* component followed by an object *transport* time.

Videography Besides these simple event markers, I also videotaped each of the grasping behaviors at 29.97 Hz using a downward-facing video camera. Within the field of view of the videotapes was a chair-mounted digital counter, which recorded time elapsed in each trial in 10-ms increments. Also located near the counter were two light-emitting diodes (LEDs) which flashed briefly at the beginning of each trial and could be used to synchronize the videotape frames and the EMG data acquisition to within 1-ms precision (due to the precise phase shift between the LED flashes). However, for this thesis I did not consider these videographic data except to interpret in a crude fashion the biomechanical significance of the muscular patterns I observed.

Muscle set The muscles implanted with electrodes in each of monkeys G0 and G1 are given in Table 1-1, and depicted in Figure 1-4. The implantations shown in the figure do not include additional muscles implanted in both monkeys whose signal quality had degraded sufficiently by the time of these recordings to warrant exclusion

from the dataset. These degradations were characterized by distinct increases both in electrode impedance (sampled weekly) and in co-occurring noise artifacts visible as increases in cross-correlation to other muscles. (One source of such cross-talk can be volume conduction in the tissue embedding the muscles; see Brochier et al., 2004). The remaining 18-muscle set of monkey G0 contained a larger representation of extrinsic forearm flexors and intrinsic hand muscles than that of monkey G1, whose 18-muscle set complementarily included more proximal arm muscles and extrinsic forearm extensors. Although only 12 of the muscles in each set were common to the two monkeys, this common group included an even distribution of intrinsic hand muscles as well extrinsic hand or elbow muscles with either a primarily flexor or extensor action. Several muscles were also implanted in multiple locations given known anatomical and/or functional divisions (Howell & Straus, 1971). Muscles were identified during surgery based generally on size, fiber direction, and relative anatomical location (Howell & Straus, 1971). For intrinsic hand muscles, either a hand-held bipolar needle electrode or the implanted intramuscular electrode itself were used to electrically stimulate the muscles in order to make a functional identification.

Muscle implantation Muscles were implanted using intramuscular electrodes which were wired subcutaneously to a circular connector (WPI) mounted cranially. Like Park et al. (2000), my own prior experience with monkey G0 showed that such subcutaneous tunneling to the skull both limits the chance for infection, and promotes stability because the wires are less likely to dislocate (especially for longer wires) and may even bond to tissue. The muscle implantations required three separate surgeries on both monkeys. In the case of monkey G0, these were spread over a five-month period; the EMG data presented here were recorded between one and two months following the last of these surgeries. In the case of monkey G1, the surgeries spanned only a half-month, but the EMG data presented here were recorded between three and five months following the last of these surgeries. (The data presented in Chapters 2 and 3 from this monkey were recorded between one and five months after the surgeries.) In order to reduce the surgical time, a novel surgical sequence was attempted with monkey G1. Whereas with monkey G0 the electrodes had been implanted first before connecting them to designated pins on the cranial connector, with monkey G1 the wires were first attached to the cranial connector prior to implantation of this entire assembly into the monkey (G1). This second surgical sequence did not achieve any reduction in surgical time given the time that was required to complete the electrodes after the individual wires had been implanted. (The electrodes could not be pre-manufactured since each wire first had to be drawn through the implanted muscle before they could be attached; see below.)

Electrode construction The bipolar electrodes were manufactured either prior to surgery (monkey G0) or during the surgeries (G1), according to the surgical sequence described under "Muscle implantation," above. The intramuscular electrodes were made of two Teflon-coated 50-μm stainless steel wires anchored together under the muscle belly by means of a 2-mm wax ball (Loeb & Gans, 1986). As shown schematically in Figure 1-5, a short length of each wire was stripped of 1-3 mm of insulation where it would pass through the muscle belly (itself 6-10 mm thick). When the electrodes were manufactured prior to surgery (as for monkey G0), this

Teflon coating was removed using a scalpel and microscope, and I confirmed that electrical current flow across the electrode was restricted to these breaks in the insulation by systematically monitoring the impedance of the electrode in saline. When the electrodes were instead manufactured immediately after implantation into each muscle (monkey G1), I used a soldering iron applied briefly to the wire to remove the insulation (or to weaken the Teflon prior to removal with a scalpel). With this monkey I relied more frequently on visual inspection to confirm that the implanted ends of the wires were well-insulated by the wax beads I applied. For both monkeys, the 8-15 mm spacing between wire exposures was oriented parallel to muscle fibers, and was chosen to maximize the differential voltage between the two electrodes when action potentials passed along the recorded fibers.

EMG data collection The EMG data from all the muscles implanted in each monkey were recorded together, bandpass-filtered (10-Hz highpass and 1000-Hz lowpass), notch-filtered (60 Hz), and amplified (5000×) in differential fashion using a programmable signal conditioner (CyberAmp 380, Axon Instruments) controlled by software (CyberControl, Axon Instruments). Data were then digitized at 2 kHz using a data acquisition board (National Instruments). The EMG data records were recorded discretely between start and reward times, as detected by the software acquisition and control software.

1.2.4 Analysis

Trial alignment After acquisition, the EMG signals were aligned on the time of object removal from the origin well, an event registered by either the pressure sensors (monkey G0) or photosensors (G1) located in the well. To equalize the quantity of data contributed by each object condition, I restricted the EMG data to a fixed window around the time of object removal, and selected an equivalent number of trials from each object condition as described under "Trial selection" below. Finding that monkey G0's movements were generally slower than those of monkey G1, I chose this window to be either -0.90/+0.60 s (G0) or -0.45/+0.30 s (G1) around the time of object removal. These durations serendipitously captured 67% of both the reach and transport durations for each monkeys. Note that the window also corresponded to a 1.5:1 ratio of reach-to-grasp to transport components for both monkeys.

EMG data preprocessing The EMG data of each trial were centered by median subtraction within each muscle channel, highpass filtered (50 Hz), full-wave rectified, and lowpass filtered (20 Hz). The relatively elevated highpass filter cutoff was necessitated in the case of monkey G1 by movement artifacts that occasionally characterized its EMG signals. High-frequency oscillations characteristic of genuine EMG oscillations persisted after this filtering (see Fig. 1-6a). As for the lowpass filter, the results that follow appeared qualitatively identical whether or the filter was applied. Its function was merely to smooth the results to make the average nature of the synergies more apparent. The data were further bin-averaged over 20 ms (G0) or 10 ms (G1), thereby equalizing the quantity of data points contributed by each monkey given the difference in reach/transport window durations quoted above. Then, data were normalized across muscles within each day of recording to the peak

level of activity in each muscle recorded in that day. Finally, for the analyses reported in this chapter and the next (but not Chapter 3), the 40 trials within each object condition and monkey were averaged together following these preprocessing steps. Reach or transport durations that were not as long as the averaging window were only included in the average for the duration they spanned. Hence activity at the termini of the windows could be based on fewer than 40 trials.

Trial selection I only present data from trials that were rewarded according to the task criteria quoted earlier. Among each monkey's rewarded trials, furthermore, I used the recorded event times to select an equivalent number of trials in each object condition, to balance the contribution of each object to the dataset. In particular, I selected those 40 trials in each condition that had reach and transport durations both closest to the mean values for that object. For monkey G0, this trial selection followed an initial exclusion of 1347 of its 3778 recorded leftward- and rightward-directed trials (36%) due to instability in the pressure sensor signals (and a manual correction of the object removal time in another 710 trials, or 19%). For monkey G1 (whose event times were more reliably recorded by photosensors, but whose recordings were spaced over a longer period of time), this trial selection followed two data stratification procedures designed to reduce EMG artifacts. First, I applied an initial exclusion of four and three days (from its first and second recording conditions respectively, as described under "Object sets" above) based on inspection of average daily cross-correlation between its muscle signals. (At the same time I manually removed several blocks of trials from four and three of the remaining days, finding that these blocks had channel saturation artifacts.) Second, within the remaining 5772 rewarded, leftward- or rightward directed trials in each object condition I applied an automatic exclusion of trials defining the top quartile of the average root-mean-square (RMS) of EMG across muscles. Finally, in this chapter (cf. Chapter 2) I focus only on the "rightward" movements made by the monkeys.

Data reconstruction The variable muscle activity observed in these behaviors was reconstructed by a linear summation of a small number of synergies, each coded by only two scalar coefficients c_i and t_i. (See Figure 1-1 for a schematic example, or Figure 1-9 for the actual synergies extracted from monkeys G0 and G1.) Formally, I used the results of the extraction algorithm (see below) to reconstitute the sequence of muscle activity $\mathbf{m}_s(t)$ in each episode of recording s as the sum of N synergies $\mathbf{w}_i$ each weighted by an amplitude coefficient c_{si} and shifted by an independent timing coefficient t_{si}:

$$\mathbf{m}_s(t) = \sum_{i=1}^{N} c_{si}\ \mathbf{w}_i(t - t_{si})$$

In matrix form, each synergy i was expressed as a matrix $\mathbf{W}^i$ defined by E muscle electrodes and J discrete time points. More compactly, the N synergy matrices were concatenated according to $\mathbf{W} = [\mathbf{W}^1\ \mathbf{W}^2\ \ldots\ \mathbf{W}^N]$ (dimension E by $J{\times}N$). While both the amplitude and timing coefficients were scalar quantities, the timing parameters could be expressed as a time-shifting matrix $\mathbf{\Theta}_{si}[k_{si},K_s]$ in order reconstruct the

samples of muscle data $\mathbf{M}_s$ (each of dimension E by K samples) by matrix multiplication with the concatenated synergy matrix $\mathbf{W}$:

$$\mathbf{M}_s = \mathbf{W}\,(\sum_{i=1}^{N} c_{si}\;\Theta_{si}[k_{si}, K_s]) = \mathbf{W}\,\mathbf{H}_s$$

This time-shifting matrix accomplished two things. First, it aligned each synergy i with the k-th data point ($2-J \le k \le K$) in the muscle pattern $\mathbf{M}$, according to the optimized time delay found for that behavioral episode s. Second, it truncated any of the time points t within the synergy that were shifted outside of the muscle pattern $\mathbf{M}$. (This simplifying operation does not presuppose that muscle activity outside of the recorded sample could not be accounted for by the "excised" portions of the synergies.) The matrix $\mathbf{H}_s$ encompassed both the scaling and time-shifting operations of the coefficients.

Synergy extraction The time-varying synergies were operationalized as two-dimensional matrices of muscle activity across time. In particular, synergies were defined as 1.0-s (G0) or 0.5-s (G1) periods of non-negative activity across 18 muscle electrode dimensions, each integrated over 20-ms or 10-ms bins, giving each extracted synergy a dimensionality of 18 × 50 for each monkey. The synergies were extracted using a non-negative matrix factorization algorithm adapted from that of Lee and Seung (1999). The algorithm, implemented in MATLAB (MathWorks) proceeded by iterative decomposition (see d'Avella et al., 2003). At each iteration, the data reconstruction error $\mathbf{M} - \mathbf{WH}$ over all S muscle patterns $\mathbf{M}_s$ in the dataset was calculated and used as a cost function to direct the update of the synergy matrices $\mathbf{W}_i$, the amplitude coefficients c_{si}, and the timing coefficients t_{si}. (Each of these was first initialized to random values prior to the extraction; $\mathbf{W}_i$ was initialized as a set of Gaussian muscle profiles specified by random μ and parameters.) In particular, the steps involved:

1. optimizing the timing coefficients t_{si} for all S muscle patterns $\mathbf{M}$ (given the synergy matrices $\mathbf{W}$) using an efficient "greedy search" nested matching procedure (d'Avella et al., 2003) to find the set of time delays that maximized the scalar product between the time-shifted synergies $\mathbf{W}\,\mathbf{\Theta}_i[j, K_s]$ and the data $\mathbf{M}$ (and subtracting each synergy $\mathbf{W}_i$ in order of decreasing correlation to the data after its t_i were optimized);

2. updating the non-negative amplitude coefficients c_{si} for all patterns $\mathbf{M}$ (given the synergy matrices $\mathbf{W}$, the coefficients t_{si} from step 1, and the coefficient matrix $\mathbf{H}$ defined earlier) according to the multiplicative rule:

$$c_{si} \leftarrow c_{si}\,\frac{trace\left(M_s^T W\,\Theta_i(t_{si})\right)}{trace\left(H_s^T W^T W\,\Theta_i(t_{si})\right)};$$

3. updating the columns of the non-negative synergy structures $\mathbf{W}_i$ (given the coefficient matrix $\mathbf{H}$ defined earlier) according to the multiplicative rule:

$$W_{ij} \leftarrow W_{ij} \frac{\left[MH^T\right]_{ij}}{\left[WHH^T\right]_{ij}}.$$

These steps were iteratively repeated until the reconstruction error decreased by less than $r^2 = 0.001$ over 10 iterations. The entire algorithm was repeated five times for each extraction.

Synergy set selection While the synergies from each repetition tended to be highly similar, only the set with highest EMG variance explained was selected for further analysis. The particular *number* of synergies selected for further analysis was based primarily on visual inspection of the pattern incremental variance explained by each additional synergy. In addition, for the primary synergies presented in this chapter (three from each monkey), I attempted to calculate a baseline amount of variance explained by extracting 18 one-muscle synergies from the EMG data of each monkey. These single-muscle "synergies" were operationalized as being of the same duration as the trials from which they were extracted and to which they were fit (cf. the 2/3 of this duration covered by the multiple-muscle synergies). This duration conservatively allowed the entire time-course of each muscle's activity to be fit by the single-muscle synergy (since no combination of shorter single-muscle synergies could span the data of a single muscle). Single-muscle synergies are consistent with the hypothesis that the nervous system controls each muscle independently in time and amplitude (and with a fixed command profile, typically unimodal and bell-shaped). Eighteen such synergies accounted for 75% of the variance in monkey G0's dataset, and 70% of the variance in monkey G1's dataset (maximal r^2 achieved in five repetitions of the extraction). Hence I take 75% as the minimum variance to be explained in order for the multi-muscle synergy model to explain "significantly" more variance than a single-muscle control model. As an upper limit on the number of synergies considered, I also chose a smaller number of synergies than the number of object shapes or sizes (five) given to each monkey. I did so in case EMG variability due to object shape or size was so substantial as to result in spurious extraction of object- or size-specific synergies. (Such reasoning also led me to focus (until Chapter 2) on only one of the two directions of movement performed by the monkey.)

Synergy comparison Besides visual comparison of synergies extracted from different datasets (here, those of monkey G0 and monkey G1; in subsequent chapters, between different datasets within each monkey), a more quantitative method was also used. In particular, the scalar product of each synergy in set A was computed in relation to each synergy of set B (within corresponding muscles and at every possible time difference between the two matrices). This was done in order to find the pair of synergies capable of achieving maximal cross-correlation (across all muscles and at whichever time difference maximized the scalar product). Synergies were compared without replacement, i.e. once a synergy in one set had been matched to synergy in the second set, it was not able to be matched to *other* synergies in the

second set. Muscle implantations unique to either monkey were not included in the correlation. While the auto-correlation of one synergy against itself would be scored 1.0 by this method, the minimal level of cross-correlation one might expect, even between very different synergies, is not zero. This is particularly true given the non-negative average activation profile ascribed to each muscle within the synergy. To find a baseline level of cross-correlation, I took the three-synergy sets extracted from each monkey, and randomized the order of muscles within each synergy prior to calculating its auto-correlation. (Scrambling the muscle order rather than the temporal order within the synergy matrix is a more conservative procedure as it does not change the frequency content of the muscles, which may generally be described as having only one or two activity phases within the synergy.) I repeated this procedure ten times for each monkey and synergy, and in doing so found an average "auto"-correlation of 0.73 ± 0.02. I thus consider 0.75 to be a threshold for deeming cross-correlations between different synergies "significant."

1.3 RESULTS

As described in the Methods, both monkeys were trained to transport plastic objects between two wells mounted in front of them on a tray. After many days of practice with a training sphere, the monkeys were exposed to novel objects, presented in a pseudorandom fashion. The monkeys were required to reach the object within 1 s and then bring it to rest in the target well within a further 1 s (Figure 1-2), and to complete a block of ten such successful trials (in any combination of leftward and rightward directions of movement) before being given a new object. The objects presented to the monkey included the original training sphere and a number of novel spheres, cubes, and cylinders of variable width, height, or concavity (Figure 1-3). I postpone an analysis of each monkey's behavioral trends and adaptation patterns until the next two chapters. Suffice it to say that for both monkeys the recordings presented in this chapter occurred after the monkeys had each quickly reached a stable and generally proficient level of performance.

1.3.1 Muscle activity

While each monkey was performing the task described above, I recorded EMG activity from 18 bipolar intramuscular electrodes, implanted in the muscles shown in Figure 1-4. Several of the muscles were only implanted in one monkey; others of the muscle set were common to the two monkeys. Several muscles in each monkey were also implanted in multiple locations following known functional divisions.

In Figure 1-6 I plot EMG data from a sample trial performed by monkey G1, wherein the monkey transported a small cube (*c03*) towards the right target well. The EMG activity was preprocessed as described in the Methods. Despite the greater degradation of the electrode recordings from this monkey the post-filtered EMG activity retained physiologically plausible oscillations. The behavioral event times superimposed on the data were detected by hardware sensors, and included start button release, object removal from the origin well, object arrival in the target well, and reward delivery. Sample screenshots accompany these times.

Of the event times superimposed, I judged the time of object removal to be

relatively consistent and intermediate within each trial, and so used it to align the trials before restricting the data to a fixed window in time and averaging the data within these windows and for each monkey and object condition. Given the longer duration apparent for monkey G0's movements, I used a larger window (1.50 s) than for monkey G1 (0.75 s). For each monkey, however, I found that the ratio of reach-to-grasp and transport times was equivalent at 1.5:1 (see Methods), prompting me to place the removal time at 0.9 or 0.45 s into the windows of the two monkeys, respectively.

Prior to extracting muscle synergies from these data, I also looked for qualitative differences in activity between object conditions and subjects. Hence I averaged the removal-aligned and rectified (but not filtered or integrated) EMG activity over all rightward trials each monkey performed with each object. In Figure 1-7 I depict the results for both the canonical sphere and the small cube of Figure 1-6. Even without a direct measure of the kinematics it was apparent that at the level of individual muscular recruitment, the two monkeys may have used different motor strategies (see Discussion). Differences in muscle recruitment for different objects were considerably more subtle. Given the multiple muscles and time-points over which these small differences were manifest, I proceeded to extract a small number of time-varying muscle synergies in order to parsimoniously capture any systematic trends.

1.3.2 Synergy extraction

From each monkey's time-aligned, fixed-window, integrated and condition-averaged EMG activity I extracted between one and eight muscle synergies according to the time-varying synergy extraction algorithm (see Methods). In Figure 1-8 I plot the amount of variance within this dataset accounted for when the same data were reconstructed by a linear summation of individually weighted and timed muscle synergies. I do not plot the reconstruction achieved by a single synergy, as the duration of all synergies was only 2/3 the duration of the fixed-window trials (1.5 or 0.75 s). Only two or more synergies could (at least theoretically) span the entire trial duration. Qualitatively, these plots suggest that only a rapidly diminishing amount of variance was explained by any more than three synergies. Coincidentally, 79% of the EMG variance in each monkey's data was accounted for by three synergies. This amount also exceeded the 75% significance threshold estimated from reconstruction of the data by 18 single-muscle "synergies" (see Methods).

The three synergies that I selected for each monkey by the above reasoning are shown in Figure 1-9. (Although I do not show them here, additional synergies tend to resemble very closely those of smaller extractions, except that individual synergies will "split" into two partitions when additional synergies are allowed.) Each synergy appeared to capture a different set of monophasic or biphasic relationships between the muscles. Only the first synergy of the three appeared to have even modest similarity between the two monkeys, one that was above a conservative 0.75 cross-correlation threshold (see Methods). This synergy described a relatively prolonged phase of cocontraction across many extrinsic and intrinsic muscles. The second synergies of each did not score nearly as similar to each other, but at least both appeared to possess a biphasic structure across the more distal muscles. Little between-subject homology was evident in the third synergy of the set. The relatively poor correspondence between the monkeys' synergy structures was also evident when

I extracted synergies from only the twelve common muscles of each monkey (data not shown).

1.3.3 Synergy modulation

After time-varying synergy extraction, I looked at how the EMG in individual object conditions could be reconstructed by a linear combination of the synergies. Figure 1-10 depicts several of these conditions for monkey G0. Variation in the EMG activity of each trial average (e.g. that of the flexor digitorum profundus) was well-captured by changes in these coefficients, particularly the amplitude factors. Conversely, "muscle activity" that was not well-captured, for instance the brief phases at the beginning of trials with the largest cube (*c07*), may represent noise that persisted despite averaging—particularly at the beginning and end of the trial where fewer than 40 trials were included in the average (see Methods).

Figure 1-11 summarizes each synergy's modulation with object properties. At least one synergy—the second shown for each monkey (Fig. 1-9)—had what appeared to be a systematic increase in scaling with object size. In the case of monkey G1, this amplitude modulation could be seen particularly well for the cylindrical objects, suggesting a nonlinear relationship with object size dimension but perhaps a more linear relationship with object mass. The relationship of this synergy's scaling coefficient to object mass (regardless of size or shape) is plotted in Figure 1-12a. Particularly in the case of monkey G0, the synergy modulated strongly (r^2 = 97%; cf. 76% for G1) with object mass. The amplitude modulation of the remaining synergies appeared less consistent, although a small, inverse relationship with object size for at least some object shapes may have described the third synergy of each monkey (Figure 1-11). Also, the first and third synergies of each monkey displayed a modest either negative (G0) or positive (G1) relationship with each other (Fig. 1-12b). The direction of these correlations, like the structure of the third synergy, was not consistent between monkeys. There was relatively little evidence for a modulation of synergy recruitment by object shape, although interactions of shape and size may have characterized the modulation of monkey G1's third synergy.

I applied the same qualitative analysis to the timing coefficients, as shown in Figure 1-13. In contrast to the amplitude modulation shown in Figure 1-11, the same synergies showed little modulation of timing with respect to object shape or size. The first synergy of monkey G0 and G1 may have been assigned onset times later into the trial for objects of intermediate size (or very late into the trial for the largest cylinders, in the case of G1). The temporal relationship of the first and second synergies (insofar as they could be equated) was generally consistent between the two monkeys, in that the peak of the first synergy appeared to precede that of the second for most objects. But the timing of the third synergies again indicated no correspondence between the monkeys.

1.4 DISCUSSION

1.4.1 Evidence for reach- and object-related synergies

Two synergies appeared either structurally or functionally comparable between

monkeys when they performed a reach-to-grasp and rightward transportation movement. For instance, the scaling coefficient of one of three synergies extracted from each monkey (#2 in each case) was strongly correlated with object mass (Fig. 1-12a), and consisted of largely biphasic intrinsic muscle activity supported by some upper arm and flexor activity (Fig. 1-9). A similar size-related kinematic principal component underlying human grasping was described by Santello and Soechting (1997). The finding that the peak activity in the object-related synergy occurred at (G0) or before (G1) the time of object contact (Fig. 1-13) is also consistent with the results of Santello and Soechting (1998). They found that the posture of the hand could predict an object to be grasped with monotonically increasing accuracy that reached a maximum when the object was contacted. I speculate that this synergy thus describes the monkey's grasp and initial lift of the object per se.

The remaining two synergies of each monkey appeared modestly related in their scaling coefficients, though inconsistently between monkeys (Fig. 1-12b). One of these two synergies (#1 in each case) appeared structurally consistent between monkeys and seemed to specify a co-activation of many muscles (Fig. 1-9) that occurred consistently prior to the object-related synergy described above (Fig. 1-13). I tentatively identify this synergy as having spanned the end of the button-pressing behavior and the reach towards the object. A dynamic correlate of this synergy may have been the synchronous inter-digit force application observed in an isometric grasping task by Santello & Soechting (2000), who argued that it reflected a common drive to extrinsic finger muscles.

The third synergy extracted from each monkey was more difficult to interpret, particularly given its inconsistency both structurally (Fig. 1-9; cf. #1) and functionally (Fig. 1-11; cf. #2) between monkeys. It was at least characterized by a predominance of upper arm muscles (although only one of these was sampled in monkey G0), and may thus be thought of as having a role in the whole-arm transportation movements. This may particularly have been the case for monkey G1, for whom this synergy spanned the final portion of the trials (Fig. 1-13).

Whatever the biomechanical interpretation of these synergies, the chief results in this chapter have been the following: 1) A small number of time-varying muscle synergies were able to explain a large portion of the EMG variability observed when two monkeys performed a reach-to-grasp and transport behavior, and 2) at least one synergy from each monkey displayed a systematic increase in amplitude when it was fit to trials performed with successively larger objects. Some problems with these conclusions will be addressed in the following two chapters. In particular, while in this chapter I have reconstructed data using synergies extracted from the *same* data, Chapter 2 will address the generalization of muscle synergies to additional datasets. Furthermore, in Chapters 2 and 3, I will consider whether EMG variability can still be captured by the synergy account when trials in the same task condition are *not* averaged together as done here (and in a related study of EMG in primate grasping by Brochier et al., 2004). Also, in Chapter 4 I will test whether systematic changes in task parameters could be reflected in changes of synergy *structure* rather than coefficient—a finding that would challenge the idea of muscle synergies as invariant motor programs. For now I address two other features of the results: the prominent between-subject differences observed, and the evidence that three synergies is an appropriate number to have analyzed.

1.4.2 Between-subject differences in synergistic recruitment

Brochier et al. (2004) found dissimilarity between monkeys in muscle-space vectors they extracted from a muscle set (comparable to the one here) while two monkeys grasped different object shapes. Only for some objects (e.g. a small cylinder, like G1's *w02*) did these muscle vectors overlap well; for others (like G1's *h04*), both extrinsic and intrinsic muscle activity differed between the monkeys. Nevertheless I initially expected only moderate between-subject differences in the structure of the time-varying synergies I extracted from my EMG data, based on reports of minor inter-subject variability in hindlimb time-varying synergies extracted from frogs (d'Avella et al., 2003). I expected greater differences in the coefficients associated with matched synergies, e.g. given Cheung et al.'s (2005) finding of substantial variability between deafferented frogs in the activations ascribed to extracted hindlimb synergies. Similarity between the muscle patterns of different animals would have justified a more detailed biomechanical analysis of those patterns in relation to the observed behavior.

As shown in Figure 1-9, however, three synergies extracted from the two monkeys were too dissimilar even to identify more than a single matched pair. This was the case even if the synergies were extracted only from the common twelve muscles (not shown), a procedure which should have removed any biasing effect on extraction of muscles highly involved in the grasping task but only recorded in one monkey (in particular, the more proximal muscles included in G1's set). Only the variance explained by the two synergy sets was similar (79% by three synergies; Fig. 1-8), a result that might also not have been predicted given that monkey G1's dataset was slightly larger and more variable in shape, with 13 rather than 11 objects and five rather than two basic shapes. (But as I demonstrate in Chapter 3, the fact that monkey G1 experienced a wider range of object shapes would not likely have affected its extracted synergy structures, which were apparent even if extracted from trials with only a single object.)

There are at least three explanations for the differences observed in the synergy structures of monkeys G0 and G1 (Fig. 1-9). First, it is possible that the synergy set selected for each monkey (out of the five repetitions of the extraction algorithm) was biased by the initial settings to find a local solution that did not generalize well between monkeys. These settings include randomly chosen initial amplitude and timing coefficients, and a synergy structure that specifies Gaussian muscle activation profiles with random parameters. However, despite these randomized initial conditions, multiple repetitions of the extraction tended to converge to the same synergy solution for the same dataset. On average, the correlation between matched synergies in each three-synergy repetition was 0.91 ± 0.06 for G0 and 0.95 ± 0.02 for G1 (not shown). Moreover it seemed reasonable simply to choose the repetition producing the highest variance explained as the "best" set of synergies to describe each monkey's data.

Second, the muscles identified as "common" between the two monkeys may have had very different activity profiles, depending on placement within each muscle. This may be especially true for muscles extrinsic to the hand with anatomical (Cheng & Scott, 2000) or functional subdivisions (Schieber, 1993). Within such muscles (in human subjects), Weiss and Flanders (2004) indeed found that single EMG "units" could have quite distinct activity profiles. Johnston et al. (2005) also found that the

coherence between the activity of extrinsic hand muscles during grasping can be as strong—or stronger—between muscles (e.g. the flexors digitorum profundus and pollicis longus) than within muscle compartments (of the former muscle). The muscle signals I recorded frequently contained single-unit activity, at least initially during recording (not shown) and therefore would not be expected to reflect the global activation of the muscle. Over time all the channels came to contain more multiunit activity, but conversely the increasing noise pickup could well have differentiated the two monkeys' records even more. Any of these possible differences in muscle identity or quality may be reflected not only in synergistic patterns but also in raw, averaged EMG activity (Fig. 1-7).

Third, monkey G0's movements were uniformly slower, perhaps attributable to differing motor strategies. (This observation led me to look at only within-subject synergy modulation in the following two chapters.) It is unlikely that monkey G1 was globally faster than monkey G0, given that its movements in the reaching paradigm (described in Chapter 4) were unusually slow. Both monkeys had also received over one year of training in the grasping paradigm, and their performance even with the relatively novel objects presented in this study was quite accurate (see Chapter 2). It is possible that these differences in timing reflect an underlying difference in hand preference. As in the all the non-human primate chapters that follow, each animal was trained to perform with its putative non-dominant hand, to facilitate maximal learning. But the evidence for an *overall* hand dominance in nonhuman primates is inconsistent (Deuel & Dunlop, 1980; Deuel & Schaffer, 1987) and may not indicate homology to the strongly lateralized human condition (Warren, 1987; Corballis, 1989). Dhall and Singh (1977) as well as Falk et al. (1988) argue for a right-hand dominance in most rhesus macaques based on greater muscle weights and bone dimensions typically found for the right versus the left forelimb, indicating preferential use of the right forelimb and thus hypertrophy of the left forelimb muscles. Alternatively, some investigators have suggested that prosimians and monkeys demonstrate *differential* hand preference in certain tasks (MacNeilage et al., 1987). Thus, while I had found empirically that the left hand of the two monkeys appeared dominant in untrained food retrieval, it is possible that a different pattern of hand dominance would have emerged in the grasping task.

1.4.3 Sensitivity of synergy extraction algorithms

The synergies described in this study were extracted using an adapted non-negative matrix factorization algorithm (NMF; Lee & Seung, 1999). The algorithm is conceptually similar to principal component analysis (PCA: e.g. Brochier et al, 2004) and to competing dimensionality reduction techniques such as independent components analysis (ICA: Bell & Sejnowski, 1995; Hyvärinen & Oja, 2000; Kargo & Nitz, 2003; Hart & Giszter, 2004). An analysis applying several of these factorization techniques to the same simulated or empirical EMG data set from the frog by Tresch et al. (2005) suggests that all these techniques produce comparable synergy structures and degrees of variance explained. However, an important distinction of NMF is its "non-negativity" constraint. Applied to EMG patterns, this constraint requires that the synergies (essentially trajectories through muscle space) include only positive (or zero) activation values for each muscle. This constraint reflects the physiological reality that muscles themselves can be activated but not

"negatively" so. Lee and Seung (1999) similarly justified this constraint by pointing out that neurons have non-negative firing rates. This technique has previously been used in the sensory domain to extract a "parts-based" representation of a family of face images (Lee & Seung, 1999)—consistent with the feature-based solution to the "binding problem" described in the introduction.

The particular model used here was adapted from NMF by d'Avella et al. (2003) in another key respect. The majority of the techniques above consider muscle synergies to be static patterns of coactivation between muscles. The algorithm used here is "time-varying" in that the synergies specify a dynamic profile of activity for each muscle (d'Avella & Tresch, 2001; d'Avella et al., 2003; d'Avella & Bizzi, 2005). This allowance incorporates a physiological assumption that muscle coordination can involve invariant but non-synchronous relationships between muscles. A further implicit assumption built into the present model of synergistic control is that of a "refractory" period: in a given behavioral episode, a synergy can be invoked only once, even if the duration of muscle activation within the synergy is less than the duration of the movement.

Synergy decomposition, like other methods of dimensionality reduction, could be considered appropriate if the amount of EMG variance explained by a small number of synergies (smaller at least than the number of EMG signals) is relatively high. However, no consensus has emerged in the literature as to a minimum threshold of variance explained that is required to accept or reject such a synergistic approach. Nor is there agreement on an appropriate level of cumulative or mean variance explained to accept a given component as behaviorally "relevant" (Hart & Giszter, 2004).

Even if there were such a level, it would be highly sensitive to data preprocessing and processing steps. For example, in preliminary analysis of the G1 dataset I found that halving the integration interval led to a ~10% decrease in variance explained by three synergies, while doubling the synergy duration was associated with a greater than 10% increase of r^2. In this study I have simply reported the variance explained by the synergy approach, and compared it to the level expected by a model assuming independent control of the timing and amplitude of each muscle (activated with the same time-varying profile). I find that even three multiple-muscle synergies were able to explain more variance than 18 single-muscle controllers (Fig. 1-8). This number of synergies was also justified by the diminished returns in variance explained accompanying further synergies (Fig. 1-8).

Proper evaluation of different synergy definitions may not depend solely on the degree of muscle variance explained. This is particularly true in studies of muscle activity in grasping, where a large amount of variance is often explicable by a single component (particularly when the task variability is highly constrained—cf. Chapter 3). For instance, Mason et al. (2004) found that the largest-eigenvalue principal component extracted from EMG data recorded during reach-to-grasp movements of the rhesus macaque was able to explain 93.5% of the EMG variance in their study. Or, conversely, components that explain very little variance may actually be very informative about the task conditions. Thus in a similar task with the macaque, Brochier et al. (2004) found that while the highest-eigenvalue principal component could explain over 60% of the EMG variance, the set of five lowest-eigenvalue PCs were together able to correctly sort 90% of the objects handled by the monkey in a discriminant analysis. Similarly, Santello et al. (1998) found that over 80% of the

variance in human kinematic joint recordings could be explained by only two principal components, but that additional higher-order principal components were informative (in an information theoretic sense) about the objects subjects were asked to imagine holding. (In Chapter 2 I perform a similar discriminant analysis.)

Such results, in combination with qualitatively consistent studies applying PCA to human hand posture (e.g. Santello, Flanders & Soechting, 1998), suggest that the variance in kinematic and EMG data in manual tasks is predominantly the result of overarching postural transitions (e.g. opening of the hand), and is relatively independent of proposed grasp taxonomies. In the present study, one or even two time-varying muscle synergies may have explained far less of the variability in the task than in the above studies (Figure 1-8), though as described earlier this level of variance explained is highly sensitive to data preparation parameters. The extraction algorithm also does not lend itself to identification of "significant" synergies in the way that PCA identifies components with large or small eigenvalues. Nevertheless, the results seem to indicate that three synergies are appropriate to explain a large amount of the variance in the data (Fig. 1-8), and in doing so identify distinct muscle coordination patterns (Fig. 1-9). In linearly reconstructing the data (Fig. 1-10), these synergies furthermore demonstrated instances of parametric relationship to object properties (Fig. 1-11), in particular object mass (Fig. 1-12). They were also recruited at consistent but distinct points that spanned each averaged trial (Fig. 1-13).

Table 1-1 Muscles implanted. Muscles are grouped both by crude anatomical location, and within each region by a general caudal-rostral or radial-medial ordering. Monkeys G0 and G1 (Chapters 1-3) and R0 and R1 (Chapters 4-6) were each implanted over the course of one to three surgeries. Muscles implanted in common between the two "grasping" or two "reaching" paradigm monkeys, and still viable by the time of the primary recordings presented here, are indicated by × symbols. Muscles recorded uniquely in one monkey are shown by × symbols. Muscles that had degraded and were excluded in the primary analyses (Chapter 1, 2, and 4) are coded by — symbols. (Some of the muscles were still viable in the recordings presented in Chapters 3 and 5.) Several muscles (e.g. abductor pollicis longus) were implanted only once in one monkey but twice in another monkey.

location	*muscle*	*grasping*		*reaching*	
		G0	*G1*	*R0*	*R1*
back region	rhomboideus major			×	×
	trapezius (caudal)			×	×
	trapezius (rostral)			×	×
pectoral region	pectoralis major (caudal)		×	×	×
	pectoralis major (rostral)			×	×
scapular region	clavodeltoideus/cleidodeltoideus (anterior)		×	×	×
	acromiodeltoideus (medial)			×	×
	spinodeltoideus (posterior)		—	×	—
	infraspinatus				—
	supraspinatus			×	×
	teres major			×	—
upper arm	biceps brachii (lateral)		×	×	×
	biceps brachii (medial)			×	×
	brachialis			×	×
	brachioradialis	×	×		
	triceps brachii, long head			×	×
	triceps brachii, short head (radial/medial)		×	×	×
	triceps brachii, short head (ulnar/lateral)		×	×	×
forearm	flexor carpi radialis	×	—		
	palmaris longus	×	×		
	flexor digitorum sublimis (radial)	×			
	flexor digitorum sublimis (ulnar)	×			
	flexor digitorum profundus (radial)	×	×		
	flexor digitorum profundus (ulnar)	×	—		
	flexor carpi ulnaris (lateral)	×	×		
	flexor carpi ulnaris (medial)		—		
	extensor carpi radialis brevis		×		
	abductor pollicis longus	×	×		
	abductor pollicis longus (proximal)	—			
	extensor digitorum communis (distal)	×	×		
	extensor digitorum communis (proximal)	—			
	extensor digiti secundi & tertii proprius	×	×		
	extensor digiti quarti & quinti proprius	×	×		
	extensor carpi ulnaris	—	×		
hand (intrinsic)	opponens pollicis	×	×		
	abductor pollicis brevis	×	×		
	adductor pollicis	×	×		
	dorsal interossei manus I	×			
	abductor digiti quinti manus	×			
	flexor digiti quinti brevis manus	—	—		
	opponens digiti quinti manus	×	×		

Figure 1-1 Time-varying synergy model. **a**) Two schematic, three-muscle synergy matrices W_i describing activity profiles over three muscles $\mathbf{m}_j$. Muscle activity is denoted by the brightness within the plots. Note that these synergies are able to capture non-synchronous coactivation between the muscles. The time profiles below each matrix are icons depicting the average activation across the three muscles. In **b**) the synergies are used to fit two behavioral episodes. The muscle activity is represented by the black envelope. The reconstruction is achieved by solving for optimal, independent activation weights c_{si} and and timing coefficients t_{si}, specific to each episode *s* and synergy *i* (Adapted from d'Avella et al., 2003).

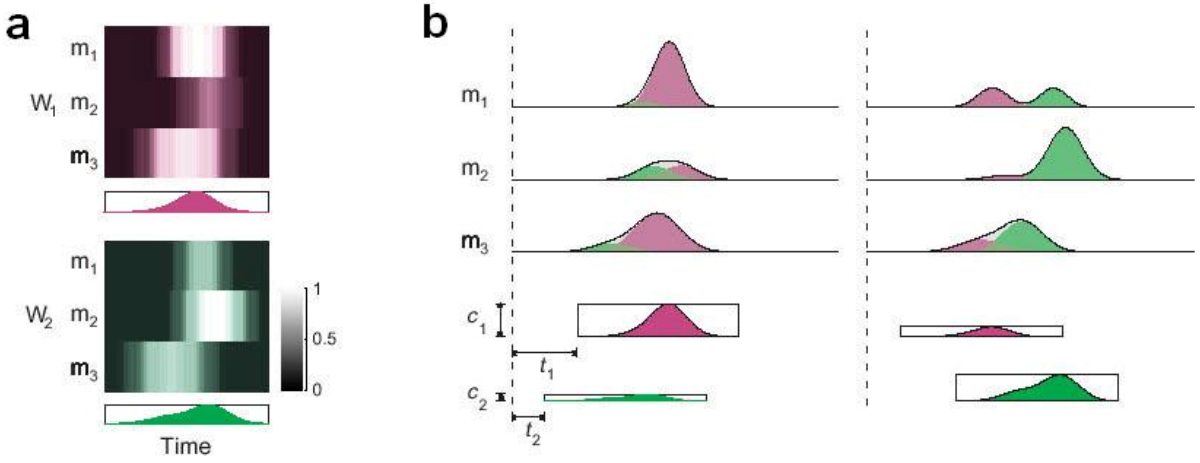

Figure 1-2 The transportation task. Each monkey was trained to transport plastic objects between two wells mounted in front of it on a tray. After many days of practice with a training sphere, the monkeys were exposed to novel objects, presented in a pseudorandom fashion. The monkeys were required to reach the object within 1 s and then bring it to rest in the target well in 1 s, and to complete ten such successful trials (in any combination of the two possible target locations) before being given a new object. Behavioral information was limited to event times triggered by pressing the start button or crossing the photosensors.

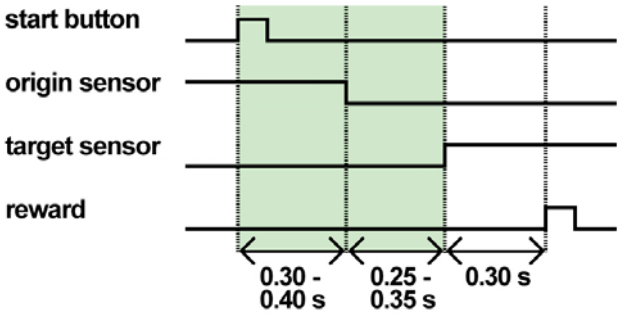

Figure 1-3 Object set used in grasping paradigm. The objects presented to each monkey included the training object (a sphere) and 23 novel objects including **a**) five additional spheres, **b**) five cubes, and five cylinders each of variable **c**) width, **d**) height, or **e**) concavity. One of the cylinders was common to each of the three cylinder shape categories (and was presented to the monkeys in equal frequencies with each of the other objects). For each object shape, the critical object dimension (e.g. width) was varied in a regular fashion. In Chapter 1, I describe each monkey's exposure to only a subset of these objects. For each monkey the remaining objects were presented in a subsequent object set described in Chapter 2. In Chapter 3 I used only the training sphere size, one of the cube sizes, and the prototypical cylinder, but in one of the experiments I varied the mass of these objects.

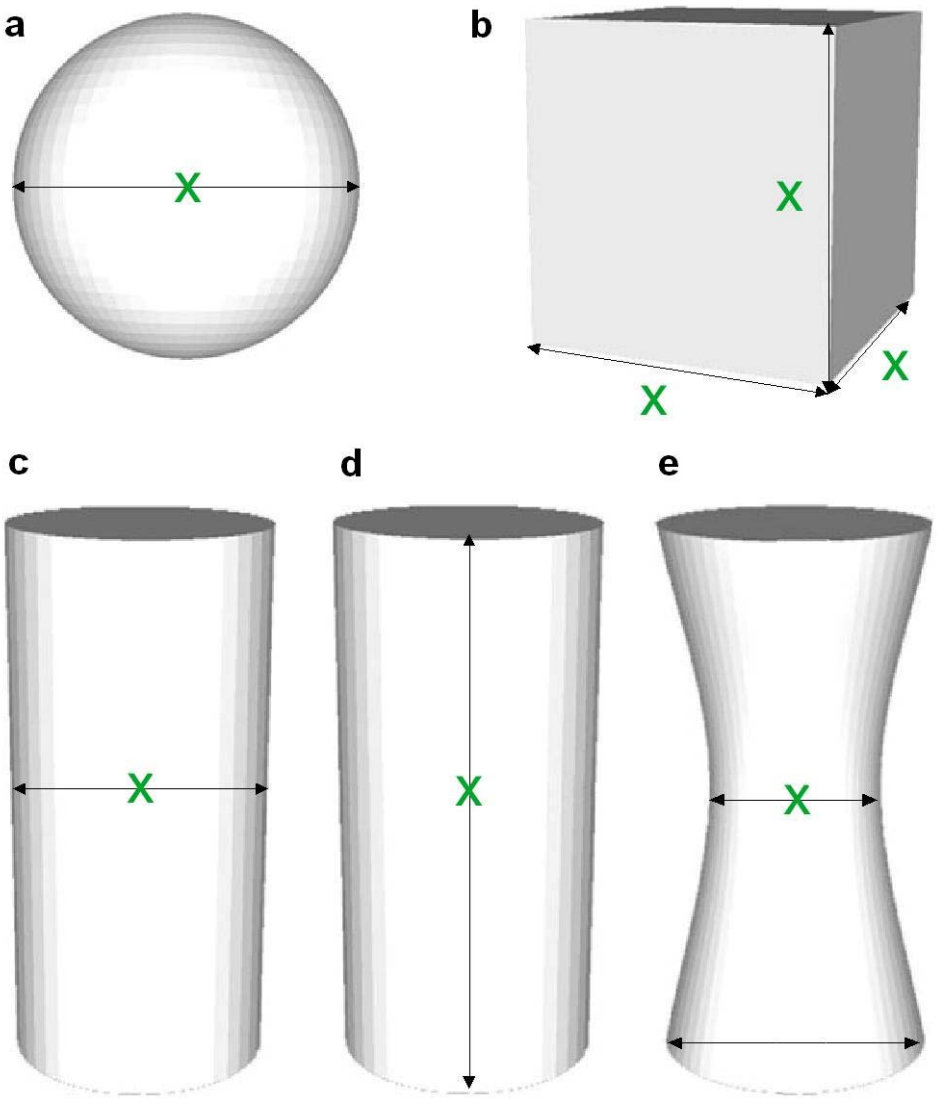

Figure 1-4 Muscle locations targeted in grasping paradigm. Between 18 and 24 intramuscular EMG electrodes were implanted in the muscles of the shoulder, upper arm, forearm, and hand, in three separate surgeries on both monkeys G0 and G1. The muscle set presented here includes 18 electrodes from each monkey, the others having been rejected based on high cross-correlation or other artifacts that developed within the months between implantation and these recordings. These muscles are colored and labeled in views of the **a**) lateral arm, **b**) ventral hand, and **c**) medial forearm. (Figures adapted from Howell & Straus, 1971.)

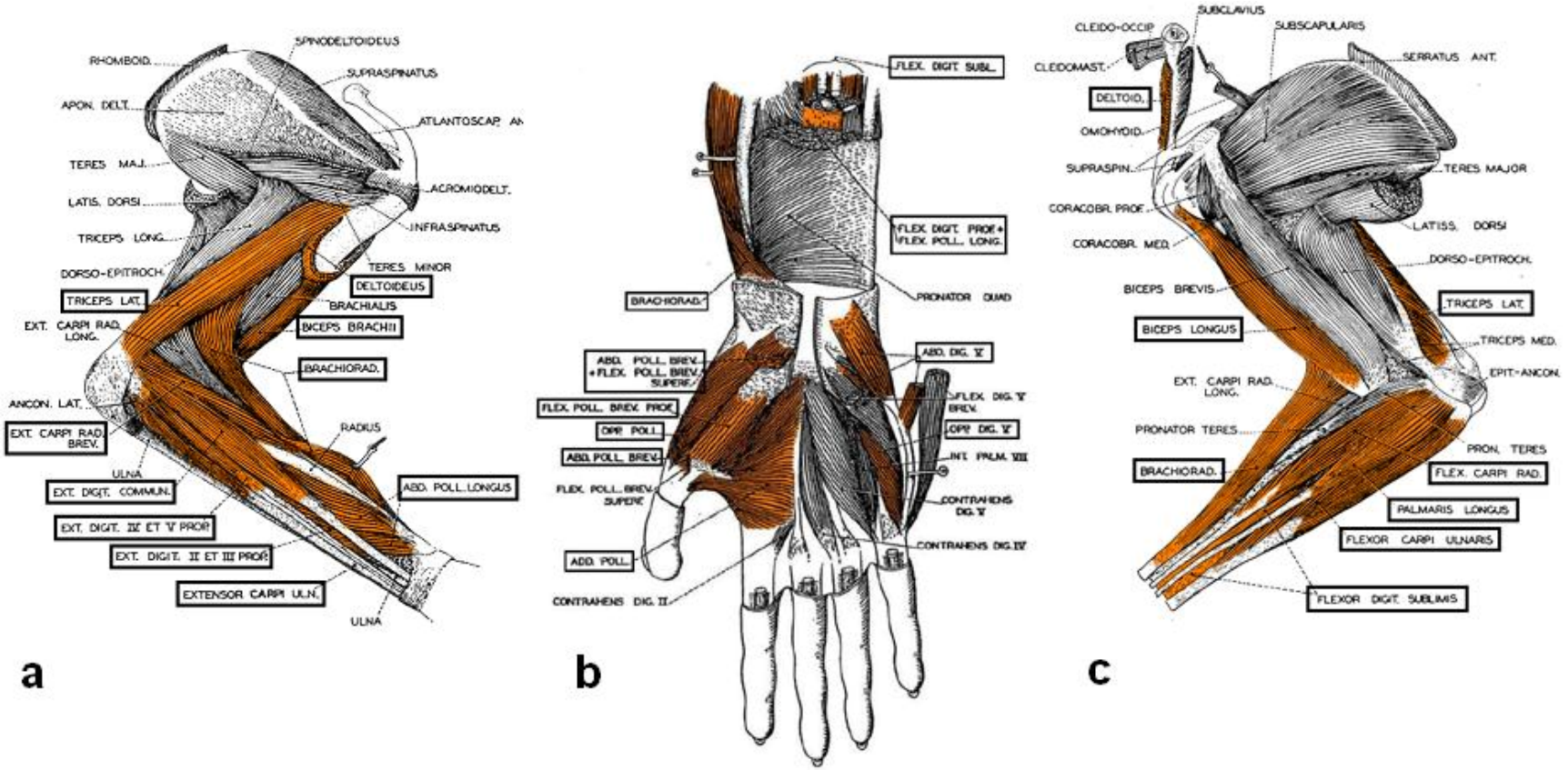

Figure 1-5 Intramuscular electrode construction. The electrodes were designed to maximize the differential voltage recorded between the two electrode wires penetrating the muscle when action potentials pass along the recorded fibers. From the spatial wavelength of these action potentials the proper spacing of the exposed wire lengths (d) was calculated to be on the order of 10 mm; I used distances between 8 and 15 mm. The size of the exposure on each wire (l=[1,3] mm) and its placement with respect to the 2-mm wide wax bead was chosen relative to the expected muscle thickness (t=[6,10 mm]). The wax bead attached the two wires physically but not electrically, and anchored them on one side of the muscle.

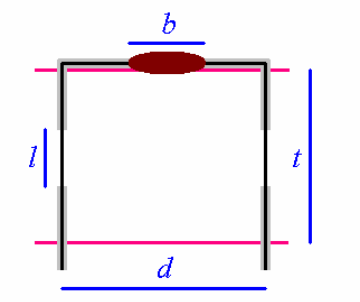

Figure 1-6 Sample transportation task trial. **a**) Highpass-filtered EMG activity is shown for a sample rightward-directed trial performed by monkey G1 with a small-sized cube (*c03*). The ordinate of each muscle represents voltage normalized to the peak voltage recorded on *any* muscle during the trial. Behavioral events are estimated based on signals from pressure sensors (monkey G0) or photosensors (G1) mounted in the wells. Sample screenshots accompanying these times at right were taken from video recorded by a camera suspended above the monkey. The events included: **b**) start button release (green), **c**) object removal (yellow), **d**) target well arrival (orange), and **e**) trial success and reward delivery (red). Despite the kinematic markers placed on the joints of the fingers and hand of monkey G1, the movements for both monkeys were difficult to characterize with precise 3D kinematics, particularly given only a single overhand camera view.

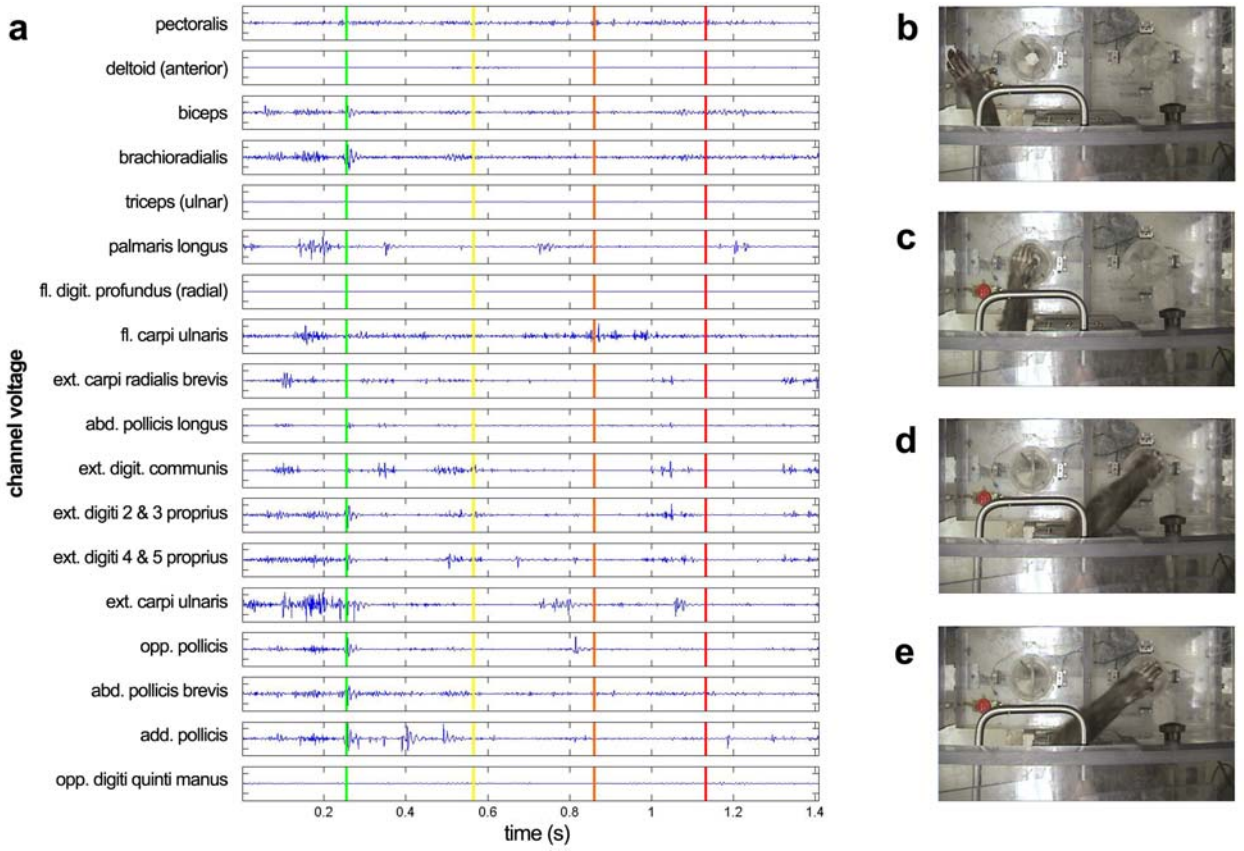

Figure 1-7 Event-aligned, averaged EMG in the transportation task. For the purposes of this figure (but not subsequent analysis), the rectified but pre-filtered and pre-integrated EMG activity was averaged across all trials transporting the canonical sphere to the right target well by monkey **a**) G0 and **b**) G1. The event used to align the EMG prior to averaging was the time of object removal registered by the sensors located in the origin well. I found empirically that this time divided the reach and transport components of the behavior into a 1.5:1 ratio of reach to transport times in both monkeys, despite the two-fold difference in the two monkeys' movement latencies. EMG activity in a -0.9/+0.6 s (G0) or -0.45/+0.3 s (G1) window around this alignment time of was averaged over all 40 selected, rightward trials performed by each monkey with each object. The ordinate represents voltage at the same scale for all muscles. (*fl.*: flexor; *ext.*: extensor; *abd.*: abductor; *add.*: adductor; *opp.*: opponens; *digit.*: digitorum.)

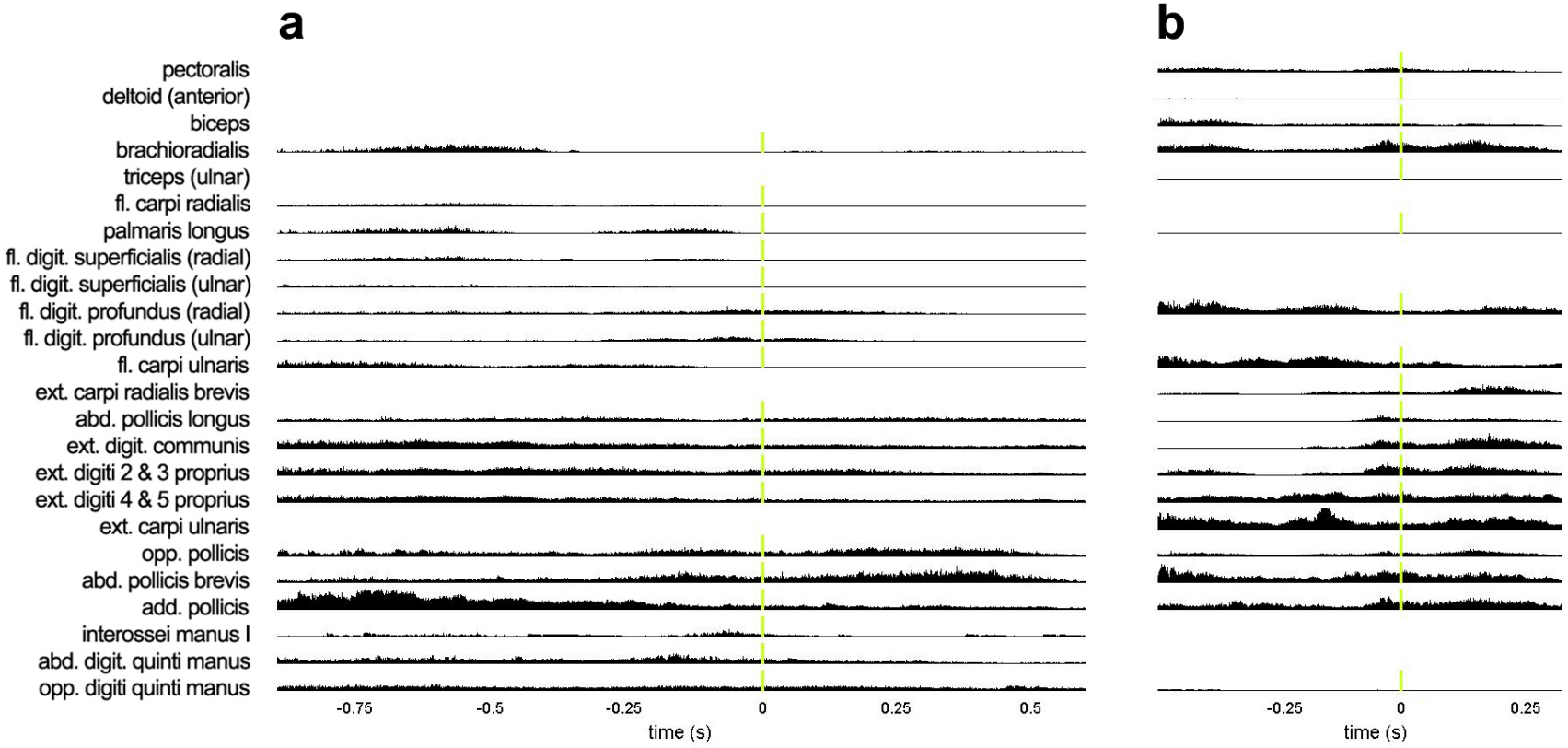

Figure 1-8 EMG variance accounted for in the transportation task. A small number of time-varying synergies were extracted from the 18-muscle, 11- or 13-object, single-direction, 40-trial-subselected, object removal-aligned EMG data, after additional processing including median baseline removal, 50-Hz highpass-filtering, half-rectification, 20-Hz lowpass-filtering, 20- or 10-ms integration, and normalization to the maximum EMG activity in each muscle across the entire experiment. Each extraction was repeated five times; the solid lines represent the maximal variance accounted for by two to eight synergies. The curves were roughly similar for both monkeys **a**) G0 and **b**) G1. The amount of EMG variance accounted for by fitting these synergies to the same dataset was dependent on each of the procedures enumerated above, and hence cannot be taken as an absolute measure of the success of the algorithm. Nevertheless, it was clear that while successively higher numbers of synergies can explain more variance in these datasets, this gain was diminished beyond three synergies. The dotted line shows the threshold variance explained conservatively estimated by reconstructing the data by 18 single-muscle "synergies."

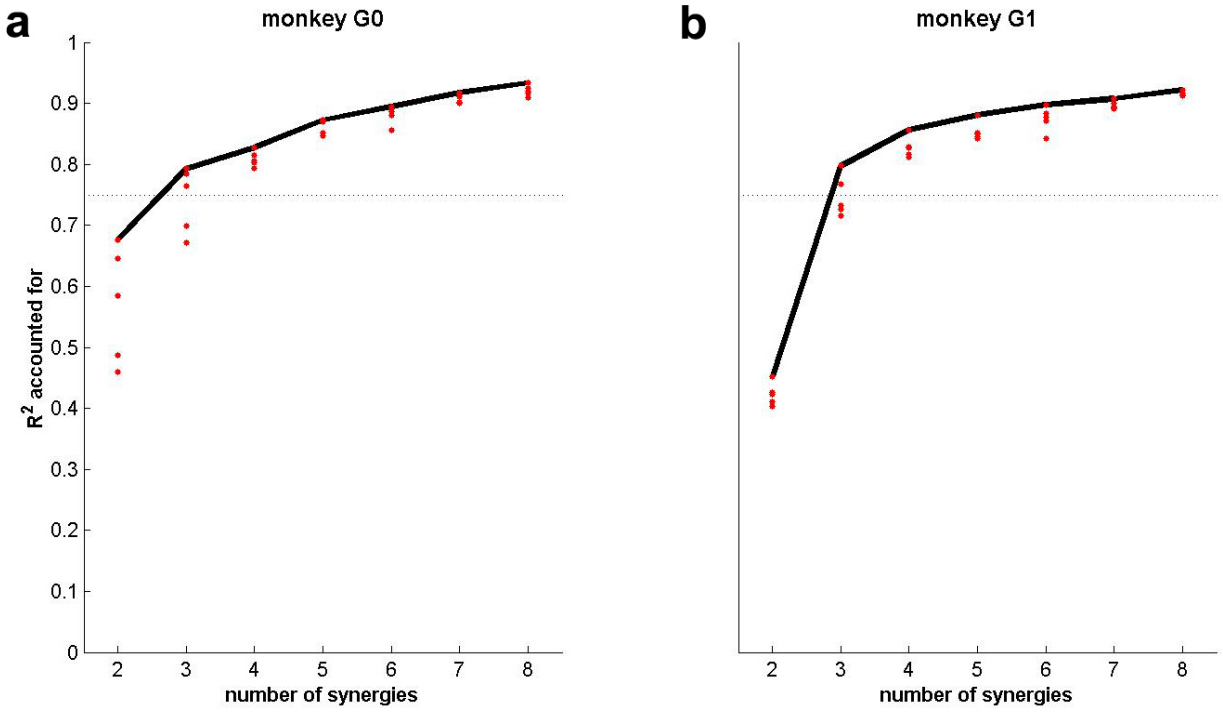

Figure 1-9 Synergy structures in the transportation task. The extractions that generated the maximal variance-explained score (79%) at three synergies in Figure 1-8 produced the synergy matrices shown in for monkey **a**) G0 and **b**) G1. Note that monkey G0's synergies were operationalized as twice the duration of G1's. Color intensity refers to the degree of ascribed EMG activity, as per the reference bar on right. (The colors themselves are chosen arbitrarily to help give visual continuity with the figures that follow in this chapter and beyond.) Muscle channels not recorded in either monkey are filled in with black in the synergy matrices. Synergies have been normalized to the same level of peak intensity within each matrix. For each monkey the synergies have been ordered in terms of decreasing similarity, as indicated by the cross-correlation score above the synergies of monkey G1.

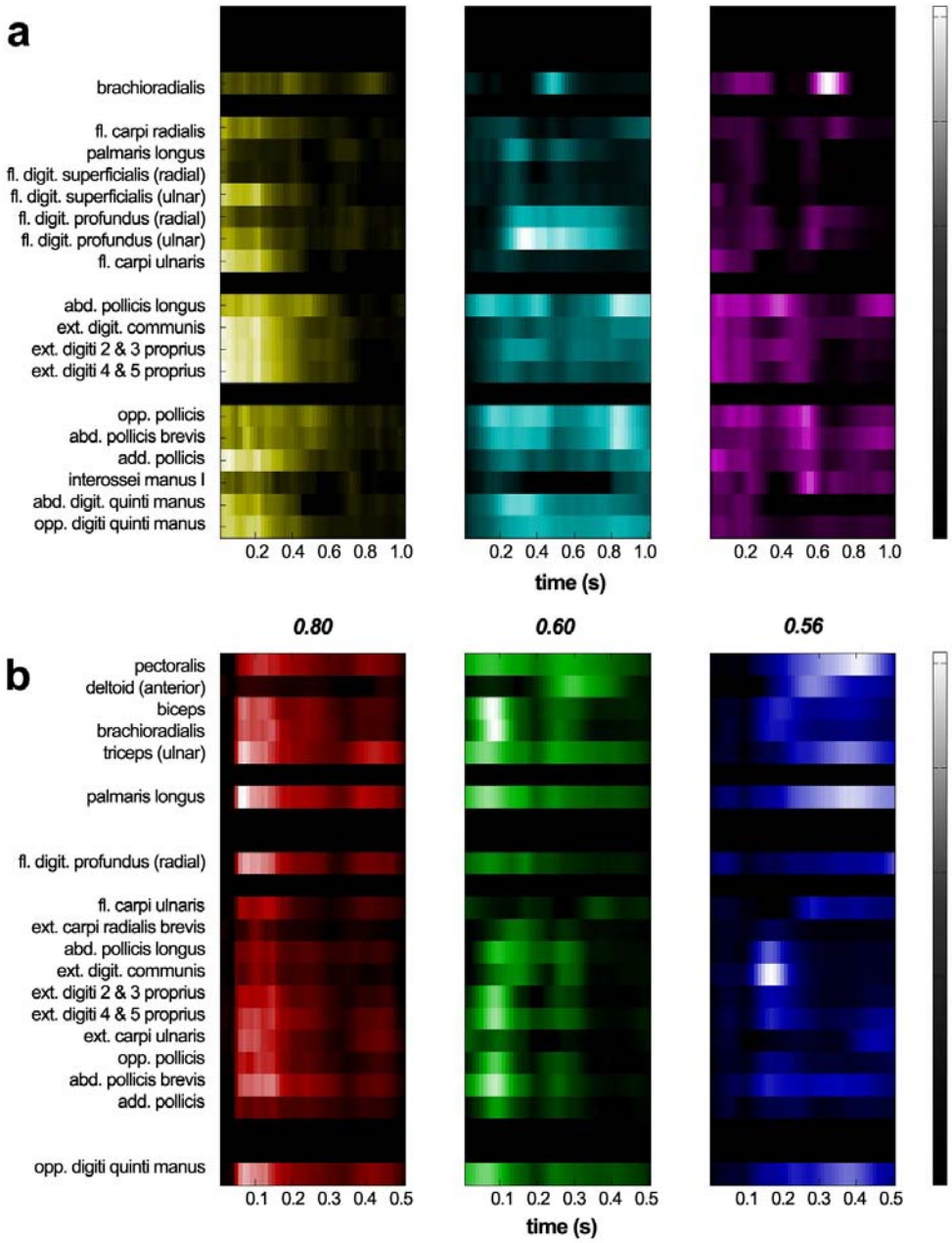

Figure 1-10 EMG reconstruction by linearly combined muscle synergies. Shown are the trial averages from the series of cubes transported in the rightward direction by monkey G0. In each case the EMG activity can be reconstructed by linear summation of the three independently scaled and shifted synergies (colored as in Fig. 1-9). The integrated EMG activity is shown as the grey envelope for each muscle; superimposed on this in red is the reconstructed activity. The scaling and timing are represented by the height and offset of the icons representing each synergy at bottom.

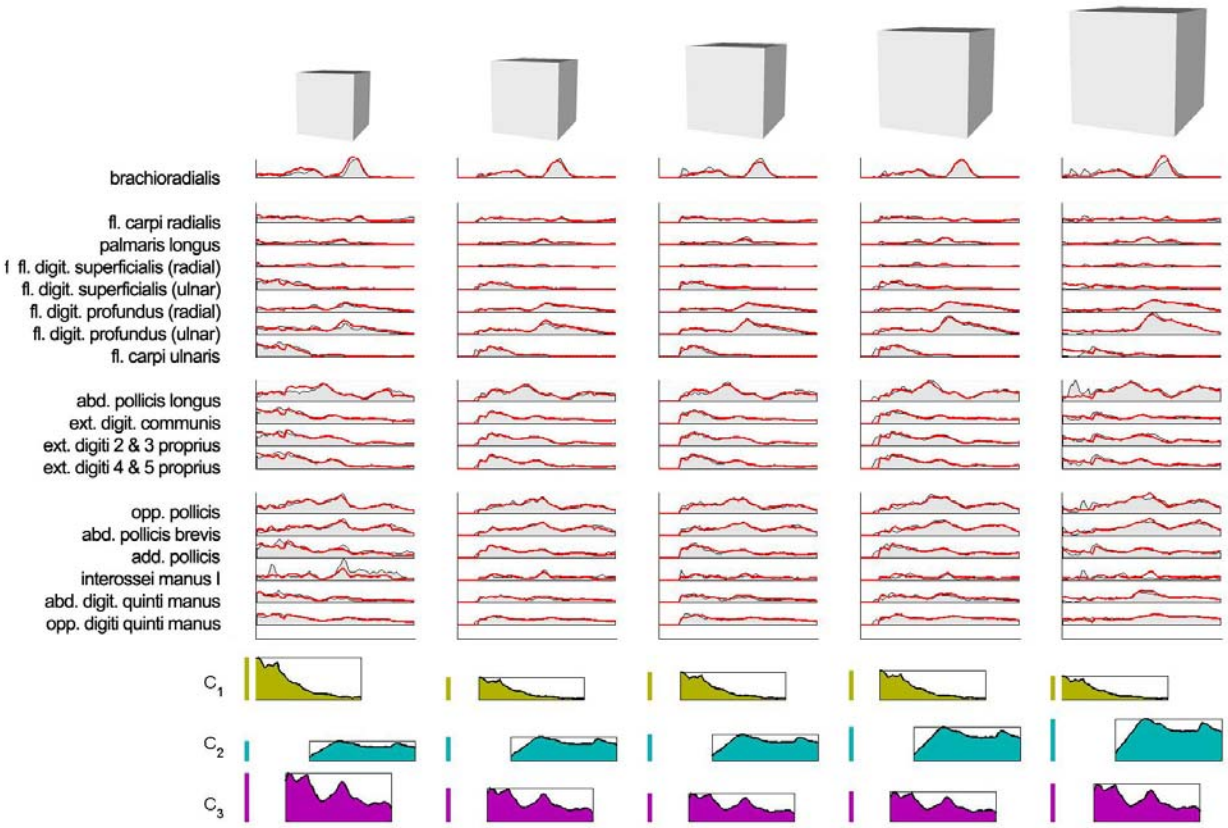

Figure 1-11 Amplitude modulation of synergies by object properties. The data are grouped by object shape and size, as shown schematically below the abscissa. Note that no error bars can be plotted as each point represents a single, averaged condition fit by the synergies. Also note that the coefficient units on the ordinate are somewhat arbitrary as they are based on the reconstruction of normalized EMG data by the extracted synergies. Finally, note that for monkey G1, the three cylinder sets were united by a prototypical cylinder, plotted thrice.

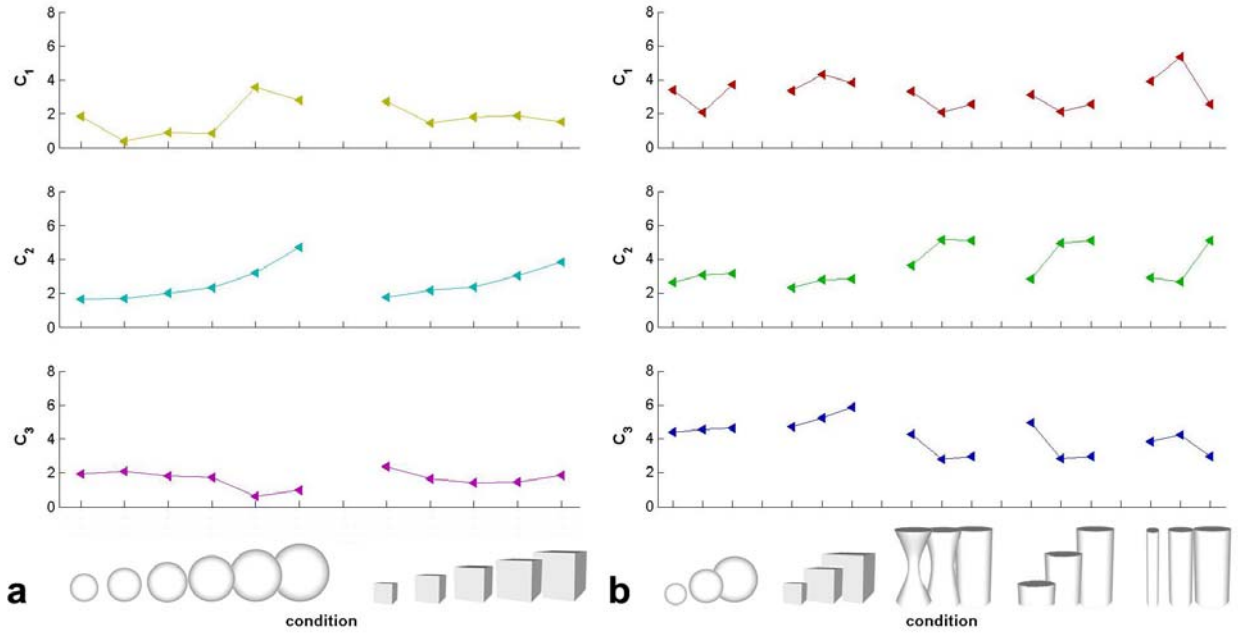

Figure 1-12 One synergy from each monkey appears correlated with object scale. **a**) The amplitude coefficient assigned to the second of the two synergies for each monkey and object condition in Figure 1-11 is plotted against object mass (rather than the dimension I explicitly manipulated, such as cylinder height). The correlations between these variables are given in the legend. **b**) A modest correlation between the amplitude coefficients of the remaining two synergies is also evident for each monkey.

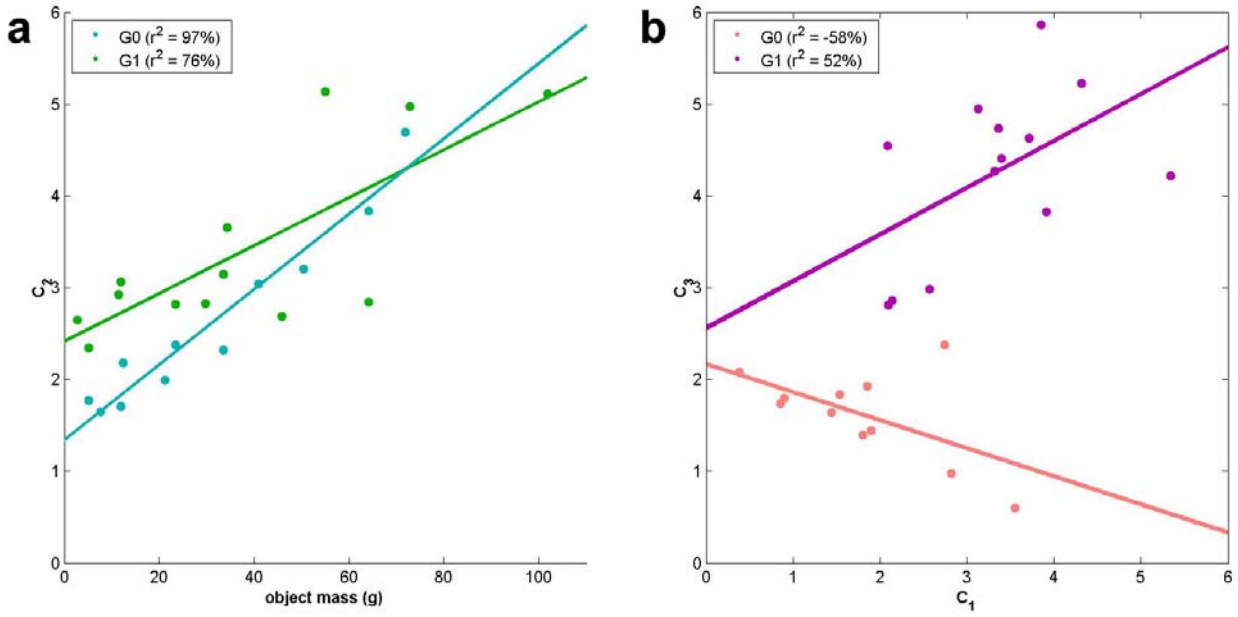

Figure 1-13 Timing modulation of synergies by object properties. The ordinate plots the time of each synergy's peak activity (after averaging across muscles) relative to the time of object removal, itself fixed at 0.9 or 0.45 s into the trials of monkey **a**) G0 or **b**) G1, respectively.

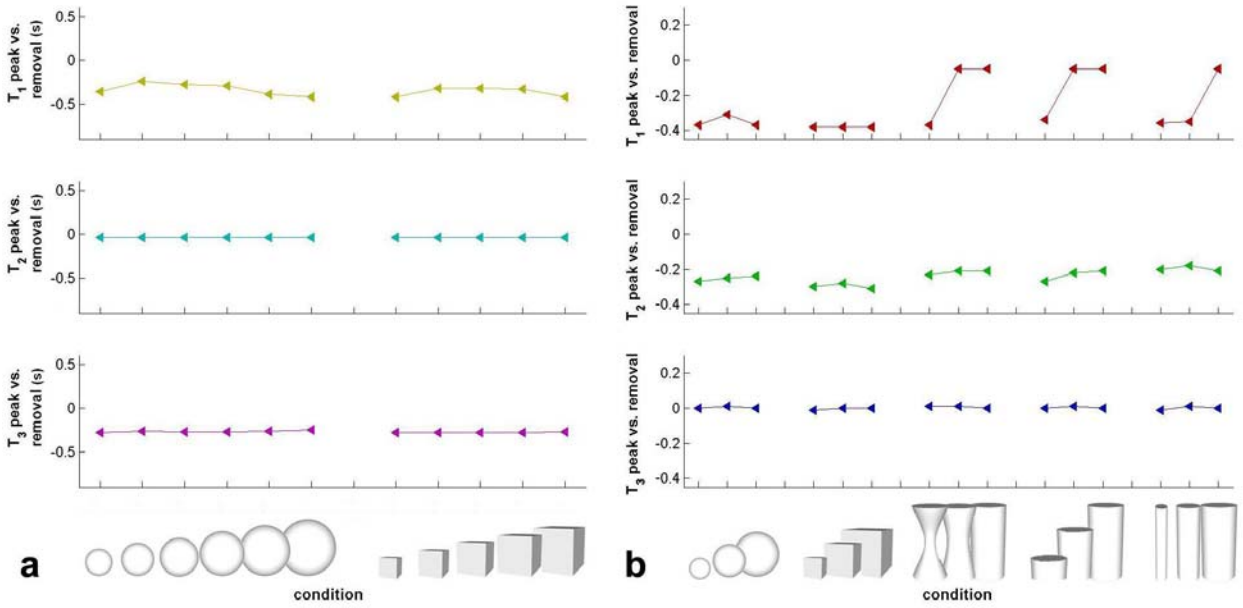

2 Muscle Synergy Generalization in Grasping Behaviors

I examined the generalization of three muscle synergies derived from each of two monkeys performing a reach-to-grasp and transport behavior with a variety of objects. While I previously found that only one of the three synergies was reasonably conserved between monkeys, here I found that two of each monkey's synergies were present regardless of whether the monkey transported the objects in a leftward or rightward direction, and despite direction-related changes in the EMG patterns and the duration of both the reach-to-grasp and transport movements. A similar degree of generalization was evident when each monkey was later exposed to a set including novel object shapes or sizes, despite the passage of time between these objects sets. When one of the monkeys was presented with cylindrical objects after having first been trained on spheres and cubes, two of its three synergy structures were preserved. When the second monkey was presented with spheres, cubes, and cylinders interposed in size between its familiar objects, all three of the synergies appeared to be present. In all of these contrasts both a reach-related synergy and an object-related synergy were evident, based either on comparisons of synergy structure and/or of the modulation of synergy scaling coefficients with object mass, respectively. The moderate degree of generalization evident in these contrasts may have been compromised by the time-varying synergy model's inability to characterize non-parametric changes in the involvement of muscle subsets or in the relative timing and duration of muscle phases within the synergies, each likely due to over-representation of one variable (e.g. movement direction) uniquely present within one of the datasets. In all of these contrasts, a similarly low number of synergies appeared appropriate for describing the data, based on the profile of EMG variance explained by reconstruction of the dataset as a linear combination of the synergies (79-88%). A reduced but still substantial degree of EMG variance (50-56%) was captured by only three synergies when the data across behavioral conditions defined by object location and identity were pooled together, and the trials representing each condition were not averaged together. Moreover, the scalar coefficients associated with these synergies were able to convey a reasonable amount (42-48%) of the information defined by these task parameters.

2.1 INTRODUCTION

2.1.1 Tests of within-subject muscle synergy generalization

In the previous chapter I identified a small number of synergies in the patterns of EMG activity observed in natural reach-to-grasp and transportation movements of the hand as two monkeys interacted with a variety of objects. I demonstrated that different behavioral conditions could be generated with good accuracy by combinations of just three synergies, each specified with particular amplitude and timing coefficient. I further demonstrated a parametric modulation of one of these synergies as a function of object mass.

One caveat about these data was that they were reconstructed by synergies derived from the *same* dataset. In this chapter I therefore compare synergies extracted from different datasets to see whether they are similar. In Chapter 1 I introduced the primary methods of comparison when I contrasted the synergy sets extracted from

the two monkeys. In doing so I found that two of the three muscle synergies extracted from the monkeys appear markedly different, even among the subset of muscles that were implanted in common between the monkeys. However, one additional synergy from each monkey demonstrated a *functional* correlation (with object weight) even though its structure (represented as a matrix of muscles and time points) was not shared.

In this chapter I consider several *within*-subject tests of the generalization of these synergies. In particular, I consider: 1) how well synergies derived from reach-to-grasp and transportation movement in one direction across the workspace (as in the previous chapter) generalize to movements in the opposite direction; and 2) how well the synergies explain muscle activity variation in handling an entirely novel set of objects. The first comparison involves two datasets that were collected in an interleaved fashion (wherein rightward and leftward movements were alternated according to the monkey's choice). The latter comparison involves datasets that were separated temporally, and hence allows me to discuss retention of these synergies over time. (Conservation of synergies over *learning* rather than the simple passage of time is something I discuss in the chapters that follow.) In the second comparison, the novel object set presented to each monkey was also distinct. Monkey G0 had previously experienced a set of 11 spheres and cubes (as described in Chapter 1) but then was exposed to a new set of 13 cylinders of variable curvature, height and width. Monkey G1, like G0, was presented over two months with two consecutive sets of objects. However, its second set contained objects systematically interposed in scale between the first-set objects, allowing more concrete predictions about the patterns of generalization.

2.1.2 Predictions about the generalization of synergy structure and modulation

All of these tests are correlational in nature, given that I attempt to describe previously-recorded EMG activity as a linear superposition of several muscle primitives. Here I test the conservation of these synergies between the dataset of the previous chapter and the novel datasets, primarily in terms of both their spatiotemporal structure and their modulation with object properties. I consider a synergy structure to be "conserved" across two datasets if the correlation *between* the best-matched synergies in these datasets is superior to a baseline level of at-chance correlation (calculated as in Chapter 1). Conservation is further indicated if the same patterns of synergy coefficient modulation are observed.

An additional basis for synergy generalization could be a comparable degree of variance explained by the two sets of synergies in their respective datasets. Another reasonable test of synergy conservation would be to fit the novel dataset with synergies derived from the baseline dataset. Although I have employed this approach in the past, I do not do so here given that it could obscure the emergence or disappearance of synergies within the novel dataset.

Beyond drawing correlations between the datasets, I am able to make hypotheses about the modulation of the matched synergies when they are fit to the novel data, based on the trends I observed in the previous chapter. In particular, in Chapter 1 I found that the scaling coefficient of one of three synergies extracted from each monkey (#2 in each case) was strongly correlated with object mass (Fig. 1-12a). Another synergy that I tentatively identified as underlying the reaching portion of the

trials (#1 in each case) appeared structurally consistent between monkeys (Fig. 1-9). The third synergy extracted from each monkey may have had a role in generating more proximal joint rotations.

Hence I expect that in comparison 1—with the same object set but a different movement direction—both the reach-related and object-related synergies (#1 and #2) will still be present, and the latter will still possess a strong correlation to object mass. Recall that the start button was located on the left of the tray, and hence the initial reach-to-grasp involved a rightward movement regardless of object location. The transportation component of each trial, in contrast, involved a different movement direction, and this may be reflected in a substitution of another synergy (for #3 above). In comparison 2—with the same rightward trials but a different object set with novel shapes (G0) or interposed sizes (G1)—I make the same predictions, except that I expect all synergies (including each monkey's synergy #3) to be preserved since the overall movement of the arm was similar. I expect particularly well-conserved synergies from monkey G1, given both that its novel objects spanned the same object dimensions as the familiar objects, and that the objects were introduced one-a-day into old dataset (displacing one familiar object each time). Given the lack of any systematic synergy scaling with object shape, I do not expect to see shape-specific synergies to be extracted from the trials performed by monkey G0 with novel cylindrical objects.

2.1.3 Trial-to-trial variability described by synergy modulation

The foregoing analyses involved trial-averaged datasets (Brochier et al., 2004) specially prepared to minimize non-systematic variability in the EMG data. To study the variation of synergistic recruitment with task parameters, and to demonstrate the predictive power of the synergy coefficients alone, I introduce in this chapter a discriminant analysis (Johnson & Wichern, 2002). This technique has been used previously in studies of human hand kinematics (Santello & Soechting, 1998; Santello, Flanders & Soechting, 1998) to discriminate between a large set of objects grasped by subjects while wearing kinematic gloves.

Here I demonstrate discriminability of behavioral conditions based on scaling and time coefficients associated with extracted EMG synergies. The result of the analysis can be presented as a $b \times b$ "confusion matrix" (Johnson & Phillips, 1981) of b behavioral conditions, defined here by objects and movement directions. Each element of the matrix represents the proportion of trials for which the given task condition (row) was successfully assigned to the target task condition (column) rather than another task condition. The assignment to a target task condition is made by a least squares fit in a linear discriminant space formed by a combination of the synergy scaling and timing coefficients (rather than within the original muscle space).

The overall probability of making a correct assignment according to the discriminant analysis above can be succinctly described by an information theoretic estimate of the "information" about behavioral conditions transmitted by the synergy coefficient dimensions (e.g. Hatsopoulos et al., 1998; see Shannon, 1948). This quantity is also known as "mutual information". Previous investigators (Santello & Soechting, 1998/2000) have converted this quantity into a "sensorimotor efficiency index" (SME) by taking the ratio of the information transmitted by kinematic or postural primitives with the maximum amount of information that could

theoretically be transmitted about behavioral conditions. (A related "visual-motor efficiency" statistic was calculated by Sakitt, 1980.) I describe the derivation of these quantities in the Methods, below.

2.2 METHODS

2.2.1 Subjects

As in Chapter 1.

2.2.2 Paradigm

Transportation task As in Chapter 1.
Objects As in Chapter 1.

Object sets As described in Chapter 1, each monkey experienced the same set of 24 objects (with the exception of two spheres unique to each monkey). However, this set was divided into two separate sets, the first containing either 11 (monkey G1) or 13 (G0) objects. Here I look at the similarity of the monkey's synergies derived from the first and second object sets. For monkey G0, this second set was presented pseudorandomly on four sessions spanning 8 days, and included all 13 cylinders (the prototypical cylinder plus *h01-h04*, *w02-w05*, and *a02-a05*). In contrast, with monkey G1 I tried to remove any confound of object presentation sequence and object shape. This monkey's second set thus included an interleaved subset of the object span defined by the first object set (e.g. spheres *s03*, *s05*, *s07* and cubes *c04*, *c06*; cf. Chapter 1 Methods). Three of the objects (*s03*, *a01*, and *h01*) were actually outside of this span, instead extending it towards the "small" end of the span. All these objects were presented over fourteen sessions spanning 21 days. Unlike the prior object presentations for both monkeys G0 and G1, the second set of monkey G1's objects was introduced one object per day, each time replacing one of the objects presented in the earlier dataset. My analysis only considers the novel objects handled during this period, not the accompanying familiar objects that were gradually being displaced by the novel objects. (During these latter days, monkey G1 also handled three additional objects not experienced by monkey G0, and not reported here.) Note that while only one day passed between the two object sets experienced by monkey G0, nine days passed between the two object presentation schemes described above for G1. Each monkey performed "leftward" and "rightward" trials in alternation, allowing me to study generalization of movement patterns between these two datasets without possible confounds of time.

2.2.3 Recording/Stimulation

Event markers As in Chapter 1.
Muscle set As in Chapter 1.
Muscle implantation As in Chapter 1.
Electrode construction As in Chapter 1.
EMG data collection As in Chapter 1.

2.2.4 Analysis

Trial alignment As in Chapter 1.
EMG data preprocessing As in Chapter 1.
Trial selection As in Chapter 1.

Data reconstruction As in Chapter 1.
Synergy extraction As in Chapter 1. For the discriminant analysis described below I also pooled together the first and second object sets and the leftward and rightward trials performed by each monkey, and did not average together the 40 trials in each behavioral condition (as I did in the other analyses of this chapter and Chapter 1). I was only able to extract up to three synergies (rather than eight) as further extractions from such a large dataset were too computationally demanding. I did repeat the three-synergy extraction extraction five times, however (as in previous analyses).

Synergy set selection As in Chapter 1.
Synergy comparison As in Chapter 1.

Sensorimotor efficiency For the 48 behavioral conditions (2 directions × 24 objects) the entropy of the behavioral variations was straightforward to calculate since the probability of any of these conditions (after selecting 40 trials per condition) was identical. In particular,

$$H(behavior) = -\sum_{b=1}^{B} p(b)\log_2\ p(b) = -\sum_{b=1}^{48}\left(\frac{1}{48}\right)\log_2\left(\frac{1}{48}\right) = \log_2(48) = 5.58$$

The entropy defined by all the possible combinations of synergy coefficients, *H(synergy)* was calculated in a similar fashion (although all these possible combinations were weighted by the frequency with which each actually occurred in reconstructing the data). A joint entropy *H(behavior,synergy)* was derived in the same manner, by taking the possible and observed combinations of behavioral states and synergy coefficients observed in the dataset. The "mutual information" between *H(behavior)* and *H(synergy)* is the degree to which one set of data (e.g. synergy coefficients) can be used to predict the other set of data (behavioral states), as measured by the informational "bits" that are shared. Its formulation was:

$$I(behavior, synergy) = H(behavior) + H(synergy) - H(behavior, synergy)$$

The sensorimotor efficiency was expressed as:

$$\text{SME} = \frac{I(behavior, synergy)}{H(behavior)}$$

This expression takes as denominator the entropy (or information content) contained within the variability of task conditions experienced by the monkey, and as numerator the information transmitted about these conditions by synergy scaling

and timing coefficients. As a baseline level for the SME, I simply randomized the behavioral conditions before calculating *I(behavior,synergy)* and computed the resulting SME. Over ten repetitions, the value for monkey G0 was 9 ± 1%, while that for G1 was 10 ± 1%. I thus take a value of 10% to be a minimal SME threshold.

2.3 RESULTS

2.3.1 Stability of behavior

Figure 2-1 summarizes for each monkey and tranportation direction the performance on each block of trials with both the first and second object sets, as measured by the fraction of trials that were rewarded. These plots demonstrate that, given the behavioral measures available, the behavior was generally stable over days of practice. Although there were reductions in performance (e.g. on G0's day 7 and G1's day 10), these were not associated with the introduction of the second set of objects on day 6 for each monkey. (Also, several days of monkey G1's recording were not included in the analysis due to EMG artifacts; see Chapter 1 Methods.) Hence this dataset was not ideally suited to address questions of motor learning or adaptation (cf. Chapter 4). The monkeys' overall accuracy levels were similar even though they differed both in their experimental history (see Chapter 1 Methods) and in their motivation (completing between 17 and 62 10-trial blocks a day in the case of monkey G0, or between 26 and 174 blocks in the case of G1).

The overall stability of performance is further evident in Figure 2-2, which depicts the duration of each of the reach and transport components among the rewarded trials of each monkey and target well location. (The nonsystematic variability that remained in the timing measures was one motivation for my subselection from among all trials in each object × movement direction condition those 40 whose reach and transport durations were both closest to the mean durations; see Chapter 1 Methods).

One additional feature apparent from the data in Figure 2-2 was an interaction between reach and transportation movement durations as a function of transportation direction. This trend is shown more clearly in Figure 2-3, which plots the distributions of each of these durations. These histograms reveal a complementarity of these durations between leftward and rightward trials. Even though the reach component necessarily varied with object placement (because the start button was on the left side of the tray while the object could be placed either on the left or on the right), an inverse modulation of the *transport* component is also visible. This sensitivity of transport duration is apparent even though the distance between the left and right wells was a constant 20 cm.

2.3.2 Generalization across object locations

The unexpected dependence of transport (as well as reach) duration on object location (Fig. 2-3) prompted the single-movement-direction analysis in Chapter 1, where I focused on synergy modulation with a richer set of behavioral conditions as defined by object size or shape. Further rationale for this initial restriction was the dependence of EMG activity on object placement (e.g. for monkey G1 in Fig. 2-4)—

even in the initial reach-to-grasp portion of the trials, which invariably required a rightward movement of the arm from the button towards the object on the tray. Here I consider how well synergy structures were nevertheless preserved across object locations. Figure 2-5 depicts monkey G0's synergies extracted from leftward as well as rightward transportation movements. Figure 2-6 does the same for G1. The r^2 curves shown in Figures 2-5c and 2-6c suggest that extraction of more than three synergies explains relatively little further variance in the EMG data for either the leftward or the rightward movements. Furthermore, the leftward transportation data are even better explained than the rightward data with three synergies—or only two synergies in the case of monkey G1.

For both monkeys (in particular G0), two of the three synergies were matched at above the 0.75 correlation threshold (Fig. 2-5ab and 2-6ab). For each monkey the synergy that was best-correlated across reach directions was the first of the three (#1), which was also the only synergy that was well-correlated between the two monkey's rightward-trial synergies (Fig. 1-9). Even in these well-matched synergies, however, there were differences evident at the level of individual muscles, for instance the second phase of activation ascribed to many muscles of G1's first synergy (Fig. 2-5ab), or the involvement of the deltoid in monkey G1 (Fig. 2-6ab).

Among the less well-matched synergies, the synergy that demonstrated a dependence in its amplitude coefficient with object mass among rightward trials (#2 of each set) also appeared to be present in monkey G0's leftward movements, with the same dependence on mass (Fig. 2-5d). In monkey G1's leftward movements, its mass-related synergy appeared to have been replaced by another synergy having a similar dependence on mass (Fig. 2-6d). For both monkeys, the mass-dependence of this synergy appears to have been modulated by reach direction, as shown by the slopes of the linear fits. For both monkeys, the relation to mass of the object-related synergy was accentuated for the leftward trials.

The remaining synergy (#3) did not appear to have been conserved between monkey G0's leftward and rightward datasets (Fig. 2-5ab), or was only marginally similar in monkey G1's extractions (Fig. 2-6ab). The amplitude coefficients associated with the novel synergy #3 had either an inverse (Fig. 2-5e) or no (Fig. 2-6e) relationship with the coefficients assigned to the first synergy, again suggesting no homology with the remaining synergy of the rightward-transport datasets.

2.3.3 Generalization to a second set of novel objects

In contrast to the foregoing results, there was a superior conservation of synergies when they were extracted from different object sets, either introduced all at once one day after the first object set (monkey G0) or one novel object per day beginning nine days after the first object set (G1). In terms of variance explained by the synergies, independent extraction of 2-8 synergies from each dataset revealed a consistent profile (Figs. 2-7c and 2-8c). In terms of synergy structure, Figures 2-7ab and 2-8ab reveal that two of monkey G0's synergies, and all three of G1's, had correlation scores above the baseline 0.75 level. Monkey G1's synergies, in particular, were all matched with correlation scores of 0.89 or above.

The exception in monkey G0's case had a near-threshold score; the novel synergy in the pair appeared to be distinguished principally by greater involvement of forearm flexors (Fig. 2-7ab; e.g. flexor carpi radialis). I considered the possibility that

three synergies were an insufficient number to retain both G0's original synergy #3 and its novel, cylinder-set-related synergy. Also, based on the r^2 explained curve in Figure 2-7c, four synergies appear to have considerably greater explanatory power in reconstructing the second dataset than do three synergies. However, after comparing the highest-r^2 extraction of three synergies from monkey G0's first dataset and four synergies from its second dataset, the three best matches (scored 0.94, 0.80, and 0.73) still contained only two reasonably well-matched synergy pairs (data not shown).

Although monkey G0's third, novel synergy may have been structurally unrelated to its prior third synergy (Fig. 2-7ab), its modulation in reconstructing the different object conditions was similar. In particular, this synergy's coefficients remained modestly, and negatively, correlated to those of the preserved reach-related synergy. This functional conservation was also evident between monkey G1's reach-related and third synergies (Fig. 2-8e), although (as before) the direction of the relationship was positive for this monkey. As for the object-related synergy, both in the familiar and the novel object sets its amplitude coefficient remained strongly, and positively, modulated with object mass (Figs. 2-7d, 2-8d).

2.3.4 Discriminability of object location and identity

Figures 2-9a and 2-10a depict the synergies that were extracted from each monkey's data when these data were pooled across objects and movement directions, and not averaged within each of the 48 resulting movement conditions. Despite the much greater quantity of data, these synergies were able to explain 56% and 50% of the variance in monkey G0 and G1's pooled datasets, respectively. (When three synergies were extracted from the same population of trials without these having first been averaged together, the variance explained was 66% and 68% respectively; not shown) For each monkey two of these synergies could be paired (with a similarity score between 0.76 and 0.94) to two of the monkeys' synergies presented in Chapter 1 and reprinted in Figures 2-5a and 2-6a. Recalling the pattern of similarities evident in comparisons of the separate leftward and rightward datasets, the matched synergies in G0's case were the first two shown in the plots, while the matched synergies in G1's case were the first and the third. The unmatched synergies again bore little structural similarity to each other (correlation scores of 0.64 and 0.57 for G0 and G1).

Figures 2-9b and 2-10b give the confusion matrices describing the correct assignment of object location and identity based only on knowledge of these synergies' coefficients. The clustering of assignments along the diagonal indicates that trials were frequently assigned a correct task condition (or a related one, as per the ordering of these conditions along the axes). For monkey G0, the set of just three amplitude and three timing coefficients could correctly predict the object location (with only two possibilities) on 86% of the trials, the object location and shape (10 possibilities) on 41% of trials, and the location, shape, and size (48 possibilities) on 26% of the trials. For monkey G1, the discriminability was superior. The coefficients could correctly predict the object location on 99% of the trials, the object location and shape on 51% of trials, and the location, shape, and size on 37% of the trials. Particularly in the case of monkey G0 (e.g. with the sphere and cube classificiation in Figure 2-9b), it may have been the case that objects at the extremes of each shape

class were classified better than those of intermediate mass. Summarizing these relations over all conditions, the relative degree of information contained in this small set of coefficients, as measured by the SME index (see Methods), was 42% for monkey G0 and 48% for monkey G1. For both monkeys these values well exceeded the 10% threshold defining coincidental mutual information between the coefficient and behavioral condition data.

2.4 DISCUSSION

2.4.1 Time-varying synergies and changes in temporal scaling of muscle activity

Despite the poor conservation of synergy structures found between monkeys in Chapter 1, some within-monkey generalization across behavioral conditions was evident in the comparisons presented in this chapter. Object location was the first variable presented as a test of generalization. The behavioral analysis of the rightward- and leftward-trial conditions revealed a surprising modulation of transport as well as reach durations as a function of object placement (Fig. 2-3). Given that the monkeys were each given a limited time to complete each of the reach and transport components, this complementarity may reflect the monkeys' compensation for the longer reach required on leftward trials (given that the start button was on the left and the object was on the right). However, for both monkeys (particularly G1) the movement durations were generally well under the 1-s limits, so the complementarity of reach and transport times cannot be said to have been explicitly enforced by the task design. It is possible that the complementarity was instead a carry-over from the monkeys' training, when their movements could be expected to have been slower.

Because both the reach and the transport components of each monkey's movements appeared to be scaled by object location (Fig. 2-3), this first test of generalization proved to be more challenging than I had expected. Indeed, I found structural or functional similarity in only two of each monkey's three extracted synergy structures across movement direction conditions (Figs. 2-5 and 2-6). Even the synergy I tentatively identified as being involved at or just before the time of object contact (i.e. between the reach and transport movements) appeared to be modulated by reach direction (Figs. 2-5d and 2-6d). Judging by the slopes of the linear fits in these figures, this object mass-related synergy was recruited even more strongly for heavier objects on leftward trials, perhaps associated with the monkeys' apparent strategy of accelerating their transportation times on leftward trials (Fig. 2-3).

Time-varying synergies such as the ones I extracted (d'Avella & Tresch, 2001; d'Avella et al., 2003) do not have the feature of capturing (within a single synergy) muscle coactivations that can scale in duration. Rather, each synergy reflects a pattern of muscle coordination that can only be scaled in amplitude across all muscles, or shifted to any point in time within the trial, in order to maximize reconstruction of the muscle data. EMG bursts that are prolonged in one dataset will be captured by novel synergies—as may have been the case with monkey G1's second synergy in Figure 2-6b. A future modification of the extraction algorithm may allow for a temporal scaling parameter as well as the two parameters currently fit to the synergies

(Andrea d'Avella, personal communication).

2.4.2 Time-varying synergies and changes in the relation between muscle phases

Another problem for the time-varying synergy model is that fixed, task-imposed temporal relationships between multiple phases of muscle activity will be captured by synergies extracted from the data but will transfer poorly to a second dataset in which this timing is systematically changed to define a new, fixed relationship between the muscle phases. Thus the second phase that was evident in monkey G0's third, leftward-set synergy (Fig. 2-5b) may have occurred at too great or variable a delay to be captured in the best-matched synergy in Figure 2-5a. This failing was arguably more a result of the paucity of object locations presented to the monkey rather than a limitation of the model (something I attempt to rectify in Chapter 4). Nevertheless, a second future modification to the time-varying synergy model that I am pursuing is to restrict muscle activation within each extracted synergy to a monophasic burst (still not necessarily synchronous between muscles). This will be accomplished by iteratively optimizing not only the synergy amplitude and timing coefficients but also three parameters describing a pseudo-Gaussian waveform of variable scaling, width, and temporal delay of each muscle. (The distribution of ascribed muscle activity would be "pseudo-Gaussian" because of the independent scaling and width parameters.) These latter parameters will be optimized by gradient descent, so that the algorithm would iteratively converge towards a minimum of residual EMG error within the space defined by the parameters. In order to capture complex, multiple-motion behaviors like the reach-to-grasp and transportation task studied here, the modified algorithm could also allow for multiple instances of each synergy (d'Avella & Bizzi, 2005).

This modification of the algorithm may also achieve a reduction in the number of fixed parameters assumed to give rise to the invariance of the synergy. Note that the time-varying synergy algorithm used in this thesis achieves reasonable data reconstruction with only a minimal number of free parameters. In particular, each synergy is composed of M = 18 muscles vs. T = 50 time points (20- or 10-ms bins), but only the amplitude and time delay parameters of S = 3 synergies are allowed to vary in reconstructions of the data. Hence a dimensionality of S(MT) (=2700) can be said to be coded within the nervous system. (Physiologically-speaking, these dimensions would undoubtedly be dependent. For instance, the activity of any one muscle within a time-varying synergy is highly related to its activity in the preceding timepoints.) Because of the large number of fixed parameters, time-varying synergies can hypothetically be recruited by only 2S (=6) free parameters—a dramatic reduction of control parameters relative to other data reduction techniques. Models of synchronous (or "time-static") synergies (of dimensionality SM) specify only a small fixed dimensionality SM (=54 in this example), but require a much larger free-parameter dimensionality ST (=150) even when reconstructing a single behavioral episode of T samples. (For an empirical comparison of time-varying and synchronous synergy extractions see d'Avella and Bizzi, 2005.) Although time is a "free" control parameter in the synchronous models, this may also imply a greater control demand on the central nervous system. My monophasic restriction, in contrast, assumes both a small, fixed set of intrinsic parameters (three pseudo-Gaussian parameters for each muscle and synergy; 3MS=162) as well as the few, freely-varied synergy amplitude

and scaling coefficients of the time-varying synergy model (2S=6).

2.4.3 Time-varying synergies and changes in the relation between muscle subsets

A final limitation of the synergy algorithm as applied to these data may have been that it was unable to describe non-parametric changes between muscle groupings (like muscle phases above) within the synergy. In particular, the structure of the synergies suggested some independent modulation of more proximal and more distal muscles. Consider the novel synergy found in monkey G0's cylinder-set data (Fig. 2-7b), in which the principal difference evident in comparison with the matched synergy from the first dataset (Fig. 2-7a) was the involvement of a group of forearm flexors. I speculate that the closure of the monkey's hand involved less individuation of the fingers for these cylindrical objects in comparison to the hand postures necessary to enclose cubes and spheres; hence the greater involvement of extrinsic flexors.

Similarly, the third synergy observed in monkey G1's performance on leftward trials (Fig. 2-6b) may have recruited a coactivation of forearm extensor and intrinsic muscles, along with the more proximal muscle involvement evident in the matched synergy in the rightward-trial dataset (Fig. 2-6a). Again, the paucity of movement directions given to the monkey may have led to only two predominant patterns of coordination between these muscle groupings, such that both leftward and rightward datasets were characterized by unique relationships between these groups.

Only when confounds of transportation direction and object shape were removed did the synergies derived from multiple datasets yield the same structures (Fig. 2-8ab). As I had predicted, synergy structures in this comparison were well conserved, given both that the objects were introduced one-a-day into old dataset (displacing one object from the familiar set each time), and that the novel objects experienced by the monkey spanned the same task dimensions as the familiar objects. Without this tight behavioral control, the time-varying synergy extraction algorithm may require that synergies be extracted separately from different possible combinations of muscles specified a priori according to known anatomical or functional relations between the muscles. (The mechanism to do so was introduced in the Methods of Chapter 1, where I described the extraction of single-muscle "synergies" derived by a restriction of each muscle's activity to one each of 18 synergies.)

2.4.4 Variability explained vs. behavioral discriminability

In terms of EMG variance explained by the synergies, both the rightward- and leftward-trial datasets were reasonably well-explained by a small set of synergies (Figs. 2-5c, 2-6c). That a greater fraction of EMG variability appeared to be explained in the leftward dataset (even by two synergies in the case of monkey G0) was an unexpected result. Neither monkey's performance on the leftward trials was more accurate than their performance on the rightward trials (Fig. 2-3). Hence the greater variance explained by three synergies in the leftward dataset (Figs. 2-5c and 2-6c) is not likely due to more stereotyped performance on the left-directed trials. The greater variance explained in the leftward dataset is also surprising given that these trials involved both a *rightward* reaching movement from the start button to the target followed by a *leftward* transportation movement. In the rightward dataset, in

contrast, both the reaching and transportation movements were directed in a rightward direction, and could presumably have involved a similar set of muscles.

The profiles of variance explained as a function of synergy number were more consistent when the synergies were extracted from trials performed in the same transport direction but with multiple object sets (Figs. 2-7c, 2-8c). Nevertheless, the overall level of variance explained in each of these comparisons (r^2 = 79-88%) may appear low considering that the trials within these datasets were averaged together within each object condition. Indeed, the variance explained was substantially lower (r^2 = 49-54%) when the 40 trials in each condition were not averaged, and when the two object sets and two movement directions were pooled together for each monkey prior to extraction of the three synergies (Fig. 2-9a, 2-10a). This is arguably still an impressive reduction in variability considering that these pooled datasets contained 160× the data of the previous analyses. But while one synergy in each extraction demonstrated a systematic relationship with object scale (Figs. 2-5d, 2-6d, 2-7d, 2-8d) the absence of further parametric relationships with object properties suggests that the residual EMG variance itself may not be reducible to explicit task dimensions.

This does not mean that the synergies are unable to give a compact description of the behavioral variables at play, however. Without regard to the systematic relationship of each synergy to task parameters, I found that the coefficients of just three synergies were able to convey a large degree of information about object properties including shape, size, and location (Figs. 2-9b, 2-10a). Indeed I observed an apparent dissociation between the variance-explained scores and SME indices between the monkeys: three synergies could account for more of the EMG variance for monkey G0 (56% vs. 49%) but for less of the behavioral variability it encountered (42% vs. 48%).

I was not able to extract more than three synergies from the pooled dataset due to computational resources. With greater resources or a different set of extraction parameters selected to reduce the volume of data, the SME index could be a useful, independent estimate of the number of dimensions underlying datasets such as these. This is particularly true because it takes into account the number of synergies used to convey information about the behavioral conditions, unlike the variance-explained metric. For this latter quantity, various curve-fitting methods, or model order estimates that make particular assumptions about the structure of the data, have been proposed but not widely accepted or systematically contrasted with the competing approaches (Tresch et al., 2005). Unlike variance-explained estimates, the SME index would not be expected to necessarily increase monotonically as a function of synergy but might rather peak at a certain number of synergies.

Figure 2-1 Stability of performance in the transportation task. Shown for all trials in the first and second datasets towards the left (**a** and **b**) and right (**c** and **d**) target well for monkey G0 (**a** and **c**) and G1 (**b** and **d**) are the monkey's performance on each block of trials, as measured by the fraction of trials in which the reach and transport components of the trial were within the set time limits. (As in the following figures those trials, blocks of trials, or entire days with sensor or EMG artifacts, in the case of monkeys G0 or G1 respectively, were removed from the dataset prior to this analysis; see Chapter 1 Methods.) Vertical lines represent divisions between days of recording; the thicker black line divides the first and second datasets of each monkey. Note that the first set comprised five days for both monkeys. Note that "blocks" are sets of ten consecutive trials performed with the same object, in any combination of leftward or rightwards trials as the monkey preferred. The blocks on the abscissa of this figure represented the variable numbers of leftward or rightward trials performed *within* these 10-trial blocks.

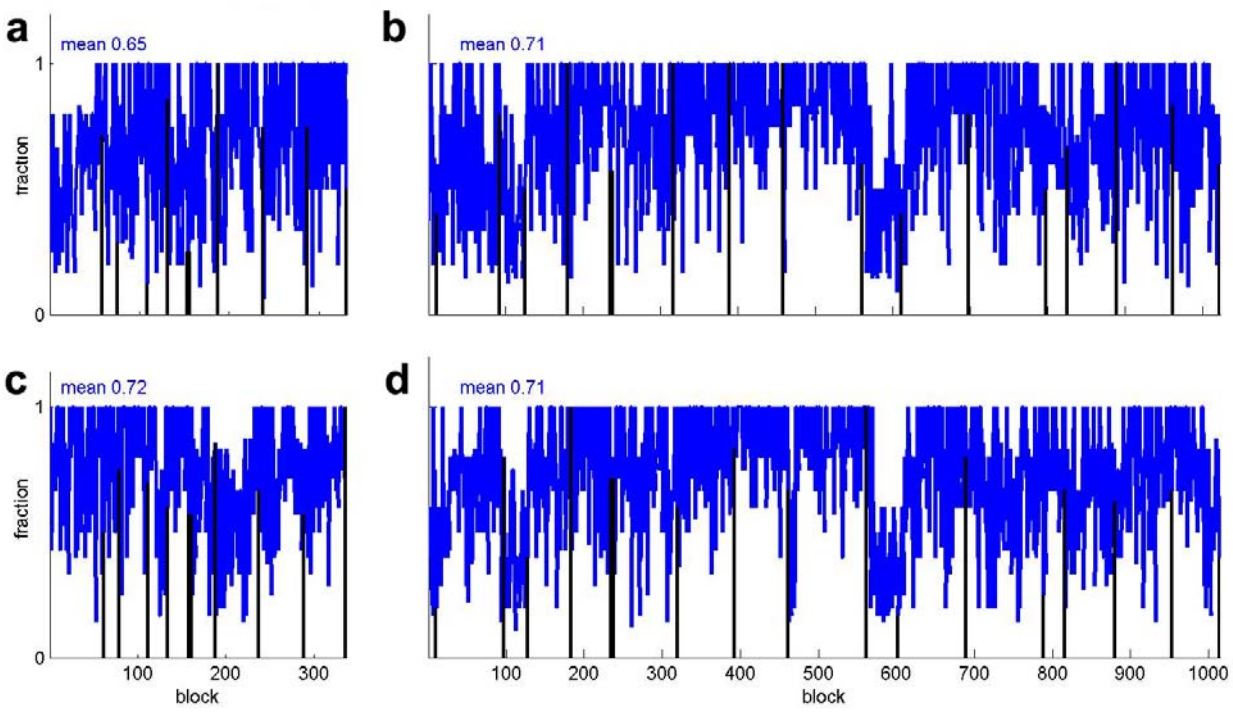

Figure 2-2 Stability of movement times in the transportation task. Shown for all rewarded trials towards the left (**a** and **b**) and right (**c** and **d**) target well for monkey G0 (**a** and **c**) and G1 (**b** and **d**) are the duration of each of the reach and transport components in each trial. Both sides of zero on the ordinate are positive. Mean ± S.D. times are displayed for each set of movements. Vertical day boundaries are displayed as in Figure 2-1.

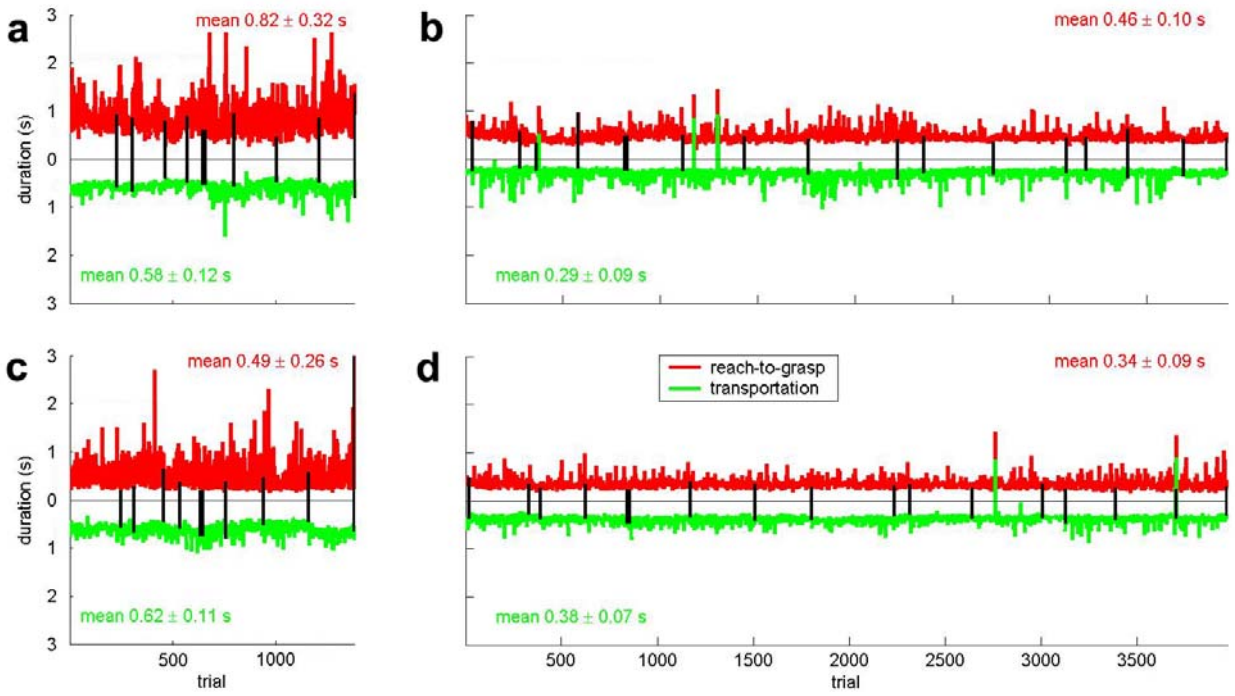

Figure 2-3 Distribution of movement times. Histograms of the reach and transport movement durations are shown for all rewarded trials towards the left (**a** and **b**) or right (**c** and **d**) target well for monkey G0 (**a** and **c**) and G1 (**b** and **d**). Superimposed over the histograms are Gaussian fits that include the mean ± 2 S.D. of the reach and transport times.

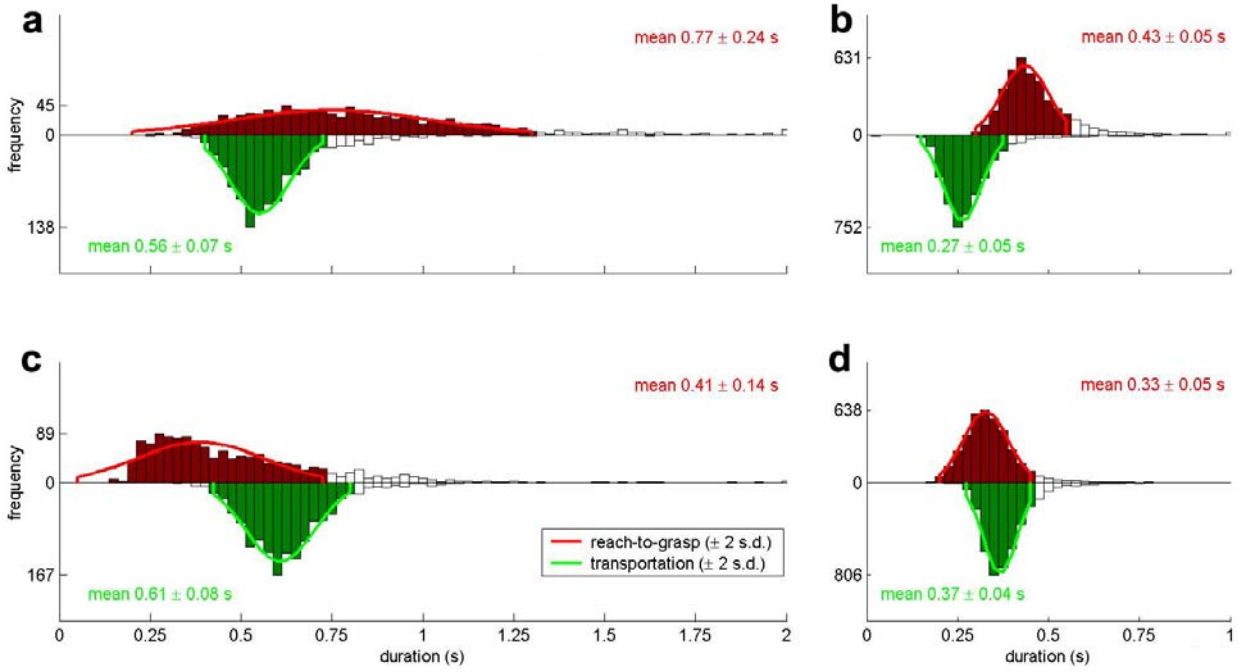

Figure 2-4 Event-aligned, averaged EMG in each direction of transport. For the purposes of this figure (but not subsequent analysis), the rectified but pre-filtered and pre-integrated EMG activity was averaged across all trials selected from the **a**) leftward and **b**) rightward transportation trials performed by monkey G1 with object the training sphere (*s08*). The event used to align the EMG prior to averaging was the time of object removal. EMG activity outside a -0.45/+0.3 s window around this alignment time was truncated. Each muscle's activity has been normalized to the same voltage level across the two directions, equal to the maximum level of averaged activity observed in the muscle in either of the directions. Each muscle's maximum activity relative to the maximum found across all muscles is represented by the scale bars at right. (*fl.*: flexor; *ext.*: extensor; *abd.*: abductor; *add.*: adductor; *opp.*: opponens; *digit.*: digitorum.)

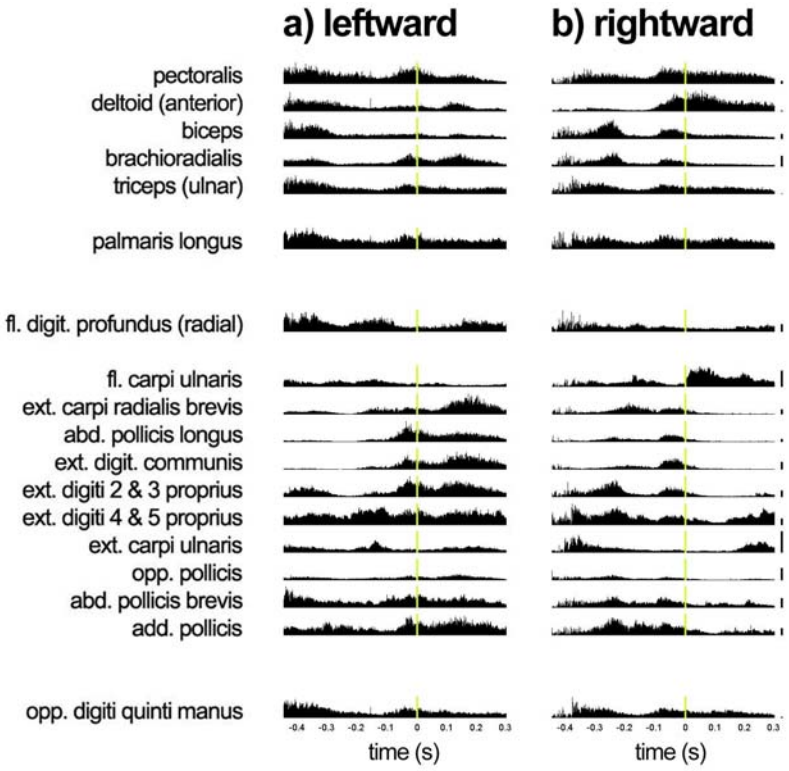

Figure 2-5 Synergies derived from G0's leftward and rightward performance. In **a**) are the three synergies extracted (as in Chapter 1) from data recorded during performance of the reach-to-grasp and transportation movements that brought the object from an origin well on the left of the workspace to a target well on the right. In **b**) are synergies extracted from the interposed trials in which the monkeys performed the same task with the same set of objects but brought the object from the right to the left well. As in the plots that follow, the correlation between these novel synergies, aligned according to the ordering of the best-matched synergies as shown in a), are given above each synergy. The r^2 curves in **c**), and the like in subsequent plots, depict the variance explained by five repetitions each extracting two to eight synergies from the rightward or leftward datasets, ±S.D. The plot in **d**) repeats for both movement directions the correlation between the scaling coefficient of the second synergy and the object masses handled by the monkey (as in Fig. 1-12a). The relationship between the remaining amplitude coefficients for both movement directions (cf. Fig. 1-12b) is given in **e**). (Note the "cleavage" evident in midway through the synergies in b is an extraction artifact related to the fixed time window allowed for each trial, the fixed temporal relationship of this window to the behavior, and the limited number and duration of the synergies used to span the behavior.)

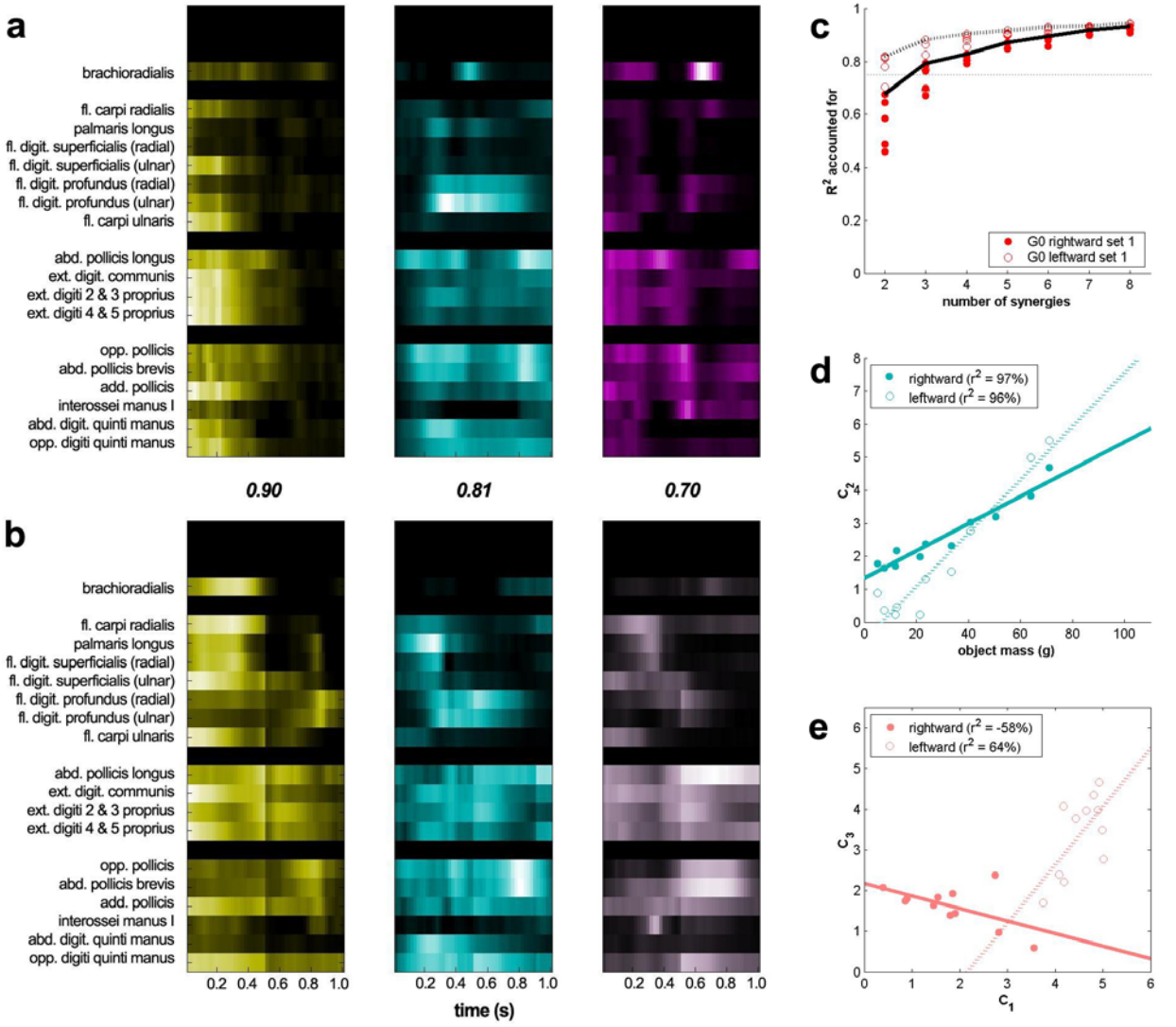

Figure 2-6 Synergies derived from G1's leftward and rightward performance. Panels were prepared as for Figure 2-5.

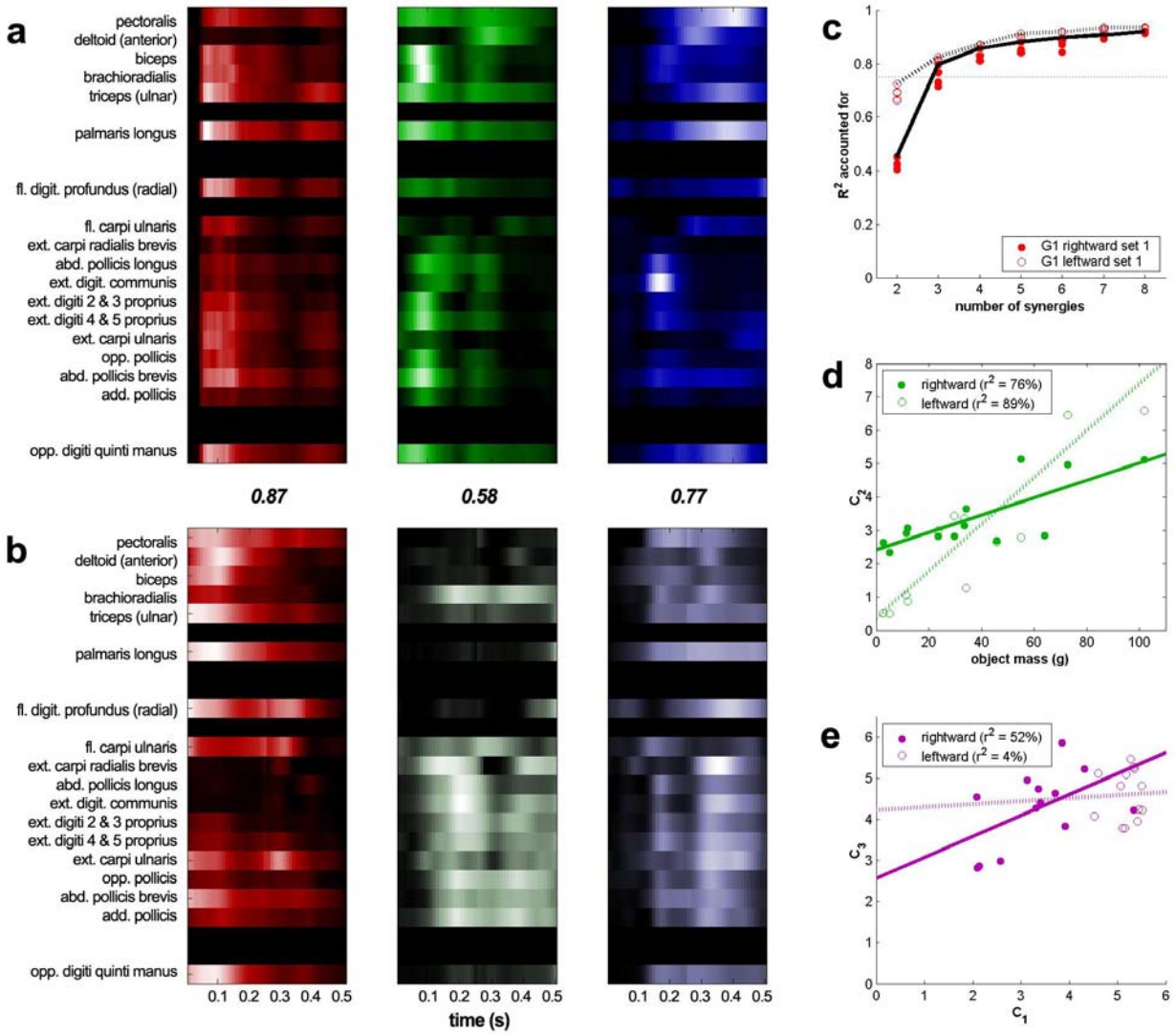

Figure 2-7 Synergies derived from a baseline and novel set of object shapes. Panel **a**) depicts the same baseline synergies from monkey G0 as shown in Figure 2-1a, extracted from EMG data describing the monkey's rightward transport of a set of 11 spheres and cubes of variable size (and mass). In **b**) are the corresponding synergies extracted from the monkey's later performance with a set of 13 cylinders of variable curvature, height, and width. Panels **c**), **d**), and **e**) are shown as in Fig. 2-5, but depict the results for G0's two object sets rather than its two initial object positions.

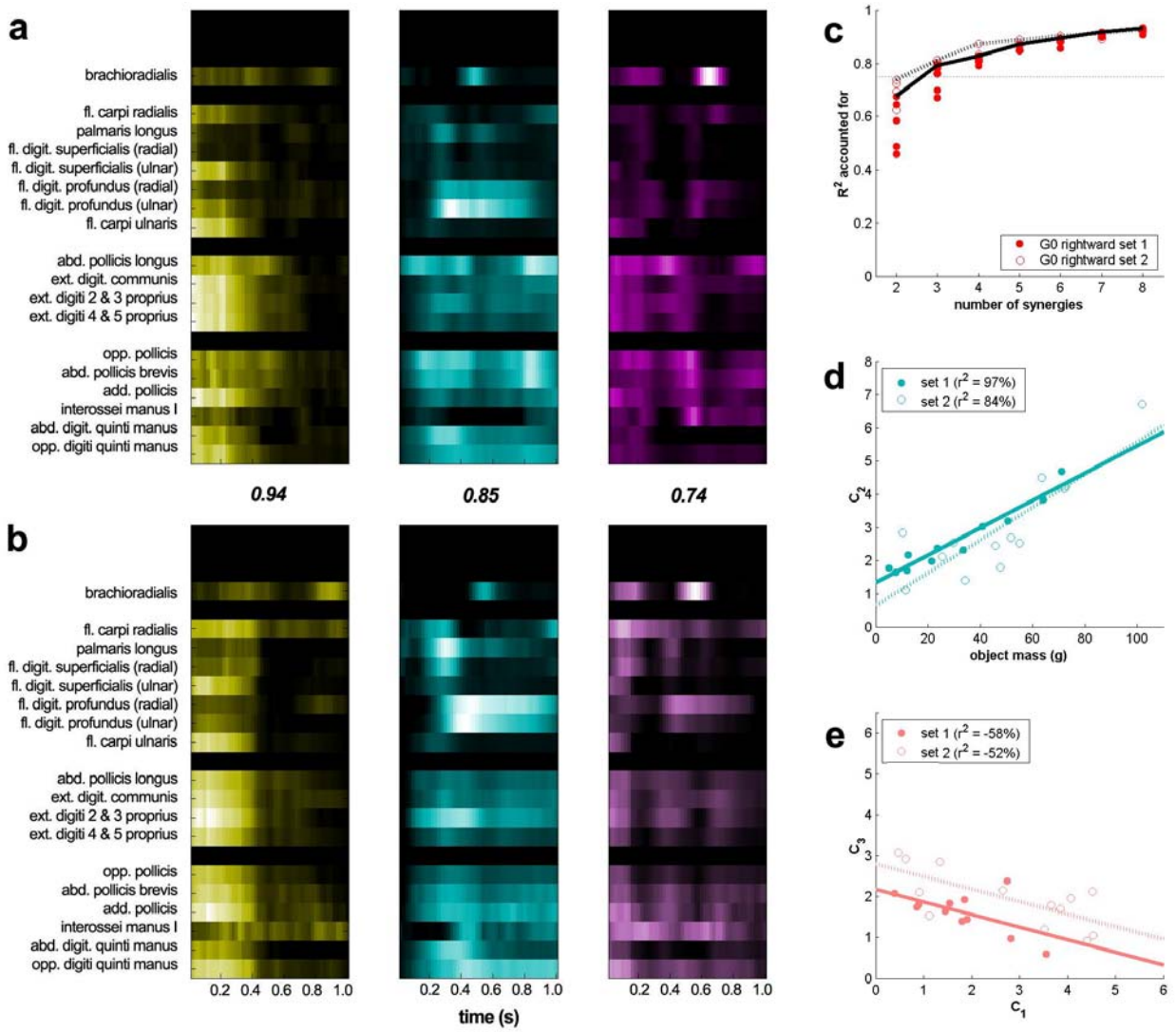

Figure 2-8 Synergies derived from a baseline and novel set of interposing object sizes. **a**) The three synergies extracted from the muscle activity of monkey G1 as shown in Figure 2-1a, extracted from EMG data describing the monkey's rightward transport of a set 13 spheres, cubes, and cylinders of variable curvature, height and width. The synergies extracted from a later dataset performed with 11 spheres, cubes, and cylinders interposed in size between the objects in its first set are shown in **b**). Panels **c**), **d**), and **e**) are shown as in Fig. 2-5, but depict the results for G1's two object sets rather than its two object positions.

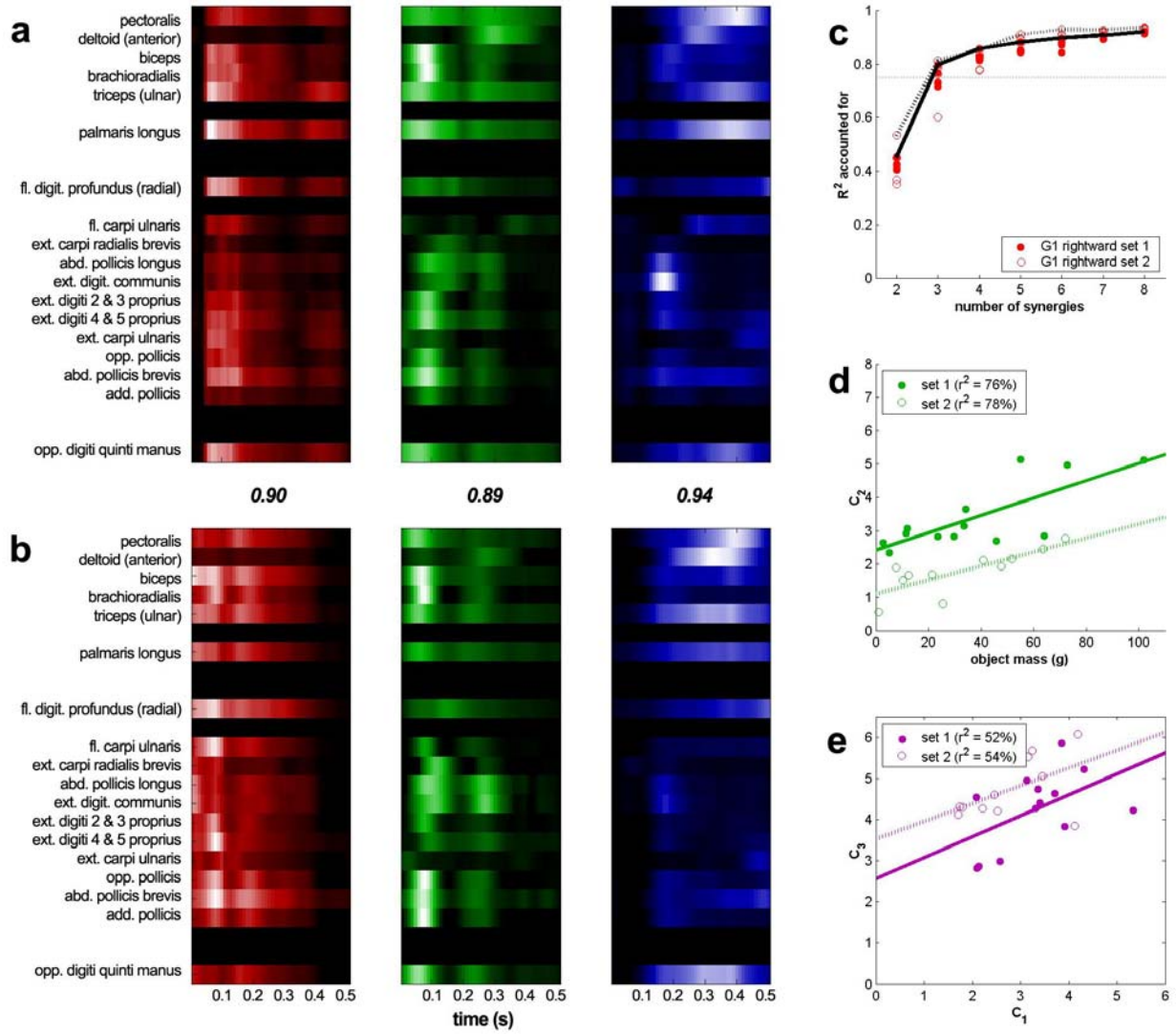

Figure 2-9 Discriminability of behavioral conditions by synergy coefficients of monkey G0. **a**) Confusion matrices for 48 task conditions (24 objects × 2 directions of movement) performed by monkey G0, using the three synergies derived from this pooled dataset, shown in **b**). Predicted and actual task conditions are represented by the matrix columns and rows, respectively. Horizontal and vertical black bars divide object classes. The objects within each of these classes were ordered in terms of increasing mass, as shown schematically by three example objects from each class beside the ordinate and the abscissa. The coefficients associated with each of three synergies extracted from these trials were computed for individual trials and used to predict which task condition was involved in given trials. The average number of condition "assignments" is represented by the color of each cell, as shown in the reference bar at right.

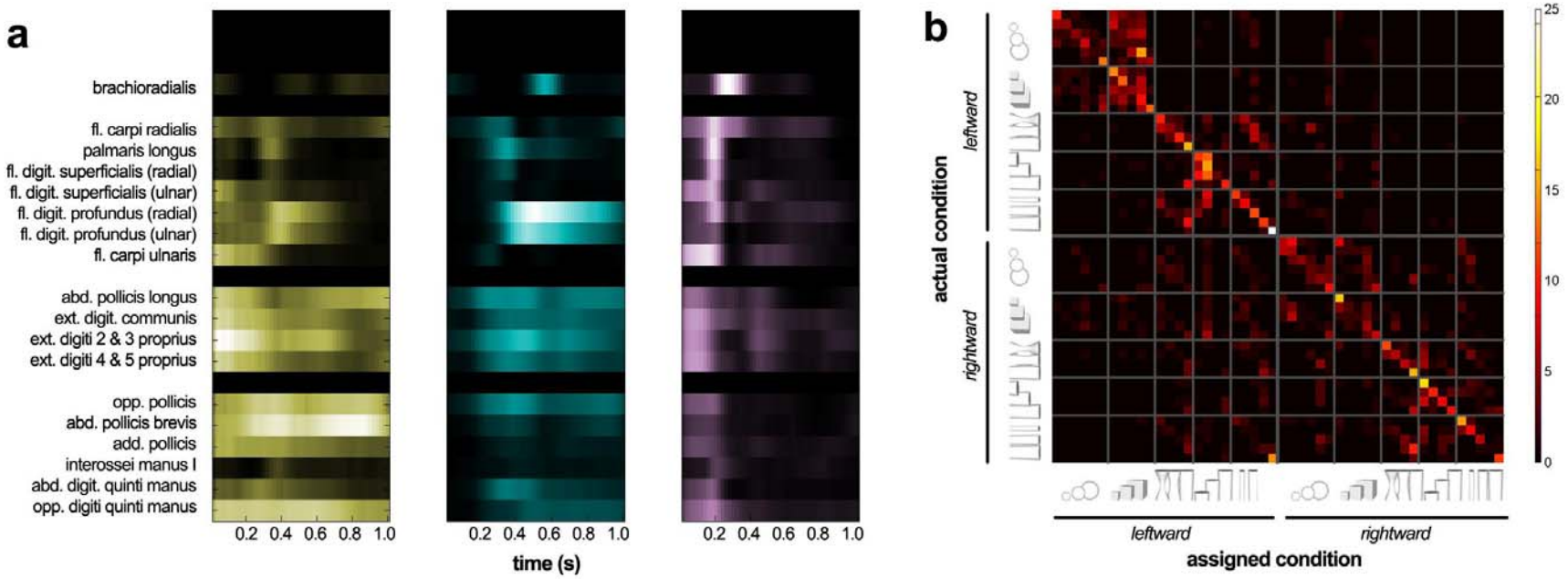

Figure 2-10 Discriminability of behavioral conditions by synergy coefficients of monkey G1. Panels are shown as for monkey G0 in Figure 2-9. (The correlation scores in **b**) give the relation of the synergy structures to those in Fig. 2-6a.)

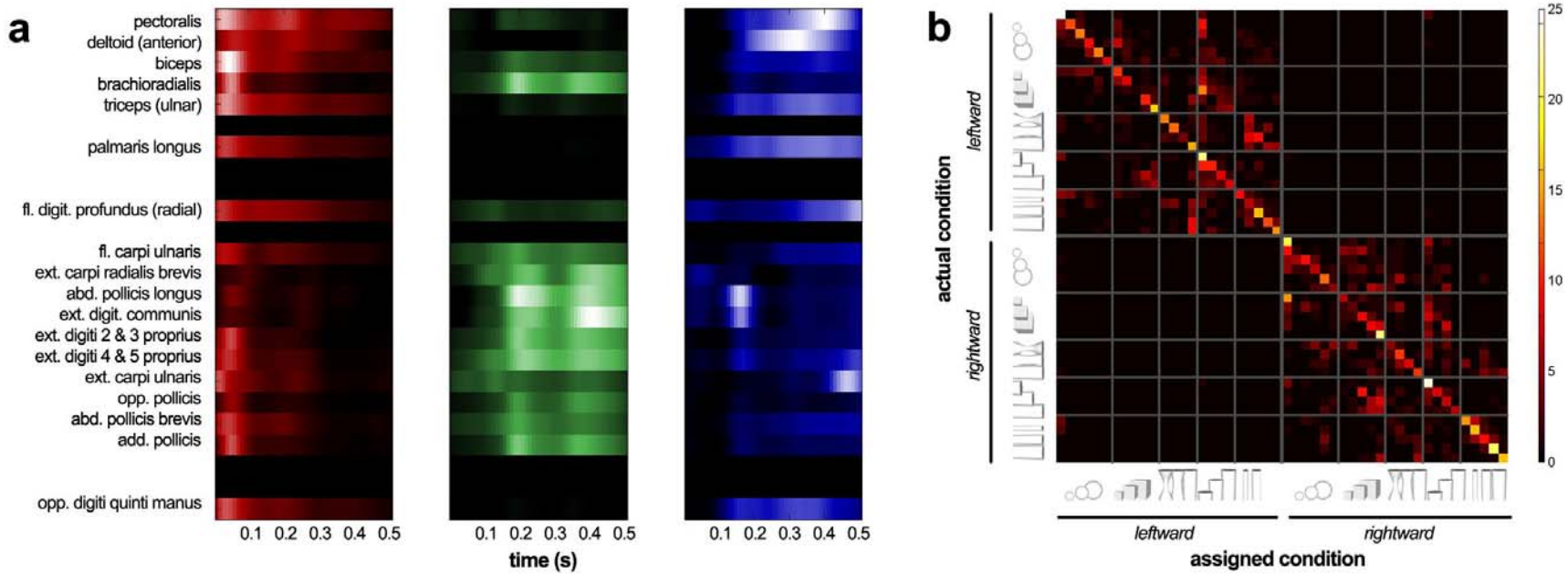

3 Muscle Synergies and Task-Specificity

To examine generalization of time-varying muscle synergies beyond a single behavior, I presented one monkey with three separate tasks involving the same object. The "transportation" task, as before, was designed to elicit a precision grip. A "force" task required the monkey to isometrically pull on the object with sustained and controlled force. A "sip" task was a spontaneous behavior wherein the monkey translocated the object to its mouth and manipulated it as necessary to direct a liquid-filled cavity on the object towards its mouth. In all three tasks I considered the EMG activity recorded from a set of 24 intramuscular electrodes chronically implanted in shoulder, arm and hand muscles. In all tasks, I restricted the analysis to a subset of 50 trials and a uniform time window around the time of object retrieval or isometric force application. Other spurious differences between the datasets were minimized in the task design. Nevertheless, a small number (three) of time-varying synergies extracted separately from each task revealed only a single common synergy describing a component of the common reaching portion of each movement. When I minimized this final, categorical confound by pooling together the EMG dataset from each task, I found that only four synergies appeared to be appropriate to capture the main variability in the EMG data. This choice was made not only on the basis of the error reconstruction curve, but also a consideration of the structural distinction between the four synergies (vs. increasing relatedness among other numbers of synergies extracted from the dataset). None of these four synergies appeared to be specific to one behavior. Rather each appeared to be recruited to a task-specific degree and with task-specific timing.

3.1 INTRODUCTION

3.1.1 Precision grips vs. power grasps

Primate hands are capable of more than grasping and holding objects. Iberall and MacKenzie (1990) characterize the "output" behavior of the hand with the following scheme. As an output device it either manipulates an object by imparting motion to it, or stably grasps the object by applying forces needed to keep it in place. Morphologically, the prehensile grasps a hand may apply include either a precision grip or a power grasp (Iberall & MacKenzie, 1990). *Precision grips* permit fine stabilization and sensory interaction with an object, and allow for small movements applied by the fingers. Such movements have been the focus of my analyses up to this point.

Power grasps, by contrast, are used when larger stabilizing forces are anticipated, and more contact with the hand surface is needed. With the ulnar-directed deviation associated with power grasps (Napier, 1956), motion may be forcefully imparted to an object through the arm and wrist (Iberall & MacKenzie, 1990). In the transportation task it is unlikely that power grasps were well-sampled. The most massive object presented to each monkey in the datasets I described in the previous chapter (cylinder *w06*) was 102 g. Among the objects in the variable-weight set to be described in this chapter in the context of adaptation, the most massive was still only 215 g. In order to stably hold these objects against gravity only 2 N were required.

Similarly modest levels of force output can be inferred from the task designs used by Brochier et al. (2004) and Mason et al. (2004) in their studies of primate grasping.

In this chapter I therefore introduce another task, the "force" task. For this behavior the monkey was required to apply to an object a sustained and controlled force exceeding 30 N and directed back along its arm. Early tests with this monkey demonstrated that this level of force application was well within its range: I found that the monkey could displace at least 4.5 kg of mass attached to a pulley in order to pull towards it a connected food reward. Nevertheless, the task required a greater length of time to train compared to the transportation task. (An earlier version of the task in which I tried to train the monkey to apply an upward force rather than one directed towards itself proved too difficult to train.) This task differed from the transportation task not only in the degree of force required, but also in being an isometric task. (Such behaviors are frequently studied because they avoid various biomechanical complexities such as muscle viscosity and inertial forces.)

3.1.2 Grasps vs. manipulatory behaviors

Grasping rather than manipulatory behavior was the focus of my previous investigations as both precision and power grasps can be more easily classified, both in terms of appearance and function. Cutkosky and Howe (1990) have proposed a preliminary hierarchy of grasp choice, based on detailed observation of the grasps chosen by human machinists. They suggest that grasp choices are made according to both object geometry and, following Napier (1956), task requirements. Even a simple task like opening a jar may involve different grasps as the torque requirements change (Napier, 1956). Their taxonomy thus includes more power grasps and precision grips, as well as side opposition postures, than have traditionally been considered based on object characteristics alone (e.g. Schlesinger, 1919). Still their taxonomy includes a finite number of fundamental grasps, with perhaps 100 rules needed to choose between them (Stansfield, 1988; Cutkosky, 1989).

While power and precision grasps are relatively easy to characterize, Klatzky et al. (1990) and Lederman and Klatzky (1996) do provide a further classification for manipulative and exploratory hand movements, as well as other non-prehensile postures in which the hand interacts with an object but the fingers do not close about it. Such behaviors have also been studied in nonhuman primates; for instance, Lawrence and Kuypers (1968) used a "Klüver board" containing wells from which monkeys could extract morsels of food using their index finger with help from the thumb. A similar setup was used in studies by Miller et al. (1993), Nudo et al. (1996), and McKiernan et al. (1998, 2000).

I have similarly recorded data during both monkeys' interaction with a Klüver board setup. But for this analysis I sampled from manipulatory behaviors in another, more controllable fashion, by having the monkey reach for an object and rotate it as required in order to extract a small volume of liquid contained inside. This task differs from both the transportation and the pulling behavior not only in the kinematics but in being an untrained behavior. As I discovered, the monkey was spontaneously able to recognize (and extract) the intrinsic reward value of these liquid-loaded objects.

All of these tasks were presented to the monkey over the course of several days of recording. Only one object—the canonical sphere—was used. In an additional

analysis, I thus tested whether EMG recorded during reach-to-grasp and transport with only this one object decomposed into the same muscle synergies as did a dataset recorded with a larger variety of objects. A positive set of matches was expected given the conservation of two out of three synergies between monkey G0's EMG data from different object shape sets, as described in Chapter 2. Next, in extracting synergies separately from each behavior, I predicted that the categorical differences between these tasks would lead to few if any matches in the extracted synergies. But when pooling the data together from the three behaviors, I expected that invariant muscle patterns common to the three behaviors would emerge.

3.2 METHODS

3.2.1 Subjects

The data in this chapter were all collected from monkey G1 (see Chapter 1). Additional EMG data from a reduced set of intramuscular electrodes were collected during performance of the force tasks by monkey G0 but these are not considered here.

3.2.2 Paradigm

Transportation task As described in Chapter 1, in this task the monkey was trained using its left hand: 1) to press a start button located to the left of its workspace; then 2) within 1 s to reach for and remove a clearly visible object in one of two conical wells fixed on a tray; and finally 3) to release it in the opposing tray location (where it had to remain stably for at least 0.1 s, and not bounce out) following either a "leftward" or a "rightward" transport of 1 s or less.

Sip task This task was an untrained extension of the transportation task, involving the same steps 1) and 2) as in that task, followed by the monkey's retrieval of liquid reward (~0.3 ml) placed within the object. I used a syringe to load the object with liquid prior to presenting it to the monkey on each trial, via the same small orifice through which the monkey was able to extract the liquid by the capillary action of its tongue. (No additional reward was given via a liquid dispensation spout, as in the transportation and force tasks.) The orifice on the object was small enough that the liquid remained inside due to surface tension even as object was turned around. I generally placed the object in the origin well with the orifice facing upwards, although this did not noticeably limit the monkey's tendency to rotate the object several times in order to direct the orifice towards its mouth. This manipulatory behavior was evident after the monkey had brought the object towards its face, and often involved unrestricted bimanual motions. The liquid contents of the object were typically removed over the course of several seconds while the monkey held the object (generally with the right hand). When the liquid was extracted the monkey would return the object to one of the wells on the tray (typically the left well, closest to the start button). As in the transportation task, the initial object location (on the right or left of the tray) was varied between trials, although in the sip task this variation was imposed by the experimenter. As in both of the other behaviors, the

monkey had full vision of its hand and the object during the task (Fig. 3-1). Not shown in the figure are the EMG cranial connector or the cortical recording chamber through which I recorded motor cortical activity, not presented here, in this and the other tasks.

Force task In this task, the monkey was trained: 1) to press the start button; then 2) within 1 s to grasp the object mounted on a horizontally-oriented, six-axis force-torque transducer (ATI Industrial Automation) on the monkey's left (Fig. 3-2a), and apply at least +30 N of force in the "critical" direction of the transducer/object axis (i.e. along the monkey's left arm towards the left of its torso) while applying less than ±3 N of force in the orthogonal ("extraneous") directions and less than 1 N·m of torque in any angular direction; and finally 3) to hold the object within this force/torque target window for 1 s. The force/torque data were collected via a dedicated acquisition board at 36 Hz. Training was accomplished by gradually narrowing the "cone" of allowable force and torque values around the transducer/object axis. The placement of the transducer was chosen to closely match the placement of the object in the left well in the move and sip tasks. (There was still a vertical difference of 4 cm between the position of the center of the training object in the transportation/sip and force tasks. The difference in the vertical placement of other objects in the transportation/sip tasks varied with object shape and size since these objects rested at the base of the origin well.) As in the transportation and sip tasks, the trial requirements were imposed by a software controller written in LabVIEW (National Instruments).

Objects The densities of the objects described in Chapter 1 were constant at 1.4 g/cm^3, and no attempt was made to equalize the mass of the objects within this set—hence mass was a confounding variable with object size and shape. To study the relation of synergistic activation with object mass, another 15 hollow objects were created that were restricted to three basic shapes (spheres *x01-x05*, cubes *y01-y05*, and cylinders *z01-z05*). In order to minimize the confound of object size, the objects were closely matched on approximate horizontal hand aperture needed to fully grasp the object (spheres 3.7 cm, cubes 3.6 cm, and cylinders 3.8 cm). Within this set I varied the mass systematically by filling each with a different balance of brass ball bearings and Styrofoam, distributed as evenly as possible within the object to maintain a fixed center of mass. I consider in the analysis both the synergies derived from the entire set and those derived from the data of sphere *x02*, which had nearly the same mass as the training sphere (31 vs 34 g). (The cylinder was of the same shape and size as the protypical cylinder used in the experiments of Chapters 1 and 2.) The three tasks involved another copy of the training sphere *s08* that had been bored and tapped so that it could be mounted on a force-torque transducer (for the force task) or could be filled with a small quantity (~0.3 ml) of liquid reward (for the sip task).

Object sets With the variable-weight and variable-mass object sets, the objects were introduced in pseudorandom 10-trial blocks as in Chapter 1, and the monkey could alternate between leftward and rightward transportation at will. The variable-weight object set was each presented over four consecutive days (i.e. with no breaks longer than a day between recordings). On the first day when the weight dataset was

introduced, I allowed the monkey to first practice on ten, 10-trial blocks with the training sphere, and on 40 blocks with a restricted set of three of the shapes that was already familiar to the monkey. The monkey performed between 32 and 166 blocks on each day of this paradigm. In the sip and force tasks the monkey was only exposed to a single object (*s08*, the training object), and this object was only presented to the monkey on its left side. It was not feasible to pseudorandomly interleave the three tasks given that the force task required a unique experimental assembly (Fig. 3-2a). The variable-behavior datasets spanned two, three-day periods separated by six days. The first period included a day of transportation-task recordings, followed by two days of sip-task recordings. The second period included only force-task recordings. The number of complete 10-trial blocks performed in each of the three tasks was 100 (transportation), 87 (sip), or 79 (force).

3.2.3 Recording/Stimulation

Event markers As in Chapter 1, except that no pressure sensors were used and photosensors were only used to track the removal or deposit of the objects in the transportation and sip tasks. In the sip task the end of the trial (analogous to the target well contact event in the transportation task) was an experimenter-logged time identifying when the monkey had begun retrieving the liquid contents of the object (and was generally lowering its freed left hand back towards the start button). This was by no means a precisely-defined time. In the force task, I derived behavioral events on-line from the three force and three torque dimensions recorded by the force/torque transducer. (See Figure 3-2b for an example.) Off-line, I interpolated these analog samples to 2 kHz (the same sampling rate as the EMG signals). From these signals I defined event times analogous to the object contact, removal, target well arrival, and settling that I defined in the transportation task (see Chapter 1 Methods). The "contact" time was the time at which the monkey first exceeded a +3-N threshold on the critical force direction. The "removal" time analogue was the first time at which the critical force channel exceeded +30 N and the extraneous force and torque channels registered under ±3 N and ±1 N·m, respectively, prior to the longest continuous period during the trial in which these conditions continued to be met. Similarly, the force-task analogue of the "arrival" time was the point in the trial when the continuous satisfaction of these conditions had ended, and the "settling" time was the last time in the trial when the critical force channel exceeded a +3 N threshold.

Muscle set As in Chapter 1. The additional six muscle implants available in each of the recordings of this chapter were listed previously in Table 1-1. The variable-behavior data were collected between 2.5 and 3 months after the surgeries. Inspection of the impedance within electrodes, and the cross-correlation between them, revealed that all were still recording independent, physiological signals. The sole exception was a relatively high level of cross-talk observed on four of the channels on two of the days during recording of the force task (the last dataset in this chapter to be recorded). I have therefore restricted my trial selection in the force task to those trials recorded on the remaining, less-affected day.

Muscle implantation As in Chapter 1.

Electrode construction As in Chapter 1.
EMG data collection As in Chapter 1.

3.2.4 Analysis

Trial alignment Because the average duration of the post-retrieval behavior in the sip task was considerably longer and more variable than in the transportation task (see Fig. 3-3), I have elected to restrict this analysis only to a fixed length of time near the beginning of each trial, generally prior to the sipping per se. In the force task, the monkey's motions were more stereotyped but the average duration of the pulling movement per se was still considerably longer than the object translocation time in the transportation task. For direct comparison of EMG patterns in all three behaviors I simply focused on the monkey's EMG data surrounding the time of object contact by applying the same -0.45/+0.3 s window around the time of object removal (as in Chapters 1-2). In the sip task, this restriction also helped to remove the effect of the monkey's relatively variable behavior *before* the time of object contact. As I discovered on the first day of recording, the monkey was so eager to complete the sip trials that after clearing the liquid out of the object it would return the object to the tray and—before I had time to retrieve and refill it—would begin pressing the start button without pause until the object had been refilled. (I corrected for this artifact in the experimental control on the second day of recording on the sip task, and do not consider data from the first day in this analysis.)

EMG data preprocessing Parameters were set as in Chapter 1. As in the final analysis of Chapter 2, I did not average the EMG data between trials in each behavioral condition, but instead concatenated these trials and performed EMG analysis simultaneously over all trials in each dataset.

Trial selection As in earlier analyses, I focused only on rewarded trials. I did not have to exclude trials based on EMG or sensor artifacts (except for the two days of force task recording referred to above under "Muscle set," the first day of sip task recording described under "Trial alignment," above, and several blocks on the final day of the weight set, which had to be excluded because of an acquisition hardware error). In the transportation and sip tasks I only considered those trials where the object was initially placed in the left well on the tray. (In the force task the object was always mounted on the left.) In the transportation task, I selected the 50 trials whose reach-to-grasp and transportation times were both closest to the *means* of their Gaussian-fit distributions (as in Chapters 1 and 2; see Fig. 3-3b). In order to minimize differences in reach-to-grasp and secondary movement latencies between each of the three behaviors behaviors, the 50 trials I selected in sip and force tasks were those with reach-to-grasp and movement times both closest to the *minima* in each of the distributions (Fig. 3-3ac).

Data reconstruction As in Chapter 1.
Synergy extraction As in Chapter 1.

Synergy set selection Because of the greater number of muscles (and of trials) in these datasets I calculated a new baseline level of variance explained by single-muscle

time-varying "synergies." I used a similar procedure as in Chapter 1, by extracting 24 single-muscle "synergies" from the dataset and then calculating the amount of EMG variance explained by these synergies. Given computational resources available, it was not possible to perform this extraction on the entire set of 150 trials (50 trials × 3 tasks) selected in the multiple-task dataset. Instead I separately extracted the single-muscle synergies from each of the three behaviors. Note that this procedure actually generated a considerably more conservative significance threshold than used in Chapters 1 and 2, since I technically allowed the entire 150-trial dataset to be fit by *three* single-muscle controllers, each specific to one task. Over a single repetition of each extraction, the reconstruction fidelity in these extractions averaged out to 63%. Given the conservative nature of this baseline, I therefore consider the threshold r^2 to be 65% in order claim that "significantly" more variance is explained by the multiple-muscle synergies than independently-scaled and -timed muscle bases.

Synergy comparison As in Chapter 1. Because of the differences in number and identify of the muscles in this analysis relative to those of the previous chapters, I empirically determined a new baseline criterion for determining whether two synergy structures were correlated. I repeated this procedure described in Chapter 1 ten times for each behavior and synergy, and in doing so found an average "auto"-correlation of 0.77 ± 0.02. I thus consider 0.80 (or greater) to be a minimal threshold for deeming cross-correlations between different synergies "significant."

3.3 RESULTS

3.3.1 Differences between the behaviors in timing and muscle recruitment

The three tasks presented to the monkey differed in a number of respects, including the degree of training required before recording, isometric vs. per-movement force application. Both of these features may have been reflected in a difference between these tasks in accuracy, i.e. the fraction of trials in each 10-trial block that were successfully completed. This crude measure of performance demonstrated that the (rightward) transportation trials were completed 78% of the time, while only 63% of the force trials were likewise recorded. (In the sip task, the performance could not be summarized in an analogous fashion, given that the sole condition for success was effectively the ability of the monkey to retrieve the object within 1 s following button press.)

Two additional and better quantifiable differences that have particular bearing on the analyses here were the latencies of the movements and the muscular involvement in each behavior. Figure 3-3 demonstrates that each task was characterized by a unique distribution of reach-to-grasp and secondary movement times. Based on the design of each task (see Methods) it was possible to identify several analogous points in time within each behavior, including the button press and release, object contact, and object displacement—or critical force application, in the case of the force task. Using this lattermost time to divide each of the trials in the dataset, Figure 3-3 nevertheless demonstrates that the duration of not only the secondary behavior following this displacement but also the prior reach plus grasp phase was systematically different depending on the task. Even after this subselection, the

average reach-to-grasp durations (± S.D.) were 0.33 ± 0.01 s (transportation), 0.47 ± 0.05 s (sip), and 0.64 ± 0.07 s (force). The average secondary behaviors lasted 0.30 ± 0.01 s, 1.6 ± 0.2 s, and 1.3 ± 0.1 s, respectively. (Note that in the force task the monkey pulled on the object on average for longer than the required 1 s, perhaps related to the small delay in reward administration following each successful trial.)

In terms of the recruitment of individual muscles, there was also a clear division of the three behaviors, even in a restricted window around the time of initial object contact. As shown in Figure 3-4, there were differences in the involvement, amplitude, and timing of various muscles. (Note that I have normalized each muscle to its maximal activity in any of the behaviors; such normalization across monkeys was not possible for the muscle sets in Figure 1-7. Such normalization makes it easier to compare the behaviors in terms of the relative modulation of activity in each muscle across tasks.) The sip task, for instance, involved a strong activation in the adductor pollicis following object retrieval, while at this point in the transportation trials there was a coactivation of the extensors digiti quarti and quinti proprius. Both the transportation and force tasks appeared to involve strong coactivation of the pectoralis and anterior deltoid, but the timing of these in relation to the alignment time differed, Although the monkey's arm was applying a great deal more force to the object in the force task, it was not evident that the maximal EMG activity in this task was higher than in the other behaviors. (I will consider the relationship of EMG activity and force application in Chapter 6.) The force task was instead characterized by relatively tonic activation, particularly in extrinsic muscles of the forearm.

3.3.2 Similarities in the muscle synergies underlying the behaviors

Before extracting synergies from the multiple-task dataset, I first considered whether the same synergies captured in earlier chapters could emerge in this analysis given that only one object was used. In particular, one of the synergies observed in previous analyses appeared to be strongly related in its recruitment to object weight. Prior to the multiple-task recordings, I therefore collected a set of data while the monkey performed the reach-to-grasp and transport behavior with a set of objects varying systematically in weight (but not size) among three prototypical shapes (see Methods), including the sphere used in training and included in the recordings in the multiple-task dataset. I then simply extracted synergies from both this entire dataset and from those trials performed with the training sphere. This analysis revealed that the same synergies were matched between the single-object and pooled datasets—all with a correlation score of 0.94.

As in Chapter 2, I then proceeded to extract synergies from the multiple-task in two ways: separately from each task condition and then from all conditions pooled. Given that the behavior was stereotyped within each task (particularly in the force task, where there was not only a single object but also a single placement of the object), I expected that any synergies I extracted separately from each task would be highly dissimilar. Indeed, I found that three synergies extracted from each behavior (selected without respect to the reconstruction r^2 curve, for the moment) possessed only one common primitive, as computed by their scalar product (Fig. 3-5). The same synergy was robustly identified in each of the prior analyses (as reproduced in Figure 3-5), and appeared to characterize the reaching portion of those trials—the one overtly common movement in these three tasks.

When the data from the three tasks were pooled together, I focused on four synergies rather than three. I made this decision in part based on the shape of the r^2 curve (Fig. 3-6a). Four synergies were also the minimal number needed to meet the r^2 = 65% threshold derived in the Methods. As an additional consideration, I computed the degree of muscle-by-muscle cross-correlation of the synergies *within* each extraction (e.g. between the four synergies extracted in the four-synergy repetition explaining the greatest degree of variance). Averaging over these relations, I found that the synergies within a set were most distinct when four synergies were extracted (Fig. 3-6b). Schematic examples of these relations are shown in Figure 3-6c.

The four synergies so selected are depicted in Figure 3-7. Each is quite distinct as suggested by the inter-synergy correlation scores of Figure 3-6. However, they do not appear to each be specific to a single behavior. As demonstrated by sample trial reconstructions in Figure 3-8, what differentiates the behaviors may be more the relative involvement and timing of each of the synergies. Over all trials, Figure 3-9 depicts the clustering of the behaviors within the four-dimensional space of the synergy coefficients.

3.4 DISCUSSION

3.4.1 Common muscle synergies emerge when confounds are controlled for

I observed a commonality between these behaviors of only one of three synergies (Fig. 3-5). This was not a trivial result given the clear differences in typical EMG records in these tasks (Fig. 3-4), even during the early phases of the trial described by this reach-related synergy. Nevertheless, the correlations were modest, and differences in muscle involvement were evident. In particular, both the transportation (Fig. 3-5ab) and sip (Fig. 3-5c) synergies appear to have involved a second phase of muscle activity, particularly in forearm extensor muscles. This phase is absent in the more tonic patterns present in the force synergy. In much the same way, I demonstrated in Chapter 2 how non-parametric variation of movement direction or object shape could confound the generalization of muscle synergies between behavioral conditions. The generalization of muscle synergies over a behavioral dimension (e.g. object size) may only be evident with parametric variation of the variable, ideally presented in a balanced and interleaved fashion so as to remove confounds of time or over-representation of any one condition.

In this experiment it was not sensible to parametrically modulate the task, nor was it experimentally feasible to interleave the force task with the remaining behaviors. However, I was able to pool together the data from the three tasks with minimal concern about confounding differences between these datasets. The recording sessions spanned only ten days, making systematic changes in electrode recording quality a less serious concern than in the data of previous chapters. I selected trials only from a single day with each behavior, and in any case its performance was sufficiently trained (transportation and force tasks) or spontaneous (sip) that I did not consider possible learning-related trends in the data. The object shape and size did not vary and so were not confounds. In the transportation and sip tasks, the monkey did perform trials with two initial object placements (as in Chapter 2), but I have removed this confound in this analysis by considering only

the left-side object placement corresponding to that in the remaining two tasks. The monkey performed a comparable number of 10-trial blocks (79-100) in each paradigm, and in any case I have selected an equal number of trials to represent each task.

With the confounds above controlled for and the data pooled together, I again extracted a number of time-varying synergies from the data. In doing so it was therefore possible to estimate the number of muscle synergies underlying the dataset, and to compare them directly in terms of recruitment (rather than structure). The overall level of variance explained by a small number of synergies (Fig. 3-6) is comparable to that reported in Chapter 2 when I similarly did not average the trials in each behavioral condition. Four synergies appeared to be an appropriate number to compactly describe the behavior, given both the profile of the reconstruction error curve and the degree of relatedness between the synergies (Fig. 3-6).

The finding that only four synergies appeared to be appropriate to capture substantial EMG variability in all three datasets (Fig. 3-6) alone suggests that the behaviors were united by a common set of only a few synergies. Recall that separate extractions from the three datasets each seemed to imply one common synergy and two unique synergies each—a total of at least seven synergies (and likely more if I had extracted and compared four synergies from each behavior). Functionally, Figures 3-8 and 3-9 suggest that the behaviors were distinguished by their relative involvement of the same set of synergies, but no synergy was exclusively used in any one task. Unfortunately the "relative involvement" associated with each behavior is difficult to visualize in a comprehensive fashion. Figure 3-9 only shows correlations between the amplitude coefficients, for instance, without considering timing differences evident in reconstruction of each behavior's EMG data (Fig. 3-8). In the next chapter I will briefly introduce a novel method for representing this high-order clustering in coefficient space.

3.4.2 Common muscle synergies do not reflect stereotopy in each behavior

One concern with this analysis is that it was restricted to a limited time window around the time of object contact, and thus failed to capture the full range of motions within each task. Indeed, I was concerned with temporally similar patterns of EMG activity in the three tasks because I restricted myself to using the same time-varying synergy algorithm on each of these behaviors. In the sip task, the cumulative unpredictability and duration of the post-object-removal behavior might have been better captured by a modification to the algorithm allowing multiple instances of each synergy (d'Avella & Bizzi, 2005). For the force task, the relatively tonic muscle activations (at least on average: compare Fig. 3-4c vs. Fig. 3-8c) might have been better captured by a modification of the algorithm allowing extraction of both time-varying and synchronous synergies (d'Avella & Lacquaniti, 2004).

But although the time window I selected should have been favorable to similar muscle patterns between tasks, Figure 3-4 reveals that this was not necessarily the case. The temporal placement of this window was designed in order to capture the preshaping and grasping behaviors of the transportation task, the ramping of force application in the force task, and the initial manipulatory movements in the sip task. In each case any synergy strictly related to the hand's grasp of the object should have been evident. The duration of the restriction was also chosen carefully, in order to

capture the majority of selected trials in each task (including the shortest, transportation trials). The selection of these trials (in particular in the force and sip tasks, where I chose those trials with minimal reach and secondary behavior durations) was likewise designed to increase similarity in the trial latencies in the dataset. Although these trials were not as "representative" as those selected from the transportation task (where the selected trials had reach and transport durations closest to the mean of each distribution), they were nevertheless still drawn from the unimodal distributions of trial movement times (Fig. 3-3). Finally, my truncation of EMG data outside of the -0.45/+0.30 s should have enforced (and not just selected for) some degree of analogy between the behaviors.

Of this analysis it may also be objected that the three behaviors were each so stereotyped that it was indefensible on those grounds to have extracted more than three synergies from the pooled dataset. In particular, given that the monkey was only exposed to a single object in each case (and the analysis was only restricted to a single object starting location), the actual space of hand postures and movements available to the monkey may have been poorly sampled (e.g. relative to the previous two chapters). One counter-argument is that each behavior (particularly the sip and transportation tasks) clearly involved more than a single motion and phase of muscle activity (Fig. 3-3).

But to address this concern more directly, I briefly introduced an earlier dataset recorded from the same monkey with the same muscle set but a wider variety of objects, each transported between tray locations. I pointed out that with the only confound between the single-object and pooled-object datasets being the relative representation of object weights, three synergies derived from each of these datasets could be easily matched. Thus I consider the synergies I extracted from the transportation behavior (at least) in the multiple-task dataset to be representative of the synergies present when the monkey interacted with a wide array of object shapes and weights. The high level of correspondence between the single- and multiple-object synergies may indicate not only the absence of confounds between these datasets, but also the fact that the monkey had considerably more experience with the single (training) object examined separately, and was only learning appropriate muscle recruitment for the remaining objects (as will be discussed in the next section). Incidentally, this result also suggests that time-varying synergies emerge from a high-level controller's optimization of muscles in order to satisfy particular task exigencies (Roy et al., 2002; Todorov, 2004). Instead it may be that—with confounding variables removed—similar motor primitives are recruited both for stereotyped behavior and the same behavior in a novel, more diverse environment of objects.

3.4.3 Motor adaptation in the context of manual behaviors

The results of these first three chapters indicated a moderate degree of generalization of muscle synergies between tasks and task dimensions including transport direction and object shape, even despite the passage of time. However, this generalization may have been compromised by the time-varying synergy model's inability (at present) to capture non-parametric changes in the involvement of muscle subsets or in the relative timing and duration of muscle phases within the synergies. Also, in the case of the synergies derived from two datasets separated by time,

temporal degradation of the electrodes (particularly in the case of monkey G0)—or behavioral adaptations made by the monkey—may have led to differentiation of the extracted synergies even when the underlying task was the same. In this chapter I therefore consider an additional and more critical experimental variable: the course not only of time but of adaptation.

In addition to the many musculoskeletal degrees of freedom, animals are required to compensate for changing external conditions. I suggest that muscle synergies may also facilitate motor learning, insofar as this learning involves coordinated changes in muscle activation across—rather than strictly within—muscles. Unfortunately, neither monkey's dataset from these chapters lent itself well to investigations of motor learning. Consider Figure 2-8. Do the changes in synergy structure (Fig. 2-8a vs. 2-8b), and the lateral shift of the second synergy's amplitude dependence on weight (Fig. 2-8d), reflect non-systematic measurement noise? Systematic increases in the noise of some electrodes? Variability in the extraction process due to randomized initial conditions? Adaptations made by the monkey? Both monkeys (particularly G0) had previously been exposed to several of the objects prior to the dataset introduced in those chapters. Several of monkey G1's days of recording (including the first three days with the first object set) were furthermore excluded from the analysis due to EMG artifacts. Moreover, the datasets in the first three chapters generally did not involve consecutive days of recording. My inspection of these and other datasets suggested that EMG patterns could demonstrate gradual adaptation over consecutive days but that interruptions of practice (e.g. on weekends when the monkeys received ad lib) were associated with dramatic reversals of these adaptations.

In this chapter, I introduced a variable-weight dataset to investigate how the monkey compensated for unpredictable mass when transporting otherwise identical objects. Although I do not analyze the EMG data for learning-related trends here, I include Figure 3-10 in order to demonstrate that behavioral trends can be crudely captured with this paradigm. As in other manual tasks (in particular the serial reaction time tasks discussed in Chapter 9), motor skill is often characterized in terms of progressive decreases in reaction time (cf. Smith, 1981). Figure 3-10 captures this same pattern using an expanded definition of "reaction time" that includes not only the reach duration but also the time the monkey spent grasping and removing each object, over four consecutive days. In addition to the differences in performance according to object weight (with heavier objects simply taking longer to remove), it also appeared that there was a systematic decrease in the reach and grasp duration. The decrease in this time may reflect the monkey's incentive to learn, since the limiting factor it its rate of reward was effectively its own movement times. The increase in times on day 2 may be associated with an initial increase in "generativity" in the monkey's motor performance, as has been documented in the domain of birdsong adaptation (Tchernichovski et al, 1999). I have previously observed this same profile to describe the variability in the coefficients associated with time-varying synergies extracted from this behavior (not shown here).

This task, too, was not ideally-suited for addressing motor learning, for several of reasons. First, the learning measure was not kinematically precise. I had kinematic *control* (in the form of different object shapes and weights designed to elicit different hand postures) but not *characterization*. In a separate project (not reported here) I have been developing a novel piezoresistive flex sensor glove for the monkey hand, in combination with a wrist-mounted 6-axis electromagnetic position sensor, in order

to address this deficiency in further recordings. A similar combination of angular and position sensors has been used in human kinematic studies (e.g. Santello & Soechting, 1998; Santello et al., 1998), and is advantageous over videographic systems (e.g. Mason et al., 2001; Roy et al., 2002) in efficiently capturing movements in three dimensions (without concerns of sensor occlusion). A second problem with this task was that the monkey's adaptation to the variable object weights was not likely driven by a feedforward strategy—at least not on the first trial of each 10-trial block, when the monkey would not have been able to predict the object weight. The "size-weight illusion" operating for human subjects (Flanagan & Beltzner, 2000) also suggested that the monkey's expectation of object mass may have been inaccurate even after having had several trials with an object.

Finally, the primate hand is perhaps the least favorable system for seeking motor primitives underlying motor learning—and indeed motor control. Although independent finger movements do involve the contraction of multiple muscles (Schieber, 1995), the greatly enhanced fractionation of muscle activity in primates (Bennett & Lemon, 1996) is known to support relatively independent movement of the fingers. Most notably, the increased mobility of the thumb, along with its anatomical evolution, afford apes and Old World monkeys (including the macaques studied here) opposability (Iberall & MacKenzie, 1990). And beyond the extensive sensorimotor cortex area devoted to the hand (see Chapters 11-12), anatomical and electrophysiological studies in monkeys suggest that the motor cortex sends monosynaptic projections to the distant forelimb motoneurons (Lemon, 1993). Because of all these concerns, I restrict my analysis of motor learning to a task with superior (if restricted) kinematic characterization: the manipulandum reaching task, introduced in the next chapter.

Figure 3-1 The sip task. **a**) The monkey (G1) was able to see the object and its hand during reach-to-grasp and removal of the object. Re-orientation of the object in order to position the orifice of the object (not shown) to face the monkey's mouth could be performed at any time between grasp and sip, and could involve both hands. During the sip per se, the monkey generally continued to hold the object with a single hand while using its tongue to remove the object's liquid contents. (The Plexiglas barriers shown were designed to keep sensitive equipment out of reach and to maintain a consistent posture.)

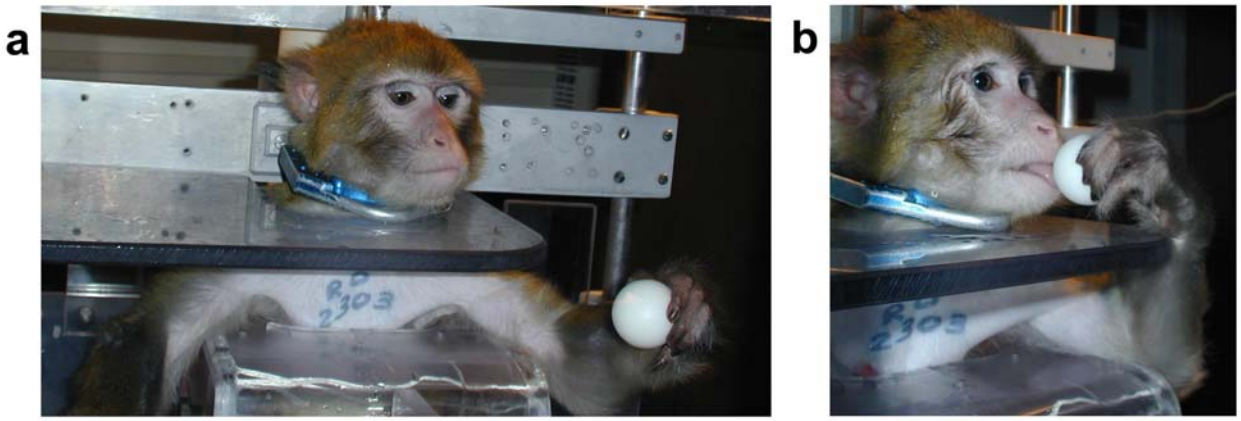

Figure 3-2 The force task. **a**) The apparatus surrounding the monkey allows the object mounted on the shaft of a force/torque transducer to be pulled isometrically strongly and backwards towards the monkey's left side. The red start button (common to all three tasks) is visible at the left of the workspace. **b**) Sample transducer records from a successful trial demonstrate the monkey's controlled force application and my selection of relevant event times. The horizontal lines define the minimum threshold of 30 N required on the critical (F_z) channel and the maximum limits (3 N or 1 N·m) allowed on the extraneous force and torque channels. The times at which the critical force crossed either two force threshold are given by the vertical lines. The second of these times was taken to be analogous to the object removal time in the transportation and sip tasks.

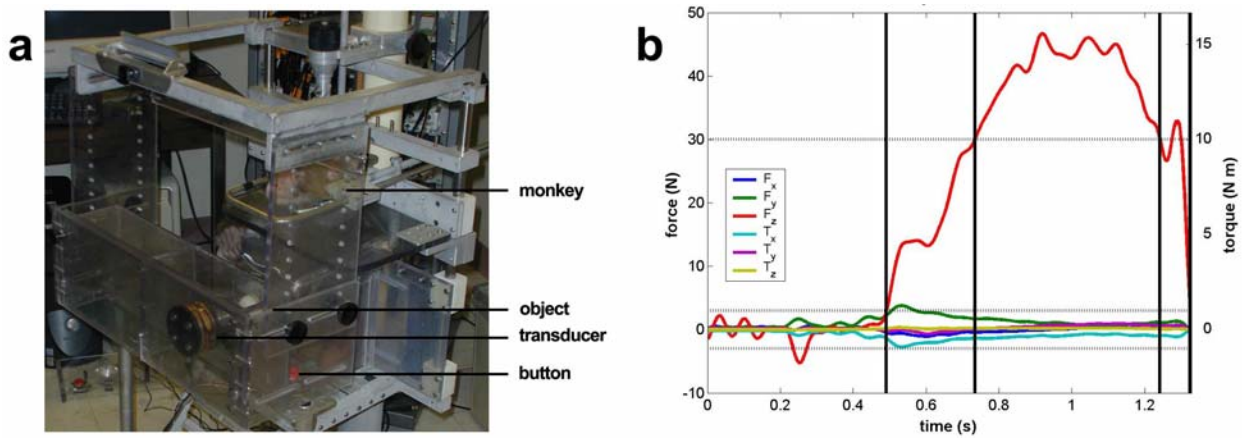

Figure 3-3 Distribution of movement times in each behavior. Histograms of the reach and transport movement durations are shown for all rewarded trials (with the object placed to the left of the tray) on each day representing the **a**) sip, **b**) transportation, and **c**) force tasks. Superimposed over the histograms are Gaussian fits that include the mean ± 2 S.D. of the reach and transport times.

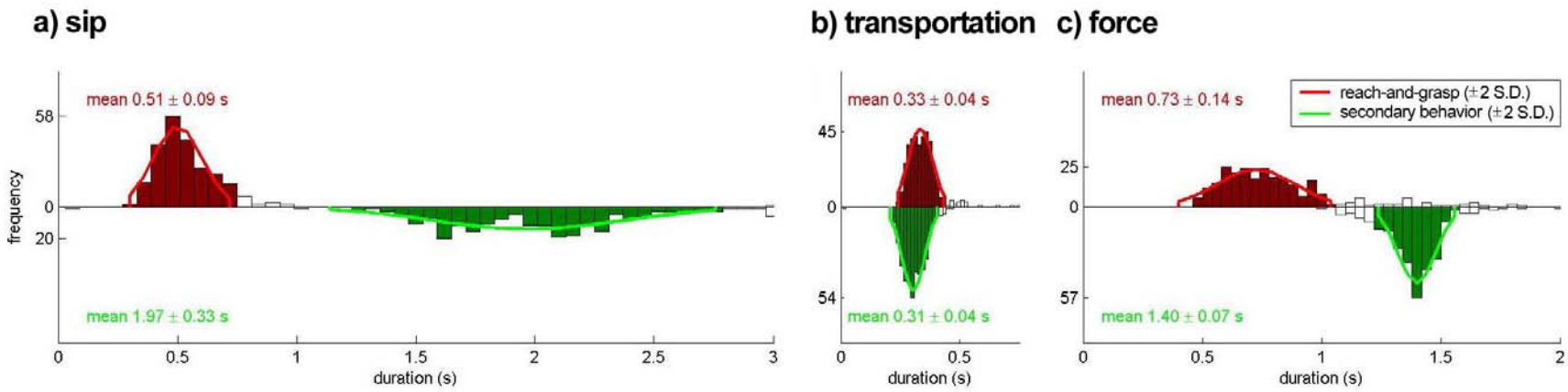

Figure 3-4 Event-aligned, averaged EMG in each behavior. For the purposes of this figure (but not subsequent analysis), the rectified but pre-filtered and pre-integrated EMG activity was averaged across all trials selected in the **a**) sip, **b**) transportation, and **c**) force tasks. The event used to align the EMG prior to averaging was the time of object removal (a and b) or critical force application (c). EMG activity outside a -0.45/+0.3 s window around this alignment time was truncated. (In the case of the transportation task, the reach-to-grasp movements were all shorter than 0.45 s and hence only the latter part of this interval is plotted.) As in Fig. 2-4, each muscle's activity has been normalized to the same voltage level across all three behaviors, equal to the maximum level of averaged activity observed in the muscle in any of the behaviors. Each muscle's maximum activity relative to the maximum found across all muscles is represented by the scale bars at right. (*fl.*: flexor; *ext.*: extensor; *abd.*: abductor; *add.*: adductor; *opp.*: opponens; *digit.*: digitorum.)

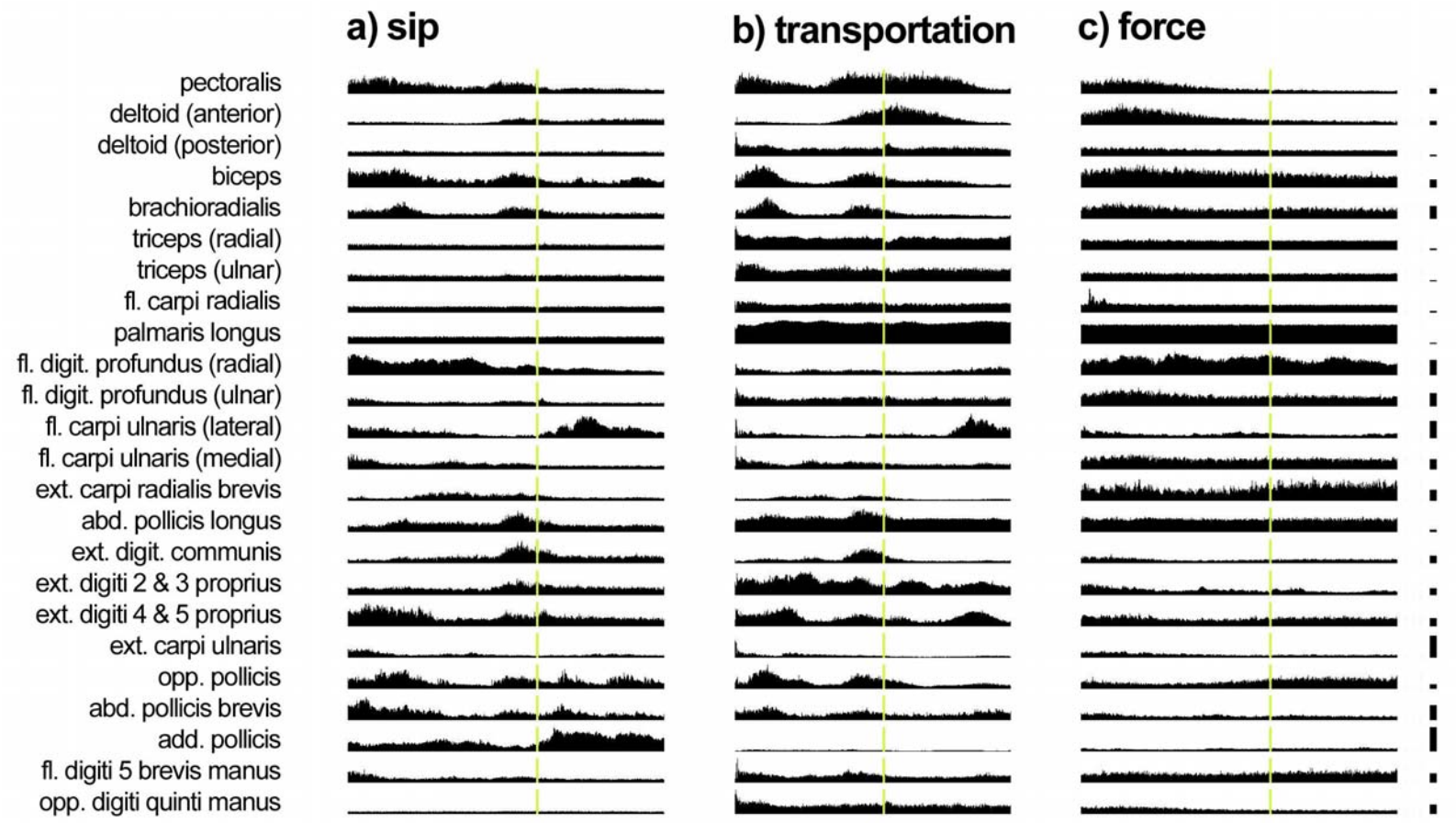

Figure 3-5 Similarity between synergies extracted separately from separate tasks. The only synergy to demonstrate a significant correlation when extracted separately from monkey G1's recorded **b**) transportation, **c**) sip, and **d**) pulling behaviors is plotted here along with its muscle-by-muscle scalar product score. Each of these behaviors is represented by a set of trials in which the object identity and placement were constant. In **a**) is the matched synergy extracted from G1's pooled movement direction and object dataset presented at the end of Chapter 2 (Fig. 2-10a). (Muscles lost from the dataset by these recordings are masked by white.)

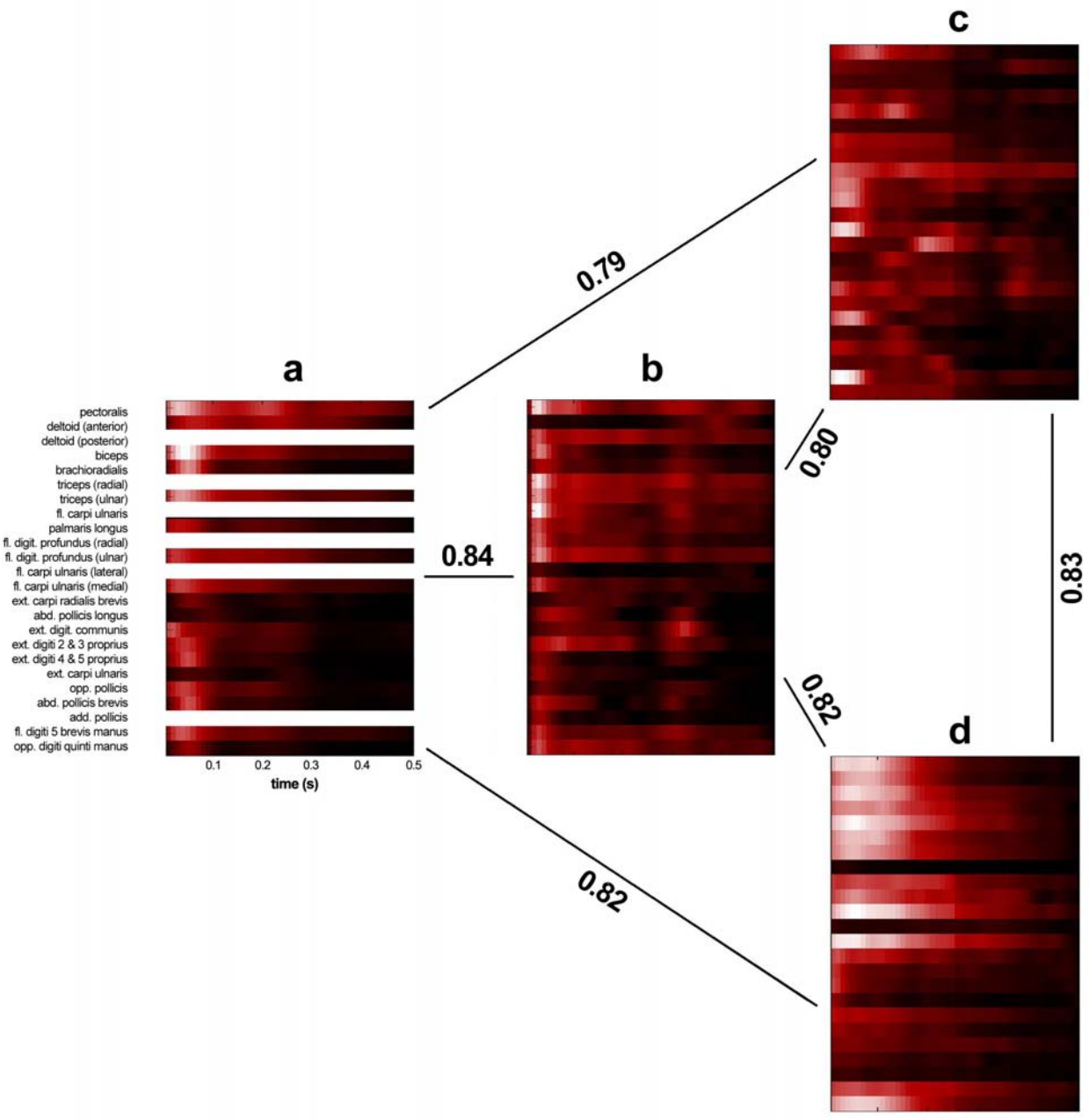

Figure 3-6 Selection of four synergies in the multiple-task dataset. **a**) Visual inspection of the reconstruction error curve suggests that four synergies were associated with the "last" sizeable increase in variance explained. **b**) The correlations among synergies within a set also revealed that beyond four synergies, the synergy structures extracted were on average more similar to each other. **c**) The relations between synergies that were averaged together in panel b), coded both by width and by color of the lines between synergies (as coded in the reference bar at top right). The nodes represent each synergy among sets of 2, 3…8 extracted.

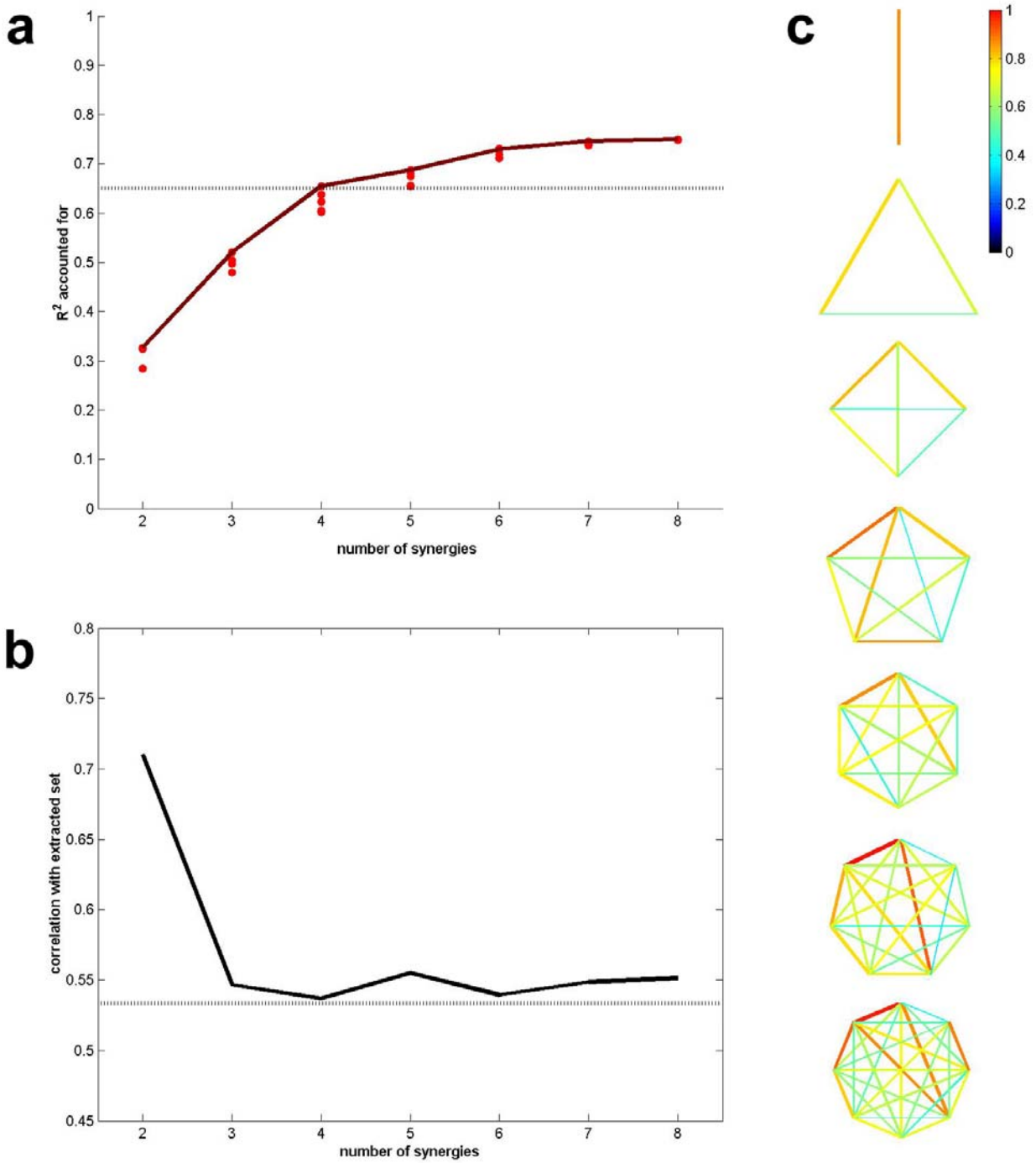

Figure 3-7 Synergies derived from the pooled set of three behaviors performed by monkey G1.

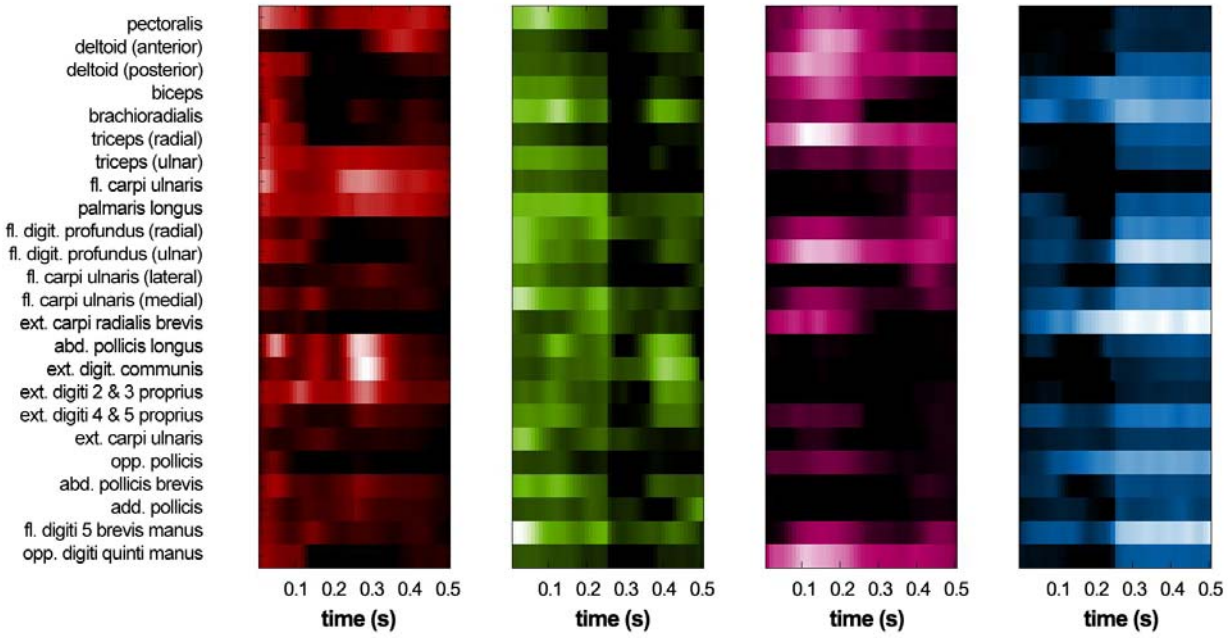

Figure 3-8 EMG reconstruction by three-behavior-derived synergies. Shown are the trial EMG data from sample trials in the **a**) sip, **b**) transportation, and **c**) force tasks. In each case the EMG activity can be reconstructed by linear summation of the four independently scaled and shifted synergies (colored as in Fig. 3-8). The integrated EMG activity is shown as the grey envelope for each muscle; superimposed on this in red is the reconstructed activity. The scaling and timing are represented by the height and offset of the icons representing each synergy at bottom.

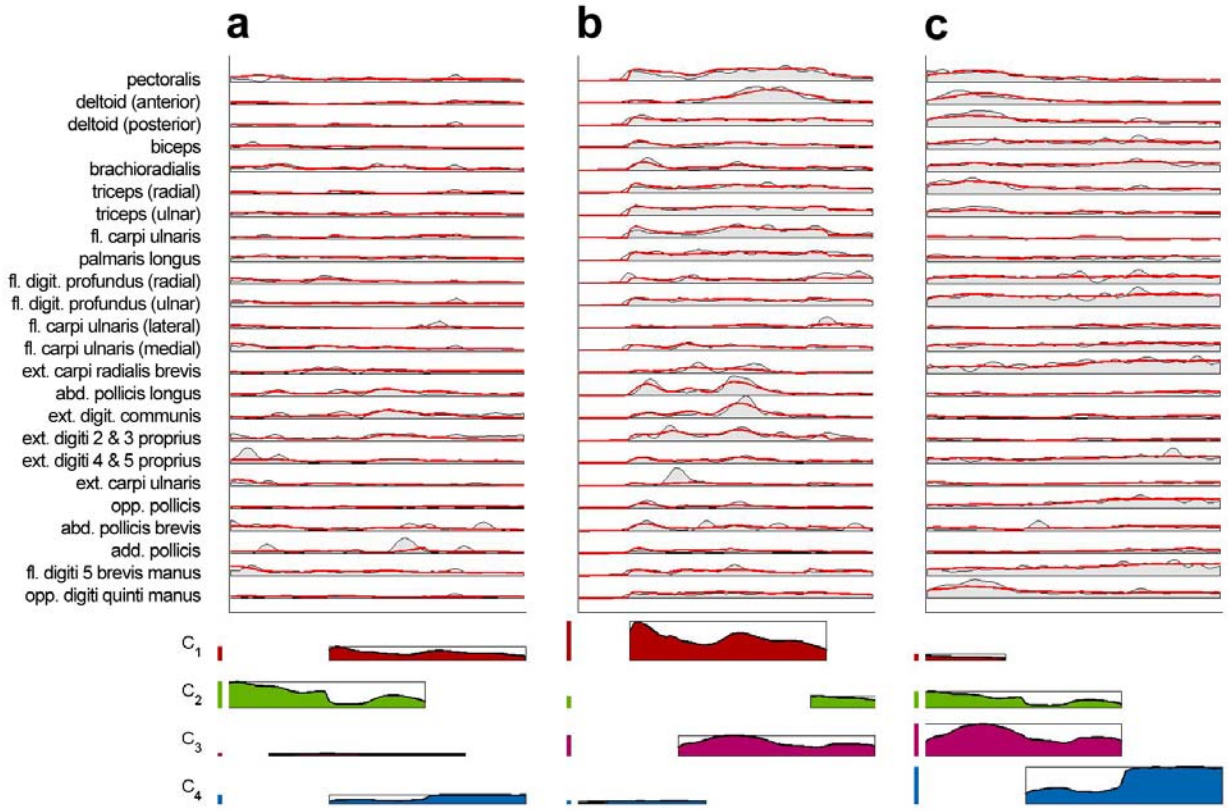

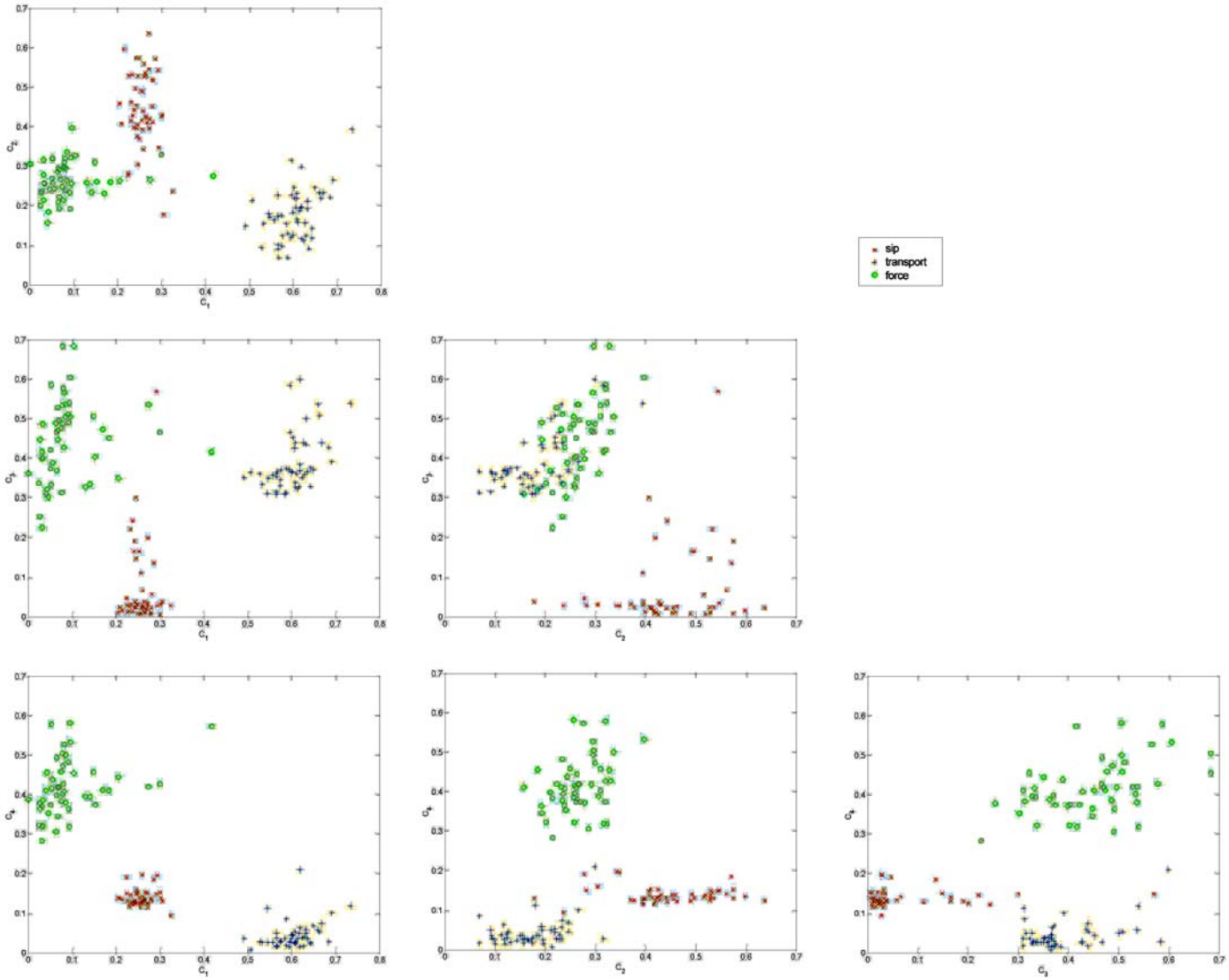

Figure 3-9 Scatterplots of amplitude coefficient relationships among synergies. For each of the four synergies plotted in Figure 3-8 the plots show the pair-wise relations between the amplitude coefficients assigned to each synergy in reconstructing the 50 trials in each behavior.

Figure 3-10 Performance of monkey G1 over four consecutive days with variable objects. The objects were defined according to shape—**a**) spheres, **b**) cubes, and **c**) cylinders—and weight (1, lightest, 5, heaviest), without the confound of object size. The reach and grasp duration spans the time from button press to the time of object removal from in its initial well in front of the monkey.

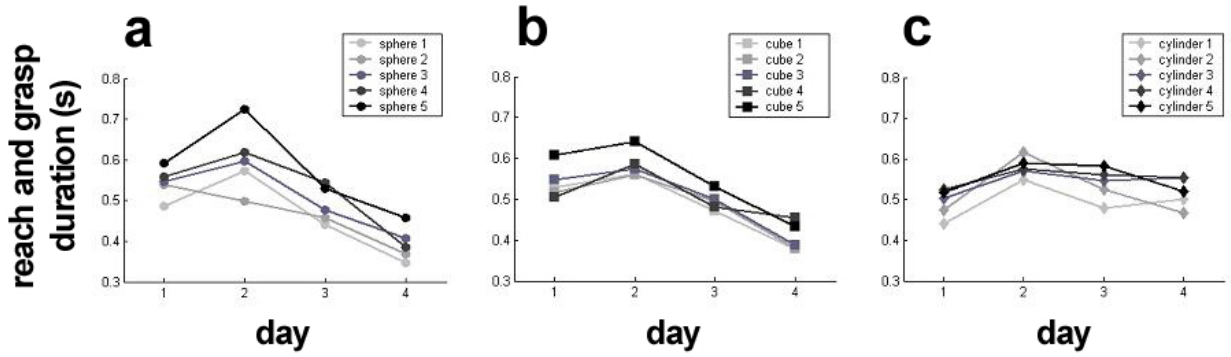

4 Muscle Synergy Recombination in Adaptation to Dynamic Perturbations

The time-varying synergy model was applied to the primate arm model. I recorded EMG activity from 14-16 intramuscular EMG electrodes implanted in the back, shoulder and arm of two macaques as they performed a center-out reaching task using a robotic manipulandum. The muscle patterns recorded during practice on this behavior could be decomposed into a small number of synergies but only with a moderate amount of EMG variance (42-48%) accounted for. A set of four synergies from each monkey were selected for further analysis as these appeared to be "tuned" to directions that spanned the workspace. When the monkeys were exposed to a velocity-dependent force field for 160 trials per day (before and after additional baseline null-field epochs), the pattern of muscular tuning was altered. Because the field chosen was a saddle field, it was possible to predict that muscle synergies whose preferred directions were aligned with the assisitive directions of the field would beceome attenuated in their recruitment, and that the converse would be true for synergies tuned along the resistive axis of the field. Evidence for this prediction was found among more tightly-tuned synergies, whose amplitude coefficients in fitting the data from both baseline and force field epochs demonstrated a pattern of modulation contrary to the applied forces. In order to visualize the recombination of synergy scaling coefficients in a two-dimensional space, I applied a nonlinear dimensionality reduction to extract a manifold containing the coefficient data. Day-by-day consistency in the overall structure of this manifold—despite extraction from successive days—suggested that there were higher-order constraints on the possible patterns of synergy recombination, and that with the learning the variability of this synergistic coordination would decline. The synergy model's assumption that only the coefficients associated with synergies can change, but not the structure of the synergies, was tested by monitoring the structural similarity between synergies derived from the baseline data and separately from each day's force field epoch. For at least one of the monkeys, the average degree of similarity appeared to decline gradually over days, suggesting that adaptation could be reflected in a rebalancing of muscle activity.

4.1 INTRODUCTION

4.1.1 Learning in the context of reaching movements

In contrast to the grasping paradigm used in Chapters 1-3 to study motor control, I have selected whole-arm reaching movements as a model system for motor learning. Reaching movements *without* an explicit learning component have been previously used as a model of cortical coding of endpoint movement kinematics in the monkey (e.g. Georgopoulos, 1982; Wessberg et al., 2000). To dissociate cortical activity related to kinematic and dynamic variables, investigators have modified the task to involve: 1) isometric vs. movement conditions (Sergio & Kalaska, 1998); 2) different upper arm (Scott & Kalaska, 1997; Scott et al,. 1997) or forearm (Kakei, Hoffman & Strick, 1999, 2001) postures during reach; or 3) loads assisting or resisting one-dimensional (Evarts, 1968, 1969; Alexander & Crutcher, 1990;

Crutcher & Alexander, 1990) or two-dimensional (Kalaska et al., 1989) reaching movements.

By retaining assistive or resistive perturbations such as those above and making them predictable environmental disturbances, motor adaptation can also be studied in the context of reaching. Both the relevant kinematic data and the resulting behavioral analyses are simpler and more standardized (though see Discussion) than in studies of manual behavior. This task has now become a classical paradigm of motor learning both kinematically and electromyographically in humans (see Chapters 8-10) and cortically in monkeys (Gandolfo et al., 2000; Li et al., 2001; Padoa-Schioppa et al., 2002).

But while neural correlates of control variables and motor learning (e.g. Li et al., 2001) have been shown to exist, the interpretation of their activity has been complicated both by the diversity of coding schemes ascribed to motor cortex (see Todorov, 2000), and the difficulty of chronic neural recording over a timecourse appropriate for studies of motor learning. Thus it seemed appropriate to seek organizational principles of motor learning at the intermediate level of muscular activation.

A note about handedness: While visually-guided food reaching is typically performed with the left hand in monkeys (Deuel & Schaffer, 1987; King et al., 1987), at least three species of macaque prefer the right hand in complex, stereotyped manipulation tasks (Kuhl, 1988), and certain monkeys have a right-hand preference in manipulating joysticks (Hopkins et al., 1989) or other tasks requiring fine control of applied pressure (Preilowski et al., 1986). Hence while I had selected the nondominant left forelimb for study in the grasping paradigm, here I train movements of the right arm.

4.1.2 Tests and representation of a modular basis for muscular adaptation

In this chapter I not only monitor changes in synergy coefficients, but I explicitly test whether learning can better be described as a recombination of existing synergies, or as a replacement of one synergy set for another. A simple test of this hypothesis could be to extract muscle synergies from early in learning a new field, and use these synergies to reconstruct the EMG activity of subsequent days. Provided there are no systematic, confounding changes in the quality of the EMG signals over this time, I would interpret a progressive decrease in the amount of variance explained by the "early" synergies as evidence for a change within the synergy structures latent in the data, rather than an adaptive rebalancing of synergy coefficients. Another test of synergy conservation based on reconstruction error might be to examine the shapes of the r^2 vs. synergy number curves derived on successive days. If the number of synergies justified by this inspection increases over learning, this might be taken as indirect evidence for the emergence of a novel synergy. However, as I have discussed in Chapter 2, model order estimates based on reconstruction error curves are controversial.

As in previous chapters, however, I avoid both of these comparison approaches because of the possibility that they would obscure the emergence of novel synergies. Instead I repeat the technique of previous chapters, wherein I directly compare two datasets on the basis of the synergy structures extracted from each (after mitigating confounding variables). My hypothesis regarding the conservation of synergies over

the course of learning can then be stated thus: the degree of structural correlation between synergies derived from each day in the novel environment and synergies derived from an unchanged environment should not progressively decrease over days. That is, the patterns of muscular activity I extract from a familiar and a novel condition should not systematically diverge in their correlation over learning. Of course, this hypothesis is predicated on the assumption that learning actually occurs, and hence it will be necessary to demonstrate a functional modulation of synergy parameters (i.e. the amplitude and timing coefficients).

To the extent that it is possible to describe motor adaptation as a recombination of existing synergies, it will also be of interest to see if there are constraints on these combinations. (Chapter 5 examines this issue more in a more direct experimental fashion.) As experimental evidence for such constraints, Saltiel et al. (2001) described not only synchronous synergies in hindlimb behaviors of the frog but also "preferred combinations" of these synergies. To this end I have implemented and compared two nonlinear dimensionality reduction algorithms—locally linear embedding or LLE (Roweis & Saul, 2000) and Isomap (Tenenbaum et al., 2000)—in order to visualize two-dimensional surfaces, or "manifolds," joining these data within the space of synergy coefficients (see Discussion).

4.2 METHODS

4.2.1 Subjects

I collected EMG and behavioral data from two rhesus macaques (*Macaca mulatta*) while they performed object transport behaviors. In the text that follows I refer to these monkeys as R0 and R1 (5-year old male and 10-year old female monkeys, respectively). Cortical data was recorded separately (monkey R0) or simultaneously (R1) but is not presented here. All procedures were approved by the MIT Committee on Animal Care.

4.2.2 Paradigm

Reach task Each animal performed the reaching task using its right hand (which I found to be non-dominant for this behavior, at least for monkey R1 in whom I tested this explicitly). During the recordings presented here the monkey was head-fixed by means of an implanted cranial post, but still able to see the manipulandum handle and screen in front of it. Each monkey was trained to move a handheld, two-link manipulandum handle using its arm following visual cues on a computer screen placed in front of the animal, as shown in Figure 4-1a. The monkey's hand was loosely tied to the handle, but its arm was not restricted to the same planar workspace as the manipulandum. Thus the movements may have involved joint rotations at the wrist, elbow, shoulder, and back. The endpoint of the manipulandum was represented by a 3×3 mm (~0.2° of visual angle) cursor; the targets by 14×14 mm (~1°) squares. In each trial the monkey is rewarded (with 0.2-0.4 ml liquid reward) for: 1) maintaining the cursor within the central square for an initial 1 s; 2) moving the cursor to a peripheral target square within 1.2 s (R0) or 2 s (R1), without deviating from the ideal movement direction by ±60°, following (in

sequence) the appearance of this target, a delay period (randomly chosen between 0.8-1.2 s), and the disappearance of the original square; and finally 3) holding the cursor within the peripheral target for 1 s. Note that rewarded trials are known as "hits" in this paradigm.

Epochs In each day of training and recording the monkey performed (if it was willing) 160 hits before (*baseline*) and after (*washout*) a *test* epoch during which the manipulandum controller generated either a null (i.e. no) force or a velocity-dependent force field. The test epoch normally spanned 160 hits. In the case of monkey R1, ~8% of these trials were randomly selected by the software as "catch trials" on which the motors are turned off without warning to the animal, leading to characteristic trajectory errors that indicate the formation of an internal model of the force field. In the case of monkey R0, the catch trials were added to the 160-hit test epoch by experimenter control, in order to ensure a relatively equal frequency of the catch trials among the hits (and not only the trials) and among the eight possible targets. (Technically these should be called catch "hits" in the case of R0, since it was required to successfully complete at least 11 catch trials each day.) If the monkey was not sated it was frequently allowed to perform additional trials under washout conditions. There was no break between epochs.

Sessions I consider all four, consecutive days that monkey R1 performed under the selected force field conditions (see "Forces," below). Monkey R0 was exposed to the force field over seven sessions spanning 15 days. I consider days 1-6 even though there was a break of several days between day 2 and 3. (But see Chapter 7 Discussion for an example of how such interruptions between days of practice can disrupt learning trends.)

Targets The eight peripheral targets were located radially around the central square at distances of 10 cm (R0) or 9 cm (R1), both on the screen and in the manipulandum workspace, at 22.5° (to the right), 68.5° (ahead and to the right) etc. in 45° increments. The target presentation was pseudorandom, with all eight targets present and ordered randomly within repeated blocks of eight trials. On incorrect trials the missed target and any remaining targets within the block were reordered randomly. A block was not considered complete until all eight targets were reached successfully.

Forces During training the test epoch involved only the null forces. Prior to the recordings presented here, monkey R0 was also exposed to a clockwise curl field and on a few days, to counterclockwise forces. Monkey R1 experienced these same fields, but for consistency this chapter considers only the field that was novel to each: a saddle field which tended to displace the hand along one axis and resist motions of the arm along the perpendicular axis (Fig. 4-1c). (In chapters 5 and 7 I consider additional force fields experienced by monkey R1.) The curl forces, of magnitude 4 N·s/m, were calculated on-line as $f = \mathbf{B}\dot{x}$, where $\mathrm{B} = \begin{bmatrix} 0 & -4 \\ -4 & 0 \end{bmatrix}$ and $\dot{x}$ was the movement velocity. The gain factor was comparable to that used in Chapters 5 and 7, and in prior literature (Li et al., 2001), but was lower in order to facilitate the

monkey's adaptation to the unstable, assistive axes of the field. Each force field was presented over multiple days until a speed profile criterion was achieved (see Li et al., 2001), or in the case of monkey R1, until 4 consecutive days on which the entire 480-hit was completed. Within the force epoch, ~8% of the trials were pseudorandomly selected as catch trials, as described under "Epochs" above.

4.2.3 Recording/Stimulation

Kinematics Rather than the combination of discrete event markers and qualitative video records that served to characterize the monkeys' behavior in Chapters 1-3, the manipulandum used in this chapter was able to provide a continuous record of the monkey's hand—insofar as it could be assumed to be holding the manipulandum, which was invariably the case on at least the reaching portion of correct trials. Mechanical potentiometers were mounted along the torque motor axis and rotated with the motors, thereby providing angular position estimates of each of the two joints of the robot arm. These data were collected at 100 Hz (monkey R0) or a software-limited rate of between 30-80 Hz (R1), hardware-filtered, and then digitized via acquisition boards (National Instruments). For velocity measurements, the system performed a differentiation of the potentiometer signals prior to digitization. Forward kinematic calculations were then used on-line to project the cursor properly and to generate the velocity-dependent force fields, and off-line to reconstruct the monkeys' trajectories. More analogous to the event markers in the previous chapters were the times associated with software-controlled events. The appearance/disappearance of the central origin and the peripheral target, and the cursor's entry/exit from the origin and target, defined a total of eight such event times.

Muscle set As in Chapters 1-3. The muscles implanted with electrodes in each of monkeys R0 and R1 are given in Table 1-1, and depicted in Figure 4-2. Three of the implants in monkey R1 were excluded from this analysis based on cross-correlations and high electode impedance. The remaining muscle sets comprised 16 (R0) or 14 (R1) muscles, of which 14 were common muscles.

Muscle implantation As in Chapter 1, the muscles were implanted using intramuscular electrodes which were wired subcutaneously to a circular connector (WPI) mounted cranially. The muscle implantations required two separate surgeries seven days apart on monkey R0 and a single surgery on R1. (The procedures to implant proximal muscles were less involved than those needed for the more distal muscles of Chapters 1-3.) In the case of monkey R0, the EMG data presented here were recorded within 1.5 months following the last of its surgeries. In the case of monkey R1, the EMG data presented here were recorded between 1.5 and 2 months following its surgery. The "novel" surgical sequence described in Chapter 1 ("connect-first") was used also on monkey R0; the more traditional sequence ("implant-first") was used with monkey R1.

Electrode construction As in Chapters 1-3.

EMG data collection The EMG data from all the muscles implanted in each

monkey were recorded together, bandpass-filtered (10-Hz highpass and 1000-Hz lowpass), notch-filtered (60 Hz), and amplified (5000×) in differential fashion using a programmable signal conditioner (CyberAmp 380, Axon Instruments) controlled by software (CyberControl, Axon Instruments). Data were then digitized at 1 kHz (monkey R0) or 2 kHz (R1) using a data acquisition board (National Instruments). The EMG data records were recorded either continuously over the session (R0) or in single-trial records divided by the software-determined inter-trial period.

4.2.4 Analysis

Trial alignment I did not align trials on an event time midway between the trials, but I did restrict the recordings to the data between the time the central target disappeared to the time the monkey reached the target (Fig. 4-1b). As in Chapters 1-3, this duration encompassed two broad phases: a reaction time and a movement time. The minimum of each time was set by the monkey's attention and/or movement speed.

EMG data preprocessing As in Chapters 1-3, the EMG data of each trial were centered by median subtraction within each muscle channel, highpass filtered (50 Hz), full-wave rectified, and lowpass filtered (20 Hz). (In the case of monkey R1, the median subtraction followed rather than preceded rectification.) The data were further bin-averaged over 25 ms. (Whereas in Chapters 1-2 the integration interval was chosen to balance the overall data volume from each animal, given differences in movement speed between them, in this experiment the average hit duration on null-field trials across the dataset was 1.3 s.) Data were normalized across muscles, but over the entire multi-day dataset rather than *within* each day of recording, to the peak level of activity in each muscle recorded in that dataset. Trials were not averaged together as was done in Chapter 1.

Trial selection As in Chapters 1-3, I considered only hits, i.e. rewarded trials. Note that I did not need to subselect among the trials in order to equalize each kinematic condition, as this equalization was already afforded by task design (i.e. by the pseudorandom equalization of target direction frequency). In addition, the representation of each epoch was balanced as each was represented by 160 hits. (In actuality, the test epoch contained catch trials, and as a result a slightly higher number of total hits (171-173) in the case of monkey R0, for whom these catch trials were randomly interleaved into the remaining force trials. For this chapter I have not excluded or separately considered these catch trials. Instead I postpone discussion of them to Chapter 10.) Synergies were derived both from individual-day and multiple-day datasets, and from individual or pooled epochs, as will be described.

Data reconstruction As in Chapters 1-3. Whereas in Chapters 1 and 2 a difference in the average speed of the movements between the monkeys prompted me to choose particular synergy durations for each animal, here I use a fixed synergy duration parameter of 0.5 s for both animals. This was the same duration as used for monkey G1 in the previous studies. Note, however, that at 1.3 s the overall duration of these trials was substantially longer than in the grasping paradigm.

Synergy extraction As in Chapters 1-3.
Synergy set selection As in Chapters 1-3.
Synergy comparison As in Chapters 1-3.

Nonlinear dimensionality reduction Both Isomap and LLE are applicable under the assumption that low-dimensional manifolds embedded in a space are "open" (shaped, for instance, as a cone rather than a sphere) yet potentially highly nonlinear. Isomap is a variant of classical multidimensional scaling or MDS (Cox & Cox, 2001), explicitly designed to allow for complex nonlinearities in the extracted manifolds. Like MDS, Isomap computes a non-sparse distance matrix for each point in the workspace. Unlike MDS, the distances are not Euclidean but are the sums of the geodesic distances, hopping from the center of one local neighborhood to the next. (This neighborhood can be determined either by including a fixed number k of neighbors, or through a Euclidean sphere of fixed radius containing a variable number of neighbors.) LLE, in contrast, only computes distance matrices for the points within a neighborhood, and tries to find a locally linear manifold containing these points (as if it were performing PCA on the local neighborhood). I have found LLE to be more sensitive to changes in the neighborhood size parameter, suggesting that Isomap manifolds are more topologically stable (cf. Balasubramian & Schwartz, 2002). Isomap is also less sensitive than LLE to heterogeneous sampling on a manifold; dense sampling can bias such algorithms into assuming a linear manifold where none exists. The results I present here are therefore restricted to those generated with Isomap. Nevertheless, nonlinear dimensionality reduction of synergy coefficient data collected on single days of EMG recording in the reach task produced generally similar results using either the LLE or Isomap algorithms. Recent techniques combining these approaches, such as curvilinear distance analysis (Lee, Lendasse & Verleysen, 2002), could also apply.

4.3 RESULTS

4.3.1 Dynamic adaptation evident among synergy coefficients

Figure 4-3 demonstrates the performance trends evident in the reaching paradigm. One classical measure of performance is the monkey's recovery from an initial decline in the correlation of its test- and baseline-epoch speed profiles as it adapts to the forces in the test epoch (Fig. 4-3a). The return to null-force conditions in the third epoch is typically associated with a smaller "aftereffect" recalling the larger decline in performance at the beginning of the force epoch. A similar pattern of performance can be measured in various ways from the subject's trajectory error (see Discussion). In Figure 4-3b, a monkey performing under saddle forces in the test epoch exhibits trajectory errors characteristic of the saddle field: movements are accentuated along one axis and repressed along the perpendicular axis as expected (Fig. 4-1c).

The EMG data collected from 14-16 intramuscular electrodes implanted in monkeys R0 and R1 (Table 1-1; Fig. 4-2) yielded the time-varying synergies plotted in Figure 4-4. Each set of synergies was able to explain only a modest amount of variance: 46% in the case of R0, and 42% in the case of R1. (Bear in mind that the

baseline-epoch datasets from which these synergies were derived included 640—or more in the case of monkey R1—non-averaged trials.) Although a similar level of variance was explained in each case, the structures of the synergies were clearly very distinct, with no significant similarities evident among the scalar product scores. In particular, the synergies of monkey R0 appear to encode more phasic muscle activations than those of monkey R1. (I continue to investigate the source of the tonic activation patterns reported for monkey R1.)

Despite the structural dissimilarity, the recruitment of several of each monkey's synergies appeared to be tuned to movement direction, and tuned to divergent parts of the workspace, as shown in Figure 4-5. (This result, evident for both monkeys, was derived after averaging the scaling coefficients used to fit each across-day, within-baseline epoch synergy to all trials performed in each movement direction in the baseline epochs.) Based on the relative alignment of these tuning fields with the resistive and assistive axes of the saddle field (Fig. 4-1c), I expected to see an upwards or downwards modulation of the synergies aligned with the resistive or assistive axes of the force field. As hinted by Figure 4-6, and in particular for the bottom two synergies shown, this may indeed have been the case.

To test for learning-related changes in synergy structure rather than coefficient, I extracted synergies separately from each day's test epochs. A visual comparison of the resulting synergy structures, as in the example of Figure 4-7, suggests both general conservation of muscular coordination and day-by-day variation in the precise structure of the extracted synergies. To examine whether this variation is systematic (and not likely a result of measurement noise), I used the scalar product method (Chapter 1) to compute the maximal correlations evident for each of the above baseline-epoch synergies with a set of four force-epoch synergies. As shown in Figure 4-8, there was again a substantial difference between the monkeys: by the 0.75-0.80 thresholds established for correlational significance in previous chapters, few of monkey R0's synergies would be considered consistently preserved between null and force conditions, while for monkey R1, all of the synergies were consistently preserved.

It is not clear that within- or between-subject ANOVAs apply in this analysis, as each synergy is considered its own population represented by a single extraction. Nevertheless, the synergies whose coefficients progressed most gradually in correlation appeared to do so with decreasing correlation over days. This is particularly true in the case of monkey R1, for whom inspection of Figure 4-4 suggests that synergy 3 came to replace 1 in the set shown. The primary difference between these two structures appears to have been the involvement of the long head of the triceps.

4.3.2 Nonlinear dimensionality reduction of synergy coefficients

After the time-varying synergies had been fit to all epochs in each day's dataset, a two-dimensional Isomap manifold was extracted from the space defined by the coefficients. (Because of computational limits, this analysis could not be performed on a dataset pooling all days together.) Although in principal this technique applies both to scaling and timing coefficients, I demonstrate the technique by applying it to the former alone. In this case the two embedding dimensions (E_2) can be described in terms of the nonlinear correlation to each of the scaling coefficient dimensions (C_i),

as demonstrated in Figure 4-9. Note that the embedding dimensions appeared to describe consistent covariation between coefficient dimensions.

The manifold embedded in this four-dimensional coefficient space is plotted in Figure 4-10. The axes of this figure are the two embedding dimensions. Each panel of the figure shows the *projection* of trials in each epoch and day onto the manifold. Each point in the plot represents a single trial, color-coded according to the target direction in that trial. The topology of the embedding surfaces is divisible into sectors corresponding to different directions of movement. The topological organization of movement direction on the within-session manifolds appears to be similar between the baseline and washout epoch, but varied upon introduction of a saddle field. Figure 4-10 also suggests that the variability of synergy recombination within the manifold is greater in the force field epoch. The manifold appeared to transform over days in a manner consistent with the change in force production needed to reach the peripheral targets. In particular, after several sessions the warp of the manifold in the force epoch appeared to reflect resistive directions in the saddle field.

4.4 DISCUSSION

4.4.1 Adaptation of synergy recruitment in reaching movements

In previous chapters I have discussed several methods for estimating the appropriate number of muscle primitives required to account for a behavior. These have principally included methods based on the reconstruction error curve (introduced in Chapter 1), the amount of incremental information provided by each element extracted (discussed in Chapter 2), and the structural similarity between the synergies (applied in Chapter 3). Here I give a further rationale in my selection of four synergies: namely, that four synergies were required to span the monkey's workspace in a non-negative fashion. Positions within the workspace could be specified by two Cartesian dimensions, but muscle synergies are restricted to positive axes. (However, in Chapter 6 I discuss further whether the non-negative nature of muscle recruitment may in turn be reflected in a similar restriction on movement endpoint encoding.) d'Avella and Lacquaniti (2004) and Ting and Macpherson (2005) have similarly shown that reaching movements in humans, or postural responses in cats, can be decomposed into four muscle synergies with very differentiated directional tuning. In the case of movement tasks, though, the directional tuning of muscle synergies is a result that deserves some qualification. Such tuning was shown in a fashion similar to that shown for motor cortical cells (e.g. Gandolfo et al., 2000; Li et al., 2001; Padoa-Schioppa et al., 2002), wherein the behavioral measure (e.g. firing rate) is averaged within those trials defined by a common target direction.

Such binning by target direction makes statistical comparisons simpler, but it can also obscure the actual relationship between central commands and movement trajectories (particularly when the latter are inferred only from endpoint position; Mistry et al. 2005). For example, the cortical work above as well as EMG recordings from human subjects (Shadmehr & Moussavi, 2000) have found that the preferred direction of cortical neurons, and in some cases of muscles, tends to rotate in a

direction *consistent* with an applied curl (e.g. clockwise) force field. This result may appear surprising, given that adaptation to such a field is thought to involve active compensation for the forces—as revealed by aftereffects (e.g. in the counterclockwise direction) when the forces are suddenly removed (Thoroughman & Shadmehr, 2000; see Chapter 10). However, if muscle activity is not binned within target direction but is rather considered in relation to movement direction, then it can be seen that the muscles remain tuned to more or less the same direction of force application despite the force field. What "rotates" between targets instead is the direction of this force application required to reach each target.

My decision to focus on saddle field data in this analysis, despite the relative novelty of this field relative to the curl fields (Shadmehr & Mussa-Ivaldi, 1994) was motivated by a desire to combine the analytical advantage of within-direction binning without the complication of expected changes in the direction of required force output. In so doing, ironically, I have avoided the superior kinematic classification of reaching movements available in this paradigm (cf. the grasping task), and have instead chosen to examine modulation of synergy parameters according to kinematic (direction) and dynamic (force field) variables (in the same manner as I differentiated manual synergies by variables like object shape and weight).

However, these experimental procedures afforded me with a simple hypothesis not only about the conservation of synergies over learning, but about the direction of expected synergy modulation (Fig. 4-5a). In particular, I predicted, and tentatively showed, that among more highly-tuned synergies, one aligned with the resistive directions of the force field tended to become attenuated in their recruitment, and conversely for a synergy aligned with an assistive axis (Fig. 4-6). Despite this evidence for adaptive modulation of synergy coefficients, however, I was unable to show that the structures of the synergies derived independently from each day's force field recordings (Fig. 4-7) were consistently similar to the null-field synergies (Fig. 4-8). Indeed, in at least one of the monkeys there was a gradual decrease in correlation to the baseline synergies over four days of recording. Furthermore, the one force-field synergy whose null-field correlation did *not* decrease appeared related to one of the waning synergies but for a single muscle substitution. While this replacement may have been due to changes in electrode quality between days, it is also consistent with a single-muscle rather than synergistic control scheme.

4.4.2 Kinematic correlates of learning

Most analyses of performance on the reach task are predicated on changes in the movement speed or the movement path over trials (Fig. 4-3). In human studies using the center-out reaching task, these have historically been based on the correlation coefficient calculated from a correlation of the average speed profile in the force epoch relative to the baseline epoch (Brashers-Krug et al., 1996; Shadmehr & Brashers-Krug, 1997). This is true even for the saddle field (Shadmehr & Mussa-Ivaldi, 1994), a perturbation used far less frequently than curl fields. This measure is thought to show reliable improvement followed by plateauing over the course of learning, reflecting in part the subjects' ability to reach targets without making corrective submovements at the end of the reach. Although the time to plateau in

monkeys performing the same task is longer, the correlation coefficient has demonstrated learning in center-out reaching of the macaque (Li et al., 2001).

More recent analyses, including some with EMG recording (Thoroughman & Shadmehr, 1999; Shadmehr & Moussavi, 2000) have considered movement path as well as speed, perhaps because path is more sensitive to deviations resulting from unexpected changes in external forces (e.g. on catch trials). For instance, measures may be based on the total movement length (Shadmehr et al., 1998); or directional error (Shadmehr et al., 1998; Osu et al., 2004), perpendicular displacement (Shadmehr & Moussavi, 2000; Thoroughman & Shadmehr, 2000; Donchin et al., 2002), and perpendicular (Thoroughman & Shadmehr, 1999) and parallel components of velocity (Thoroughman & Shadmehr, 2000), each calculated a short time (typically 0.15-0.3 s) into the movement.

Beginning in Chapter 8, I consider and contrast several measures of learning—and describe why I favor more robust and direct measures based not on speed but on trajectory error. Even such measures of learning deserve qualification when compared with changes in muscle activity, however, as they are based only on the path of the hand. While endpoint trajectories tend to return to relatively undeviated levels with adaptation, the underlying joint rotations may remain distinct in null and force conditions (Mistry et al. 2005). And as trajectory "aftereffects" on catch trials reveal (Chapter 10), the dynamics generated by the arm as a result of adapting to a force field are very distinct from those necessary under null field conditions. Thus my primary measures of learning here have been those visible at the level of muscular coordination.

4.4.3 Embedded dimensionality in synergy recombination

My primary purpose in applying this nonlinear dimensionality reduction was to better observe the pattern of synergy combinations in natural behavior, in particular over the course of learning (Fig. 4-10). Consider the complexity of the coefficient combinations demonstrated earlier in Figure 3-9. This complexity only grows when consideration is extended to the timing coefficients associated with the extracted synergies, as these are more difficult to intuit than the activation coefficients. Indeed, in the reaching task, some modulation of timing dimensions was observed (Fig. 4-5b), perhaps reflecting the involvement of invariant muscle groups either as agonist or antagonist depending on the direction of movement.

Nonlinear dimensionality reduction may further allow several questions to be addressed in a more quantitative fashion than is possible with simple two-dimensional projections of the data. In much the same way, cortical flattening has been a useful tool to study topological organization in cortical sheets (e.g. Fischl et al., 1999; see Chapter 12). For instance, how are the coefficients for different directions of motion distributed over the embedded manifold? Figure 4-10 suggests not only that the embedding surface is open (Tenenbaum et al., 2000), but that movement directions could be programmed according to highly differentiable combinations of muscle synergies. How is the manifold transformed by the presence of a perturbing force field? Most critically, how is learning over days reflected in the structure of the manifold—i.e. is the monkey's recruitment of muscle synergies constraint to the preferred combinations of primitives implied by the manifold?

I do not pursue these questions in a quantitative fashion here, in part because computational resources made it difficult to test whether each manifolds extracted from different days varied in structure, or whether a common manifold could have been fit to all these data—in the same way that movement direction, another variable, could be plotted on to a single surface. But the nonlinear dimensionality reduction of the synergy coefficients did at least indicate that there were nonlinear relations between synergy combination and movement direction, external forces, and learning, and that these relations are well captured by lower-dimensional embedded manifolds. The overall continuity of the directional clustering on the maps of Figure 4-10—extracted independently from each day's data—also suggested that a common manifold was being retained.

More generally, nonlinear dimensionality reduction may be viewed as a method of capturing nonlinear patterns of synergy combination that cannot be described by the linear addition assumed by the time-varying and other related algorithms. For example, these algorithms do not allow for nonlinear interactions between synergies due to muscle saturation (i.e. of muscles encoded in each synergy). Higher-level constraints dictating preferred combinations of synergies may also be possible (Saltiel et al., 2001), to the extent that synergies are programmed centrally. However, development of a fully non-linear (and time-varying) synergy extraction algorithm is outside the scope of this thesis.

Figure 4-1 The reach task. **a**) Each monkey was trained to hold on to a vertically-oriented joystick mounted at the end of a robotic manipulandum, and use it to guide a cursor on the screen towards one of eight radially-arranged peripheral target squares, starting from a central origin. **b**) Much of the training involved teaching the monkey to maintain both the 1-s central and peripheral target hold periods (the former being a variable duration centered at 1 s). (Compare to Fig. 1-2.) The monkey's movements between the central and peripheral targets had to occur following the center-off event but before the maximum 1.2-s or 2-s time allowed for the movement. The movement paths also had to remain inside a ±60° angular window around a straight line joining the central and peripheral squares. The monkeys were required to complete one successful trial in each of the eight pseudorandomly-interleaved target directions before another 8-target set would be generated. After many days of practice with a null field, the monkeys were exposed to novel, endpoint velocity-dependent force fields generated by the manipulandum over a "test" epoch of 160 trials. **c**) Two examples of such fields were the "saddle" field (left)—the focus of this chapter—and the "clockwise" field (right), each schematically depicting the pattern of forces experienced in two-dimensional velocity (not position) space.

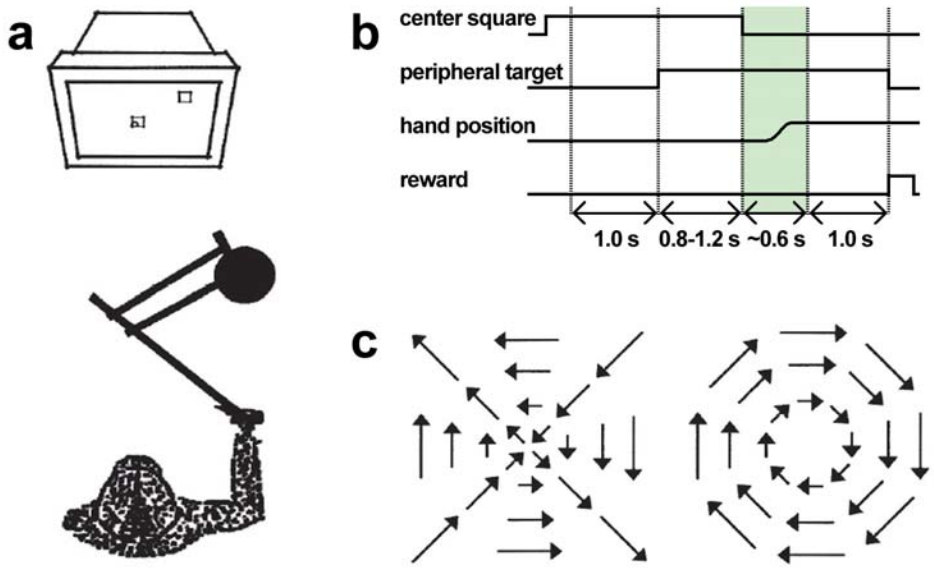

Fgure 4-2 Muscle locations targeted in the reaching paradigm. Between 16 and 17 intramuscular EMG electrodes were implanted in the muscles of the back, shoulder, and upper arm in two and one surgeries, respectively, on monkeys R0 and R1. The muscle set presented here includes 16 or 14 electrodes from each monkey, respectively, the others having been rejected based on high cross-correlation or other artifacts that developed within the months between implantation and these recordings. These muscles are colored and labeled in views of the **a**) lateral arm, **b**) ventral hand, and **c**) medial forearm. (Figures adapted from Howell & Straus, 1971.)

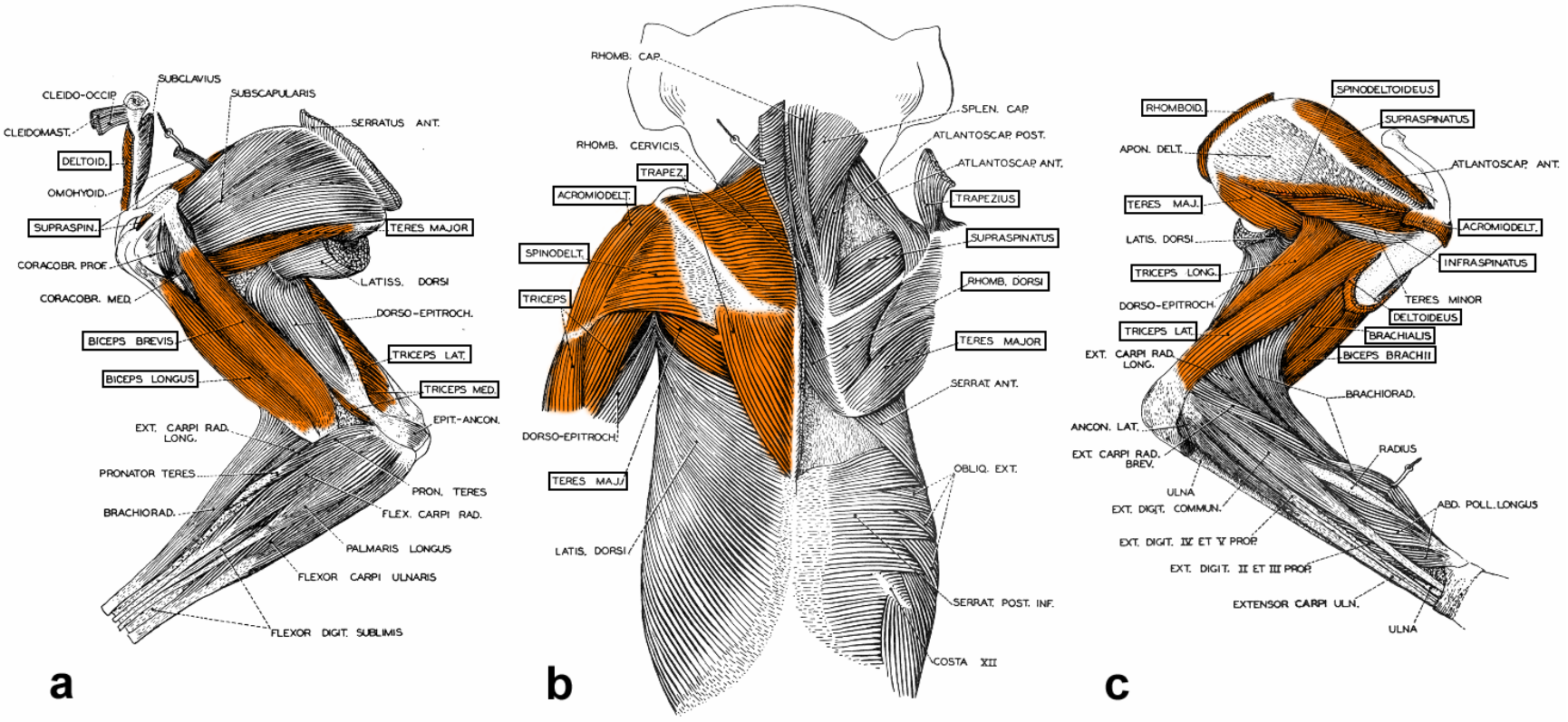

Figure 4-3 Sample performance on the reach task. **a**) Within-day learning is evident in monkeys performing the center-out task, as shown here for a monkey performing under clockwise field conditions. **b**) At the level of trajectory, force fields (like the saddle field shown here with sample trajectories from monkey R0) are associated with distinct, transient deviations.

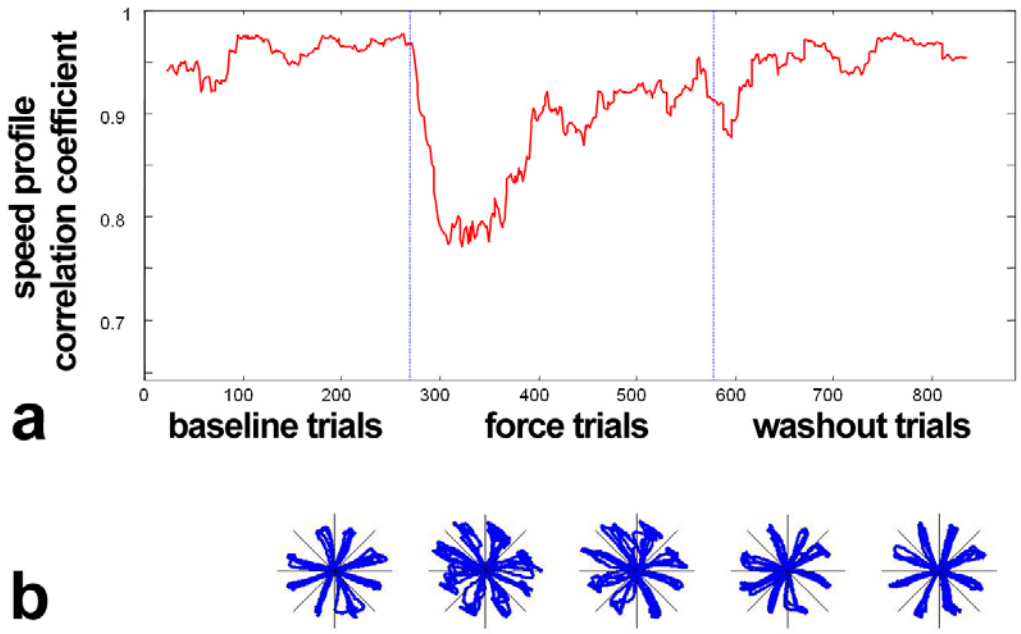

Figure 4-4 Time-varying synergies. Shown for monkey **a**) R0 and **b**) R1 are four 0.5-s time varying structures extracted from their EMG data recorded from the baseline-epoch center-out reach task (collected across all days on which the monkey subsequently experienced the saddle field). Electrodes not included in the recordings from monkey R1 are masked black. Note that color as well as intensity is used to code for muscle activation (cf. Fig. 1-9), as per the scale bar at right.

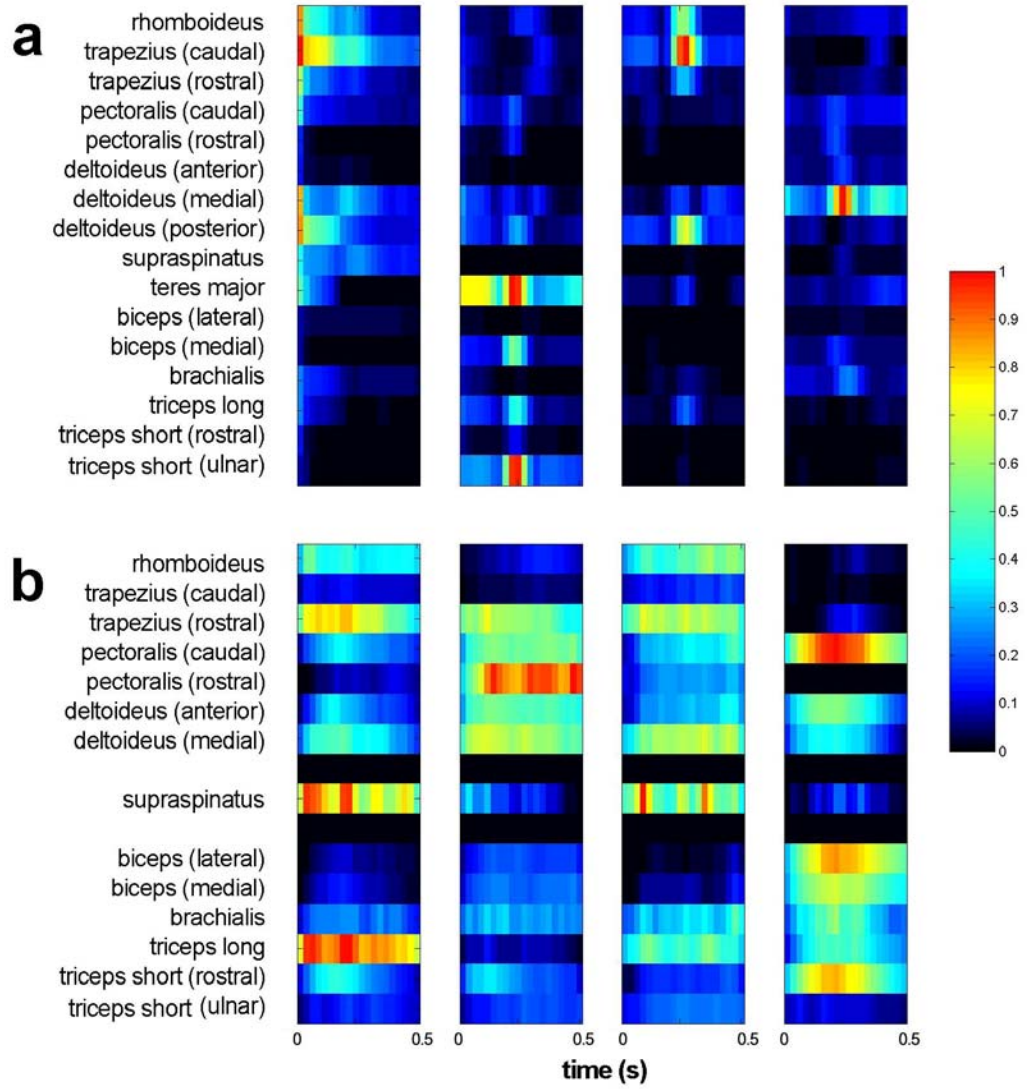

Figure 4-5 Directional tuning of synergy coefficients. As shown for the four synergies extracted from monkey R1's synergies (numbered as in Figure 4-4a), each synergy appeared to be tuned to a particular direction of the workspace, both in terms of the **a**) scaling and **b**) timing coefficients fit with the synergy in reconstruction of the data.

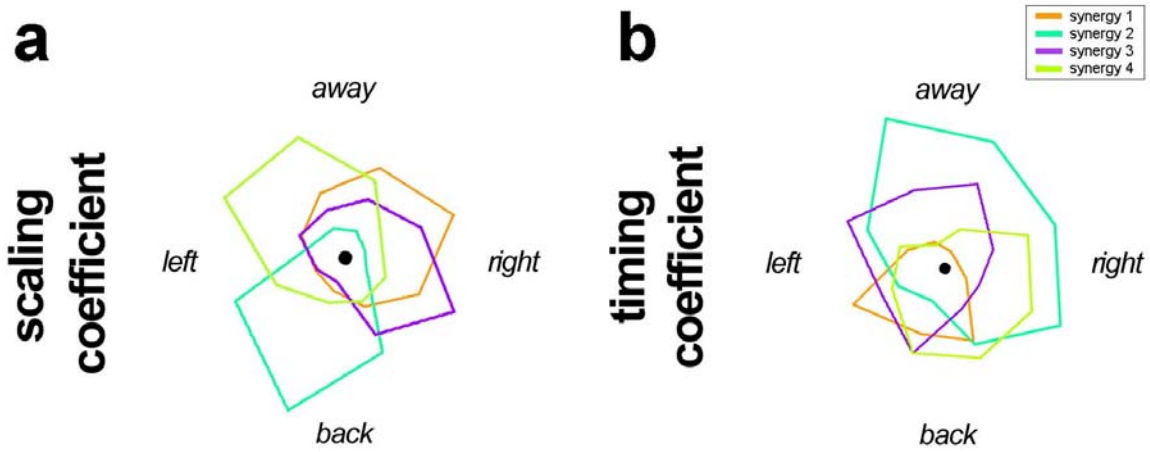

Figure 4-6 Day-by-day changes in scaling coefficient tuning. Shown for monkey R0 are the target direction-averaged tuning profiles for each synergy's scaling coefficient, as found in reconstructing the day's data with time-varying synergies extracted from its multiple-day (baseline+test epoch) dataset. The bottom-most two synergies are the most highly-tuned to target direction. (Workspace orientation and synergy color code as in Fig. 4-5.)

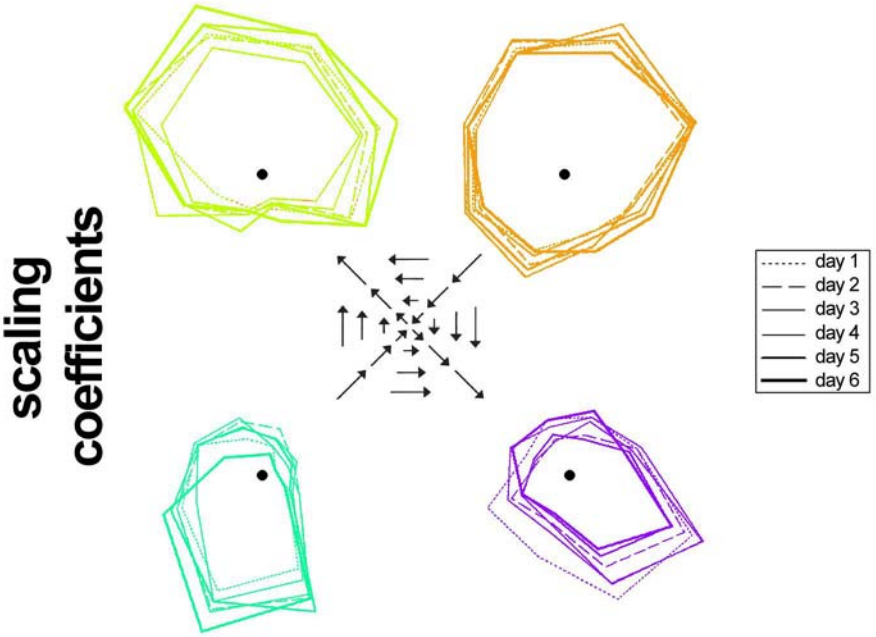

Figure 4-7 Day-by-day changes in synergy structure. Shown for the four consecutive days of force-field training by monkey R0 (following two prior, non-consecutive days) are the four synergies extracted independently from each day's force field epoch. The synergy matrices have been matched according to correlation with the synergies extracted from the full-day dataset (see Fig. 4-4) and have been sorted and colored according to the best-matched synergy within this dataset as in Figures 4-5 and 4-6.

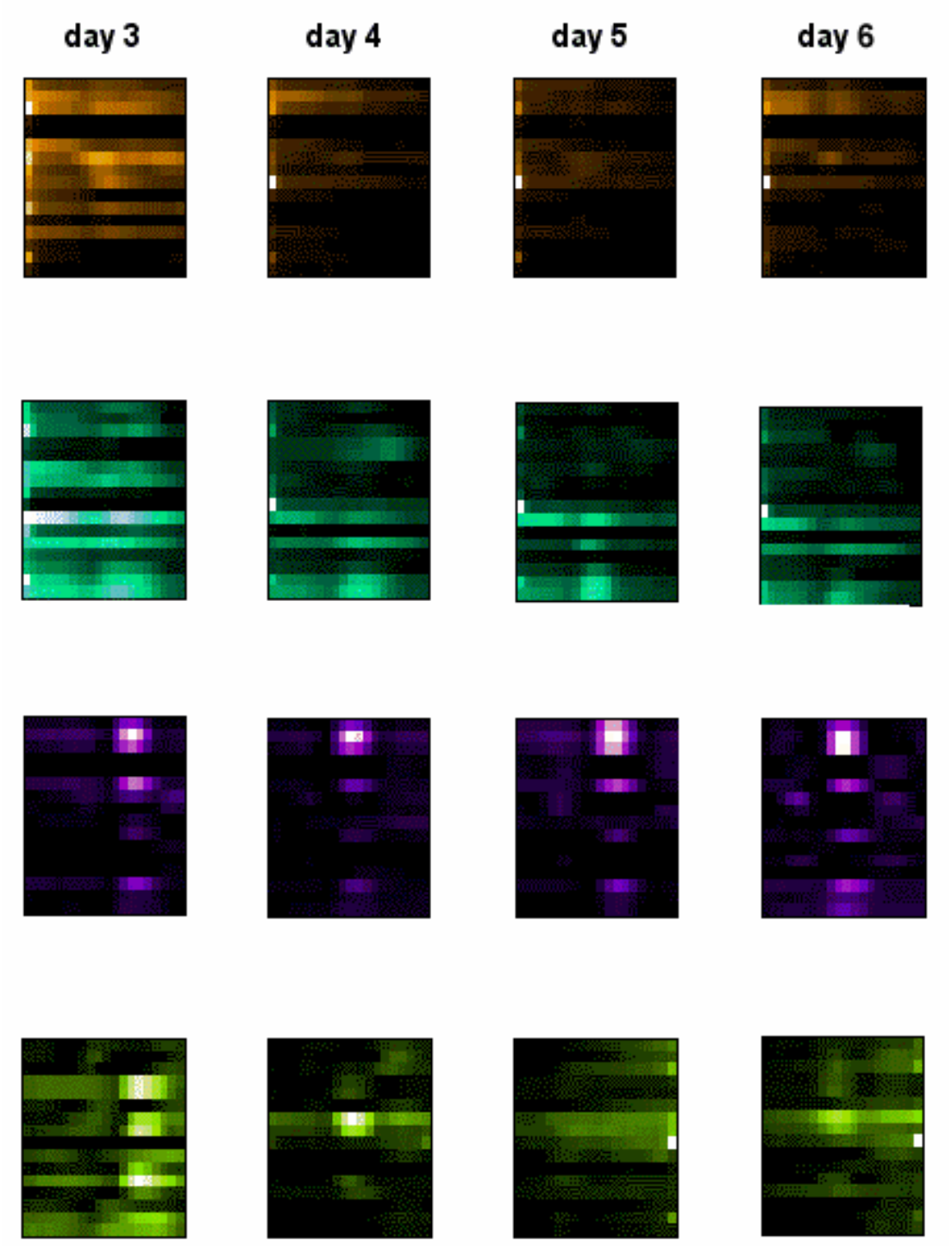

Figure 4-8 Day-by-day changes in synergy similarity. Shown for monkey **a**) R0 and **b**) R1 are the maximal correlations observed for each of the synergies shown in Figure 4-4a and 4-4b, respectively, with sets of four synergies extracted independently from each day's force field epoch. The separation of R0's plot indicates the break between days experienced by this monkey. Both curves are aligned over the four days on which each received consecutive saddle field practice. Colors as in Figures 4-5 through 4-7 (with no similarity between each monkey's synergy sets implied).

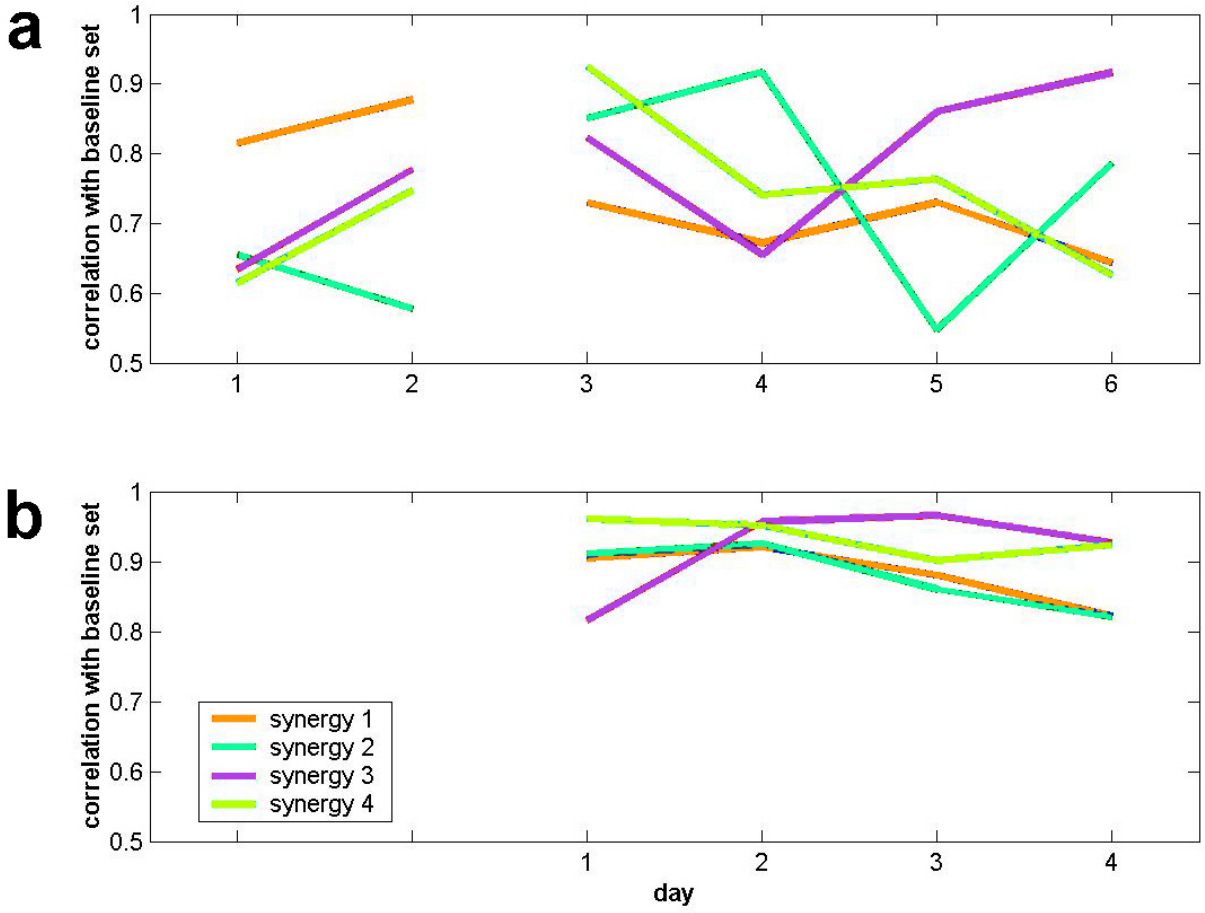

Figure 4-9 Relationship of Isomap embedding dimensions and synergy coefficient dimensions. An intrinsically two-dimensional manifold defined by dimensions E_i was extracted from the space defined by the scaling coefficients (C_i) associated with four synergies extracted from monkey R0's data on the sixth day of its recording.

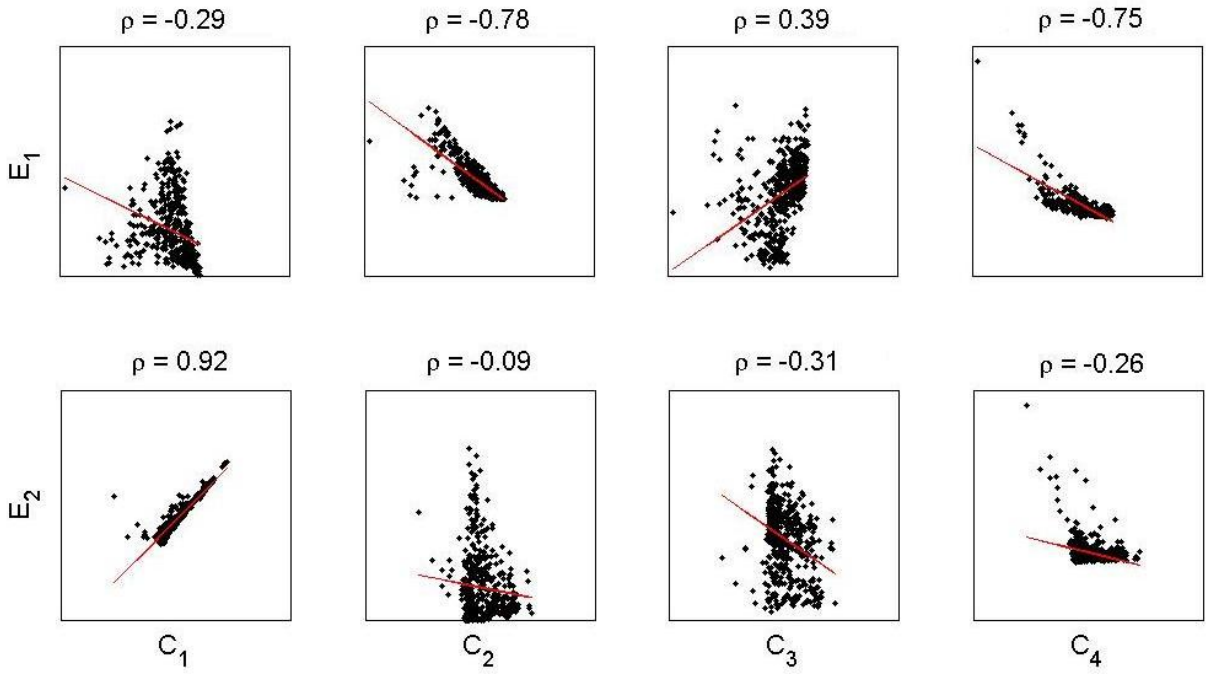

Figure 4-10 Visualization of higher-order constraints on synergy recruitment over learning. In this example from monkey R0, separate two-dimensional Isomap manifolds were extracted from each day's dataset (including all three epochs and all eight target directions in each case). Colors code the movement directions as shown; separate plots are used for each epoch and day. The central points of each target direction cluster are connected together by straight lines to illustrate the continuity of directional mapping on the manifold. Ordinates and abscissae represent the two embedding dimensions extracted from each day's data, and do not necessarily map on to those extracted from prior or following days.

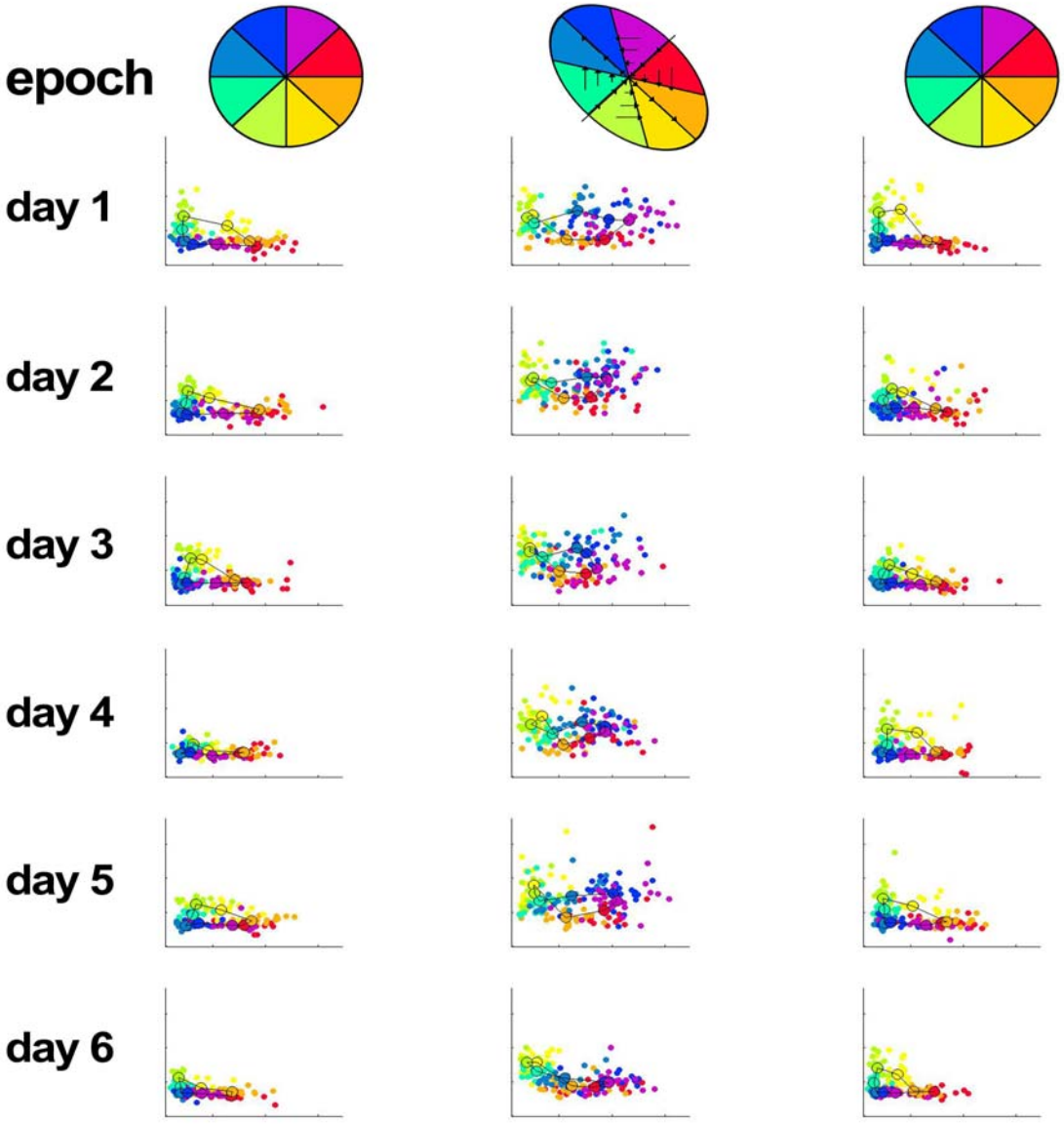

5 Muscle Synergy Resistance to Myofeedback Perturbations

I propose a novel paradigm for directly testing the synergy hypothesis in which an organism is required to modulate the activity of individual muscles. Although muscle synergies could theoretically accommodate single-muscle modulation through appropriate rebalancing of associated activation coefficients, the synergy model could be falsified by evidence showing individual muscle modulation independent of changes in the activity of other associated muscles. Experimentally, I have implemented this test by having a macaque perform the whole-arm center-out reaching task with a robotic manipulandum, while it generates viscous forces that vary in proportion to the on-line activity of a target muscle. Over twelve days in this task, I targeted a dozen different muscles or muscle divisions. Preliminary analysis suggested that the monkey was able to accommodate the forces in the case of certain muscles, as reflected both in its ability to complete the set 160 trials, and in the attenuation of activity observed within the target muscle. Consistent with the synergy hypothesis (although not exclusively so) other muscles besides the target muscle were observed to modulate in their degree of tuning. However, cortical microstimulation trains delivered to MI following these experiments were often associated with transient decreases in the activity of the target muscle, but not of similarly attenuated muscles, relative to its baseline activity, suggesting a rapid and centrally-driven reweighting of muscle coordination.

5.1 INTRODUCTION

In Chapters 1-4 I have shown how EMG data from forelimb muscles of macaques as they make grasping or reaching movements can be reconstructed as combinations of a small number of time-varying muscle primitives. These muscle synergies provided a description of motor output that is compact, requiring specification of independent, scalar activation and timing coefficients for a group of muscles rather than individual time courses of activation for each muscle. Such synergies were able to explain a substantial amount of the variance present within the muscle data, and at the same time could be informative about behavioral variables such as object shape and movement direction. The synergies appeared to be stable in structure, available for different tasks, and adaptable to changing dynamical conditions. For instance, when a robotic manipulandum controlled by the monkey generated forces counteracting movement to a target, I observed a gradual and compensatory increase in the coefficient of activation for synergies aligned with that target direction.

In Chapters 1-3 the methods I used were esssentially correlational. In Chapter 4 I substituted reach direction for my former control kinematic control variables, chiefly object shape and mass, and was able to test a prediction about how the muscle patterns would be recruited under novel dynamic conditions. Here I provide more direct evidence for the existence of these muscle synergies, by delivering perturbations dependent not only on the velocity of the hand but also on the activity of individual muscles. The synergy hypothesis predicts that muscles are activated in a coordinated fashion with other, functionally-related muscles. Hence, to vary the activity of a single muscle the nervous system should have to vary the activity of other

synergistic muscles simultaneously, both those that are part of the same synergy and those of other synergies that are needed to compensate for the change in the target muscle.

In this pilot study I am currently testing this hypothesis, with one rhesus macaque trained to make reaching movements using the manipulandum. Over 12 days, I presented the monkey with a null-force baseline period and then a pure viscous (resistive) force field epoch, created by the robot's torque motors. The gain of this force field was set proportional to the real-time EMG (sampled, rectified, and integrated at 30-80 Hz) of a particular target muscle selected for that day. As a result, the monkey experienced a resistive force during movement any time that it activated the target muscle. I predicted that the monkey would learn to adapt to these forces as it had done with pure velocity-dependent forces (Chapter 4). In this task, however, I expected that this adaptation would involve an attenuation of activity measured in the targeted muscle. By the synergy account, I hypothesized that this attenuation would also extend to other muscle related to the target muscle in a synergistic fashion, even if these muscles were agonists that might otherwise be expected to increase in activation in order to compensate for the attenuation of the target muscle.

5.2 METHODS

5.2.1 Subjects

As in Chapter 4. The sole subject (female, 10 a.) was the same as subject R1. Below I briefly describe the cranial and cortical procedures undergone by the monkey prior to and during the experiment in Chapter 4.

5.2.2 Paradigm

Reach task As in Chapter 4.
Epochs As in Chapter 4.

Sessions The monkey performed twelve sessions on separate days spanning a one month period (beginning five weeks after the monkey's EMG implantation surgery). On these days the monkey completed at least the baseline epoch and 40 trials of the test epoch. Only eight of these days were completed in blocks of four consecutive days, as in Chapter 4.

Targets As in Chapter 4.

Forces During the test epoch the monkey experienced novel viscous forces, calculated on-line as $f = \mathrm{B}\dot{x}$, where $\mathrm{B} = \begin{bmatrix} -1 & g \\ g & -1 \end{bmatrix}$ and $\dot{x}$ was the movement velocity. The matrix B was multiplied by a further scalar gain factor upon each iteration of the program, set proportional to the real-time EMG (sampled, rectified, and integrated at 30-80 Hz). The gain factors were chosen subjectively to approximately normalize for the range of muscle activity observed during the baseline

epoch.Within the force epoch, ~8% of the trials were either pseudorandomly selected as catch trials, as described under "Epochs" above.

5.2.3 Recording/Stimulation

Kinematics As in Chapter 4.

Muscle set As in Chapter 4. However, only 12 electrodes continued to have reasonable signal throughout most of the investigation, which included days before and after the experiment in Chapter 4. The muscles included rhomboideus, rostral trapezius, infraspinatus, supraspinatus, medial and anterior deltoid, rostral and caudal pectoralis, long head and rostral short head of the triceps, and lateral and medial biceps (Fig. 4-2).

Muscle implantation As in Chapter 4.
Electrode construction As in Chapters 1-4.
EMG data collection As in Chapter 4.

Craniotomy Following training a craniotomy was performed on the monkey and a 1.9-cm diameter metal chamber was implanted on the skull around the exposed dura surface. The location of the craniotomy center (AP = 17.0, ML = 15.0) was chosen to cover the forelimb area of primary motor cortex contralateral to the implanted limb, as well as neighboring premotor and somatosensory cortex. This position was estimated based on reported values (Park et al., 2001; Holdefer & Miller, 2002), as well as vasculature-revealing infrared observation of the dural surface during surgery.

Dura maintenance I thoroughly "scraped" the monkey's dura every seven to ten days during these recordings. Scrapings were performed with Ketaset and Atropine IM, under a microscope set to about 3.5× magnification, using an aspirator mounted with glass pipettes whose ends had been broken off. Cooled saline was used to periodically rinse the chamber. An accidental evagination over its left postcentral cortex had become sealed over by connective tissue prior to the experiment, but was still associated with particularly heterogeneous tissue that was difficult to remove or penetrate with microelectrodes (and may have been related to the subsequent difficulties reported in Chapter 7 concerning this monkey's dura.)

Microelectrodes I used the same multiple vinyl-coated tungsten microelectrodes (FHC) for cortical and LFP recording (not presented here) and for intracortical microstimulation (see below). Thee electrodes were measured to have impedances above 250 k as measured in saline. These were positioned on a custom grid with 1-mm spacing between holes, and lowered into cortex by means of a custom manual microdrive (each turn translating the electrode 0.3 mm in depth). The signals were monitored both on a software oscilloscope function and aurally through a speaker connected to the amplifier. No systematic attempt was made to place the electrodes in a particular layer of cortex.

Microstimulation Following each experiment I performed repetitive intracortical microstimulation (R-ICMS) at 2-7 sites in motor cortex shown in prior sessions to

have muscles fields including the target muscle. (In a minority of cases the stimulation sites were chosen 1 mm from such target sites.) A custom switch-box allowed stimulation current to bypass the sensitive recording headstage. The pulses were bipolar (cathodal-first) and were created by staggering two pulse trains (S48 Stimulators, Grass Medical Instruments) and inverting the polarity of one train (BSI-2 Biphasic Stimulus Isolator, BAK Electronics, Inc.). The parameters, including 2×0.2 ms pulse duration, 330 Hz pulse frequency, and 50-ms train duration are consistent with settings used by other investigators (e.g. Asanuma & Rosén, 1972; Strick & Preston, 1978; Cheney, Fetz & Palmer, 1985; Sato & Tanji, 1989; Baker, Olivier & Lemon, 1998), although most of these investigators used strictly cathodal current. The range of current amplitude used (10-150 mA current) exceeded the conventional bounds (see Chapter 6 for the motiavtion). Delivery of stimulation pulses was periodically confirmed during experimental sessions by means of a custom 100× isolated amplifier that magnifies the stimulation current on a digital oscilloscope (TDS-210, Tektronix). These trains were initiated by manual experimenter control, and were delivered while the monkey was at rest.

5.2.4 Analysis

Trial alignment As in Chapter 4.
EMG data preprocessing As in Chapter 4.
Trial selection As in Chapter 4.
Data reconstruction As in Chapters 1-4.
Synergy extraction As in Chapters 1-4
Synergy set selection As in Chapter 4.
Synergy comparison As in Chapter 4.

5.3 RESULTS

Preliminary analysis of the behavioral data suggests that the monkey *was* able to compensate for some of the muscle-dependent forces. In the sample day shown in Figure 5-1, the monkey did experience difficulty reaching targets in the presence of the rhomboideus (Rho) dependent viscous force field, but its performance (as measured crudely but intuitively by the average duration of each movement, averaged over 32-trial bins) plateaued to a lower level of error by the end of the force epoch.

In general, days when this learning occurred also appear to be days on which the monkey was able to decrease the activity of the target muscle, thereby lessening or making isotropic the experienced forces (Fig. 5-2a). Consistent with the synergy hypothesis, these changes were associated with changes in the recruitment of other muscles that were not directly targeted. Particularly prominent modulations (Fig. 5-2b) were observed on fellow electrodes in the rostral trapezius, infraspinatus, medial biceps, and rostral short head of the triceps. Activity in the rostral trapezius decreased even though this muscle may be considered an agonist of the rhomboideus based on the similarity of its directional tuning, and thus to have been available as a "substitute" for the target muscle. Given the opposite tuning of several of these muscles, it appeared in this example as though the average direction of force application could have been conserved as a result of these modulations.

These changes appeared to be related to the pattern of attenuation or facilitation following cortical microstimulation. The most common trend that I observed in such microstimulations was a transient decrease in the activation of the targeted muscle. As shown in Figure 5-3, the muscles sympathetically modulated by the rhomboideus-dependent force field also appeared to undergo a synchronous modulation of activity during microstimulation. In this particular example, the sign of these modulations appeared to be related to each muscle's similarity of tuning to the rhomboid, and not to the *degree* of modulation shown by each (Fig. 5-3). This pattern is suggestive a rapid re-weighting of corticomuscular efferents, unconstrained by synergistic relationships between the muscles.

5.4 DISCUSSION

Although the results of my analysis are currently very preliminary, I have included this chapter because it represents an important and direct test of the synergy hypothesis. In particular, the synergy hypothesis does not disqualify the possibility that individual muscle modulation is possible (Fig. 5-1). Rather it constrains the manner in which such modulation might occur: modulation of the muscle's activity should not occur without "sympathetic" changes in its synergists, and complementary changes in other muscle patterns that may be required to stabilize the behavior despite the absence (or addition) of the targeted muscle. The initial analysis does at least suggest that individual muscles are not modulated in isolation of other muscles (Fig. 5-2b). Even simple, reciprocal modulation of agonist muscles is not observed. Rather, adaptation may involve coordination of both agonists and antagonists in such a way as to preserve the overall pattern, but not amplitude, of force production (Mussa-Ivaldi et al., 1985; Shadmehr, 1993).

This chapter is also important because it may help to relate my analysis of motor control and learning strategies at the level of muscle recruitment (Chapters 1-4) with the involvement of descending cortical control (Chapters 6-8). My finding that cortical microstimulation may reveal non-synergistic effects on muscles will be framed by a wider discussion of the mechanism of cortical microstimulation, and the relation of muscular and kinematic invariants evoked by microstimulation, in the next chapter. In Chapters 7 and 8, I will consider two additional techniques thought to have effects on cortical excitability.

I have also included this brief report because the paradigm is novel. Several previous studies have used real-time control neurophysiological sensorimotor signals including extracellular recordings from cortex (Fetz, 1969; Fetz & Finocchio, 1971) and functional MRI (deCharms et al., 2004). Electromyographical feedback, or "myofeedback" (Johnston & Lee, 1976), has received relatively little research but has been evaluated clinically for treatment of conditions including emphysema (Johnston & Lee, 1976), stroke (Shiavi et al., 1979), and myalgia (Vollenbroek-Hutten et al., 2004).

Overall, the clinical success of myofeedback has been limited. Possible reasons may include: 1) stability issues arising from surface (not intramuscular) EMG recording; 2) associated perceptions of pain; and 3) reliance on auditory feedback, which (in contrast to the sensorimotor feedback used here) has relatively little access to the motor system. In addition, the effects of clinical myofeedback training have

been observed to be nonspecific to target muscles (Lee et al., 1976). This evidence is consistent with my finding that the nervous system may be limited in its ability to modulate the activity of target muscles independently of other muscles.

Figure 5-1 Behavioral adaptation to a novel muscle-dependent perturbation paradigm. In this sample day, the monkey appeared to be able to adapt to a rhomboideus (Rho) dependent viscous force field (right) following an initial null-field baseline epoch (left), as measured simply and directly by its trial-binned movement time.

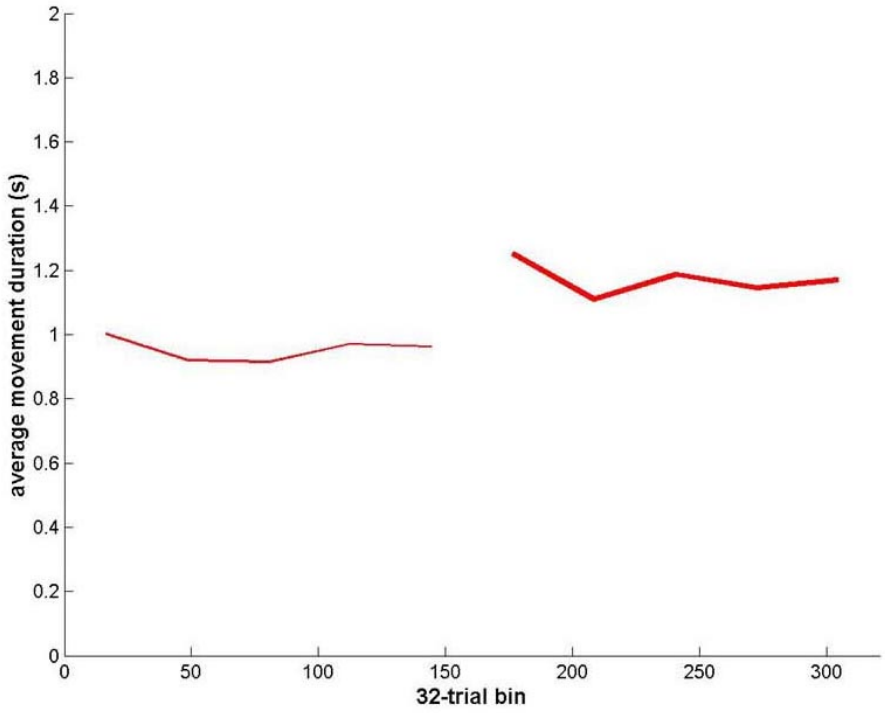

Figure 5-2 Attenuation of target and non-target muscle activity. **a**) Comparing the average degree of muscle activity in Rho in the second half of the baseline and force fields (using the same sample experiment presented in Figure 5-1), it can be seen that the monkey learned to attenuate its Rho activity, particularly in directions in which it was originally tuned. **b**) Several other muscles that showed large modulations in activity included rTra (rostral trapezius), iSpi (infraspinatus), mBic (medial biceps brachii), and rTri (rostral triceps brachii, short head). Of these, rTra demonstrated a similar attenuation of muscle activity, while the remaining muscles, tuned to opposite directions of movement, appeared to attenuate their activity in these directions in a fashion that may have balanced the overall direction of extrinsic force output by the monkey.

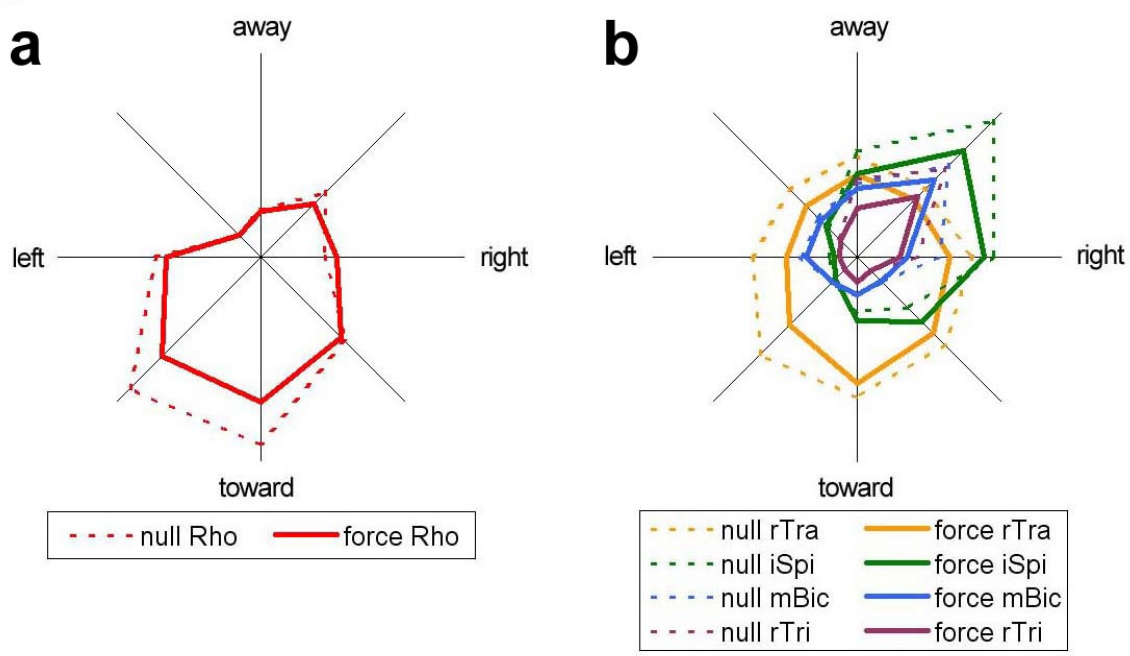

Figure 5-3 Relative attenuation of stimulation-evoked activity in target-aligned muscles. Following the experiment demonstrated in Figure 5-1, the five muscles in Figure 5-2 were also those that experienced the largest changes in activity following 40 ms of cortical microstimulation (at t = 0 s), here summed over 10 trains delivered at 5 separate sites. Perhaps relating to the tuning direction of each muscle, both Rho and the related muscle, rTra, displayed a common attenuation, while iSpi, mBic, and rTri displayed complementary facilitation.

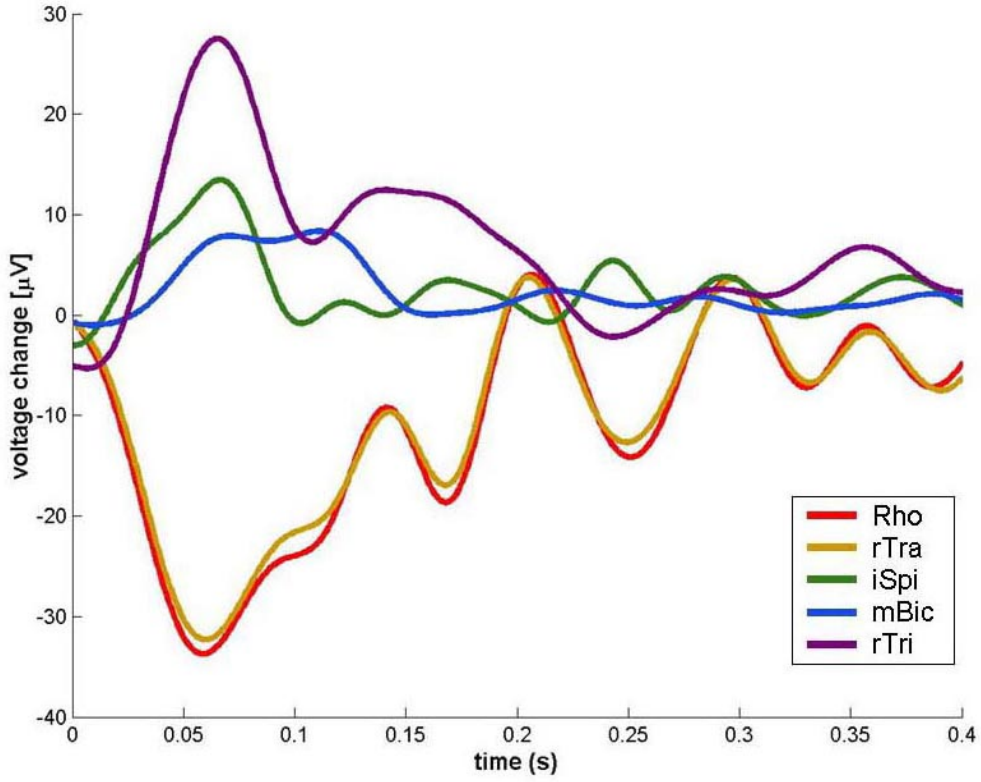

6 Convergent Movements Elicited by Stimulation in Motor Cortex

I review the historical antecedents of the synergy model, including both kinematically defined motor primitives and the more recent definition of primitves at a muscular level. I contrast both of these biologically-inspired and empirically-driven models with EMG/force control theories of motor function. I introduce my own evidence for a central encoding of equilibrium positions rather than invariants of muscle recruitment, in the form of motor cortical microstimulation results. Consistent with recent reports, I find that long-train stimulation elicits complex multijoint behaviors of the arm that tend to converge towards a single point in the workspace regardless of initial arm posture. I confirm many details of these reports despite the restriction of the monkey's hand to a planar workspace. I discuss the controversy surrounding the microstimulation parameters used to evoke these complex movements, and argue that the critical parameter, stimulation train length, may be critical for recruiting the spinal interneuronal pools that may be involved in organizing movements according to motor primitives. I also show that these kinematic invariants may describe the monkey's natural movements, by extracting time-varying synergies including both non-negative muscle, displacement, and velocity records from the monkey's center-out reach task performance under null-field conditions. Although these "musculokinematic" synergies are dominated by muscle channels, a small number of such primitives captures kinematic rather than muscular invariants. These basis movements consist of short velocity profiles and trajectories translocating the hand through the workspace (to points along the displacement axes, not to the targets the monkey actually reached towards), Only with additional numbers of extracted synergies did relatively kinematically-dominated muscle synergies emerge.

6.1 INTRODUCTION

6.1.1 Motor primitives defined as equilibrium postures

Previous chapters have found limited support for the muscle synergy hypothesis. I have shown that they are capable of explaining a sizeable amount of EMG variance; of providing compact information about behavioral conditions experienced by a monkey; of underlying distinct behaviors; and of being associated with an adaptive balance of activation coefficients over the course of learning. On the contrary, however, I have shown that time-varying synergies may be highly dissimilar between animals; that their generalizability across behavioral conditions may be highly sensitive to categorical differences between the conditions; that they may fail to capture small but meaningful changes in the relative phase or duration of muscle activations; and that they may change in structure as much as in coefficient modulation over learning.

Muscle synergies are only one definition of motor primitives. Earlier work by Bizzi and coworkers defined motor primitives and their combination at the level of force production within two-dimensional space. This elegant work showed that microstimulation of the premotor layers in the frog spinal cord lumbar grey matter tended to drive the hindlimb to discrete endpoint locations within the workspace around the frog, as inferred by isometric measurements of force generation at the

ankle when placed at multiple points around the frog (Bizzi et al., 1991; Giszter et al., 1993). Several such force fields appeared to be encoded in the spinal cord, suggesting a spinal map of invariant motor postures. Microstimulation at multiple sites in the spinal cord would lead to a linear superposition of these isometric "force fields" (Mussa-Ivaldi & Giszter, 1992; Mussa-Ivaldi et al., 1994). Similar experiments in the decerebrate or anesthetized cat have confirmed the conservation in mammals of spinally-encoded convergent equilibrium postures (Lemay & Grill, 2004).

These results suggested that spinal cord circuits could simplify postural control, and beyond this also movements and the learning of new movements (Mussa-Ivaldi & Bizzi, 2000), by specifying an "equilibrium point" as a linearly-interpolated position intermediate between hardwired endpoints around the organism. This idea extended well to the behavioral evidence collected from primates performing reaching movements. In particular, Polit and Bizzi (1978, 1979) found that monkeys trained to point to a seen target (without sight of the arm) were able to continue doing so after bilateral dorsal rhizotomy, even if the arm was displaced (unbeknownst to the monkey) at the beginning of the movement. The implication that the monkeys had coded the endpoint of the movement as a particular posture was further supported by the finding that the deafferented monkeys were unable to point to the target if the configuration of their body with respect to the apparatus was altered (Polit & Bizzi, 1979).

The equilibrium point idea was even able to describe stabilizing movements made by (intact) human subjects using a robotic manipulandum (Shadmehr et al., 1993), if not movements between targets per se (Lackner & Dizio, 1994). Convergent force fields were evident both in the "restoring" forces measured at the handle when the robot drove the hand in different directions away from a resting position (see also Mussa-Ivaldi et al., 1985), and in the static "evoked" forces measured when subjects attempted to move to a target but were prevented from doing so by sudden braking of the handle. The force fields were similar in either case, and consisted of individual force vectors that were not necessarily directed to the target posture or location (or of a magnitude dependent on displacement from the target) but were a function of hand position and arm configuration (Shadmehr et al., 1993). Hence the results suggested that (at least slow) hand movements in humans may be specified by shifts between arm postures, and not by a direct specification of trajectories between the hand and target.

6.1.2 Motor primitives defined as muscle synergies

The work described above focused on a dynamic, or force-related, description of motor primitives. Computationally, each postural primitive encoded in the spinal cord was hypothesized to represent a local minimum in an "energy landscape" (Shadmehr, 1993) defined by the potential energy of each agonist and antagonist muscle (and stored within the limb). Experimental measures of endpoint force fields would then reflect a joint "torque field" describing the gradient of this energy function with respect to joint angles (Shadmehr, 1993). This formulation did not require a close correspondence between muscle synergies and postural primitives. Shadmehr (1993) proposed that the nervous system could independently control limb position and stiffness by selecting a muscle synergy associated with a postural

primitive and then scaling its activation (without changing the location of the minimum in the resulting joint torque field).

In more recent modeling work, Berniker (2005) suggested that, while muscles in general are nonlinear actuators (i.e. in the dependence of their force output with muscle length and velocity), in the frog the forces generated by hindlimb muscles generally scale linearly with activation. In a physiologically realistic model of the frog hindlimb, he found that within the workspace of the hindlimb the muscles generally operated within a restricted, pseudo-linear range of their activation workspace. The linear, spinally induced isometric forces observed in the frog are a natural result of the linearity of muscle forces. But experimentally, while invariant patterns of EMG activation and force generation had both been observed following microstimulation in the frog spinal cord (Loeb et al., 1993), the finding of invariant, convergent force fields has not directly been shown to involve invariant, synergistic cocontraction of muscles (Bizzi et al., 1995).

The transition from earlier, kinematic demonstrations of motor primitives to studies of muscular synergies, again in the frog (Tresch et al., 1999; Loeb et al., 2000; Saltiel et al., 2001, d'Avella et al., 2003), may have several origins. For instance, computing power was originally unavailable to perform the computationally-demanding synergy extraction procedures. Investigators may also have shifted their interest to intact preparations rather than the deafferented frogs first characterized as having convergent force fields (e.g. Giszter et al., 1993). Perhaps most relevant was a renewed interest in motor primitives in movement and impedance control rather than posture and stiffness regulation (see Shadmehr et al., 1993), despite the great dynamical complexity required for postural behaviors (Hogan et al., 1987). Finally, investigators may have followed "force-control" formulations of motor control (Ostry & Feldman, 2003), which often assumes that the nervous system specifies EMG activity, or a directly related quantity, in order to generate desired force levels—as will be discussed shortly.

6.1.3 Central specification of muscle activity

Whatever the reason for the recent focus on muscle synergies and endpoint positional equilibria, these two notions have generally not agreed well with each other. The simplest explanation for this discrepancy—namely, that there is no one-to-one correspondence between measured EMG and posture (Ostry & Feldman, 2003)—appears sometimes to have been forgotten. When a limb is placed at different positions within the workspace, any given arm muscle may have zero EMG activity (Gottlieb et al., 1989; Suzuki et al., 2001); hence, EMG signals *cannot* be predicted from postural information. Conversely, any one position in the workspace may be associated with multiple combinations of muscle activation; hence posture *cannot* be predicted from EMG activity. This correspondence failure extends also to movements, where the transient EMG activity observed during transition of a limb can be a function of the original and final postures (e.g. Graziano et al., 2002a, 2004b), the particular trajectory of the limb between those postures, intrinsic limb impedance, joint interaction forces, and external forces acting on the limb.

Motor control models based on EMG activity and/or force production (rather than transitions between equilibrium points) generally posit that the central nervous system specifies motor commands—inferable from EMG signals—in the form of

desired muscle forces. These commands are thought to be translated from desired endpoint positions via inverse kinematic and inverse dynamic calculations (Ostry & Feldman, 2003). Indeed, EMG activity may vary with changes in applied force, once passive muscle resistance is no longer able to oppose the forces (Henneman et al., 1965; Desmedt & Godeaux, 1977). However, this is a feedback-dependent process rather than one that is solely centrally-driven—one that is not observed in deafferented patients (Levin et al., 1995). Proprioceptive feedback may also modify cortical excitability, further complicating the putative role of the central nervous system in specifying EMG outputs. The postural dependence of muscle activity is thought to be a result of changes in cortical excitability driven by posture-modulated proprioceptive afferents (Landau, 1952) as can also be inferred using transcranial magnetic stimulation in humans (Wasserman et al., see Maeda & Pascual-Leone, 2003).

Central specification of forces also appears to be absent in normal subjects during sudden unloading of the limb, when there is a transient, short-latency silencing of muscle activity (Merton, 1951; Angel et al., 1965). This silencing, even during rapid point-to-point movements (Adamovich et al., 1997), can be attributed to decreases in muscle spindle afferents accompanying muscle shortening, rather than interference with putative descending commands. To the extent that EMG signals are a measure of force generation, therefore, it is questionable whether the nervous system specifies these muscle activations and forces directly. This is particularly true given the immense computational challenge posed by the inverse kinematics, dynamics, fiber recruitment etc. problems.

6.1.4 Central specification of muscle thresholds

Alternative models to EMG/force control formulations have generally dealt with the non-correspondence of postures and EMG signals by treating the latter measure (if at all) as a byproduct of equilibrium point transitions. One classical resolution has been to treat an equilibrium posture as specified by a target level of coordinated elastic stiffness between multiple muscles. Movement between such postural primitives may then involve re-selecting this reference set of stiffnesses. This formulation has been key to explanations of impedance control in deafferented animals, in particular the "alpha" model of Bizzi et al. (1992). The idea that active muscle reflexes as well as muscle impedance may be determined by displacement from a set point of the muscles in intact organisms has driven the "lambda" model of Asatryan and Feldman (1965) and subsequent "threshold control" models of motor control (see Feldman & Latash, 2005). Notably, each of these models—unlike most EMG/force control schemes (Ostry & Feldman, 2003)—also offers a simple resolution of "Von Holst's paradox" (Von Holst & Mittelstaedt, 1950/1973), namely that movement exists despite the powerful EMG- and force-generating reactions that can follow any deviations from an initial posture.

I do not wish to enter any further into the debate between these "equilibrium control" schemes or between them and the "force control" schemes currently en vogue (Ostry & Feldman, 2003). Instead I simply wish to point out the problem faced by electromyographers: relative muscle stiffness and activation thresholds may be more direct measure of central control signals, but are not as easy to measure as is the propagation of action potentials through muscles. EMG activity may correlate

with movements (if not postures before and after movements), but it does so in a highly nonlinear fashion that is very much dependent on a host of other motor variables, and may thus make it an inadequate metric of descending motor commands. This appears to be the case even if these central signals take the form of direct muscle activation commands (as in the EMG/force control formulations), rather than instructions to change the target limb impedance and/or thresholds for reflexive muscle activity (as in equilibrium point formulations).

6.1.5 Synergies organized around centrally-specified endpoint equilibria

In previous chapters I have attempted to circumvent the mis-correspondence of EMG activity and kinematic variables by controlling for some of these parameters. In the reach task, in particular, the movement origin is equivalent between trials, and trials begin and end with zero velocity. In the grasping task the movement origin and endpoints were equivalent at the level of the arm, and the movements generally began and ended with the hand devoid of the grasped object so it is at least possible that there was some consistency of hand postures at the termini of each trial. Here, instead, I attempt to investigate a more central specification of motor plans by examining the movements that result from microstimulation within monkey sensorimotor cortex. I leave the topic of cortical encoding to the Discussion and to subsequent chapters. But to anticipate these considerations I show here that sensorimotor cortex may encode movement endpoints in much the same way as the frog spinal cord may encode convergent force fields.

Extending this work, I also consider the involvement of stereotyped muscle activity in these evoked movements, measured simultaneously with the movements themselves. In particular, I consider an expanded definition of function muscle synergies that incorporates invariants both at the muscular and the kinematic levels. This synergy model includes both muscle channels, and non-negative endpoint displacement and speed profiles in both negative and positive x and y directions in the workspace. Related definitions of time-varying sensory-motor primitives (Todorov & Ghahramani, 2003) and time-invariant force-muscle "functional synergies" (Torres-Oviedo et al., 2005) have similarly been proposed. The division used here between both positive and negative displacement and speed allows each quantity to express distinct relationships with simultaneous muscle activity, which is expected not only to reflect movement intention but to vary with position in the workspace, displacement from equilibria, movement direction, and movement speed.

As a simple test of this "musculokinematic" synergy model, I extracted time-varying synergies from the data recorded during null-field center-out reach movements of the arm. I predicted that the extracted synergies would define invariant movements towards a discrete set of locations in the workspace.

6.2 METHODS

6.2.1 Subjects

As in Chapters 4-5. The sole subject (female, 10 a.) was the same as subject R1.

6.2.2 Paradigm

Reach task On each day of recording, the monkey first performed between one and three 160-trial epochs using the robotic manipulandum (as described in Chapter 4). The first epoch, considered here, was always a null-field epoch. Following this epoch the monkey performed between trials in a non-null force field, either a viscous counterclockwise field or a "myofeedback" force field as described in Chapter 5. On 9 of the 13 days the monkey completed this condition, and continued on to a further null-field washout epoch (completing this epoch on 7 of the 13 days). I do not consider the data from these test and washout epochs in this chapter, or the influence they may have had on subsequent cortical activity (cf. Li et al., 2001) or on the results of cortical microstimulations done after the monkey had completed as many trials as it was willing to attempt. I only consider the EMG and kinematic data collected following these experimental sessions when I performed cortical microstimulation on the monkey.

Sessions I consider thirteen sessions performed on separate days spanning a three-week period (beginning 6.5 weeks after the monkey's EMG implantation surgery).

6.2.3 Recording/Stimulation

Craniotomy As in Chapter 5.
Dura maintenance As in Chapter 5.
Microelectrodes As in Chapter 5.

Microstimulation Repetitive intracortical microstimulation (R-ICMS) was performed as described in Chapter 5. Long-train R-ICMS was performed with parameters including 2×0.2 ms pulse duration, 200 Hz pulse frequency, 25-150 mA current, and 0.5 s train duration. Stimulation trains were delivered by manual experimenter control without warning to the monkey. However, I generally timed the trains to periods when the monkey sat calmly while holding on to the manipulandum, so it likely had a general awareness of when it was liable to receive stimulation.

Motor response determination I classified the motor response of each stimulation site by visual observation of which body part, if any, moved in response to stimulation. I made note of leg, torso, and digit movements, but used more specific terms to describe movements of the arm when these were clear—see Table 6-1. In some cases, e.g. when the microstimulations were applied near-threshold or when the monkey's arm posture had changed between trains, I was unable to be as specific. For this reason and for simplicity here, I have collapsed these arm movements into three gross anatomical categories: those acting at the scapular/Glenohumeral ("shoulder"), "elbow," or radioulnar/wrist ("wrist") joints. I generally repeated the stimulation train 5-10 times in order to determine the current threshold at which microstimulation could reliably evoke the response. I did not perform a sufficient number of these stimulations to find the exact threshold at which 60% of the trains could elicit the behavior (a standard criterion). Nor did I attempt to use fine gradations (< 25 μA) of current in order to attempt to identify the precise thresholds,

if indeed these existed. I did use on-line observation of EMG to guide my observations to the monkey's motor responses, but the unrecorded responses I report here are joint-kinematic and not muscular. In a few (<5) exceptions the microstimulations appeared to elicit complex but unreliable actions at a particular joint. I only include these sites with the other sites evoking motor actions at that joint if the pattern of elicited muscular activity or proprioceptive responses reliably confirmed my observations of the monkey's overt actions.

Muscle set As in Chapter 5. The twelve muscle implantations used here, as in Chapter 5, were a subset of the seventeen implanted in the monkey for the purposes of the recordings presented in Chapter 4.

Muscle implantation As in Chapters 4-5.
Electrode construction As in Chapters 4-5.
EMG data collection As in Chapters 4-5.

6.2.4 Analysis

EMG data preprocessing As in Chapter 5.

Synergy extraction I used the time-varying synergy extraction algorithm, as in Chapters 1-5. However, in this chapter I describe a slight variation of the procedure, wherein I combined the position and velocity traces with the muscle recordings prior to extracting "musculokinematic" synergies (see Introduction). The dataset on which this algorithm was applied were the thirteen complete null-field baseline epochs performed by the monkey on the same days that I performed the R-ICMS recordings outlined above.

Convergence estimation Rather than model the field of convergent movements as a summation of basis functions (Shadmehr et al., 1993), I used a geometrical algorithm to identify the approximate convergence of the trajectories. I did this by first dividing the workspace up into square cells (1 cm^2 to a side), and then by computing (at each grid cell) the displacement between it and each site where the hand was located at the beginning of stimulations (i.e. a "stimulation site"). For each grid cell I then computed the overall *displacement* vector at each cell grid site across all stimulation sites. I developed a similar vector sum of the population of *stimulation* traces, defined from the manipulandum endpoint position at the end of the stimulation trace (again, set at 250 ms after stimulation) to the endpoint position at the time the stimulation began. These two vector sums were defined both by radial and angular coordinates (i.e. in polar space). In the first case this vector sum was defined relative to each grid cell (and computed repeatedly over the entire workspace). In the second case this vector sum was defined relative to the stimulation sites (as if these sites were all overlaid) and was computed only once. After these vector sums were generated, I converted the vectors back to Cartesian space but with a radial distance of unit length. In doing so I restricted my comparison of the two sets of vectors to differences in their direction, not length. At each grid cell, therefore, I could compare the direction of the grid-cell-dependent displacement and the grid-cell-independent stimulation trace vectors, by computing the direct Cartesian

distance between the intersection of these two vectors and a unit circle around the grid cell. Because this Cartesian distance varied monotonically with vector direction divergence, I could simply locate the grid cell where this calculated divergence was minimal. This site I then identified as the convergence point.

6.3 RESULTS

6.3.1 Movements evoked by microstimulation

Repetitive microstimulation trains were applied to on 182 occasions to the sensorimotor cortex of monkey R1, spanning premotor, primary motor and somatosensory cortices. (These areas were estimated by sulcal borders visible during the craniotomy.) Most of these stimulation experiments were designed to provide a map of cortical motor and sensory responses in order to guide cortical recording (not reported here). These stimulations were performed at the end of behavioral recording sessions and each involved multiple microstimulation trains (330 Hz, 50 ms). Shown in Figure 6-1 are the subset of these stimulation sites where EMG and kinematic signals (n = 45) or EMG alone (n = 24) were recorded while I applied either these stimulation trains or longer trains (200 Hz, 500-ms). Of the sites where I recorded EMG and kinematic data, most (n = 42) were recorded while performing long-train R-ICMS. A crude lateromedial somatotopy can be observed, but the joints are clearly represented in a mosaical fashion. Along the orthogonal axis, more posterior sites appeared to require lower stimulation thresholds. (The apparent post-central extension of the low-threshold sites is a surprising finding that demands closer scrutiny of the monkey's sulcal anatomy, which currently awaits magnetic resonance imaging.)

When I applied the longer microstimulation trains, I frequently observed complex multijoint movements of the arm. Because the monkey in this study was very placid, it was possible to have it sit and hold the manipulandum handle calmly while microstimulation trains were applied. Even though the manipulandum handle was restricted to moving in a planar workspace, the evoked movements were often able to translate into movements of the robot. The first two movement records are shown in Figure 6-2. Even though the distribution of initial hand positions in Figure 6-2b was less uniform than in Figure 6-2a, the geometric method I introduced for calculating an approximate "convergence point" in the workspace appeared robustly able to do so. This was the case even though the movements were not straight and only brought the monkey's hand a short distance towards the convergence points. (As another confound visible in Figure 6-2, the circular extent of the manipulandum's reach constrained the hand movements to the right part of the workspace in each examples.)

The examples in Figure 6-2 coincidentally demonstrate some of the larger-amplitude movements elicited by this long-train microstimulation. The amplitude of the movements appeared to be independent of the stimulation current applied, at least when averaged across all sites chosen (Fig. 6-3). The amplitude of the movements did appear to relate to stimulation duration, with greater displacements elicited by long-train microstimulation. (Only at three sites did I test both of these types of stimulation, however, so it was not possible to directly compare the two

techniques.)

Considering only the long-train R-ICMS experiments, Figure 6-4 demonstrates that the population of evoked movements could be mapped cortically according to evoked movement amplitude, but not to locations in the workspace. In particular, it is evident in Figure 6-4b that the largest movements were elicted by relatively lateral (i.e. "ventral") and stimulation within primary sensorimotor cortex. There was otherwise little in the way of a mapping between the cortical distribution of these stimulation sites and the actual convergence point estimated for the sites. Within the workspace, there was also no evidence for a strong clustering of the convergence points, except that the largest-amplitude sites tended to lie directly in front of the monkey.

6.3.2 Structure of musculokinematic synergies

In considering the relation of EMG activity to kinematic variables, I combined the muscle activity data with transformed kinematic variables together coding non-negative displacement and velocity. The four resulting "musculokinematic" synergies shown in Figure 6-5a were able to account for 49% of the EMG and kinematic variance, a result comparable to the values reported in Chapter 4 with a smaller set of channels (and all of them derived from EMG electrodes) and fewer days of recording. Each appeared to describe a particular trajectory among the non-negative displacement dimensions, which could be converted back to Cartesian coordinates as in Figure 6-5b. The velocity profiles appear to describe bell-shaped movements like those seen in natural movements. However, note that the orientation of these trajectories did not align with the movement paths, which were spaced at 45° with an angular offset of 22.5° from the axes shown.

The EMG activity associated with these kinematic invariants was relatively similar between synergies, and appeared to involve less modulation of activity than synergies based solely on muscle activity (cf. Fig. 4-4). Only with extraction of higher numbers of such musculokinematic synergies (e.g. of eight synergies in Fig. 6-5c, able to account for 71% of the varince) do invariant patterns dominated by movement activity appear.

6.4 DISCUSSION

6.4.1 Kinematic characteristics of convergent movement fields

The movement vectors composing the set of responses to microstimulation generally converged (Fig. 6-2), but the movements themselves rarely reached a final position (cf. Graziano et al., 2002a). Possibly this incomplete convergence may be attributed to the non-negligible drag on the hand from the inertia and friction of the robotic arm. Graziano et al. (2005) similarly found that at least 26% of the microstimulation sites they tested were unable to evoke full convergence when the hand was loaded with a weight. Also, the movements I observed were restricted to a planar workspace, and the endpoints observed by Graziano et al. (2002a, 2005) generally occupied a three-dimensional workspace—hence the movements I observed may only represent a planar projection of those movements, themselves impeded by

the tether to the manipulandum handle. Similar reasoning could explain why the component movement vectors—like the isometric force field vectors measured in human subjects holding the manipulandum (Shadmehr et al., 1993) did not point directly towards the convergence point.

Interestingly, most of highest-gain convergent locations in the manipulandum workspace appeared to lie in the "central" region (Fig. 6-4a). It is possible that convergent locations more to the right of the workspace—spanning the most distal targets—would have been observed had we been able to access cortical sites located further laterally. But it is worth noting that Graziano et al. (2004a) found that about 40% of both microstimulation-evoked movements and natural movements generated by the monkey while in its cage kept the hand in, or brought the hand into, the central zone (defined both horizontally and vertically) in front of monkey. When the hand was observed to perform grasping or manipulation behaviors, the time spent in this central zone vs. the surrounding eight zones exceeded 50% (Graziano et al., 2004a).

The movement primitives I observed had a time-varying structure. A similar result was found in the central point of the convergent force fields obtained by long-train microstimulation in the frog (Giszter et al., 1993), and described as evidence for a "virtual trajectory." Such evolution has also been observed in corrective responses made by spinalized frogs as they encountered obstacles during rapid, aimed contralateral wiping reflexes (Kargo & Giszter, 2000). By comparing the frogs' kinematics and EMG with and without the obstacle and with and without feedback, Kargo and Giszter (2000) found that the corrective response (an added hip flexion) was dependent on intact cutaneous afferents. Under isometric conditions, this response was shown to be a structurally invariant force field that could be scaled by obstacle force magnitude and time independently of the wiping reflex. Moreover, the "corrective field" itself had temporal dynamics, changing in its component vector directions even as its overall duration (~0.5 s) was relatively fixed.

In contrast to Graziano et al. (2002a), I was able to achieve different starting postures in the monkey while it was actually at rest, not while it was performing a simple task designed to bring the hand to different parts of the workspace. (I rejected from the analysis those few cases where the monkey started to move its hand just before the stimulation train began,) As a result, I was able to exclude prior movement as a confound in the interpretation of the muscle activity.

6.4.2 Cortical relationship to convergence points

The cortical topography of the responses I observed did not have a clear, linear relationship to the planar workspace of the monkey. This finding is not inconsistent with the crude topography observed by Graziano et al. (2002a), who divided their cortical map of endpoint locations into "lower," "middle," and "upper" space in a 3D region around the monkey. Once again, the workspace in this experiment was at best a planar projection from this more complicated 3D map. For one monkey, Graziano et al. (2002a) also showed the "horizontal" topography of the hand and arm postures. Like me, they show that contralateral space (here, the left side of the manipulandum workspace) is represented more anteriorly (towards the arcuate sulcus) while the "central" region in front of the monkey is represented on the caudal portion of the precentral gyrus and the ipsilateral region is represented just as

posteriorly but also more laterally. Graziano (2005)'s maps appear to have even less clear-cut vertical- and horizontal-space topography, but the cortical representations divide relatively neatly into "hand-to-mouth," "defensive-like," "central space + finger movement," "reach," "leg + arm," "saccade," and "no movement" categories, all of which I was not able to distinguish using the manipulandum encoder data.

Like Graziano et al. (2002a), I have combined microstimulation results from premotor, and primary motor and rostral somatosensory cortex, finding no sharp divisions between these regions in terms of endpoint locations. Indeed, by other sensorimotor measures—threshold current amplitude, evoked movement amplitude, multi- vs. single-joint movement, proprioceptive responses, cutaneous responses, size of somatosensory receptive field—these regions appear to be divided only by slow gradients of encoding. As suggested by Graziano et al. (2002b), primary and premotor areas may be defined by a continuous map of manual space.

Whether the data shown in Figure 6-4a indicate a clustering of convergent points beyond the predominance of these points directly in front of the animal. But at least it does appear to be the case that the responses did not all lie along the edge of the workspace—as might be predicted from a simplistic assumption of directional tuning in motor cortex. The encoding of motor variables by motor cortex remains a controversial topic. Two prominent and competing schemes have suggested that the cortex either codes for movement end point locations or postures (Polit & Bizzi, 1979) or for movement direction (Rosenbaum, 1980). The latter viewpoint is now more widely accepted, generally because of experimental results based on the relation of cortical firing to movement variables observed under controlled conditions. For instance, Georgopoulos et al (1985) found that in out-center movements, m1 and area 5 cells fired according to direction and not the central end-point. However, in this case only a single end-point was tested. A proper test of different candidate coordinates may require a much richer sampling of these dimensions (Ajemian et al., 2001).

One consequence of assuming directional encoding was discussed in Chapter 4, where the apparent rotation of neural and EMG "preferred directions" along with a curl field conceals the more likely relationship between these variables and movement dynamics. Of particular relevance to the current literature on neuroprosthetic control, simple linear models of positional encoding (e.g. Ashe & Georgopoulos, 1994) have likewise implied untenable physiological assumptions, for instance that neural activity relating to arm control scales linearly with the position of the hand in the workspace, even to the extremes of the workspace. Our data suggest that the biologically no less plausible possibility of endpoint encoding by re-evaluated.

6.4.3 Validity of high-current, long-train microstimulation

In applying cortical microstimulation, researchers have traditionally used short train durations and sub- or per-threshold currents in order to map the overt response of corticomotoneuronal cell populations. The maximum current applied in such studies has been reported as 10 μA (Asanuma & Rosén, 1972); Cheney et al., 1985; Baker et al., 1998); 25 μA (Sato & Tanji, 1989); 30 μA (Strick & Preston, 1978a; Bennett & Lemon, 1994; Nudo et al., 1996); 40 μA (Lemon et al., 1986); or 60 μA (Donoghue, Leibovic & Sanes; 1992). Other parameters are generally more constant. In particular, the stimulation pulses reported above were all 0.2 ms in duration

(usually cathodal or occasionally biphasic, with the "negative" or depolarizing phase first) delivered at 300-400 Hz, for a duration lasting 10-20 pulses—i.e. in the range of 25-70 ms. Trains of much lower-frequency (up to 15 Hz) pulses have also used to perform stimulus-triggered averaging of EMG in response to an injected current without much likelihood temporal summation of the pulse effects (e.g. Cheney & Fetz, 1985; Cheney et al., 1985; Baker et al., 1998; McKiernan et al., 1998; Park et al., 2001).

The studies listed above neither sought nor reported convergent movement fields of the sort reported here and by Graziano and coworkers. Like them I have used long-train (typically 500 ms), high-current (up to 150 μA) pulses of 0.2 ms delivered biphasically at a typical rate of 200 Hz with the negative phase first. (In the published work there was some minor variation in pulse frequency and phase [Graziano et al., 2002a] and in train duration [Graziano et al., 2002a, 2004b]). Graziano's results, and the parameters used to find them, have naturally aroused some controversy (see Strick, 2002). One purpose of this project, in the proper scientific tradition, was therefore simply to replicate their results. I take this goal as having been well-accomplished, given the results discussed above—particularly given our planar restriction on movements.

In addition, there is historical precedent for these results of cortical microstimulation (besides the obvious parallels with spinal microstimulation in the amphibian; Giszter et al., 1993). Although other parameters of the microstimulation (e.g. electrode location, stimulation duration) and the species (cat) were quite different from those used here, Clark and Ward (1937) and Ward (1938) showed that motor cortical stimulation would evoke posture-dependent leg movements that seemed to drive the leg to a particular point in space. Whether the motor cortex is essential for driving these convergent movements is not clear (see Strick, 2002). For instance, similar patterns of movement have been observed (again in the cat) by medullary stimulation of the pyramidal tract (Landau, 1952).

Nevertheless, a further discussion of the validity of the microstimulation parameters that we have used is in order. Graziano et al. (e.g. 2002a) have emphasized that 500-ms stimulation trains are appropriate given that this time scale approximates that of the natural reach and grasp movements made by the monkey (e.g. Georgopoulos et al., 1986; Reina et al., 2001). Researchers using microstimulation to study oculomotor and somatosensory systems have similarly used relatively long trains. For instance, 400-ms trains were been applied to the arcuate sulcus to replicate the time scale of typical regular head movements (Freedman et al., 1996), and 500-ms trains were applied to primary somatosensory cortex to mimic a tactile stimulus (Romo et al., 1998), Shorter stimulation trains, as in Graziano et al. (2002a) and in my own data, appear to elicit truncated and incomplete movements, relative to those elicited with 500-ms stimulation. Giszter et al. (1993), in their original finding of convergent force fields coded in the frog spinal cord, similarly used long-train (typically 300-ms) microstimulation, albeit at lower frequency (40 Hz) and current (1-8 μA) than used in the primate microstimulation trains reported here and by Graziano and coworkers.

As for the relatively high stimulation currents used to elicit these complex movements, such large currents are likely to activate a cortical territory far outside the 100-μm radius assumed for about 10 μA stimulation (Ranck, 1981; Yeomans, 1990). Nevertheless, currents of up to 150 μA have been used by neurophysiologists

studying the oculomotor system, e.g. to classify particular populations of neurons in frontal eye fields such as visual neurons vs. presaccadic neurons (Bruce et al., 1985; Gottlieb et al., 1993). Graziano et al. (2004b) has also used 30-μA currents to show, as I have done above, that EMG activity (in the biceps and triceps muscle) following microstimulation in primary motor cortex is a function of arm posture. (It should also be noted that in all of these experiments only the *maximum* currents used reached 150 μA, and not necessarily the individual currents which were as low as 25-50 μA.)

Furthermore, Strick (2002) suggests that microstimulation with relatively high currents may be uniquely required to activate non-direct connections between motor cortex and spinal motoneurons. Connections by networks of propriospinal neurons in the cord may be particularly involved in mediating the convergent force fields observed in the spinalized amphibian (Giszter et al., 1993). It should be noted that the relative contribution propriospinal pathway in the primate may be small, e.g. as compared to the cat following lesions of the corticospinal tract at the C5 dorsolateral funiculus in each (Maier et al., 1998). Nevertheless it may be that the stimulation parameters used by Graziano and coworkers, and in this project, are in fact required to activate and study spinally-encoded primitives.

6.4.4 Systematic variability of EMG activity following microstimulation

In testing the "musculokinematic" synergy model (Fig. 6-5) l, I indeed found that the extracted synergies define invariant movements towards a discrete set of locations in the workspace—even though these did not correspond to the actual targets reached to by the monkey. The muscle activity in these synergies bore even less relation to the expected pattern of phasic bursts. Small numbers of musculokinematic synergies reflected relatively unvarying muscle activity, both within and between such primitives. This result might be interpreted as showing that—to the extent that muscle activity covaried with movement in this task—the monkey simply used similar muscles (e.g. rTra, rTri, aDel) to get to the left and right parts of its workspace, and similar, mostly overlapping muscles (e.g. Rho, sSpi, aDel) to get to the top and bottom parts of its workspace. What changed may have been the balance of stiffness, viscosity, activation threshold etc. between muscles.

I do not claim that the nervous system actually uses such motor primitives, though in the context of "sensory-motor primitives," the displacement and velocity signals I included might be interpreted either as sensory signals (e.g. the muscle spindle afferents) or as movement goals. My purpose in performing this analysis was merely to document whether invariance in the reach task was more a feature of the muscular recruitment or the kinematic patterns. I am not the first to claim that EMG activity during movement is dependent on limb configuration—a finding previously shown in microstimulation studies (see Lemay & Grill, 2004). One future contribution of the microstimulation dataset I have collected, despite the planar restriction of the hand and its measurement, may be in its combination of large numbers of EMG channels with the kinematic recording.

Table 6-1 Biomechanical scheme used to classify microstimulation evoked movements. Note that these movements were broadly grouped into those involving the "wrist" (as well as the radioulnar joint), the elbow, and the "shoulder" (including glenohumeral and scapular movements, insofar as these could be distinguished).

joint	*motion*
wrist	flexion/extension
	ulnar/radial deviation
radioulnar	supination/pronation
elbow	flexion/extension
glenohumeral	abduction/adduction
	flexion/extension
	horizontal flexion/extension
	internal/external rotation
scapular	elevation/depression
	protraction/retraction
	upward/downard rotation

Figure 6-1 Map of microstimulation sites according to joint and current threshold. In particular, I represent each recorded stimulation site (n = 69) according to the joint(s) where I reliably observed evoked movements (color), according to the legend shown. I simultaneously plot the sites according to the inverse current threshold needed to evoke these movements (diameter)—hence the size of each circle can be thought of as the "gain" of the stimulation. Sites with no reliable evoked movement (even at 100+ μA) are represented by × symbols, and occurred more anteriorly. Estimated sulci include the arcuate (anterior) and central (posterior). The recording chamber was centered at AP = 17.0, ML = 15.0. Grey cells indicate the cortical region accessible through the chamber.

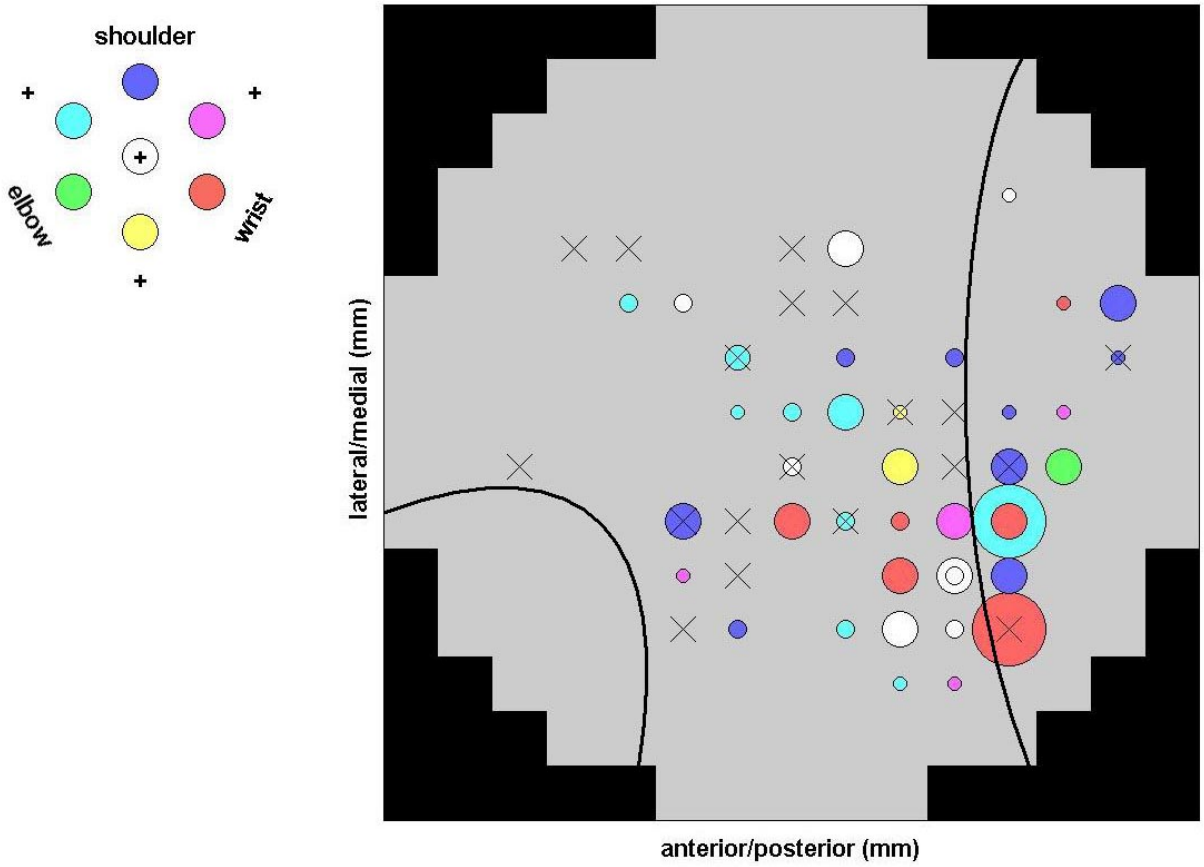

Figure 6-2 Long-train microstimulation evokes convergent movements. Panels **a**) and **b**) show two sets of evoked movements that followed microstimulation trains applied to two cortical locations on the same day. In both plots, the position of the hand at the time of microstimulation is shown as the brightest red dot. The progressively darker trace represents the position of the hand recorded over the following 250 ms. The thin black lines give the position of the hand during freely moving behavior (while still connected to the manipulandum handle) over the cumulative several minutes that elapsed between microstimulations at each site. The "convergence points" (see Methods) are projected as blue circles.

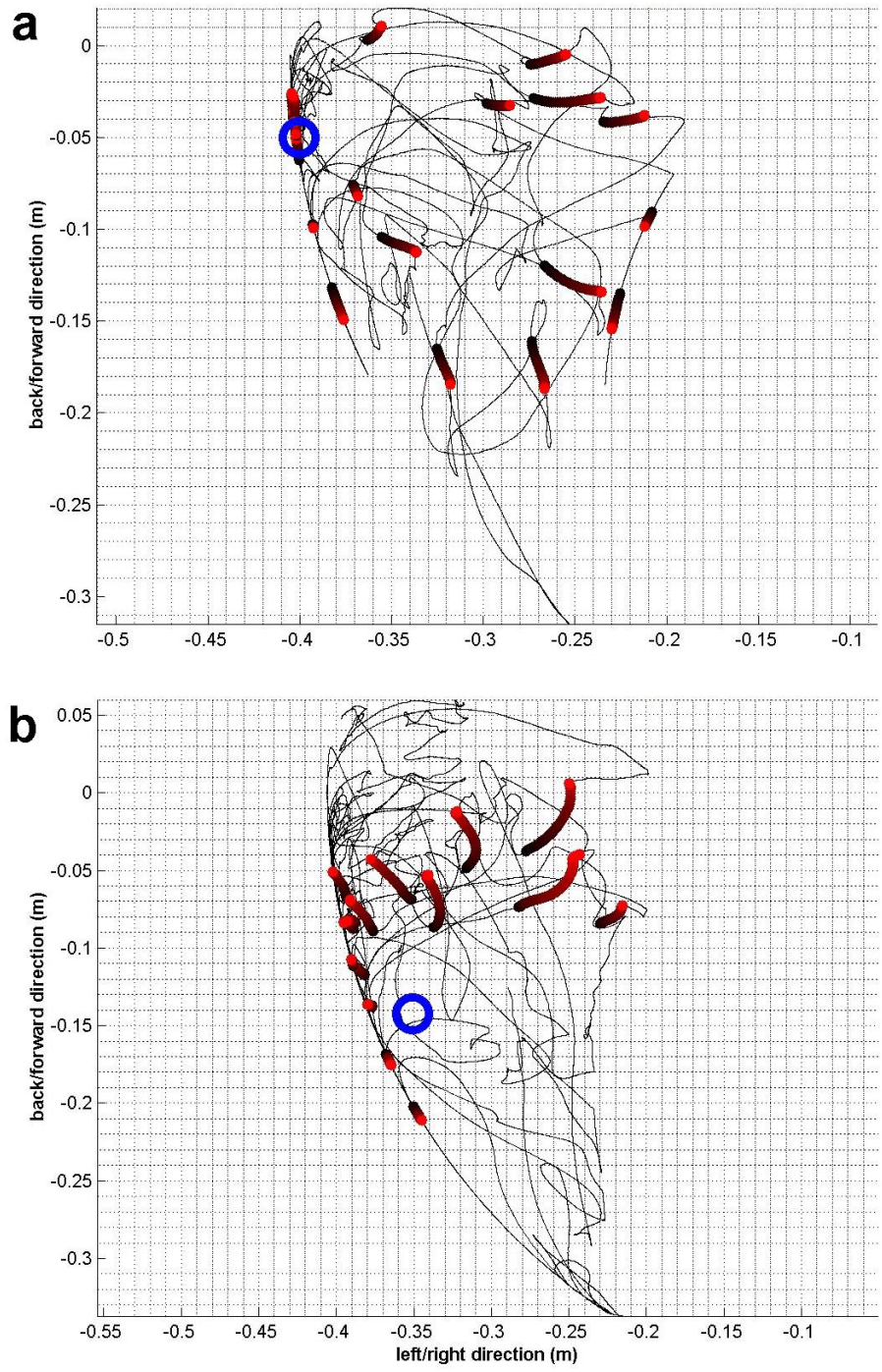

Figure 6-3 The amplitude of evoked movements was not a function of current applied. The average displacement of the hand over multiple microstimulation-evoked movements is plotted vs. the long-train R-ICMS current used to elicit the movements (not the current threshold).

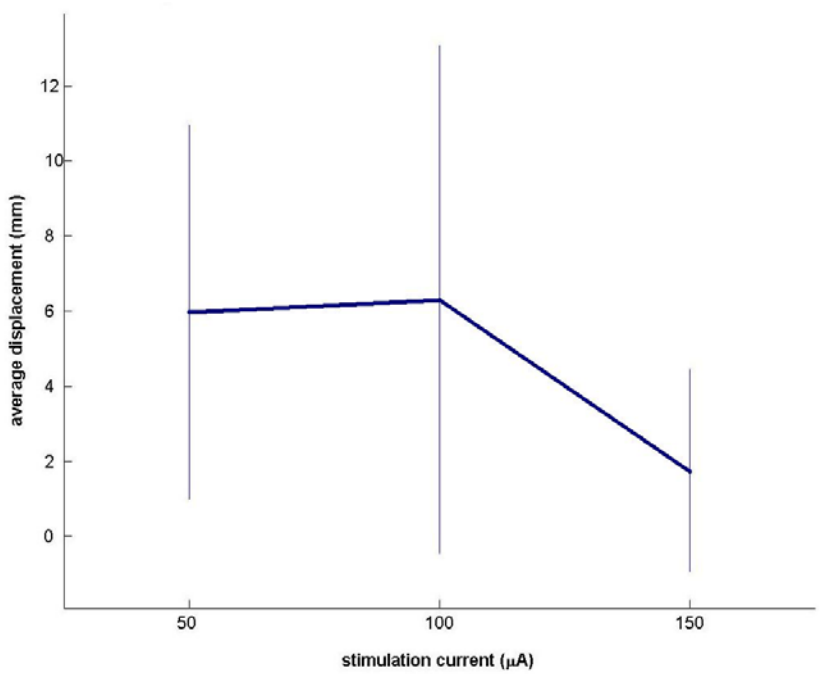

Figure 6-4 Convergent positions distributed in the workspace and over cortex. Shown for all recorded trials using long-train R-ICMS (n = 45) are **a**) the convergence point estimated for the movement and **b**) the cortical distribution of these same convergence points. The colors in a) were chosen arbitrarily to span the planar workspace with two color dimensions (x: red, y: green). The diameter of each circle is proportional to the average displacement amplitude evoked by the microstimulation trains. The square symbols in a) represent the locations of the targets experienced by the monkey in the context of the center-out reach task recordings (Chapters 4-5, 7) but not experienced here.

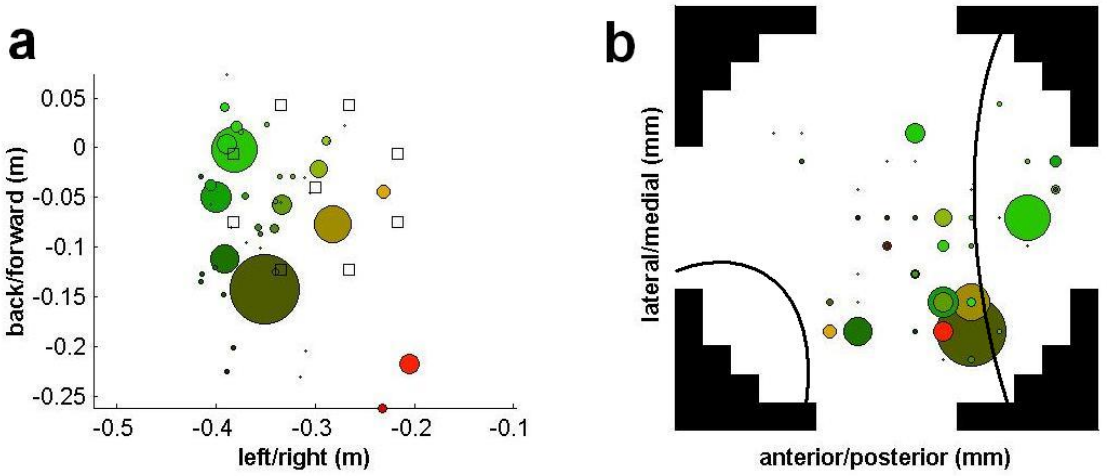

Figure 6-5 "Musculokinematic" synergies. **a**) Four 1-s synergies derived from the EMG and transformed kinematic data collected from monkey R1 as it completed null-field trials. The muscle intensity is coded by the reference bar at right. **b**) The trajectories encoded within these synergies, within the workspace of the manipulandum. **c**) Eight synergies extracted from the dataset. Channels were normalized to the same peak level of activation prior to extraction of synergies.

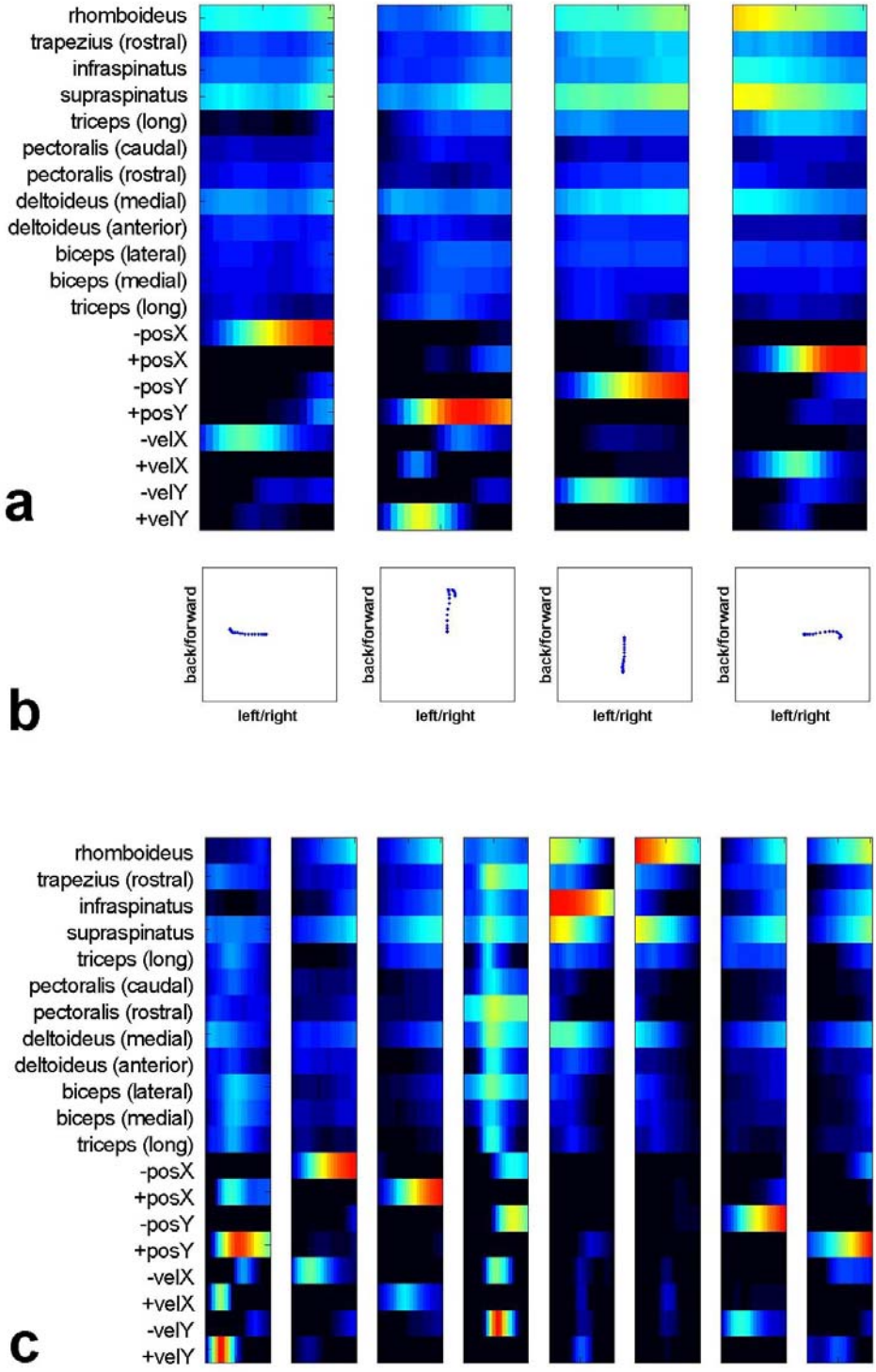

7 tPA Disruption of Acquired Adaptation in Motor Cortex

In this pilot study, I applied tPA (tissue plasminogen activator) to the MI arm representation in a single macaque as it learned to make reaching movements under a clockwise curl force field applied by a robotic manipulandum. The monkey had extensive prior experience performing under null-field conditions, which were repeated for a first epoch of 160 trials each day of recording, prior to a 160-trial force field epoch. The tPA was administered over a ten-day period separated by five days before and after from ten-day control periods, when the monkey performed the same task under similar conditions but without receiving tPA. tPA was infused at a fixed rate during force-field practice, via custom canulae to up to four sites per day. These sites wre chosen so as to span the bulk of the MI arm area (as assessed through earlier cortical mapping). The canulae were lowered along with microelectrodes in order to ensure they were lowered into cortex. Due in part to difficulty penetrating the dura, application of tPA may have been limited to 15 of the 40 canulae lowered over the experiment, most of them during the final five days of the ten-day per-tPA period. The monkey's performance, gauged by the signed deviation area of its movements, reached a stable level by the end of the control period. The error was non-zero, possibly related to the presence of catch trials in the force epochs. When the tPA was introduced, the most evident behavioral variable observed to change was the monkey's general ability or motivation to complete trials under the force field. Its null-field performance was spared. When the monkey returned to the task following the per-tPA period, its performance on both the null and force field conditions did not demonstrate lasting impairment. Various experimental confounds are addressed to discuss the lack of a behavioral enhancement. Another explanation of the findings may be that the monkey's more recently-acquired clockwise field learning was more sensitive to the effects of tPA than was the robust null-field performance.

7.1 INTRODUCTION

While non-forelimb movements may be synergistically encoded at the level of the spinal cord (e.g. Saltiel et al., 1998) there is evidence that a distributed control system in the cortex (Schieber, 1996) is directly and uniquely responsible for muscle activation patterns of the primate forearm. Beyond the extensive sensorimotor cortex area devoted to the hand, anatomical and electrophysiological studies in monkeys further suggest that the motor cortex sends monosynaptic projections to the forelimb motoneurons (Lemon, 1993). Beginning with this chapter I therefore turn my attention from the muscular basis of motor control and learning to the level of the central nervous system.

This chapter describes a pilot study that was designed to test whether motor cortical application of a pharmacological agent shown to be involved in synaptic plasticity (see below) could enhance primate motor learning. Tissue plasminogen activator (tPA) is a serine protease that converts plasminogen to its active protease form, plasmin, which in turn degrades numerous substrates. tPA or its derivatives are commonly administered for lysis of fibrin clots following thrombotic strokes to help restore blood flow. Endogenous tPA is widely expressed in the human and rodent central nervous system (Friedman & Seeds, 1994; Tessalu et al., 2004). In the mouse

central nervous system, tPA functions range from neuronal development (Seeds et al., 1999), neuronal plasticity (Qian et al., 1993), and excitotoxic neuronal cell death (Siao & Tsirka, 2002).

The onset of long term potentiation (LTP), a proposed mechanism of synaptic plasticity, is characterized by the transcriptional induction of immediate early genes. tPA was identified as an immediate early gene that is elevated after LTP (Qian et al., 1993). Inhibition of tPA prevents the late phase of LTP (L-LTP) in the hippocampus while application of tPA or overexpression of tPA in transgenic mice enhanced L-LTP and improved performance in spatial orientation learning tasks (Baranes et al., 1998; Madani et al., 1999). Recent research has shown that the LTP-enhancing effect of tPA is via its interaction with two molecules: the NR1 subunit of the N-methyl-D-aspartate (NMDA) receptor and brain derived neurotropic factor (BDNF). tPA has been shown to cleave the NR1 subunit of the NMDA receptor leading to a potentiated calcium influx (Nicole et al., 2001). tPA, via plasmin activation, converts the precursor proBDNF to its mature form, mBDNF, which is in turn critical for L-LTP expression in mouse hippocampus (Pang et al., 2004).

Apart from its effects in the hippocampus, tPA has been shown to play an important role in cerebellar motor learning (Seeds et al., 2003). tPA expression was induced specifically in the cerebellum of normal mice during the early stages (within the first 4 hours) of learning on a complex peg walking task. Knockout mice lacking the tPA gene were impaired in their rate and extent of motor learning compared to their wildtype and heterozygote littermates. It is not known whether cerebellar LTP requires tPA activity but the results of Seeds et al. (2003) suggest that the role of tPA in the cerebellum is similar to its role in the hippocampus. Little work has looked at the involvement of tPA in cortical plasticity (Mataga et al., 2002, 2004), and none in primate or motor cortical systems. In this pilot study, therefore, tPA was infused over a wide swath of arm-related motor cortex over the course of several days of learning on the conventional center-out reach task with clockwise curl forces (much as in Mataga et al., 2002, 2004).

7.2 METHODS

7.2.1 Subjects

As in Chapters 4-6. The sole subject (female, 10 a.) was the same as subject R1.

7.2.2 Paradigm

Reach task As in Chapters 4-5.

Epochs As in Chapter 4, the first two epochs of trials were a null-field baseline epoch and a test epoch with forces. In this experiment, however, the monkey was only allowed to complete these two 160-hit epochs (a baseline and a test epoch). tPA administration was consistently begun within the first minute of the test epoch, except on the first two days of the ten-day tPA period, when no tPA was administered (and when the monkey was not yet sufficiently motivated to complete both the baseline and test epochs).

Sessions The monkey's last exposure to the clockwise force field (consisting of five days of consecutive practice on a slightly weaker version of the field) had occurred over 11 weeks prior to the recordings presented here. Particular care was taken to match the control (no tPA) and tPA periods. Prior to the tPA administration, there were two ten-day control periods. (Initially only one such period was planned, but a review of its data following the first control period indicated its performance had not yet plateaued.) Following the single ten-day tPA period, the monkey performed the task for a final ten-day period. Each of these ten-day periods was separated by a 5-day rest period including ad lib water access and dura maintenance procedures. Each day of recording I would allow the monkey up to three hours to complete as many hits (up to 320) as it could. In the tPA administration period I stopped the experiment after 320 hits had been completed or if the monkey had stopped working for ~30 min. Performance of the full 320-hit experiment would reliably earn the monkey a bonus food reward.

Targets As in Chapters 4-5.

Forces As in Chapter 4, except that the force field was a clockwise curl field. The forces, of magnitude 6 N·s/m, were calculated on-line as $f = \mathbf{B}\dot{x}$, where $\mathrm{B} = \begin{bmatrix} 0 & 6 \\ -6 & 0 \end{bmatrix}$ and $\dot{x}$ was the movement velocity. "Catch trials" (trials on which the motors are suddenly turned off just as the target is presented) were used as described in Chapter 4.

7.2.3 Recording/Stimulation

Kinematics As in Chapter 4.
Craniotomy As in Chapter 5.

Canulae tPA was initially (on days 3-5 of the tPA period) delivered via commercial infusion canulae (Plastics One). As these easily succumbed to distal bending upon first or repeated contact with the monkey's dura, I manufactured custom stainless steel canulae, using 28-gauge (O.D. 0.028", I.D. 0.020") and 22-gauge O.D. (0.014", I.D. 0.010") tubes. Similar but wider stainless steel guide tubes were additionally used to protect the canulae from buckling. These were delivered to the cortex via a custom microelectrode grid made of clear plastic, with grid holes restricted to one half of the grid in order to permit (limited) visibility of the dura surface during its penetration by electrodes and canulae.

Cortical penetration Each canula was paired with one vinyl-coated tungsten microelectrode spaced 1 mm away along the grid surface. One microelectrode/canula at a time pair was lowered through the cranial recording chamber, using manual screwdriver action. Contact with the dura surface was indicated by an increase in resistance to the screw's progress. Cortex was recognized by an increase in the background incidence of "crackles" on a speaker receiving input from the microelectrode. In addition to audio monitoring of the cortical amplifier, cortical

acquisition software was used to help identify isolated neurons given a consistent and above-threshold waveform. Microelectrodes sometimes could penetrate the dura; these were subsequently confirmed by visual inspection either to have become bent or pushed back up through the microdrive. When a microelectrode was unable to reach the dura, I would nevertheless drive both it and its partnered canula to a depth 0-4 turns below the depth(s) at which I had reached the cortex with any of the other microelectrodes being lowered that day. With only one possible exception, the custom-made canulae always penetrated the dura. The saline layer was recognized by a drop in noise, since it is conductive.

tPA preparation Over the course of the tPA period I supplemented an initial supply of pre-dissolved and frozen 2-chain recombinant human tPA (American Diagnostica Inc.) with a lyophilized powder form that could be reconstituted by dissolution into sterile or 0.22 µl filtered deionized water. Before use, the tPA was diluted with room-temperature sterile injection water to a concentration of 0.08 µg/µl. Each day I prepared about 1.2 ml total of the diluted solution, i.e. 0.6 ml for each of two 1-ml syringes used for delivery. (This amount included an empirically-determined 0.35 ml to flush each set of tubes with tPA solution in place of the saline, a further minimum "overhead" of 0.1 ml to occupy the syringes when mounted in the pump due to the presence of adjustable stops, 0.04 ml to be injected into the monkey, and 0.1 ml of additional solution to buffer against inadvertent loss.) The delivery tubing (Plastics One) was flushed with room-temperature saline prior to each recording session. Each tPA syringe was inserted into the proximal end of a long (60-cm) tube, the distal ends of this tubing already having been fitted with two, two-way splitters (Plastics One) and four short (6.5 cm) lengths of additional tubing. These short tubes were then connected to the proximal ends of the canulae mounted on the grid. I confirmed that the saline could flow into each canula with minimal and equivalent resistance. After the diluted tPA solution was drawn into each of two 1-ml syringes, these being fitted with two additional blunted 20-gauge needles, 0.35 ml of tPA solution were slowly injected from each into the tubing, or more if necessary in order to set the plunger in each syringe to the same starting volume of tPA solution within the syringe. Visual confirmation was again made to ensure that fluid could pass through each canula.

tPA delivery The syringes were then attached to the canulae and loaded into a syringe pump apparatus (Harvard Apparatus). This pump allowed the tPA solution to be automatically administered from each syringe at a constant infusion rate of 20 µl/hr (i.e. not to constant target volume). The most solution that could be introduced at any one of the four target sites was thus 10 µl per hour, or 20 µl over the maximum 1.63 hr that the monkey performed in any one day's force epoch during the tPA experiment. Given the 1:10 dilution of the tPA solution, this corresponded to a maximum of 2.0 µg of tPA administered at any one site on a given day.

Performance error The monkey's performance was characterized by the signed (clockwise minus counterclockwise) area of its trajectory relative to a straight line connecting the beginning and end of its movement. The error was summed over all

directions and 8-hit sets defining either the baseline or test epoch. Catch trials were included along with other trials.

7.2.4 Analysis

Trial alignment As in Chapter 4.
Trial selection As in Chapter 4.

7.3 RESULTS

7.3.1 Application of tPA

Figure 7-1 depicts the sites over sensorimotor cortex selected for tPA delivery. Several months of motor and somatosensory response mapping had revealed both a large extent of arm-related cortical territory, and a continuum of sensorimotor response (Fig. 7-1a). Both the expected lateromedial somatotopy and the anteroposterior motor/sensory axes were broadly confirmed. The tPA sites were chosen to span the arm-related portion of this cortical map as widely as possible within the eight days during which the tPA was delivered (at up to four sites per day). The interleaving spaces were assigned to microelectrodes that accompanied each tPA canula at a distance of 1 mm.

Many of these microelectrodes, and some of the initial tPA canulae, were unable to penetrate the dura in spite of the regular dura "scraping" surgeries since the craniotomy six months prior. Effort was made to return to these blocked sites on subsequent days for further attempts at dural penetration, which were generally successful in the case of the tPA canulae used beginning on day 6 of the ten-day tPA period. Overall, I estimated that 25 of the 40 attempts were able to pass through the dura, although of these there may have been liquid flow problems affecting the tPA delivery from a further 10 of these canulae (see Discussion).

7.3.2 Behavioral trends

Figure 7-2 gives the psychophysical results of the monkey's performance over the two ten-day pre-tPA periods, and the subsequent ten-day per-tPA period. The first two ten-day periods shown involved no tPA administration. The null-field errors can be observed to plateau in terms of perpendicular displacement only in the second ten-day period. Among force trials during these control days, the monkey's mean level of error was comparable to that on null-field trials near the end of the control period. Ironically, the plateau level of performance in both the baseline and force field epochs appeared to involve a *higher* level of trajectory error than its initial performance (see Discussion).

With the introduction of tPA (Fig. 7-2), the monkey's baseline error level changed little. The deviation error among force field trials may have increased during this period—although this effect may have been confounded by the waning number of hits each day. Indeed, as shown in Figure 7-3, the most visible performance change associated with tPA infusion may simply have been in the monkey's capacity to perform the reaching task under force field conditions. As before, the monkey was

still able to perform 160 baseline hits each day, but its ability or willingness to generate the full epoch of force field hits appeared to decline soon after infusions of tPA began on day 3 of this period. (The large differences in numbers of hits performed in each epoch precluded meaningful statistical comparisons of trajectory error between these epochs.)

When the monkey returned to the task for a final ten-day post-tPA period (Fig. 7-3), it again performed complete or nearly complete epochs of both null-field and force-field trials—suggesting that whatever had affected its performance in the per-tPA period was no longer influencing the monkey's behavior. This pattern is also suggested by the profile of trajectory error (Fig. 7-2), which appeared consistent with the monkey's baseline performance in the per-tPA period and its force-field error at the beginning of the tPA period.

7.4 DISCUSSION

7.4.1 Explanations for the lack of tPA-associated enhancement of learning

The monkey's force-field performance in the per-tPA did not appear to be enhanced relative to its baseline performance, and if anything appeared to have been compromised during this period (Fig. 7-3). I have nevertheless included this report both because of the novelty of the methods and because of the relation of these results to those of Chapter 8. But with an eye to improving the experimental paradigm in the future, I consider below possible explanations of this finding:

1. *The canulae generally were not lowered into cortex.* It was clear enough when the canulae did not make it through the dura, since they would end up bent or deflected upwards (which could be ascertained by comparison of the their initial and final elevations, taking into account the displacement due to the microdrive). I found that, of the 40 canula which I attempted to lower past the dura, 25 of them (19 in days 6-10) went to the appropriate depth (based on the simultaneously cortical monitoring performed with the yoked microelectrodes). One alternative to the methods used here might be to use beveled, insulated guide tubes not only to penetrate the dura, but also to act as microelectrodes—along the same track as the injection needles, rather than parallel to them.

2. *The tPA could not be pumped into the cortex.* Visual inspection of the pump apparatus confirmed that the appropriate volume of tPA solution had been pumped from each syringe. But one concern on days 3-5 of the tPA administration was that a failure to penetrate the dura with either canula of a tube-yoked set (see Methods) likely led to all the tPA supplying the two canulae to follow the path of least resistance—i.e. into the saline of the recording chamber rather than into the denser tissue below. Of the 25 canula which penetrated the dura, flow such flow problems may have affected 10 of them, leaving only 15 (13 of them in days 6-10) to deliver tPA solution. While the risk of such shunting was clearly minimized beginning day 6 with the custom canulae, uneven flow through the two canulae of a pair remained possible. But provided that both canulae were in cortex, a differential flow of tPA solution from each would not have affected the overall quantity of tPA administered.

3. *Before reaching the cortex much of the tPA was diluted by contact with saline in the recording chamber.* Even if the dilution was minimal and local to the tip of the canulae it could have blunted the effect of the tPA, since only the distal-most ~0.01 ml in each canula was delivered into tissue. With practice I was able (by day 8 if not earlier) to reduce this time of immersion in saline to 10 min at most. The degree of dilution could be tested (in vitro) by substituting a green dye in place of the tPA solution. If it is problematic, it would suggest that beveled guide tubes should be used not only to puncture the dura but also to seal the path of the injection needle from most of the surrounding saline.

4. *The tPA was delivered in too dilute a solution to begin with.* The concentration of tPA solution was chosen to be in the same range as values quoted in the literature. For instance, Mataga et al. (2002, 2004) quote a concentration of 160 IU/µl, while the concentration here was 60 IU/µl—at each of one to four sites per day. More important than the concentration may have been the total quantity of tPA delivered, which in the literature above was 240 IU, compared to the average total here (across days 3-10) of 730 IU, and the maximum total (on day 6 with 0.0108 µl at each of four sites) of 2580 IU. Indeed, if anything a *less* concentrated solution (or a small undiluted quantity injected directly) is recommended in the future.

5. *The tPA was not applied for sufficiently many days.* Given previous experiments I expected to see an effect of the tPA after fewer than ten days' administration—indeed, even after a single day's administration (Mataga et al., 2002). If this does not apply to the primate then I might still have seen longer-term effects when the monkey was retested in the final ten-day recording period, without tPA. However, the monkey was able, or willing, to perform nearly the entire set of baseline and force epochs in this period.

6. *Any enhancing effect of the tPA was mitigated by cortical damage resulting from the canulae or the liquid volume*. On days 6 and 10, for example, I observed a small amount of dural bleeding following the recording session. It was likely that the custom canulae caused more trauma than the weaker, commercial infusion canulae I used (for the most part unsuccessfully) on days 3-5. Future experiments should use subjects with less cumulative dural growth, and/or minimize the diameter of the canulae.

7. *The monkey's learning capacity was already maximized.* Seeds et al. (2003) found that cerebellar tPA levels in mice that had already acquired a motor task (or who were stressed) were elevated, thus likely reducing the potency of further tPA infusion. Although the monkey's prior exposure to the clockwise force field was minimal, it was true that there appeared to be little learning evident within the its force field deviation scores—especially when compared to the learning trends evident in its baseline scores. For the monkey's learning capacity both in the baseline and force field epochs to have been maximized was also conceivable given that its performance did appear to plateau towards the end of the second ten-day pre-tPA period.

8. *The monkey's performance was too variable to allow for significant evidence of learning enhancement.* Initially I had planned to give the monkey only one ten-day period of training on the clockwise force field prior to tPA administration. In reviewing its performance over this period, however, I correctly predicted that the monkey's performance could reach a more stable plateau with a further ten-day period prior to tPA introduction. This additional ten-day baseline period would allowed me to enforce greater regularity in the monkey's environment and task parameters, including: the degree of its head fixation, the time of day, the quantity and nature (juice/water) of the reward, the size of the targets, and the number of additional (washout) trials it was allowed to perform on days when it completed the set 160 force hits. Considering the two pre-tPA periods together, the variability associated with the monkey's deviation area was not nearly as large as the systematic change in its baseline performance across these periods, and again in the per-tPA period. Variability was more of a concern when following behavioral trends in the monkey's force field epochs, given that the monkey often did not perform a full epoch of 160 hits, particularly in the per-tPA period.

9. *Changes in task parameters or environment factors between the pre-tPA and per-tPA periods negated any evidence of learning.* As in the second ten-day pre-tPA period, I strove to keep the monkey's environment and task parameters as consistent as possible within the ten days of recording. Nevertheless, a handful of differences between the two latter ten-day periods may have remained. For instance, during the per-tPA period the experiments typically began in the late afternoon (mean recording start time 17:05 ± 1:18) rather than the early afternoon (12:02 ± 1:31), as had been the case in the preceding ten-day period without tPA. However, in the monkey's ten-day post-tPA period I attempted to more closely replicate the per-tPA recording conditions. For instance, the post-tPA mean recording start time was also 17:05 ± 1:18. Despite these additional controls, the monkey's per- and post-tPA performance levels were clearly distinct, its post-tPA performance more closely resembling the monkey's pre-tPA performance (both at the level of hits performed and of trajectory error). Nevertheless all of these experimental conditions should be controlled both in the pre- and post-tPA periods in future experiments.

10. *tPA delivered to MI is simply ineffective at enhancing motor learning.* It was expected that tPA would have effects on motor learning because it has been implicated in neurogenesis in visual cortex (Mataga et al., 2002, 2004), perhaps via new spine growth of existing cells. While it may be the case that the monkey's performance on the force field trials did not improve over the course of the tPA administration, the data do suggest that the monkey's performance on these force trials was *selectively* impaired while its performance on the baseline null field condition was generally spared. Such a selective impairment may indicate a greater fragility of the monkey's clockwise force field learning. Whether memory of this learning was indeed impaired, or whether motivational issues may account for the monkey's inability to complete the force field epochs late into the tPA administration, was tested by the final ten-day post-tPA period. Generally the monkey's post-tPA performance followed the trends in the monkey's pre-tPA period, suggesting that it had not catastrophically "unlearned" the clockwise force field during the per-tPA period. Given that the literature on motor learning generally

implicates MI in motor execution or recall rather than dynamic adaptation (see Chapter 8), it may well be that the tPA—far from facilitating further learning—simply interfered with the monkey's expression of its clockwise force field learning.

7.4.2 Human vs. nonhuman primate motor learning

This investigation also illustrates some of the peculiarities inherent in nonhuman primate motor control. Chief among these is perhaps the longer time course involved. Whereas in human studies (see Chapters 8-10) adaptation to modified dynamical environments can be observed within one hour, a comparable degree of monkey learning is thought to require days. Hence trials in this study (Fig. 7-2) were averaged over multiple days of practice, rather than binned and compared within-day. Although I have used catch trials in Chapters 4-5 and here, the time course of learning suggests that null field blocks at the end of each day (Li et al., 2001) may serve a similar function in assessing learning through aftereffect trajectories (see Chapter 10). The relative trajectory errors observed in the monkey's plateau performance (Fig. 7-2b) are larger than observed for human subjects, making it difficult to identify a level of error that demonstrates "learning." Under altered dynamical environments, in particular, it may not be appropriate to assume that the monkey was similarly compensating for the occasional catch trials by deviating its movements into the force field (Thoroughman and Shadmehr; see Chapter 10). Even under null field conditions (which I have implicitly presented as a control for learned behaviors) clearly involve adaptation in their own right—at least when experienced by monkey subjects.

The apparent fragility of these motor memories may also differentiate monkeys and humans. For instance, an early analysis of monkey R0's EMG data in the reach task (see Chapter 4) found that interruptions of learning could reverse prior adaptations visible at the level of synergy recruitment. As shown in Figure 7-4, the monkey's adaptive pattern of epochal modulation emerged in a progressive fashion over consecutive days of practice on the field. When the learning was interrupted by a weekend break, however, the adaptive pattern of dynamic modulation appeared to have reversed upon retest in the field, only to be recapitulated by further days of practice. I have similarly made similar observations about monkeys' performance and EMG patterns in the grasping paradigm. Coupled with the longer time required in order to observe motor adaptation in monkeys, the sensitivity of this learning suggests that nonhuman primates may not be a perfect model for human motor learning. The remaining chapters of this thesis are therefore restricted to investigations of human motor adaptation and control.

Figure 7-1 Grid map of sensorimotor cortex targeted for tPA delivery. **a**) Map of monkey R1's cortical cutaneous, proprioceptive, motor, and "mirror" responses observed following either somatosensory stimulation or microstimulation in the months prior to this study. Many sites were stimulated on more than one day (not always with consistent responses) only the most recent response is shown, as coded in the legend at bottom. (Compare Figure 6-1, based only on recorded microstimulation-evoked movements.) **b**) Map of sites where tPA canulae were lowered. At certain sites there was experimental uncertainty about whether the canula had penetrated the dura, as coded by the legend at bottom. Microelectrodes lowered together with the canulae were interleaved between the chosen locations. The recording chamber was centered at AP = 17.0, ML = 15.0. (Note that a different grid size and centering was used compared to a.) Sulci borders, estimated from infrared observation during the craniotomy, included the arcuate sulcus (anterior) and central sulcus (posterior).

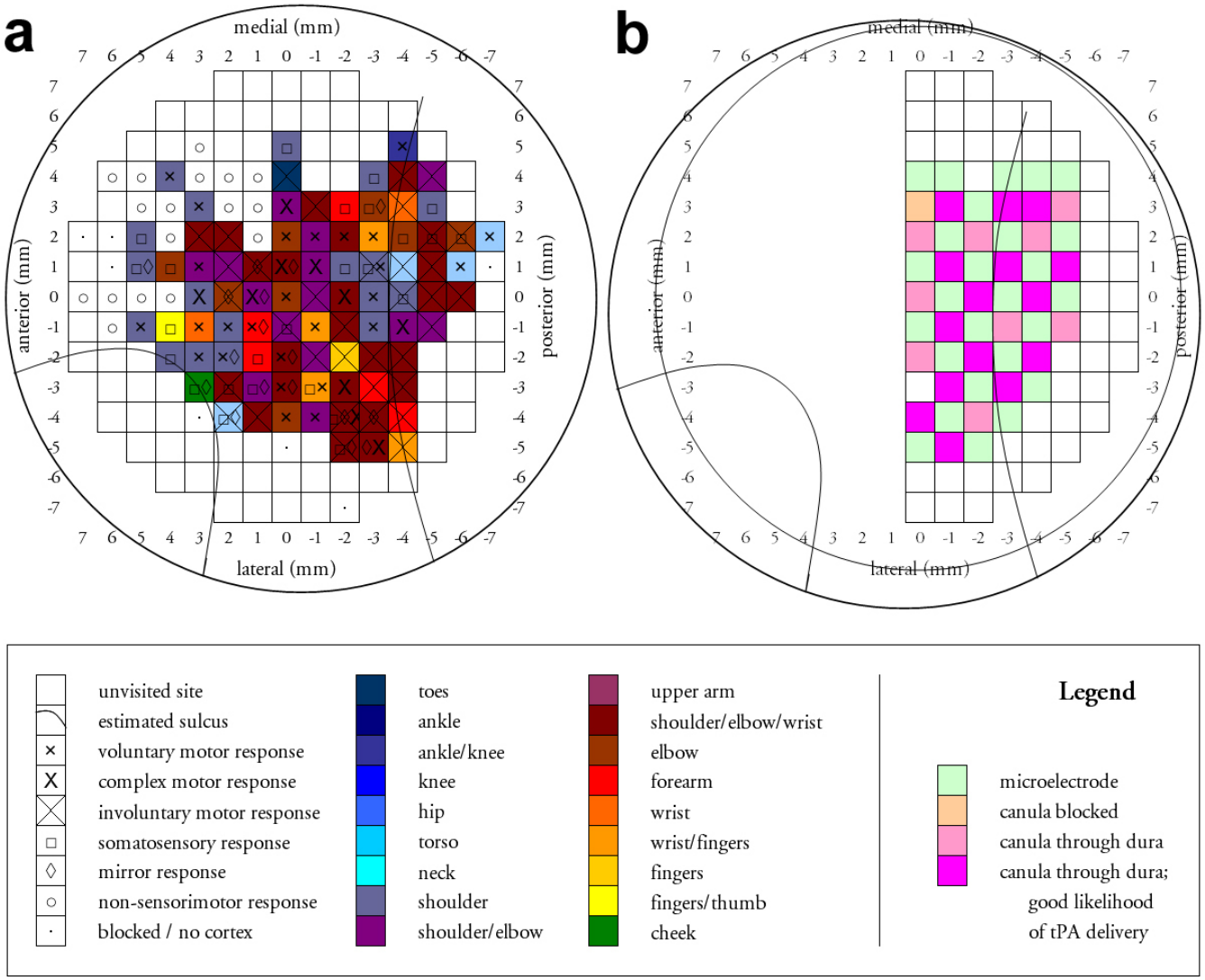

Figure 7-2 Trajectory errors upon introduction of tPA. The signed deviation area is plotted (mean ± S.E.M.) over all trials in either the **a**) null-force baseline (in black) or **b**) clockwise-force test (red or magenta) epochs. Note that there were "baseline" epochs on both tPA and "control" days, and that the left and right plots represent interleaved rather than consecutive data. Magenta depicts the epochs when the monkey was receiving both the tPA and the clockwise forces. Epochs on which the monkey failed to complete more than two 8-target blocks are not plotted.

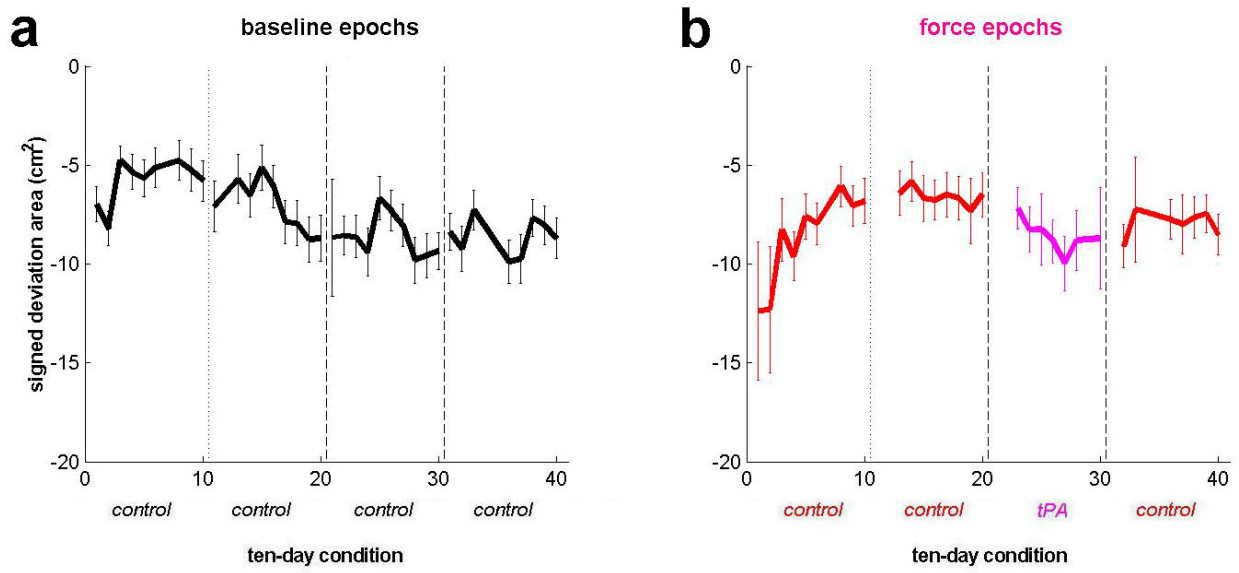

Figure 7-3 Task completion upon introduction of tPA. Task completeion was measured simply by the number of trials the monkey was able or willing to perform in each epoch or day. Colors and alignment as in Figure 7-2.

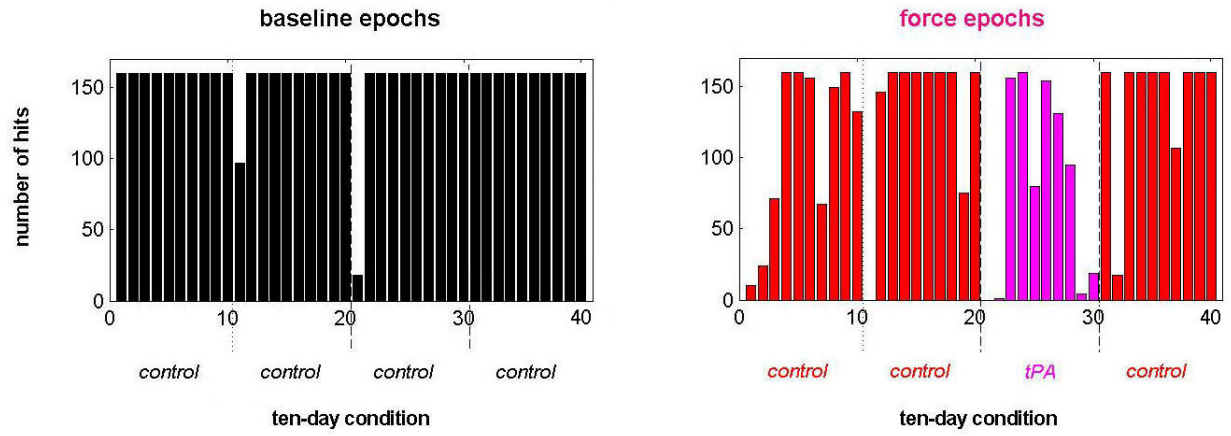

Figure 7-4 Sensitivity of monkey subjects to interruptions in learning. **a**) Four time-varying synergies extracted from monkey R0's reach task EMG (spanning the first five days of exposure to the saddle field, and including all three 160-hit epochs) were modulated in their average amplitude coefficient as a function of task dynamics (as well as movement direction, not shown). The pattern of coefficient magnitude in the force relative to the null epochs was correlated to the degree of each synergy's alignment to the saddle field (not shown) Recall that a synergy's amplitude does not reflect the average amplitude of the muscle activity it encodes. **b**) The average amplitude coefficient associated with each synergy, averaged over all trials (including null and force trials) of each day.

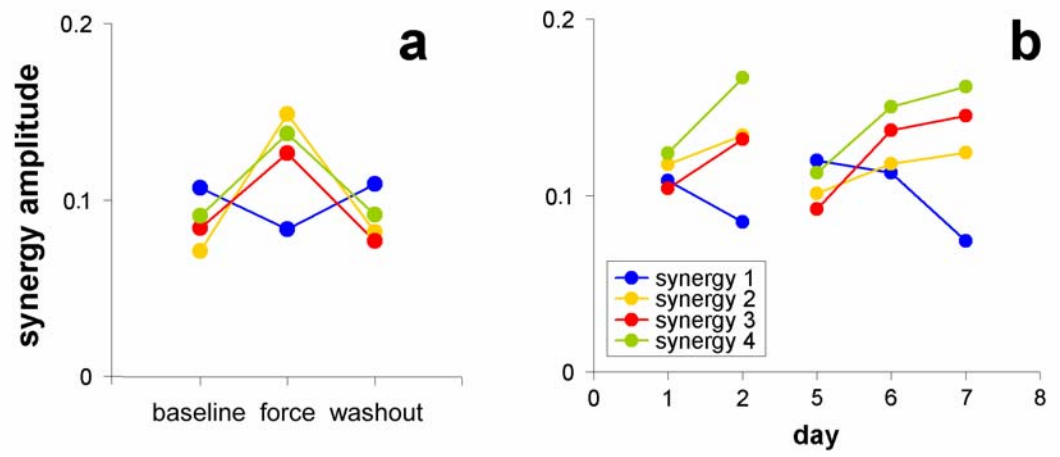

8 rTMS Disruption of Motor Cortex Impairs Off-Line Improvement

To date there has been relatively little evidence for the involvement of primary motor cortex (MI) in human motor adaptation—beyond motor execution. Investigators using repetitive transcranial magnetic stimulation (rTMS) in MI have found it either unable to disrupt retention of recent dynamic adaptations, or able to disrupt off-line improvements on a motor sequence task that would normally accrue over the day. Here we using 1 Hz rTMS to MI in an attempt to interfere with learning on the classic center-out reach task. We applied rTMS just prior to subjects' exposure to clockwise force field conditions, to decrease cortical excitability while they acquired this experience. We were thereby able to assess the role of MI in motor acquisition, rather than performance or retention of prior training. We found that subjects given rTMS performed as well as control subjects (using performance measures including deviation angle, distance, or area)—even during the block of trials following rTMS. Because the groups performed similarly during motor acquisition, we were further able to compare the groups on their retest performance 24 hr later. At retest I found that the rTMS subjects began the session with the same level of kinematic error as they exhibited at the end of training, while control subjects immediately plateaued at a level of error indicating better adaptation to the field. These results indicate that 1 Hz rTMS of MI blocks off-line improvements on a standard motor adaptation task. This result is significant both in its implication that such off-line "consolidation" describes tasks outside of the sequence learning domain, and in its implication of a role for MI and/or associated areas in the stabilization of dynamic sensorimotor learning.

8.1 INTRODUCTION

8.1.1 The role of MI in human motor learning

Adaptation to modified sensorimotor environments like the one presented to nonhuman primate subjects in Chapter 4-7 has been shown to rely on a network including nodes in the premotor cortex, cerebellum and certain thalamic structures (e.g. Shadmehr & Holcomb, 1997; Imamizu et al., 2000; Kassardjian et al., 2005). Involvement of the posterior parietal cortex in acquisition of sensorimotor adaptation has also been implicated by imaging (Clower et al., 1996; Inoue et al., 1997; Ghilardi et al., 2000) and transcranial magnetic stimulation, or TMS (Della-Maggiore et al., 2004).

Primary motor cortex (MI) has traditionally been assigned a role in motor execution rather than motor learning, or else has been thought to reorganize slower than the areas listed above over the course of learning (Ungerleider et al., 2002). For instance, Shadmehr and Holcomb (1997) found that regional cerebral blood flow to MI was correlated with baseline motor output (quantified by reach length), but did not increase over 5.5 hours between practice and retest on a novel force field (in contrast to increased activity in premotor, posterior parietal, and cerebellar areas). However, Li et al. (2001) found that in monkeys performing the same task, the preferred direction of a population of neurons within MI shifted along with the

monkeys' novel pattern of muscle recruitment—and retained this "memory" of the field even when the monkey returned to a null (no-force) field for further practice at the end of the day. In sequence learning tasks, functional imaging has also implicated MI in motor learning as well as motor execution (Karni et al., 1995, 1998; Ghilardi et al., 2000).

8.1.2 The application of rTMS in studies of motor learning

Beyond correlative evidence for the role of MI in human motor learning, a more direct test has recently been afforded in the form of repetitive TMS (rTMS). At relatively low frequencies (e.g. 1 Hz), rTMS pulses have been shown to disrupt behavior by reducing cortical excitability (see Discussion, and Robertson et al., 2003). When centered on MI immediately following implicit acquisition of a finger movement sequence, rTMS has been shown to disrupt off-line improvements that would normally accrue over the day (Robertson et al., 2005)—a common feature of motor sequence learning (Karni et al., 1998; see Robertson et al., 2004a for review). (Resistance to such rTMS-evoked disruption in motor learning tasks might almost be considered a novel, alternative definition of motor consolidation.) On a ballistic finger pinching task, rTMS applied to MI has also been shown to interfere with the retention of earlier performance gains (as measured by movement acceleration and force production), but not with subsequent adaptation (Muellbacher et al., 2002).

The involvement of MI in adaptation to environmental perturbations, as in the force field paradigm, could similarly be elucidated by an rTMS manipulation. In a comparison of ballistic finger abductions and fast finger movements under velocity- and position-dependent forces, Baraduc et al. (2004) found that rTMS of MI was unable to affect the retention of dynamic experience gained immediately before the rTMS, suggesting little role for MI in short-term memory retention. Given their novel task design, however, this null effect must be treated with some caution. For instance, the rTMS was targeted to a cortical representation of the first dorsal interosseus muscle, which may have been more involved in the ballistic finger movement than in the force-field movements, these appearing to have been dominated by finger flexion and extension. (Electromyographic data are not presented to validate the involvement of the target and other muscles in either task.) Also, an "optimal" level of performance error on this task has not been characterized, as has been done in the center-out reaching task (Thoroughman & Shadmehr, 2000). Such an analysis would be particularly informative given the large variability apparent in subjects' trajectories and their "root-mean-square deviation" scores even after learning (Baraduc et al., 2004). An additional concern about this task is that the position-dependent, i.e. stiffness, component of the field may have induced muscular cocontraction rather than coordination as a learning strategy (Burdet et al., 2001).

Learning to reach with energetic efficiency under complex dynamical conditions requires subjects to learn a novel coordination of muscle activity, as frequently occurs in acquisition of real-life motor skills—and as represented in the conventional center-out reaching task. In this paradigm, Della-Maggiore et al. (2004) used single-pulse TMS centered over posterior parietal cortex in an attempt to interfere on-line with cortical function in the acquisition of a velocity-dependent force field. In the present study, we have used the center-out reaching task and standard measures of performance (as in Della-Maggiore et al., 2004), but have focused instead on the

involvement of MI by disrupting it with a block of 1 Hz rTMS pulses (as in Baraduc et al., 2004). We applied this stimulation just prior to force field learning, rather than after (Baraduc et al., 2004) or during (Della-Maggiore et al., 2004) these trials, and did so at a relatively low stimulation intensity in order to further minimize interference with task performance per se. In doing so we investigated the role of MI in the acquisition of motor learning, rather than motor performance or retention of prior training. We hypothesized that MI has no role in such acquisition, and so subjects receiving rTMS of MI would have the same performance level during their baseline (null-field) and learning (clockwise-field) trial epochs as control subjects who did not receive rTMS. To further test whether there were delayed effects of rTMS on motor acquisition, we had all subjects return for a retest in the clockwise field one day after their training. Again we predicted no difference between the rTMS and control groups.

8.2 METHODS

8.2.1 Subjects

Sixteen right-handed subjects (mean 25 years old; 6 males) participated in the experiment. Subjects were screened for history of seizures, familial epilepsy, strokes, head injury, neurosurgery, other neuorological conditions, psychoactive medications, pregnancy, prior adverse reaction to TMS, or other TMS contraindications. Ethical approval was obtained through the MIT Committee On the Use of Humans as Experimental Subjects. Participants were paid at $10/hour, with a $15 bonus for successful completion of the study. No subjects were excluded from the study. The subjects were assigned to two experimental groups ("control" and "rTMS") prior to their first epoch. These groups were not run in a blind fashion. (One subject also underwent the rTMS localization procedure but then elected not to continue as a rTMS subject, and so was reassigned as a control subject.)

8.2.2 Paradigm

Task Participants performed the behavioral task by operating a custom manipulandum apparatus (Fig. 8-1; Fayé, 1983) with their right hand. The targets were white 1-cm-wide squares appearing on a black screen, shown to the subject via a vertically-oriented monitor above the planar manipulandum apparatus. Their backs were kept vertical by means of a seat belt. Motions of the handle were represented on the screen as continuous movements of a 0.8-cm-wide red crosshair. As a standard center-out task, movements alternated each turn between the central origin and a peripheral target, or a peripheral origin and the central target. Following each trial, a new target appeared and the former target became the "origin" for the next movement. Participants were given 0.50 ± 0.05 s to complete each movement, following the time at which they left the origin square. The target remained on the screen even if subjects failed to reach it in the allotted time. Upon acquiring the target, a further 0.5-s within-target hold time had to be observed in order for the trial to be a "success." Trial success was indicated to the subject by an expansion and disappearance of the target accompanied by an audible "quacking" sound. If either of

the conditions was not met, the trial failure was indicated by a silent transition in the color of the target to red (if the target was achieved too soon) or blue (if the target was acquired too late) prior to its disappearance.

Epochs The start time of the experiment was 2 ± 3 p.m. (mean ± S.D.) for both control and rTMS subjects (each n = 8). Subjects performed trials in four different epochs, denoted as "practice" (250 trials), "baseline" (150), "learning" (400), and "retest" (400). (There was some variability in the number of trials performed by each subjects in each block, so that these values were actually 253 ± 8, 152 ± 4, 400 ± 0, and 403 ± 10 trials, respectively, across subjects.) The latter two epochs required about 10-15 min to complete. Intervals between epochs were all measured from the end of the previous epoch to the beginning of the next. The practice and baseline epochs were separated by uncontrolled breaks of 11 ± 2 min (control subjects) or 17 ± 6 min (rTMS). During this interval we performed the rTMS localization and intensity determination procedures on the rTMS subjects, while the control subjects simply remained in the lab. The baseline and learning epochs were separated by 16 ± 1 min (control) or 16 ± 2 min (rTMS). During this time the rTMS subjects received 1 Hz rTMS over left sensorimotor cortex, while the control subjects again remained in the lab but received no rTMS. The learning and retest epochs were separated by 24 ± 2 hours (control) or 24 ± 1 hours (rTMS). During this time subjects were not in the lab but we did ask them to get a reasonable amount of sleep. Only the interval between the practice and baseline epochs varied significantly between the two groups, $t_{(14)} = 2.14$, $p < 0.01$ (one-tailed t-test assuming equal variances).

Instructions We informed participants that they were part of a TMS investigation on "motor learning." We discussed the basic mechanism, application, and possible side effects of rTMS. We described the basic task and trial success feedback, and asked subjects not to "anticipate" the targets but merely to move as "naturally" as possible. They were informed that the experiment was not overly difficult to complete, and that their performance would improve with time. As a safety precaution, subjects were warned prior to each epoch that they might experience "forces" generated by the robot during the epoch.

Targets The possible targets included four peripheral targets spaced around a central target at a distance of 10 cm (in the workspace), at 0° (to the right), 45°, 90° (ahead), and 135° (Thoroughman & Shadmehr, 1999). Each subject received one of two possible target files (each including 96 peripheral targets). The same file was repeated as many times as necessary, in each epoch, until the subject had completed the intended number of trials in that epoch (see "Epochs," above). All subjects completed each movement specified by the target files—trials were not aborted if they failed to reach the target on time. The first origin in each epoch was always the central square. The target file experienced by three of the control subjects and one of the rTMS subjects was constrained to have peripheral target frequencies of between 12 and 13% (and a central target frequency of 50%), and no more than two consecutive presentations of the same peripheral target (interleaved with trials back to the central target). The remaining subjects experienced a target sequence that had peripheral target frequencies between 10 and 15% (and a central target frequency of 50%).

Forces All subjects experienced a null (0 N·s/m) force field during the practice and baseline epochs, and a velocity-dependent clockwise field in the learning and retest epochs. The curl forces, of magnitude 15 N·s/m, were calculated on-line as $f = \mathbf{B}\dot{x}$, where $\mathrm{B} = \begin{bmatrix} 0 & 15 \\ -15 & 0 \end{bmatrix}$ and $\dot{x}$ was the movement velocity. "Catch trials" (trials on which the motors are suddenly turned off just as the target is presented) were not used in this study.

rTMS Stimulation was delivered using a Magstim (Whitland, Wales, UK) Super Rapid stimulator. The subjects who received 1 Hz rTMS first underwent a procedure (between the practice and baseline epochs) to determine the appropriate rTMS anatomical target and intensity level. This procedure involved using single-pulse TMS over motor cortex to determine: 1) the approximate location capable of reliably and maximally inducing visible contractions in the right biceps muscle, and 2) the intensity threshold necessary to reliably activate both the first dorsal interosseus (FDI) and biceps muscles (further confirmed in three subjects by on-line surface EMG recording). Across subjects, we found these thresholds to be 63 ± 6 (FDI, mean ± S.D.) and 66 ± 6 (biceps) measured at the site with the minimal biceps threshold, in the arbitrary output units of the stimulator. The intensity level of the 1 Hz rTMS used in the experiment was then calculated to be 90% of the biceps motor threshold (MT) level, or 59 ± 6 units across subjects—a level known to affect behavior and cortical excitability (Romero et al., 2002; Robertson et al., 2003). After the baseline epoch, the rTMS pulses were applied at 1 Hz for 15 min (i.e. 900 pulses) using a hand-held figure-of-eight coil (commercially-available double 70 mm coil; Magstim), positioned tangentially relative to the scalp at the same location found to evoke biceps activity during localization. (One subject received an additional 126 1 Hz pulses immediately following the regular 15 min of stimulation, during a delay before the start of the learning epoch.) A neurologist was present during TMS application, given the potential for spread of cortical excitability (Chen et al., 1997). No subjects reported adverse effects of the TMS localization or the rTMS application (e.g. Satow et al., 2002), either immediate or delayed. We did not apply sham or control rTMS to the non-rTMS subjects.

8.2.3 Recording/Stimulation

Performance error Planar position and velocity were sampled at 100 Hz using optical potentiometers and tachometers. We applied three measures of motor performance commonly used in studies of arm movement adaptation: 1) the deviation angle (Sainburg et al., 1999; Della-Maggiore et al., 2004; Malfait & Ostry, 2004; Krakauer et al., 2005); 2) the peak perpendicular deviation (Shadmehr & Moussavi, 2000; Karniel & Mussa-Ivaldi, 2003); and 3) the deviation area (Caithness et al., 2004; see Chapters 9 and 10 of this thesis). We chose all of these measures to test the validity of our results in a comprehensive (if pedantic) manner. We ignored related performance measures that nevertheless fail to indicate the directionality of the error, e.g. movement distance (Shadmehr & Holcomb, 1997). Given our earlier finding of characteristic and covaried reaction time and speed

profile changes in manipulandum reaching tasks (see Chapter 9), we also ignored measures that have expected relations to reaction time, e.g. movement duration or fraction of trials completed within the allotted time, or deviation at a certain time into the movement (Shadmehr & Brashers-Krug, 1997; Donchin et al,. 2002). We did not consider the correlation coefficient of subjects' baseline and force field trials (Shadmehr & Mussa-Ivaldi, 1994; Brashers-Krug et al., 1996; Caithness et al., 2004), a measure which can theoretically reflect various underlying trends (e.g. movement smoothness, speed, and anticipation).

8.2.4 Analysis

Comparisons Trials in which the subject failed to reach the target within a 0.50 ± 0.25-s time window (more generous than the 0.50 ± 0.05-s "success" window effective during the experiment) were excluded from the analysis. Trials were binned by 16 trials in each epoch and condition. We did not exclude the first 16-trial bin of each epoch in the analyses. For display purposes (Fig. 8-3), data within each epoch were fit by single-exponential curves (only constrained in their parameters such that the exponential "growth" or "decay" part of the curve occurred at the beginning and not the end of the epoch). Statistical results were based on the within-bin-averaged trajectory error, as defined above. Transfer of clockwise field experience between the learning and retest epochs was estimated by comparing the mean scores of the first eight 16-trial bins in the retest epoch with the last eight 16-trial bins in the learning epoch. Main and interaction effects of rTMS and Time (or Bin average, in the case of learning transfer) were assessed using repeated measures ANOVAs. One-way ANOVAs were used to test for group differences in the magnitude of these learning transfer values at each direction of movement. Differences among the "slope" parameter of exponential fits were not compared. All significant effects (at the $p < 0.05$ level) are reported.

8.3 RESULTS

As illustrated in Figure 8-2, subjects learning to reach in the clockwise force field produced trajectories that were initially deviated in the clockwise direction. With practice, the trajectories returned to a less deviated form like that exhibited under null-field conditions. We chose to examine this adaptation with three common metrics of motor performance used in motor adaptation studies: the deviation angle, peak perpendicular deviation, and deviation area swept out by each movement relative to a straight line connecting the beginning and end positions of the trial (see Methods).

8.3.1 Similarity of subjects on performance and force field acquisition

Within the 250-trial practice epoch, both groups showed a significant adaptation to the null field, as shown in Figure 8-3. Although we considered movements in all eight directions (outward to four peripheral targets and from these to the central target), the null-field errors have a non-zero, counterclockwise bias to them. However, this bias declined with practice in this epoch, as captured by a significant

main effect of Time on signed deviation angle ($F_{(14,15)}$ = 3.59, $p < 0.001$), peak deviation ($F_{(14,15)}$ = 15.01, $p < 0.0001$), and deviation area ($F_{(14,15)}$ = 13.78, $p < 0.0001$).

After subjects completed the practice epoch and had either rested (control) or received rTMS localization and calibration (see Methods), they performed an additional baseline epoch of 150 null-field trials. Subjects exhibited a small amount of further adaptation in this epoch (Fig. 8-3), suggesting that they had not fully adapted to the null field by the end of the practice epoch. However, this supposition is only supported by the signed deviation angle statistic, for which there was a small but significant main effect of Time on signed deviation angle ($F_{(8,15)}$ = 2.78, $p < 0.05$). As in the practice epoch, there were no significant differences between the rTMS and control groups (despite the small difference apparent in each of the panels).

Following the baseline epoch, the rTMS subjects received 15 min of 1 Hz rTMS centered over MI, while control subjects again waited for an equivalent time. Immediately after this interval, all participants performed a 400-trial learning epoch with a clockwise force field generated by the manipulandum. Subjects' errors were strongly deviated in the clockwise direction, but again the participants were able to adapt to the field (Fig. 8-3). This trend was supported by a significant effect of Time on signed deviation angle ($F_{(23,15)}$ = 27.77, $p < 0.0001$), peak perpendicular deviation ($F_{(23,15)}$ = 24.54, $p < 0.0001$), and deviation area ($F_{(23,15)}$ = 29.26 ($p < 0.0001$). Only by the deviation angle measure did the trajectories appear to return to their level in the null field; in terms of peak perpendicular distance and deviation area measures, the trajectories were still deviated in an overall clockwise fashion. But once again there were no significant effects of rTMS on subjects' performance by any of the performance metrics.

8.3.2 rTMS and performance changes at retest

An effect of rTMS was only apparent when the participants returned 24 hours following learning for a retest epoch. Within the 400-trial clockwise retest epoch, there was an overall change in performance, captured as before by significant effects of Time on signed deviation angle ($F_{(23,15)}$ = 4.19, $p < 0.0001$), peak perpendicular deviation ($F_{(23,15)}$ = 8.23, $p < 0.0001$), and deviation area $F_{(23,15)}$ = 4.90, $p < 0.0001$). However, this trend was largely restricted to the control subjects, as a significant main effect of rTMS was present according to all three measures: signed deviation angle ($F_{(1,15)}$ = 9.45, $p < 0.01$), peak perpendicular deviation ($F_{(1,15)}$ = 4.28, $p < 0.05$), and deviation area ($F_{(1,15)}$ = 9.62, $p < 0.01$). Although the exponential fits in Figure 8-3 suggest that the two groups began at the same level at the beginning of the retest epoch, the change in performance among the rTMS subjects to a new level of error is too rapid to create significant rTMS × Time interactions by any of the three measures.

We quantified the change in performance between the learning and retest epochs as the change in performance between the last eight 16-trial bins of the learning epoch and the first eight 16-trial bins of the retest epoch (Fig. 8-3). This analysis again shows a significant overall change in performance by the signed peak perpendicular deviation ($F_{(1,15)}$ = 7.19, $p < 0.01$) and deviation area ($F_{(1,15)}$ = 5.87, $p < 0.05$), and a nearly significant change by the deviation angle metric ($p = 0.06$). As a

measure of "off-line" performance change between the epochs, this statistic also indicates that rTMS was associated with significantly reduced changes. This effect was captured by significant rTMS × Time interactions at the level of deviation angle ($F_{(1,15)}$ = 5.44, $p < 0.05$) and deviation area ($F_{(1,15)}$ = 5.56, $p < 0.05$), and a nearly significant interaction in peak perpendicular deviation scores ($p = 0.06$).

The transfer effects described above are averaged across the eight directions of movement. We also examined the magnitude of these effects on a within-direction basis using the signed perpendicular deviation measure, as shown in Figure 8-4. As in Figure 8-3, the effects had a negative value if the performance at retest was more clockwise than the performance in the learning epoch. While control subjects exhibited a positive transfer (i.e. less clockwise deviations) in most directions, the rTMS subjects exhibited negative transfer in movements oriented towards the subject, in particular at 225° and 270°.One-way ANOVAs show that the two groups differed significantly only at 270° ($F_{(1,15)}$ = 9.31, $p < 0.01$) and to a lesser degree at 135° ($F_{(1,15)}$ = 4.95, $p < 0.05$).

8.4 DISCUSSION

8.4.1 Studies on rTMS and MI

The biological effects of rTMS remain poorly understood. At the cellular level, rTMS has been shown to evoke increases in firing rate in rodent auditory cortex, and longer-term potentiation and depression of this rate (Wang et al., 1996). Indeed, the stimulation parameters used in our experiment (15 min of 1 Hz pulses) are temporally similar to those used in studies of long-term depression (Chen et al., 1997). Valero-Cabré et al. (2005) used ^{14}C-labeled deoxyglucose (2DG) tracing to follow metabolic activity around the site of rTMS application in anesthetized cats, and found that metabolic activity was modulated not only near the target location but at sites distant to stimulated cortex, in proportion to the degree of efferent projections to those sites.

Functional imaging in awake humans similarly suggests that regional cerebral blood flow—a marker of synaptic activity—increases in response to rTMS of the motor cortex (Lee et al., 2003). This increase in blood flow is not specific to the site of stimulation, although areas immediately adjacent to the stimulated site may not be activated (Fox et al., 1997). Instead, both low- and intermediate-frequency (1-3 Hz) rTMS to primary sensorimotor cortex is associated with focal sites of activity in a wide network outside this region, including premotor, cingulate and supplementary motor areas (SMA) and the thalamus and putamen, even at stimulation intensities below the MT (Lee et al., 2003; Bestmann et al., 2004). Conversely, suprathreshold rTMS to human SMA has been shown to modulate cortical excitability in MI, e.g. as assessed by the stimulation intensity necessary to generate motor-evoked potentials (Matsunaga et al., 2005). This distributed effect of low-frequency rTMS at least appears to be more anatomically restricted when applied to MI than to dorsal premotor cortex, perhaps consistent with connectivity patterns within the motor network (Chouinard et al., 2003).

The lack of a mechanistic understanding of rTMS and the finding that its action is widely distributed make the behavioral interpretation of rTMS effects particularly

problematic (Robertson et al., 2003). It is not even possible to expect that rTMS will generally impair rather than improve behavior (Tegenthoff et al., 2005). However, it is clear that rTMS applied to primary motor areas does have behavioral consequences, and that these consequences are modulated by stimulus frequency and intensity (Pascual-Leone et al., 1994). Low-frequency (1-Hz), subthreshold rTMS, as used in our study, has been shown previously to transiently decrease motor evoked potentials (MEPs) following single-pulse TMS to motor cortex (Chen et al., 1997). On the other hand, rTMS of MI at these parameters (but not 5 Hz suprathreshold TMS of SMA; Matsunaga et al., 2005) has been shown to facilitate human spinal reflex monosynaptic responses, or H reflexes, e.g. in the flexor carpi radialis muscle (Valero-Cabré et al., 2001). Both of these effects (and their converse effects visible with higher-frequency, suprathreshold stimulation) may be mediated by a low-frequency rTMS-induced decrease in cortical excitability (Berardelli et al., 1998; Valero-Cabré & Pascual-Leone, 2005), centered in MI.

8.4.2 rTMS of MI and motor skill acquisition

To assess the effects of rTMS on motor acquisition by direct comparison to control subjects, we made sure to equalize the groups, e.g. in early-afternoon start times (see Methods). The intervals between epochs were consistent for all groups with the exception of a small interval length difference between the practice and baseline epoch (when the rTMS subjects received rTMS localization and MT determination). However, this difference in interval length, and the unique procedures experienced by the rTMS subjects therein, did not appear to lead to any significant difference between the groups during the null-field baseline epoch (Fig. 8-3).

In our experiment we did not apply "control" rTMS to non-sensorimotor regions in the control subjects. Since our task involves not only motor performance but also the integration of proprioceptive, visual, and auditory feedback as well as the involvement of both long- and short-term memory, it would have been difficult to select a control brain region to stimulate (cf. Muellbacher et al., 2002; Della-Maggiore et al., 2004). Although we could instead have used sham stimulation in the control subjects (as in Baraduc et al., 2004), we did not consider it critical in this task because the rTMS was delivered prior to the clockwise field introduction, i.e. while the subject was at rest. However, given evidence that TMS of some brain regions may have general, affective consequences (e.g. Rossini et al., 2005; cf. Miniussi et al., 2005), future replications of this study should include additional control conditions.

But most importantly, we would like to stress that the rTMS and control subjects performed *identically* in the learning epoch (i.e. just after the rTMS was applied), arguing that the rTMS had no immediate effect on motor performance (Fig. 8-3). Even at the very beginning of this epoch, both groups expressed an equivalent level of trajectory deviation (in close agreement with those of control and TMS subjects in Della-Maggiore et al., 2004). This was the case even though the rTMS immediately preceded the learning epoch—and might be expected to have disrupted retention of the prior, same-day baseline adaptation (Muellbacher et al., 2002). Subjects all completed the bulk of the learning epoch within the 10-15 min duration in which rTMS of MI has been shown to have behavioral effects, both with subthreshold (90% MT for 10 min at 1 Hz) and suprathreshold (115% MT for 15 min at 0.9 Hz,

or 120% MT for 30 min at 1 Hz) stimulation (Romero et al., 2002; Chen et al., 1997; Fox et al., 1997). Nevertheless, it should be noted that intersubject variability in the stimulation frequency dependence and the direction (Romero et al., 2002; Gangitano et al., 2002)—and perhaps the timecourse—of these modulatory effects may have been substantial. Despite these concerns, no evidence for a difference between our control and rTMS subjects emerged even by the end of the learning epoch.

Single-pulse, suprathreshold TMS, as used by Della-Maggiore et al. (2004) in posterior parietal cortex during performance of this task, was associated with a higher level of performance error by the end of learning, in contradistinction to our results. But the lack of any effect on performance in our subjects does not suggest that subthreshold rTMS of MI was ineffective. At 90% of the within-subject biceps MT (e.g. Maeda et al., 2000a,b), we expected the rTMS to be able to reduce cortical excitability while not inducing reliable or persistent contractions in the biceps. (The rTMS was also set below the MT measured for the FDI, a muscle extraneous to the task but nevertheless relevant because, like many other hand muscles, it may twitch in response to rTMS intensities lower than the MT for upper arm muscles.) Furthermore, previous studies have similarly shown that subthreshold rTMS of the motor system can modulate cortical excitability over a distributed network without affecting motor behavior (see Lee et al., 2003). As a possible resolution of this paradox, functional brain imaging by Lee et al. (2003) indicates the involvement of additional motor areas contralateral to the site of rTMS.

8.4.3 rTMS of MI and motor skill retention

The identical performance of the control and rTMS groups in their first clockwise field (and the null fields that preceded it) allowed us to investigate whether rTMS had an effect on motor learning independent of initial practice. The performance of the two groups at the very beginning of the retest epoch was comparable (Fig. 8-3). Shortly into the retest epoch, however, the control subjects displayed a level of error characteristically different from that of the rTMS subjects. The rapid divergence of the two groups suggests that the control group was expressing performance gains that had accrued over the previous 24 hours. These off-line improvements, measured well after the immediate excitability effect of rTMS would have dissipated (Maeda et al., 2000b; Robertson et al., 2005), were not present in the rTMS subjects.

The trajectory deviations of the control subjects were deviated against the direction of the force vectors, that is, in a counterclockwise direction (Fig. 8-3). In absolute terms, the performance level of the rTMS subjects actually appeared to be closer to zero by the deviation area and angle measures (Fig. 8-3a,c). However, given that all subjects were performing in a monotonous, clockwise field, their trajectories were expected to be "S-shaped" and deviated against the field at the beginning of the movement (Fig. 8-2b; see Thoroughman & Shadmehr, 2000). Hence it appears that the control subjects developed a more pronounced—and arguably more adaptive—initial trajectory, as captured most intuitively by the initial angle measure (Fig. 8-3a). The absence of a counterclockwise bias in the peak perpendicular error of control subjects' retest trials (Fig. 8-3b) indicates that these participants straightened their trajectories overall even as they may have redirected them against the force field. The

magnitude of this additional improvement in the control subjects is small, but this may be due to the extended practice they had already received on the first day of clockwise field practice.

The magnitude of the additional improvement also showed a relationship with movement direction (Fig. 8-4), as demonstrated with the signed perpendicular deviation metric. Our rTMS subjects, like the control subjects, actually did display off-line changes in performance leading towards zero mean deviation in several directions of movement (0°-90°). In other directions the rTMS subjects showed significantly less off-line adaptation than the control subjects (135° and 225°), or actually developed more pronounced clockwise deviations over the 24 hours between clockwise epochs (225° and 270°). It is worth pointing out that the biceps have previously been shown to be tuned between 180° and 270° in human subjects performing this same task under null or clockwise field conditions (Thoroughman & Shadmehr, 1999). Although we cannot claim to have targeted only the biceps with rTMS while sparing the cortical representation of other muscles, it may be that the effect of rTMS in our experiment was *relatively* more pronounced in directions of movement that involved the greatest biceps activation.

In motor sequence learning literature, consolidation is frequently sought in the form of off-line performance improvements (Robertson et al., 2004a), usually measured in speed or reaction time. These studies have also distinguished practice- vs. sleep-dependent aspects of such consolidation (Korman et al., 2003; Walker et al., 2003b), and the further dependence of each of these phases on conscious awareness (Robertson et al., 2004b). Robertson et al. (2005) found a further distinction between time- and sleep-dependent improvements: when they applied 1 Hz rTMS to MI, off-line improvements were prevented in subjects given daytime hours to consolidate, but continued to accrue overnight in subjects given rTMS prior to sleep.

Our findings are remarkable, first, in their implication that off-line performance improvements over a 24 hour period may describe dynamic motor adaptation as well as sequence learning tasks. But more than this, we have shown that 1 Hz rTMS of MI blocks these off-line improvements, pointing to a clear role of MI and/or associated areas in the stabilization of this dynamic sensorimotor learning in memory. Given the results of Robertson et al. (2005) and functional imaging evidence that MI is not metabolically more active during sleep following serial reaction time or ocular pursuit tasks (Maquet et al., 2000, 2003), we do expect the off-line improvements following force field learning to be at least partly MI-dependent and sleep-independent. Indeed, given that stabilization for such skills may occur over six hours after practice (Brashers-Krug et al., 1996; Muellbacher et al., 2002; see also Chapter 10), and that our two groups on average both completed their learning sessions in the mid-afternoon, we might predict that most of the off-line improvement occurred within subsequent daytime hours. But future studies remain to be done in order to assess the relative contribution of time- and sleep-dependent processes to off-line improvements in motor adaptation.

Figure 8-1 Task design in the human reach task. Right-handed subjects grasped the handle of the low-friction human manipulandum with their dominant hand. This handle was represented on the monitor above the robot by a cursor (not visible). Torque motors mounted above and below the robot generated forces at each of the two joints of the manipulandum, creating a null or velocity-dependent force field in endpoint space as per the computer controller.

Figure 8-2 Sample reach trajectories under null and force conditions. **a**) Subject holding on to the handle of the manipulandum while viewing its cursor representation on a computer monitor. **b**) Trajectories of sample control (top) and rTMS (bottom) subjects, made from the central square to the target at 90°. Compared to the relatively straight movement paths visible among the null-force practice trials, and especially among the following baseline trials, the trajectories are highly deviated in the clockwise direction during the learning epoch, and to a lesser extent among the clockwise retest trials. The recency of the trials plotted, and trajectory improvements *within* each epoch, are represented by the brightness of the points representing sampled hand positions.

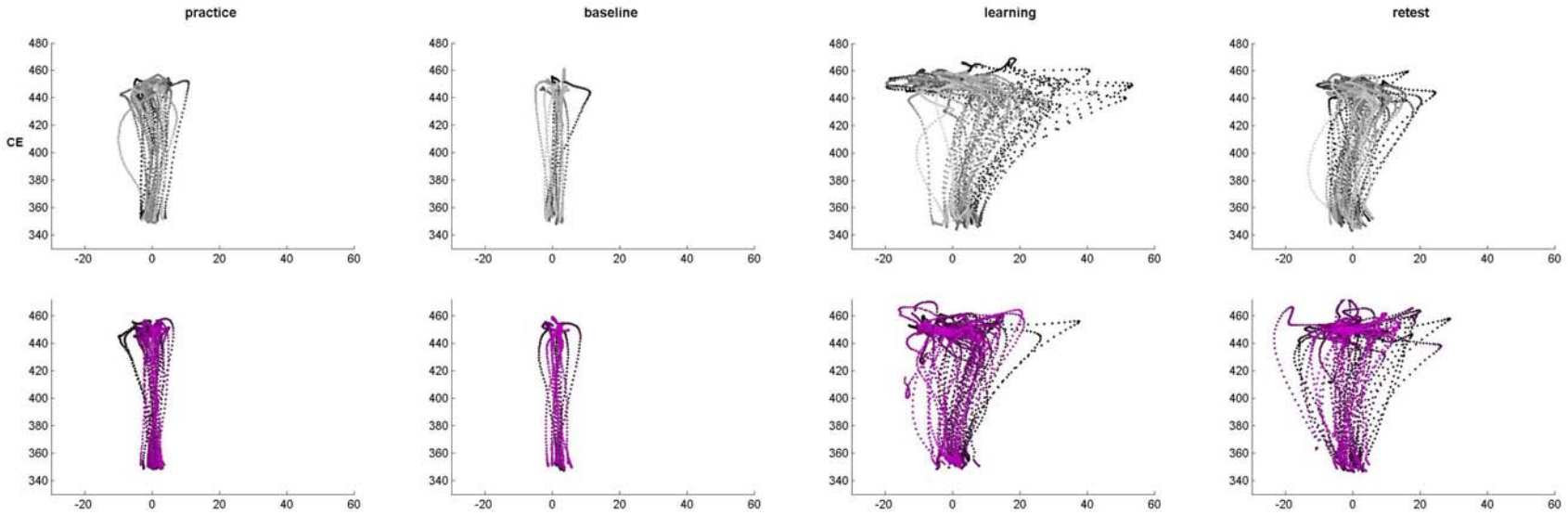

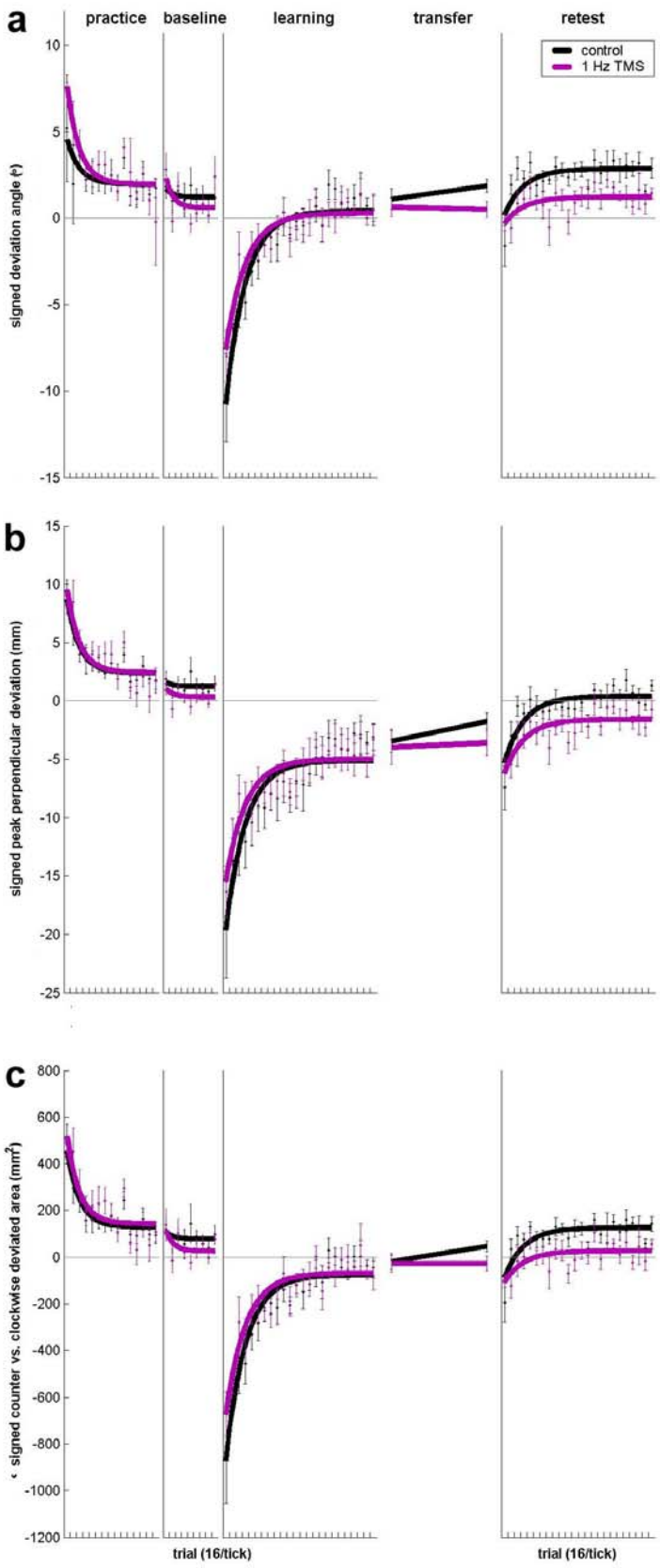

Figure 8-3 rTMS of MI spares motor performance and acquisition but disrupts off-line learning. Performance trends were described in a similar fashion by: **a**) deviation angle from the origin to the point of maximal speed, **b**) peak perpendicular deviation distance from a straight line connecting the origin and target, and **c**) deviation area relative to this same straight line. (In all plots, clockwise deviations are represented by the negative direction on the ordinate.) By all measures the subjects appeared to adapt to the basic, null-field reaching task (with initially counterclockwise-deviated error) in the "practice" epoch. Further small gains were seen in the null-field "baseline" epoch (following rTMS localization and calibration, and before rTMS application to MI in half the subjects). Upon clockwise force field introduction in the "learning" epoch, subjects' errors were all deviated in the clockwise direction, but showed adaptation over the epoch that occurs regardless of the rTMS. An effect of rTMS becomes apparent only in the "retest" epoch, when subjects who had not received rTMS rapidly displayed a level of performance distinct from that of the rTMS subjects. Although by the perpendicular deviation measure (b) the rTMS subjects actually appeared to have a less biased performance by the end of the experiment, we argue that the movements of the control subjects actually displayed superior internalization of the force field. In particular, the angular deviations came to be oriented counterclockwise with respect to the target (a), an adaptive strategy that may have benefited from off-line improvements between the learning and retest epochs. These off-line changes are shown as "transfer" effects that compare performance in the final eight blocks of the learning epoch with the first eight blocks of the retest.

Figure 8-4 rTMS subjects showed direction-specific impairments in off-line improvement. Shown for the signed peak perpendicular deviation metric (Fig. 8-3b) are the magnitudes of the two groups' change in performance between the two clockwise field epochs (radial axis). As in Figure 8-3, these "transfers" of learning are defined as the difference between performance error in the first eight 16-trial blocks of the retest epoch, and the last eight 16-trial blocks of the learning epoch. Negative values of this transfer indicate that performance at retest is more deviated in the clockwise direction than in the latter learning epoch. Whereas these transfers were summed across movement directions in Figure 8-3, here they are plotted within each direction of movement (four of which are to peripheral targets, at 0° through 135°, and the remainder of which are returns to the center). By the perpendicular deviation metric, the control subjects exhibit small positive changes in performance error between the epochs (which bring their mean deviations closer to 0 mm; see Figure 8-3). The rTMS subjects show a similar increase in error only in certain directions of movement, in particular between 0° and 90°. At other directions, the rTMS displayed less off-line improvements than the control subjects. In movement directions of 225° and 270° they exhibited more counterclockwise error at retest than at the end of learning. (Lines represent mean transfer value; shaded regions indicate ±1 S.E.M. around this mean.)

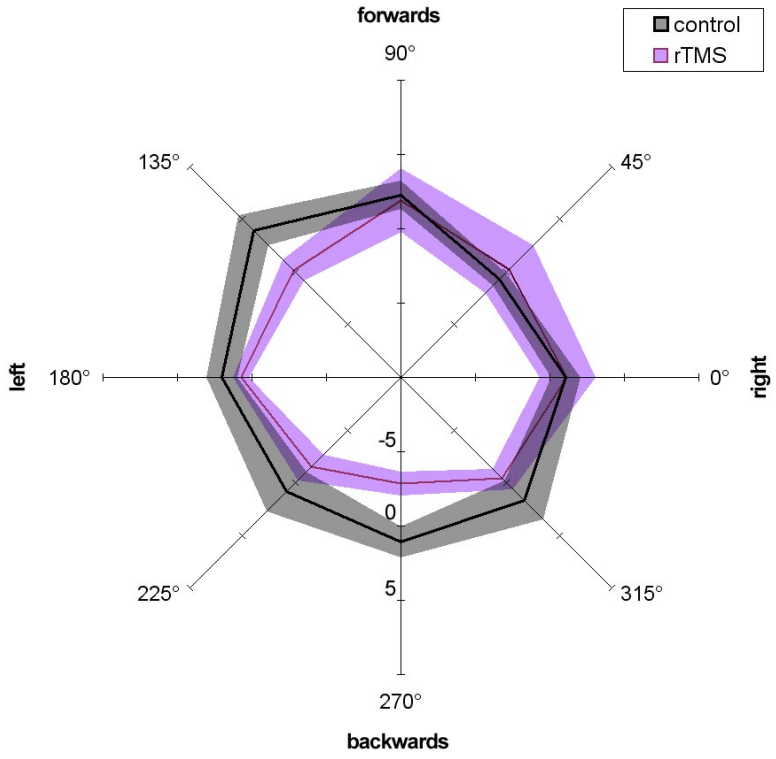

9 Acquisition in Adaptive vs. Sequence Motor Learning

Sensorimotor adaptation and sequence learning have generally been treated as distinct processes within the domain of motor learning. Each has been described as having a "consolidation" stage, but this has been defined either as a gradual resistance to retrograde interference or as off-line improvement following practice. Each has been described as having a distinct pattern of generalization, either across a workspace or between limbs. Each has been ascribed an anatomical network subserving learning, involving distinct cortical and subcortical structures (e.g. premotor and cerebellum, or supplementary motor and basal ganglia). The two forms of motor learning have also been studied by different investigators using different experimental paradigms, most commonly a reaching or a finger tapping task, with different experimental measures, typically ones based on trajectory error or reaction and movement times, respectively. Here I attempt to study the interaction of these two forms of motor learning simultaneously, by having human subjects adapt to force fields imposed by a robotic manipulandum while reaching to an implicit sequence of targets. Adaptation and sequence learning thus occur in the context of the same task performed using the same effectors by the same subjects, and even at the same time. I show that adaptation to a force field and implicit learning of a sequence of reaching movements are indeed relatively independent phenomena. When both conditions were presented simultaneously to subjects, their average kinematic errors and reaction times decreased to the same extent as those of subjects who experienced the force field or sequence independently. However, there was evidence for a unique strategy of sequence learning among subjects also given a force field. Perhaps due to the accentuation of their kinematic errors by the force field, these subjects appeared to apply a chunking strategy wherein their movements were organized around returns to the central target, as reflected in their relatively high reaction times here as well as their recollections following the experiment.

9.1 INTRODUCTION

9.1.1 Two modes of motor learning

Several recent studies of motor learning in human subjects (and Chapter 10 of this thesis) have investigated motor consolidation. This phenomenon has been described psychophysically as a gradual *resistance to retrograde interference* (McGaugh, 2000), and can be observed as subjects learn to reach with straight trajectories through novel dynamical environments created by a robotic manipulandum (Brashers-Krug et al., 1996; Shadmehr & Brashers-Krug, 1997). Another set of motor tasks, best represented by a paradigm requiring rapid finger movements, considers subjects' ability to learn a sequence underlying these movements. Recent studies using such finger opposition behaviors (Fischer et al., 2002) or tapping tasks (Korman et al., 2003; Walker et al., 2003b) to probe motor sequence learning have treated consolidation as an *off-line improvement* in performance (Karni et al., 1998; see Robertson et al., 2004a for review), and have distinguished practice- vs. sleep-dependent aspects of such consolidation and their further dependence on conscious awareness. In particular, implicit, or unintentional, acquisition of sequence

knowledge appears to occur off-line both over wake and sleep periods, but off-line improvement following explicit sequence learning appears to be limited to sleep periods (Robertson et al., 2004b).

There may be commonalities to these two disparate notions of motor consolidation. For instance, despite different rates of learning (Doyon et al., 2003) both sequence learning and dynamic sensorimotor adaptation appear to require a minimum of 2-6 hours post acquisition to appear (Robertson et al., 2005; Press et al., 2005; Brashers-Krug et al., 1996). But as adaptation and sequence learning have traditionally been measured by different groups of researchers using different tasks performed by different effectors, the relation between them is not well understood (Robertson et al., 2004a).

Indeed, consolidation defined as a resistance to interference has only recently been investigated in sequence learning tasks—and has not consistently been found (Goedert & Willingham, 2002; Walker et al., 2003a). Goedert and Willingham (2002) further contrasted consolidation in parallel sequence learning and visuomotor adaptation paradigms, but with such distinct tasks that direct comparison of the two becomes problematic. For instance, in the first case the responses were key presses (rather than direct movements towards the sequential spatial locations); in the second, they were underhanded whole-arm throwing motions made while wearing prism goggles. In motor adaptation literature, meanwhile, rapid off-line "learning" or "reminiscence" in a classical rotary pursuit task has traditionally been attributed either to a lessening of fatigue (Eysenk, 1965) more so than to active skill development (Rachman & Grassi, 1965). Among other concepts commonly applied in sequence learning, conscious awareness has been cited as a factor in the generalization of sensorimotor learning (Abeele & Bock, 2003; Malfait & Ostry, 2004). But to the extent that sleep-dependent learning has been studied for sensorimotor adaptation tasks (Donchin et al., 2002), no sleep-dependent benefits have been found at retest.

Only a handful of recent studies have attempted to investigate the relationship between these two modes of learning. These investigations suggest that motor learning can transfer only in a general way across motor adaptation and sequence learning tasks, and that sequence information does not facilitate adaptation to multiple dynamical environments. Seidler (2004) presented subjects with a variety of visuomotor tasks and a movement sequence, each involving center-out movements made with a joystick. Subjects generalized learning not only across three similar visuomotor rotations and to a novel visuomotor gain change, but also showed improved performance by a decline of reaction times on both random and sequenced trials that might indicate a general enhancement of pattern or error detection or conflict monitoring.

Wainscott et al. (2005), tested subjects who performed reaches while experiencing curl forces dependent not only on the direction of reach but also on the serial order of the movement within a simple, explicit sequence of alternating "even" and "odd" movements. Unlike the alternation of "outward" and "inward" movements typical of center-out tasks, these movements were defined only temporally and not spatially. However, their experiment does not address the learning of the even-odd "sequence" per se (or attempt to make such learning implicit, as in traditional SRT tasks). Their focus was rather on the degree to which the sequential position of each movement informs the trajectory error on the

following movement (which they find to be minimal). Furthermore, the temporally-dependent force field was both difficult to acquire (as in Karniel & Mussa-Ivaldi, 2002, 2003) and not possible to study as a physically independent phenomenon.

9.1.2 Two patterns of learning generalization

Another phenomenon distinguishing sensorimotor adaptation and sequence learning tasks is that of spatial generalization. Adaptation to a velocity-dependent field can implicitly transfer to other response locations in the workspace if the experienced torques, and not necessarily end-point forces at the hand, are either invariant (Shadmehr & Mussa-Ivaldi, 1994; Shadmehr & Moussavi, 2000; Malfait et al., 2002) or can be interpolated (Malfait et al., 2005). This pattern suggests that an intrinsic joint- or muscle-based system coordinate system underlies such adaptation. Sequence learning, in contrast, has been shown to transfer across tasks only if response locations, and not necessarily the motor actions, are kept constant (Willingham, 1999; Willingham et al., 2000; cf. Willingham et al., 1989). This pattern suggests an extrinsic coordinate system.

Interlimb generalization may operate differently from the above examples of spatial, intralimb generalization, but again may distinguish the two forms of motor learning. Force field adaptation has been shown to transfer from one arm to another (Criscimagna-Hemminger et al., 2003) despite the difference of effectors, particularly if explicit learning strategies are recruited (Malfait & Ostry, 2004). In contrast, sequential finger opposition learning has been shown not to transfer between hands (Karni et al., 1998), even when the extrinsic sequence (or matched component movements) was controlled. Future use of our unified paradigm should confirm that these distinct patterns of generalization hold for both sensorimotor adaptation and sequence learning.

9.1.3 Two neuroanatomical systems

The neural systems subserving sensorimotor adaptation and sequence learning have both unique and overlapping elements. Two different subsystems of motor memory have been proposed to underlie the two forms of learning (Hikosaka et al., 1999; Ungerleider et al., 2002; Doyon et al., 2003). According to these models and supporting evidence, acquisition and integration of sequence knowledge may depend on a frontal-subcortical network including nodes in the supplementary motor area, basal ganglia structures, and ventral anterior thalamus (e.g. Schendan et al., 2003; Shin & Ivry, 2003; Lehéricy et al., 2005). In contrast, adaptation to a modified sensorimotor environment may rely more on a network including nodes in the premotor cortex, cerebellum and different thalamic structures (e.g. Shadmehr & Holcomb, 1997; Imamizu et al., 2000; Kassardjian et al., 2005). Involvement of the posterior parietal cortex in acquisition of sensorimotor adaptation has also been implicated by imaging (Clower et al., 1996; Inoue et al., 1997; Ghilardi et al., 2000) and transcranial magnetic stimulation (Della-Maggiore et al., 2004).

However, sequence learning and adaptation tasks do appear to share some neural correlates. Both imaging (Ghilardi et al., 2000; cf. Seidler et al. 2002) and neuropsychological evidence (Inhoff et al., 1989; Exner et al., 2002; Shin & Ivry, 2003) have indicated the involvement of the cerebellum not only in motor

adaptation (as in Shadmehr & Holcomb, 1997) but in sequence learning. Imaging of premotor cortex has shown it to be involved in acquisition of both a novel dynamical environment (Shadmehr & Holcomb, 1997; Inoue et al., 2000) and a sequence (Jenkins et al., 1994). Furthermore, primate neurophysiology has demonstrated that premotor cells are responsive to a target sequence when it is visually presented rather than recalled from memory (Mushiake et al., 1991). Even primary motor cortex (MI)—while it may not similarly be responsive to the degree of sequence present between movements (Mushiake et al., 1991)—has been implicated in human sequence learning as well as motor execution (Karni et al., 1995, 1998; Ghilardi et al., 2000). Transcranial magnetic stimulation (TMS) has been used to more directly test the involvement of this area in motor learning—indeed, resistance to interference by TMS in such studies may be considered a third definition of motor consolidation. When centered on MI immediately following implicit acquisition of a finger movement sequence, TMS has been shown to disrupt off-line improvements that would normally accrue over the day (Robertson et al., 2005). My own results in Chapter 8 similarly found the TMS of MI may disrupt off-line improvements following adaptation to novel dynamical environments. And while although Ungerleider et al. (2002) suggest that MI reorganization may lag behind learning-related changes in either the striatal or cerebellar systems, TMS to this area has also been shown to interfere with the process of motor adaptation (Muellbacher et al., 2002), at least in ballistic tasks if not within novel dynamical environments (Baraduc et al., 2004). Therefore, there is reason to suspect that the two forms of motor learning share some neural resources.

9.1.4 A single paradigm for simultaneous sensorimotor and sequence learning

Here we introduce a novel reaching paradigm for studying both force field adaptation and sequence learning simultaneously, and for testing the interaction between them. In this chapter I do not attempt to study the phenomena of motor consolidation or generalization in this investigation, or the direct cortical involvement in these processes. My focus rather is on the acquisition of new motor memories. The degree to which these forms of learning interact is assessed by the presence or absence of both a curl force field applied by a manipulandum, and an implicit sequence among the targets. Both the force field and, simultaneously, sequence were either absent or present for a block of trials performed by each subject, giving a 2×2 between-subject design. Subjects not presented with a sequence were instead given a random series of targets, subject to similar pseudorandom constraints as a control for the task structure resulting from repeated presentation of the sequence to the other participants. Subjects not presented with a force field were instead given a null field on each trial, rather than a field with mean-matched but random gains (Takahashi et al., 2001; Scheidt et al., 2001). The latter likely would have led to a cocontraction strategy (wherein agonist and antagonist muscles are activated together to increase the stiffness of the arm) as well as an acquisition of the mean field structure, rather than the intended "absence of learning."

In designing the sequence component of our paradigm, we were motivated to keep the sequence acquisition as implicit as possible: 1) to parallel the relatively implicit nature of force field adaptation; 2) to minimize possible effects of awareness on motor learning (Robertson et al., 2004b; cf. Perruchet & Amorim, 1992); and 3)

to avoid spurious disruptions of either force field or sequence learning due to attentional demands (Nissen and Bullemer, 1987). In terms of visuomotor presentation, sequence length, and other parameters our design thus followed more traditional, serial reaction time tasks or SRTTs (see Nissen & Bullemer, 1987; Willingham et al., 1989) rather than the adaptation made by Walker et al. (2003a,b). The duration of the trial epoch during which this sequence was repeated was also set long enough to guarantee that subjects who experienced a force field would generally come to a plateau in their adaptation, but short enough to ensure that subjects would neither fatigue nor develop explicit awareness of a sequence as a result of overtraining (Stadler, 1994). Further, we questioned subjects immediately following the experiment for explicit awareness either of a predictable pattern among the targets presented, or of forces acting on their hand.

To probe the interaction between force field adaptation and sequence learning, it was first necessary to show that both could occur in isolation, following a "baseline" practice epoch with a random target sequence and null forces. Therefore, we predicted that subjects given a clockwise force field would initially experience large trajectory deviations that would converge over adaptation to the stable deviation level exhibited by subjects given a null field. Similarly, we predicted that subjects given an implicit target sequence in the subsequent "test" epoch would develop lower reaction times than subjects given a random target sequence. We expected that both of these phenomena would be mirrored in heightened trajectory error or reaction time aftereffects in a "washout" epoch, when all subjects again experienced the same random target sequence with null forces. As for subjects given both an implicit sequence and a force field, we hypothesized that they would simultaneously exhibit both of the trends described above. We based this hypothesis on the assumption that sensorimotor adaptation and sequence learning are independent processes, as suggested by the weight of evidence cited earlier.

9.2 METHODS

9.2.1 Subjects

Forty-six right-handed, English-speaking students (mean 21.4 years old; 34 females) participated using a custom manipulandum apparatus (Fayé, 1983). Participants were screened for history of neurological illness, epilepsy, seizures, head injuries, and neurosurgery. Ethical approval was obtained through the MIT Committee On the Use of Humans as Experimental Subjects. Subjects were paid at $10/hour, with a $5 bonus for successful completion of the study. Participants occasionally reported fatigue when asked, but none withdrew from the experiment for this reason. One subject was excluded after reporting feeling light-headed, and for talking frequently, during the experiment. Five further participants (one or two from each experimental group) were excluded for having high mean reaction time plus movement time (> 1.5 s) in the second half of the baseline epoch, when pilot experiments suggested that the subjects would stabilize in their trial times. Of the remaining 40 subjects, ten each were randomly assigned to four experimental groups prior to the test epoch. These groups were defined by the combination of null forces and random targets (NR, n = 10), null forces and sequenced targets (NS, n = 10), clockwise forces and random

targets (FR, n = 10), or clockwise forces and sequenced targets (FS, n = 10). The group mean start times ranged from 16:34 to 17:24, i.e. consistently enough to preclude any circadian influences on implicit learning (Cajochen et al., 2004; cf. Heuer et al., 1998).

9.2.2 Paradigm

Task The targets were white 1-cm-wide squares appearing on a black screen, shown to the subject via a vertically-oriented monitor above the planar manipulandum apparatus. Motions of the handle were represented on the screen as continuous movements of a 0.8-cm-wide red crosshair. The targets were spaced hexagonally to ensure equidistant separation of neighboring targets (similar to the design of Wainscott et al., 2005). The movement distances were 10 cm both in real space and as shown on the monitor. Participants were given 1 s to complete each movement, starting from the moment the target was presented and lasting until their cursor entered the target. The target remained on the screen even if subjects failed to reach it in the allotted. Upon acquiring the target, a further 0.5-s within-target hold time had to be observed in order for the trial to be a "success." Trial success was indicated to the subject by a transition in the color of the target from white to green just prior to its disappearance. If either of the conditions was not met, the trial failure was instead indicated by a target transition from white to red.

Intervals Subjects all performed a baseline, test, and washout epoch separated by 5 min. Subjects sat at the manipulandum during the 5-min breaks, either waiting for the next epoch of trials or talking with the experimenter.

Instructions Participants were informed that they were part of a study on "motor learning" and were all "control subjects" for a TMS investigation. The basic task was described, and subjects were asked not to "anticipate" the targets but merely to move as "naturally" as possible. They were informed that targets would often be difficult to reach in the allotted time, particularly at the beginning of the experiment. The trial "success" feedback was described, but participants were told it was given merely to help them make their movements as consistently as possible, and not to evaluate how successful they were. As a safety precaution, subjects were warned prior to each epoch that they might experience "forces" generated by the robot during the epoch. However, care was taken before and during the experiment not to refer to any temporal order (either random or sequenced) or spatial distribution of the targets.

Forces All subjects experienced a null (0 N·s/m) force field during the baseline and washout epochs, and NR and NS participants received a null field during the test epoch. No forces were applied by the manipulandum motors during these epochs. During the test epochs of the FR and FS subjects, the motors generated a velocity-dependent clockwise force field of 10 N·s/m (Fig. 9-1a). Forces were calculated on-line as $f = \mathbf{B}\dot{x}$, where $\mathrm{B} = \begin{bmatrix} 0 & 10 \\ -10 & 0 \end{bmatrix}$ and $\dot{x}$ was the movement velocity. There were no catch trials (i.e. trials on which the motors were suddenly turned off).

Sequence In the baseline and washout epochs all subjects experienced targets preprogrammed according to the same two pseudorandom 180-target files. The NR and FR participants received similar, pseudorandom 360-target files during the test epoch. During the test epochs of the NS and FS subjects, the 360 targets were presented according to 20 repetitions of the same sequence of 18 targets (Fig. 9-1b). There were no breaks or other indications of the transitions between repetitions, and no random target positions embedded in these epochs. All sequence subjects completed each repetition of the entire sequence—trials were not aborted if they failed to reach the target on time.

Targets Target squares were presented at six peripheral locations spaced hexagonally around a central location. Following each trial the target became the "origin" for movement to the subsequent target, as in Shadmehr and Mussa-Ivaldi (1994). The first origin in each epoch was always the central square. From each of the six peripheral origins the possible targets were restricted to one of the three neighboring equidistant targets. From the central origin, movements to only three of the six candidate directions were allowed; these were equally spaced at 120° increments (Fig. 9-1b). The 18-target sequence was chosen subject to the following additional constraints: 1) there were no "repeats" (i.e. targets ABA), and 2) there were no "semi-circles" (i.e. targets ABCDEA with A as the central target). Patterns such as "triangles" (ABCA) and "parallelograms" (ABCDA) were permitted, as in the random target files. All target files were further constrained to have equal frequencies of both the six movement directions possible from the set of peripheral targets and the three directions allowed from the central target. (The 18-target sequence itself obeys this last rule as closely as possible, with one necessary exception: of movements 5, 9, 13 and 18, only one originates from the center.) With these restrictions it was not possible to maintain equal frequencies of origin and target position, and indeed a higher proportion of the trials (27 ± 2% of the test epoch trials across groups, mean ± S.D.) originated at the center rather than the periphery.

9.2.3 Recording/Stimulation

Verbal reports Immediately following the experiment we probed all participants for explicit awareness of either a target sequence or force field structure. Subjects who answered positively to either of these phenomena were further asked to identify the epoch(s) in which the sequence(s) or force field(s) was (were) detected, and/or to describe the structure of any part of the sequence(s) or the field(s).

Reaction time As in classical SRTT studies (Nissen & Bullemer, 1987; Willingham et al., 1999; Willingham & Goedert-Eschmann, 1999), we used reaction time as an indirect measure of sequence learning. We defined reaction time to be the time into the trial at which subjects last reached 20% of their peak speed within that trial, prior to reaching the peak speed. Speed was calculated by off-line differentiation of the manipulandum joint encoder position signals that we sampled continuously throughout the experiment. Reaction times based on absolute rather than relative speed, or spatial displacement relative to the beginning of the movement, gave qualitatively similar results.

Performance error For our measure of force field adaptation, we chose to look primarily at the total deviation area swept out by the movement relative to a straight line connecting the beginning and end positions of the trial (Caithness et al., 2004). Several other measures of trajectory deviation (peak perpendicular deviation and deviation angle—i.e. measures compared in Chapter 8—and path distance) yielded qualitatively similar results. We did not consider measures (e.g. perpendicular deviation at 200 ms into the movement, or correlation to baseline speed profiles) that we expected a priori would change spuriously as a result of decreasing speed-based reaction times—our measure of sequence learning. However, we did consider total movement duration following reaction time as an additional performance measure, as it was presumably a more intuitive performance measure from the subject's point of view given the trial success criteria.

9.2.4 Analysis

Baseline correction Given our finding that reaction times varied with movement origin (see Figure 9-6a and Results)—unlike movement direction, a variable not controlled for in the experimental design—we applied a correction for movement origin location to participants' reaction times and performance errors. This correction involved taking the relative time or error each subject displayed at each origin position in the last 30% of the baseline epoch, and dividing their scores in all test- and washout-epoch trials originating from the same position by this factor.

Comparisons Trials in which the subject failed to reach the target in the allotted 1-s time limit were still included in the analysis. However, we rejected any trial in which the combined reaction plus movement time was less than 0.25 s or greater than 1.75 s. Trials were binned by 18 trials in each epoch and condition. Statistical results were based on the within-bin-averaged trajectory error, movement duration, and reaction time scores. We did not exclude the first 18-trial bin of each epoch in the analyses. Aftereffects, i.e. changes in performance error or reaction time upon initiation of the washout epoch, were estimated by comparing the mean scores of the final two 18-trial bins in the test epoch and the first two 18-trial bins in the washout epoch. Main and interaction effects of Force, Sequence, and Time (or Bin average, in the case of aftereffects) were assessed for trajectory error, movement duration, and reaction time separately, using repeated measures ANOVAs. (In this and the following chapter post-hoc tests remain to be completed.) All significant effects (at the $p < 0.05$ level) are reported.

9.3 RESULTS

9.3.1 Sensorimotor adaptation and sequence learning in isolation

As a validation of our paradigm, it was first necessary to demonstrate that force field adaptation and sequence acquisition could both occur in the task. Figure 9-2 demonstrates such trends for two sample subjects who experienced in isolation either a force field or a sequence during the test epoch. Figures 9-3 and 9-5, discussed

below, summarize these trends for all subjects, including those who experienced only null forces and random targets (NR, n = 10), null forces and sequenced targets (NS, n = 10), clockwise forces and random targets (FR, n = 10), or clockwise forces and sequenced targets (FS, n = 10). Among subjects given a clockwise force field, sensorimotor adaptation is evident as a gradual decline in trajectory deviation area. Among subjects given nonrandom targets, sequence learning is evident as a change in the latency and shape of subjects' speed profiles, captured by our speed-based measure of reaction time (see Methods).

9.3.2 Effects on performance error

Deviation area The average changes in trajectory deviation area in each group and epoch are summarized in Figure 9-3. Across groups, subjects demonstrate a significant adaptation to the null field during the baseline epoch ($F_{(9,39)}$ = 17.72, $p < 0.0001$). Application of a force field following training was initially associated with large trajectory deviations among both the FR and FS subjects. Both these groups then showed evidence of adaptation to those forces. These trends are captured by significant main effects of Force and Time, i.e. trial bins ($F_{(1,39)}$ = 10.10, $p < 0.01$; $F_{(19,39)}$ = 6.50, $p < 0.0001$), and by a significant Force × Time interaction ($F_{(19,39)}$ = 11.12, $p < 0.0001$). When the forces were removed in the null-field washout epoch, both the FR and FS groups again showed a large initial level of trajectory error but a rapid decline in this error during re-adaptation to the null-force conditions. (The relatively large variability in trajectory error across groups during this epoch may indicate global fatigue.) These washout trends are captured by significant Time and Force × Time effects ($F_{(9,39)}$ = 15.74, $p < 0.0001$; $F_{(9,39)}$ = 6.77, $p < 0.0001$). The magnitudes of these aftereffects—another measure of adaptation—were estimated by comparing the average of the final two 18-trial bins in the test epoch with the first two 18-trial bins in the washout epoch. Again the force subjects displayed the only prominent aftereffects: we found significant main effects of Force and Bin-averages ($F_{(1,39)}$ = 3.23, $p < 0.05$; $F_{(1,39)}$ = 10.53, $p < 0.01$), and by a significant Force × Bin interaction ($F_{(1,39)}$ = 10.46, $p < 0.01$). The actual magnitudes of the trajectory error aftereffects were +6 mm^2 (NR), -5 mm^2 (NS), +223 mm^2 (FR), and +139 mm^2 (FS). We found no significant main or interaction effects of Sequence in any of the epochs or transitions between epochs. (Note that the parallel temporal structure of the grouops' error reflects both the identical target files received by these groups—except for the sequenced file introduced to two groups in the test epoch—and any uncontrolled concentrations of certain targets or movement directions within these files.)

Movement duration These trends generally hold for another measure of performance, subjects' movement durations, as shown in Figure 9-4. Global adaptation of movement time in the baseline epoch is described by a significant effect of Time ($F_{(9,39)}$ = 32.98, $p < 0.0001$). Subjects continued to improve in the test epoch, as confirmed by a significant main effect of Time ($F_{(19,39)}$ = 8.71, $p < 0.0001$). By the last two 18-trial bins of the test epoch, movement times of the null-force subjects had declined to 0.88 ± 0.08 s (NR, mean ± S.D.) and 0.86 ± 0.07 s (NS), while those of the clockwise-force subjects had declined but still remained elevated at 0.99 s ± 0.06 s (FR) and 0.95 ± 0.09 s (FS). The groups' differential learning patterns as a function

of force field in this epoch are captured by significant main effects of Force and Time ($F_{(1,39)}$ = 42.84, p < 0.0001; $F_{(19,39)}$ = 8.71, p < 0.0001), and by a significant interaction of Force × Time ($F_{(19,39)}$ = 2.64, p < 0.01). In the washout epoch, these patterns were recapitulated in significant main effects of Force and Time ($F_{(1,39)}$ = 3.80, p < 0.05; $F_{(9,39)}$ = 8.31, p < 0.0001) and their interaction, ($F_{(9,39)}$ = 4.26, p < 0.001). Among the transitions between test and washout epochs, there is again a significant main effect of Force ($F_{(1,39)}$ = 19.97, p < 0.0001) which may simply reflect the FR and FS groups' failure to converge with the null-force groups by the end of the test epoch. As hinted by a small but significant Sequence × Bin interaction ($F_{(1,39)}$ = 5.63, p < 0.05), a learning aftereffect is only prominent among the FS group. We found no other significant main or interaction effects of Sequence in any of the epochs or transitions between epochs.

9.3.3 Effects on reaction time

Overall reaction time The average changes in reaction time in each group and epoch are summarized in Figure 9-5. Across groups, subjects demonstrated a significant improvement in reaction times during the random-target baseline epoch ($F_{(9,39)}$ = 13.86, p < 0.0001). Introduction of an implicit sequence following training was associated with a gradual decrease in reaction times among both the NS and FS subjects. These trends are captured by a significant main effect of Sequence ($F_{(1,39)}$ = 6.96, p < 0.01) and by a small but significant Sequence × Time interaction ($F_{(19,39)}$ = 2.05, p < 0.05). When the target presentation again became random in the washout epoch, it was the two force field groups (FR and FS) who initially showed the highest reaction times. Their reaction times then declined along with those of the NR and NS groups. (The global decrease in reaction times across groups in the washout epoch, and to a lesser extent in the test epoch, may indicate impatience as much as general skill learning.) These washout trends are captured by a small but significant main effect of Force ($F_{(1,39)}$ = 4.85, p < 0.05), and a significant effect of Time ($F_{(9,39)}$ = 4.05, p < 0.001). We found no other significant main or interaction effects of Force in any of the epochs or transitions between epochs. Indeed, the effect of force in the washout epoch disappeared when we applied a more widely-accepted and specific measure of sequence learning, namely reaction time "aftereffects" (Nissen & Bullemer, 1987; Willingham et al., 1989; Goedert & Willingham, 2002; Robertson et al, 2004b; Press et al., 2005; Robertson et al., 2005), defined as for performance error. We found that only the sequence learning groups, and in particular the FS group, experienced a relative increase in reaction time between the test and washout epochs. Statistically, the only significant aftereffect comparison was the Sequence × Bin interaction ($F_{(1,39)}$ = 9.11, p < 0.01). The actual magnitudes of the aftereffects were -17 ms (NR), +8 ms (NS), -10 ms (FR), and +24 ms (FS).

Reaction time as a function of serial order In order to better understand the uniquely large aftereffect in washout-epoch reaction times among subjects who experienced both a clockwise force field and a sequence (FS), we examined how the reaction times changed as a function of serial order within the sequence. First, we found that subjects generally showed elevated reaction times (prior to correction as described in the Methods) when launching movements from the central target location. Figure 9-6a shows this effect for the NS group, as well as their decline in

reaction times with learning over the test epoch. We hypothesized that the sequence learning subjects might organize their acquisition of the sequence around these "returns to center." Therefore we compared all groups in terms of their average reaction time change over the test epoch at all center-originating targets and the subsequent periphery-originating target. All subjects demonstrated a small drop in reaction times at center-originating trials, but the FS subjects were unique in demonstrating a large decrease in reaction times on the next, periphery-originating trial. This trend was captured by small but significant Sequence × Bin and Force × Sequence × Bin effects ($F_{(1,36)} = 4.50$ $p < 0.05$; $F_{(1,36)} = 3.20$, $p < 0.05$).

9.3.4 Implicit vs. explicit learning

Force awareness During questioning following the experiment, FR and FS subjects were reliably able to identify the presence of a force field in the test epoch (Table 9-1). This was true even though one each of the NR and NS subjects incorrectly suspected a force field in the test epoch, and one each of the FR and FS subjects also incorrectly claimed there were forces in the washout or baseline epochs. Some of the force field subjects in each group described the force field as "resistive," "counteracting," "harder to start" or "stop," or "jerky." Others in both groups emphasized the *deviations* caused by the force field rather than its *resistance*, describing it as "pushing" or "pulling" movements either "to the side" or "off course" or "off track," or otherwise making movements not "straight." One additional participant (from the FR group) included in this category described the forces as being stronger in certain directions. One FR subject and two FS subjects more specifically described the forces as resulting from a certain segment or joint of the robot. Although many of the subjects were MIT students, no subject described the force field structure using terms such as "circular" or "clockwise," or as "viscous," "velocity-" or "speed-dependent."

Sequence awareness Subjects who reported that the target positions were arranged in a regular (usually hexagonal) pattern were generally from the NS and FR groups (three and six, respectively). Only one FS subject and no NR subjects volunteered this information. Several subjects in each group further reported that there were short but salient *patterns* of movements between these targets (Table 9-1). For instance, two or three subjects in each group reported frequent two-movement lines (targets "ABC") or repeats (ABA). One or two subjects in each group reported "triangular" (ABCA) movements. Longer patterns (e.g. "parallelograms," "diamonds," "X's," and "snowflakes") were only described by two NR subjects and four FS subjects, but none described these patterns as being part of a longer sequence. Subjects who did actually claim that a *sequence* underlay their movements in a particular epoch were present in each condition (one NR, two NS, two FR, and four FS subjects), and generally incorrect. These reports were clearly incorrect in the case of the NR and FR subjects. Furthermore, of these respondents the NS, FR, and FS subjects were evenly divided in placing the sequence in the test epoch or, incorrectly (and like the NR respondent), in the washout epoch. Four of the subjects, all in the NS group, reported a definite feeling of having experienced a *sequence* during the experiment, and in particular an ability to "anticipate" the next target, but only one of these referred this experience to a particular epoch (the test epoch). None of these

participants could reproduce any part of the sequence except for one subject who drew a sequence of six movements (only four of which correctly corresponded to the any part of the 18-target sequence given).

9.4 DISCUSSION

9.4.1 Sensorimotor adaptation and sequence learning do not compete

Our paradigm allows for acquisition of either novel sensorimotor or sequence experience (Fig. 9-2). These two modes of learning occur in the context of the same task performed using the same effectors by the same subjects, and even at the same time. Because of the common task, the design precluded spurious interactions of sensorimotor and sequence learning at the level of motor performance. This was the case even though these two phenomena likely share neural substrates at the level of motor execution simply because they both involve the arm (rather than the arm and hand—more traditional experimental models). Though we included three control conditions (NR, NS, and FS) and three experimental epochs (baseline, test, and washout), we were able to apply a within-subject design, within a single block of trials, to study the immediate interaction between motor adaptation and sequence acquisition.

In so doing, we showed that adaptation to an external force field and learning of an implicitly presented sequence are relatively independent phenomena. When both conditions are presented simultaneously to participants, they show as much of a decline in trajectory error and reaction time as subjects who experience the force field or sequence independently, and like them, more of a decline than subjects who experience neither condition (Figs. 9-3, 9-5). We predicted the relative independence of these phenomena based on the psychophysical and neuroanatomical evidence cited in the introduction, with the caveat that no previous investigation had attempted to probe the interaction of these phenomena in a single task.

Although sequence learning has been shown to have some sensitivity to attentional capacity (Nissen & Bullemer, 1987; Frensch & Miner, 1994; McDowall et al., 1995), it might be argued that our task was too easy to allow competition between motor adaptation and sequence learning to exhaust neural resources. In reality, the task we set for our subjects was arguably more difficult than most SRTT or dynamic adaptation tasks. We placed a single, 1-s restriction on reaction and movement time combined (rather than a restriction on movement time alone). This gave subjects the incentive to reduce their reaction time to the extent that their prediction of the next target would allow, and simultaneously to minimize the duration of their trajectories as much as the force field would allow in order to reach the target in the allotted time. This period of time was insufficient for subjects to reach the target in time on most trials, even with learning under control conditions. By the last two 18-trial bins of the test epoch, the average movement times of the null-force subjects (not even considering the additional reaction times) had barely declined below 1 s.

While sensorimotor adaptation and sequence learning did not *interfere* with each other, we also found little evidence that sequence learning *facilitated* force field adaptation. We might have expected that shortened reaction times would have

allowed subjects more time to complete their movements, and thus would have granted those subjects experiencing the force field less of a perturbation. However, our movement time restriction was strict enough that movement times continually decreased in all subjects, independently of their experience of a force field (Fig. 9-4). Furthermore, both reaction and movement times decreased in the subjects given both a sequence and a force field, and when these conditions were removed in the washout epoch, both reaction and movement times became transiently elevated (Figs. 9-4, 9-5). Indeed, the direct relationship between reaction and movement time appears to hold for the aftereffects of each group. This phenomenon may be understood by reference to Figure 9-2b, which demonstrates that as the speed profiles are initiated earlier in time, so too do they become heightened, allowing the target to be acquired sooner.

The absence of an interaction between sensorimotor adaptation and sequence learning at the level of subjects' trajectory error is consistent with recent evidence that serial order cues do not facilitate adaptation to multiple dynamical conditions. Wainscott et al. (2005) presented subjects with forces that depended both on the direction of reach and the serial position of each movement within a two-movement "sequence." The authors developed a generalization function describing the transmission of error information from trial to trial as a function of distance in a state space defined by movement direction, and to a much weaker extent, by ordinal number. Their results, like those of Karniel and Mussa-Ivaldi (2002, 2003), suggest that the acquisition of two models of external forces occurs relatively independently of simultaneous sequential information about each movement.

9.4.2 Sequences are encoded differently depending on the dynamical context

Explicit awareness of a sequence need not impair learning of that sequence (Nissen & Bullemer, 1987; Willingham & Goedert-Eschmann, 1999), or alter the involvement of the hippocampus and cortical areas in the formation of this sequence knowledge (Schendan et al., 2003). However, the importance of conscious awareness in determining the features of motor learning has been invoked in the ability to generalize motor adaptation across movements (Abeele & Bock, 2003) or space (Criscimagna-Hemminger et al, 2003; Malfait & Ostry, 2004). Awareness has also been shown to relate to people's ability to protect the memory of a new motor sequence from later retrograde interference (Goedert & Willingham, 2002; Walker et al., 2003; see Caithness et al., 2004).

In part to make the sequence difficult for the participants to recognize, we chose a relatively long sequence of 18 targets. This was longer than the 12-item sequences commonly used in serial reaction time studies (e.g. Goedert & Willingham, 2002), and the 5-item sequences explicitly learned by the subjects of Walker et al. (2003a,b). However, it was possible that subjects used a "chunking" strategy, as occurs in other visuomotor sequence tasks (Sakai et al., 2003). Subjects' frequent returns to the central target (e.g. Fig. 9-1b) may have demarcated these chunks, perhaps because of the relatively long "rests" made by subjects prior to movements from this position (Fig. 9-6a). These elevated reaction times were not likely due simply to "indecision" resulting from a greater number of candidate targets, since all subjects' center-out movements were restricted to only three paths (Fig. 9-1b), as were movements originating at the periphery. It is possible that the elevated reaction times were due to

the greater spacing of the three possible targets—at 120°, twice the spacing of targets accessible from peripheral origins. But whatever the cause of the reaction time differences, it is clear that the most natural separations between the movements occurred at rests at the central target.

Consistent with this hypothesis, the more complicated movement patterns (e.g. "parallelograms;" Table 9-1) recalled by the FS subjects all passed through the central target. These recollections developed even though the chunked movements themselves were still necessarily discontinuous, given the 0.5 hold period that had to be maintained at the end of every trial in order for the next target to appear, and the variable reaction time that followed. (Such learning is in agreement with prior evidence for serial learning in variable and discontinuous stimulus conditions: McDowall et al.; 1995; Willingham et al., 1997.) Our finding that these same subjects also developed a uniquely and relatively large decline in reaction time in trials following center-out movements suggests that they anticipated subsequent targets. Such anticipation was evident as a reduction in the interval between chunked trials, if not at the beginning of these sub-sequences.

Robertson et al. (2004a) discuss the possibility that long sequences do not require a period of stabilization because they can be learned as a series of interleaved chunks—in the same way that two force fields can be learned when presented in a rapidly interleaved (Osu et al., 2004) rather than blocked (Shadmehr & Brashers-Krug, 1997) fashion. We found no evidence that sequence subjects actually did implicitly learn the entire 18-target sequence. Such learning can often be inferred from an increase in reaction time at the first trial of the sequence (Povel & Collard, 1982). We neither observed (e.g. Fig. 9-6a) nor expected such an "initiation cost" given that there were no explicit or implicit cues as to the transitions between sequences. But our interpretation that the FS group was at least able to chunk their movements into subsequences (if not into the longer 18-target sequence) may explain their disproportionately large reaction time aftereffect upon being reintroduced to randomly-ordered targets in the washout epoch (Fig. 9-6b).

While sequence subjects were unable to acquire the entire sequence implicitly, they were even less able to develop explicit awareness of the sequence. The minority of participants who reported after the experiment that there might have been some general non-randomness to the targets in a particular epoch were distributed across all four conditions, and half or more of these responses incorrectly identified the sequence as having been in the washout epoch (Table 9-1). These subjects may have been deceived by the presence of salient "repeats" during the washout epoch, as in the baseline epoch and, in the case of NR and FR subjects, the test epoch. (Future work with the paradigm presented here should avoid target repeats in the random target conditions, while observing as many of the remaining pseudorandom constraints that we did apply). Beyond these false positive controls, only four subjects in the study specifically asserted the presence of a discrete sequence (rather than short, frequent patterns or general target non-randomness) and/or their ability to anticipate the next target, and only one of these identified even four of the eighteen movements. Notably, each of these four subjects was in the NS group. Whether or not their level of recall qualifies the criterion for sequence "awareness" on the standard 12-item SRTT (Willingham & Goedert-Eschmann, 1999), it does suggest a low level of explicit awareness in this group. (In order to better assess subjects' explicit recall, future experiments might include an additional target prediction task

at the end of the experiment, as in Willingham et al., 1989.)

In curious contrast, all of the remaining subjects who received a sequence and *were* able to recall a salient pattern of four or more movements (e.g. a parallelogram) were from the FS group (Table 9-1). These four FS subjects were able to reproduce movement patterns that were in the actual test-epoch sequence, yet unlike the four NS subjects above, they did not claim that there actually had been a sequence containing these patterns. The inability of the FS subjects to notice their declining reaction times (in spite of their large increase in reaction times upon removal of the sequence) may have been related to the forces they simultaneously contended with—our only evidence for an interaction between force and sequence learning at an attentional level. These contrasts, though difficult to quantify, appear to suggest that without true explicit awareness, some NS subjects nevertheless recognized their ability to anticipate the targets within the sequence, while some FS subjects became attuned to their repeating movement patterns—perhaps due to the accentuation of their kinematic errors by the force field.

Table 9-1 Sequence learning study subjects' force field or sequence awareness reports by group. Bold text denotes reports from subjects who actually did receive a force field or sequence in the second (test) epoch. False reports of the force field across conditions and epochs may be attributed to initial adaptation to the manipulandum, fatigue, or aftereffects they experienced. The terms that subjects used when the force field was correctly recognized can be classified as emphasizing only its general resistance or its deviations (see Results). Three further subjects specifically described the forces with mechanical reference to a certain segment or joint of the robot. False reports of a sequence also occurred in all groups and more commonly in the random-target, washout epoch. Of those subjects who claimed to have experienced a discrete sequence, and/or an ability to anticipate the targets, all were in the NS condition. But only one referred these sensations (correctly) to a particular epoch, and only another was able to describe even four consecutive movements making up the sequence. Other subjects, notably concentrated in the FS group, did recall relatively salient patterns longer than two or three motions (e.g. "parallelograms"), but none claimed these were part of a repeating movement sequence. In all reports, note that some subjects did not volunteer or articulate a description of either the force field or a sequence, while some offered multiple descriptions or reported a field or sequence in multiple epochs.

groups	*force field awarenes*						*sequence awareness*						
	reports by epoch			*descriptions*			*reports by epoch*			*discrete*	*salient patterns*		
	1	*2*	*3*	*resistance*	*deviation*	*mechanical*	*1*	*2*	*3*	*sequence*	*2*	*3*	*4+*
NR (n = 10)	0	1	0	0	0	0	0	0	1	0	4	2	1
NS (n = 10)	0	1	0	0	0	0	**0**	**1**	**1**	**4**	**2**	**1**	**1**
FR (n = 10)	**0**	**10**	**1**	**6**	**5**	**1**	0	1	1	0	4	1	0
FS (n = 10)	**1**	**10**	**2**	**5**	**1**	**2**	**0**	**3**	**3**	**0**	**3**	**2**	**4**

Figure 9-1 Revised reach task structure. **a**) Subjects experiencing a planar, clockwise viscous force field in the second ("test") epoch felt the manipulandum apply forces to their hand that were consistently proportional in magnitude to the speed of their movement, and perpendicular to the direction of their movement. **b**) Subjects presented with a repeating, nonrandom 18-target sequence in the test epoch made movements between the seven targets in the serial order shown. Whether participants experienced a null (N) or clockwise force (F) field and/or a (pseudo)random (R) or sequenced (S) target presentation, they were required to make "natural," 10-cm movements to each new target as soon as it appeared, without "anticipating" the target location. Trials were deemed "successful" if the subject's total reaction plus movement time did not exceed 1 s, and if they then held the cursor representing their hand in place within the target for 0.5 s. Movements of all participants in each epoch were constrained to the paths denoted by the arrowheads between target locations.

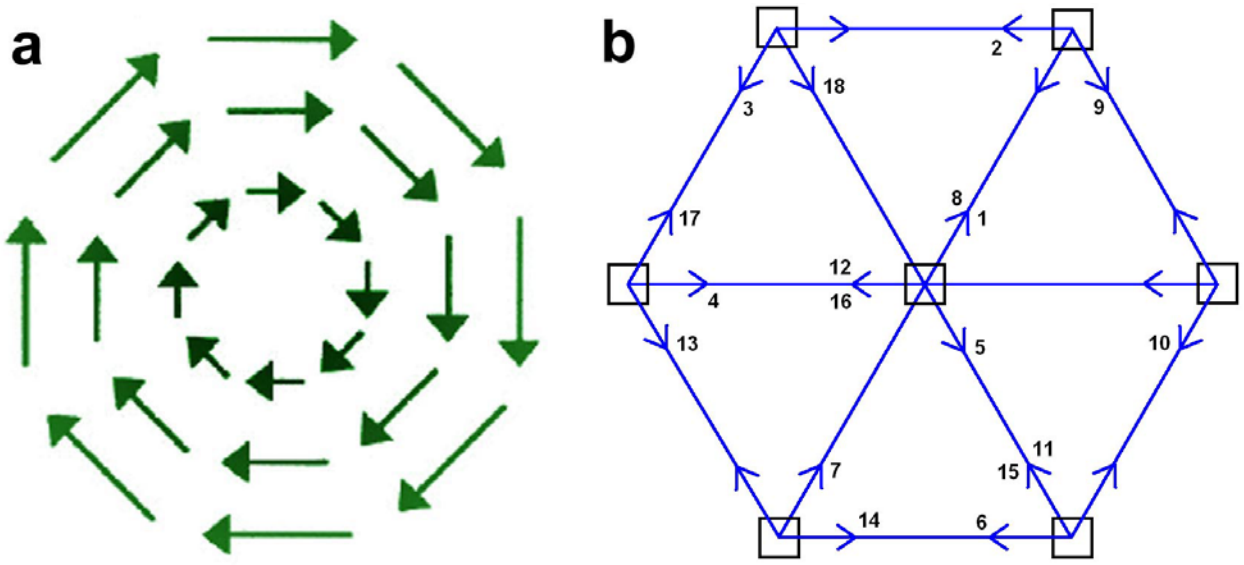

Figure 9-2 Force field adaptation and sequence learning in isolation. **a**) FR subjects experienced a clockwise force field but no sequence in the test epoch. As can be seen in the center-out trajectories of this sample participant, movement paths are deviated in the direction of the field. The paths appear more deviated at the beginning of the epoch (•) than at the end (•). This force field adaptation was well-characterized by a measure of the total area of the trajectory deviation. **b**) NS subjects experienced an implicit target sequence but no viscous force field in the test epoch. As can be seen in the speed profiles recorded in one direction of movement from a sample participant, speed profiles remained bell-shaped but movements early in the epoch (•) appear delayed and slower at peak speed relative to those late in the epoch (•). This sequence learning was well-captured by a measure of the time at which subjects reached 20% of their peak velocity.

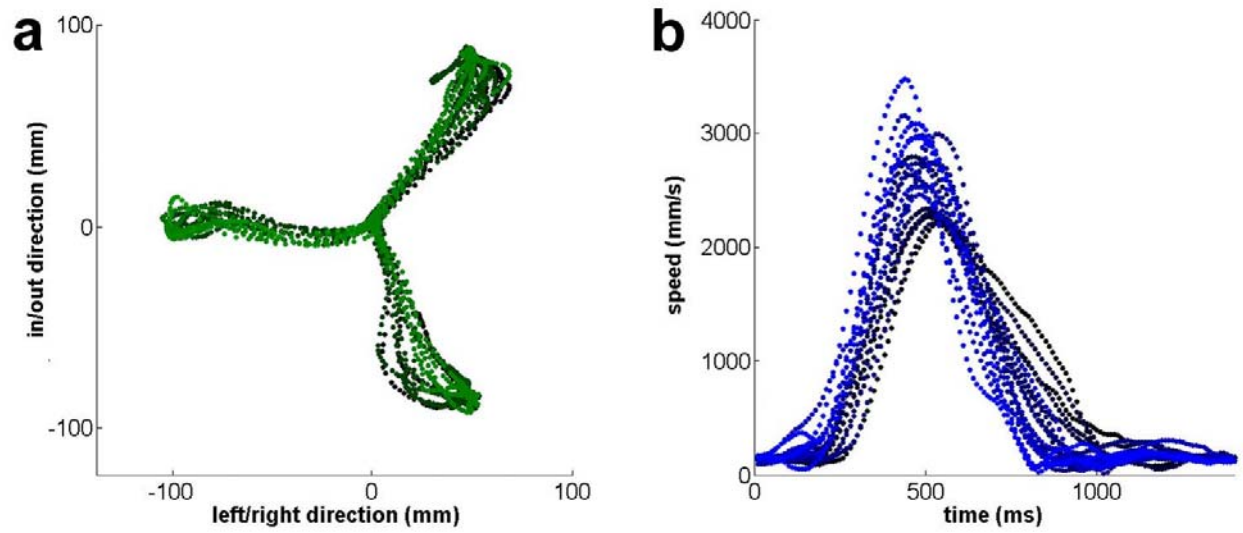

Figure 9-3 Decrease in trajectory deviation evident among subjects given a force field. After subjects had achieved a stable level of performance in the baseline epoch (left panel), the introduction of a force field in the test epoch of the FR and FS subjects (center) led to immediate, large trajectory deviations. These deviations declined over the first half of the epoch and then converged with the deviations exhibited by the subjects experiencing a null field (NR and NS). When all subjects performed a final washout epoch with null forces (right), subjects who had previously adapted to the forces show a characteristic "aftereffect," which again rapidly declined to baseline levels. (The aftereffect was defined as a change in average error between the last two 18-trial bins of the test epoch and the first two bins of the washout epoch.) These trends were consistent regardless of whether subjects simultaneously experienced an implicit target sequence. (Lines represent group averages of subjects' binned data, ±S.E.M.)

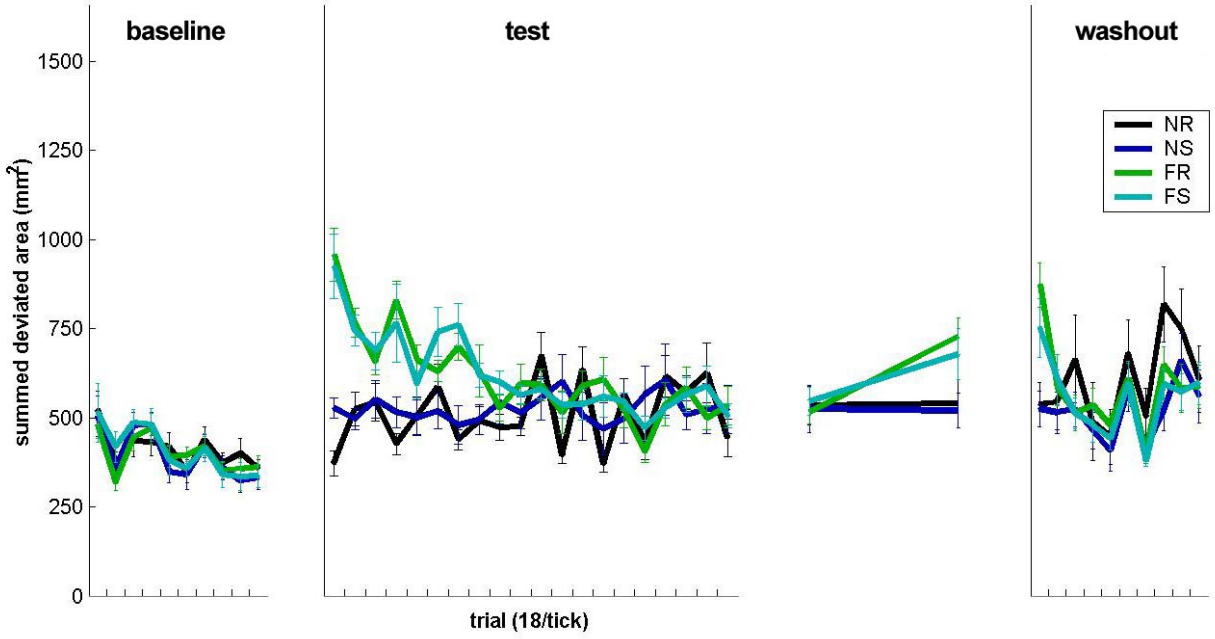

Figure 9-4 Decrease in movement duration evident among subjects given a force field. As an alternative measure of performance, subjects' adaptation is shown in terms of movement duration (following reaction time) rather than trajectory deviation area (Fig. 9-3). The trends of each group and epoch are generally consistent between the two performance measures, except that a movement duration "aftereffect" is pronounced only for the FS group. (Lines represent group averages of subjects' binned data, ±S.E.M.)

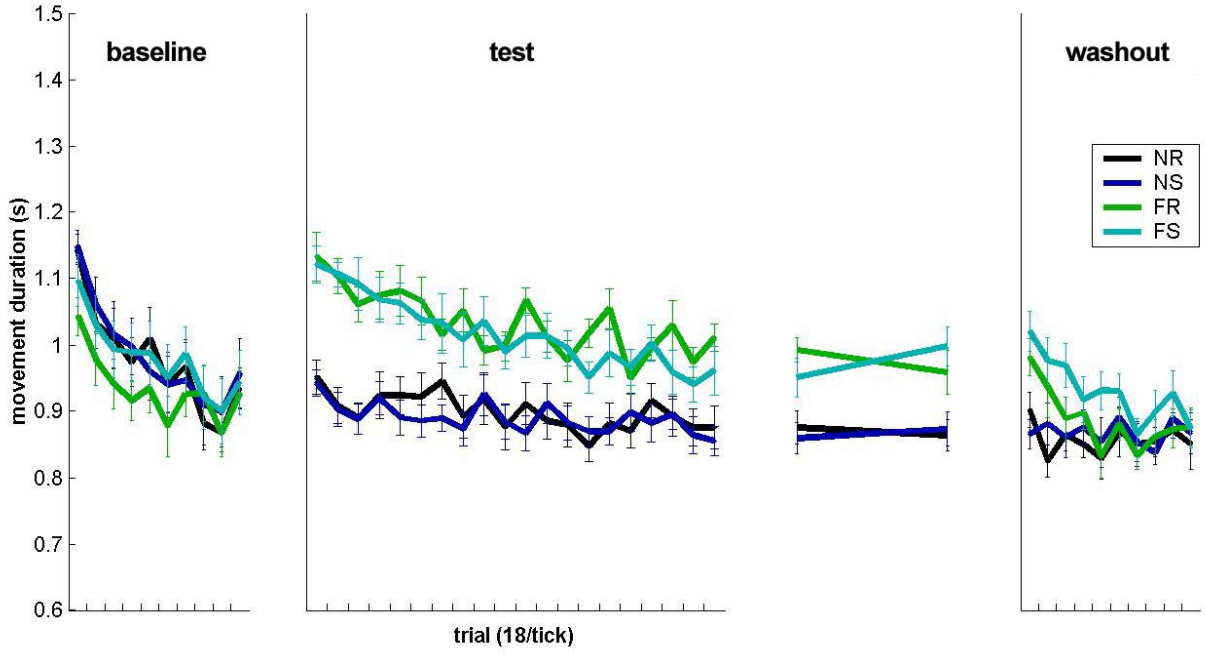

Figure 9-5 Sequence learning evident among subjects given nonrandom targets. After subjects had trained on a baseline epoch (left panel), the introduction of a repeating, implicit target sequence in the test epoch of the NS and FS subjects (center) led to a gradual decline in reaction times relative to the subjects experiencing a random target order (NR and FR). When all subjects performed a final washout epoch with random targets (right), subjects who had previously experienced a sequence exhibited an aftereffect of reaction times (defined as for performance error). This was particularly true of the FS subjects.

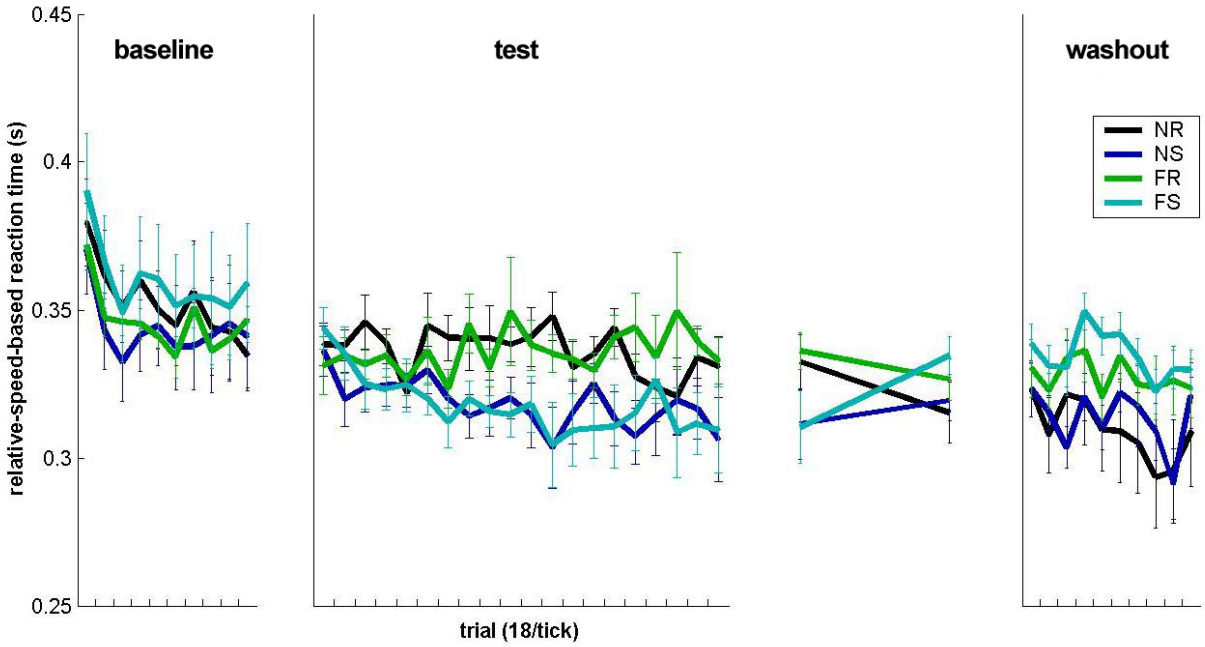

Figure 9-6 A chunking strategy may be used by subjects learning a sequence and a force field. **a**) The structure of the reaction time adaptation is shown for all NS subjects in a comparison of their initial (sequence repetitions 1-2) and late (11-20) test epoch performance. The adaptation is apparent both for trials beginning at the central target, and the variable number of trials following each such trials. **b**) FS subjects experience a greater decline in reaction time on trials immediately subsequent to trials originating at the central target. (Both sets of trials are shown boxed together in panel b.) These center-out trials, in turn, retain relatively high reaction times over learning, suggesting that they are used to organize the 18-target sequence into "chunks" of predictable, outwardly directed movements. (Lines represent group averages of subjects' binned data, ±S.E.M.)

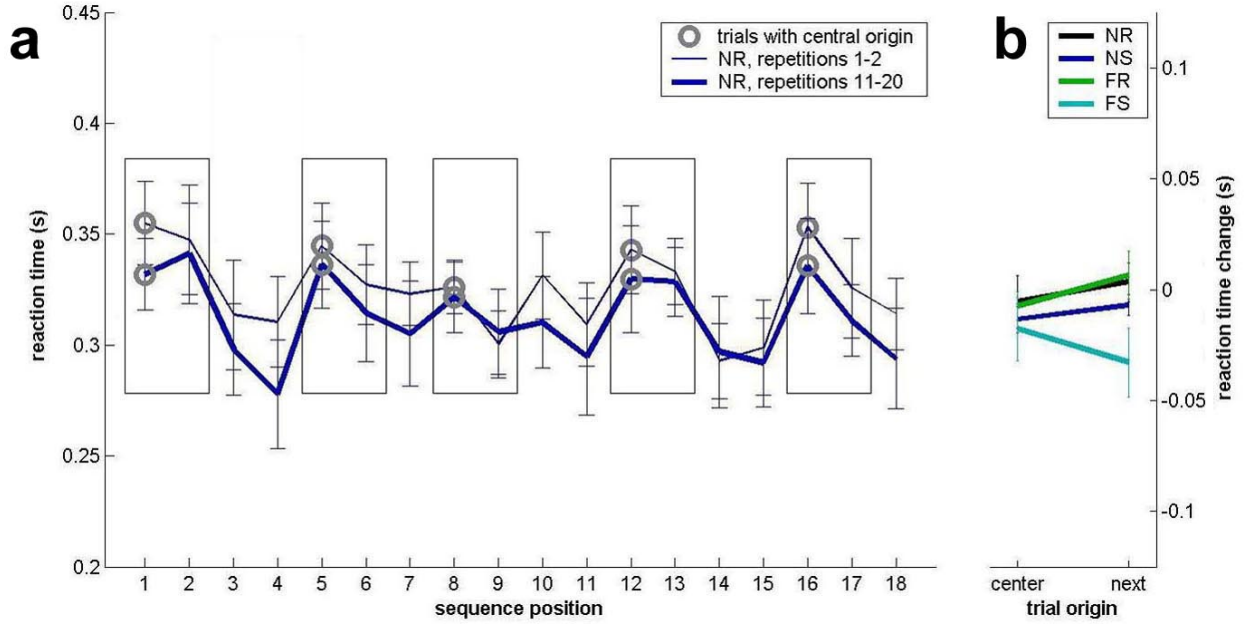

10 Consolidation and Interference in Motor Learning with Catch Trials

Motor consolidation—a gradual resistance to retrograde interference from a second, inconsistent motor program—has been shown to emerge over several hours after subjects learn to reach with straight trajectories through novel force fields applied by a robotic manipulandum. The robustness of motor memory against later interfering conditions and the time course of this stabilization have recently been questioned. In the human study presented here, I attempt to reconcile these conflicting reports by exploring the effect of catch trials, in which the forces are unexpectedly removed. I found that this methodological tool, while not consistently applied by different investigators, not only demonstrates the process of consolidation, but might itself influence motor learning. Although the mechanism is unclear, the experience of catch trials clearly altered the motor recall of our subjects, who uniquely demonstrated retention of their earlier clockwise field learning, despite an interfering counterclockwise force field presented after learning. However, this retention of learning was inconsistent with the standard understanding of motor consolidation, as catch trial subjects given 5 minutes to stabilize their motor memory prior to interference, and those given 6 hours, both *appeared able to recall this learning 24 hours after the interference. While the 6-hr group may indeed have "consolidated" their clockwise field experience, analysis of catch trial aftereffects during the interference trials suggests that the 5-min group experienced particularly severe anterograde interference that protected them from internalizing (i.e. mentally representing) the counterclockwise forces. We thus interpret the chief effect of a longer interval as allowing subjects not to consolidate their earlier learning, but to more rapidly internalize the interfering field. While catch trial performance did not reveal an effect of stabilization interval on the degree of consolidation, they were—ironically—critical in* enabling *motor recall.*

10.1 INTRODUCTION

10.1.1 The consolidation controversy

In this chapter I focus on motor consolidation, a dissociable process from the motor acquisition (Zach et al., 2005) that was the focus of the previous chapter. Several recent studies of motor learning in human subjects have investigated this phenomenon, characterized by a gradual resistance to retrograde interference (McGaugh, 2000). The time course of consolidation was classically demonstrated in the motor system as subjects learned to reach with straight trajectories through novel dynamical environments, or "force fields," created by a robotic manipulandum (Brashers-Krug et al., 1996; Shadmehr & Brashers-Krug, 1997).

The robustness of this consolidation against later interfering conditions has recently been questioned, as has its generalization to other sensorimotor adaptation tasks such as simple visuomotor transformations or prism adaptation (Bock et al., 2001; Goedert & Willingham, 2002; see Robertson et al., 2004). In particular, Caithness et al. (2004) presented subjects with visuomotor and dynamic motor adaptation tasks progressively approximating those of Brashers-Krug et al. (1996)

and Shadmehr and Brashers-Krug (1997). Yet in each case they failed to show that a learned motor memory of condition A could gradually become resistant to interference by a second condition B.

In contrast, the results of Krakauer et al. (2005) suggest that consolidation *is* a property of visuomotor learning under some conditions, in particular with null-field trials inserted prior to retest with the presumed effect of erasing any anterograde interference effects (Miall et al., 2004). But while these results demonstrated that motor memories can develop resistance to retrograde interference, Krakauer et al. (2005) also found that such resistance can emerge within just 5 minutes, rather than hours, if subjects merely double their duration of learning—even well after they have reached a stable level of performance.

10.1.2 Catch trials in consolidation studies

Here we attempt to reconcile these conflicting reports, by drawing attention to a methodological detail not consistently applied in the literature. Catch trials—in which the force field is unexpectedly removed—were originally used to track the formation of an internal model of the field (and not a reactive increase in stiffness). When applied, such trials have been presented at rates between 10% (Shadmehr & Mussa-Ivaldi, 1994) and 16-17% (Shadmehr & Brashers-Krug, 1997; Thoroughman & Shadmehr, 2000; Donchin et al., 2002; Wainscott et al., 2004). In Chapter 4, 5, and 7 I applied catch trials at a rate of 8%. Other researchers—including me in Chapter 9—have used null-condition washout epochs (e.g. Caithness et al., 2004, Krakauer et al., 2005) or have restricted the catch trials to the final blocks of the experiment (Baraduc et al., 2004) in order to test for learning "aftereffects." Others—including me in Chapter 8—have avoided null trials altogether (Bock et al., 2001; Goedert & Willingham, 2002). Randomly interposed catch trials have even been used but described as having "prevented subjects from learning the novel dynamics," e.g. destabilizing forces, that are created experimentally (Milner & Franklin, 2005).

We predicted that the presence of randomly-interposed, unannounced catch trials would demonstrate the process of consolidation, as in Shadmehr and Brashers-Krug (1997). We hypothesized that subjects given 6 hours between practice in a clockwise viscous force field and subsequent exposure to an interfering counterclockwise field would consolidate their initial learning, as measured by a superior level of performance at retest. In contrast, subjects who experienced only a 5-minute consolidation interval would not. We expected both to infer consolidation from the initial error levels of subjects at retest, and among the catch trial subjects, to track subjects' on-line internalization of the force fields via their aftereffects on catch trials. We did not predict that the catch trials themselves would influence motor acquisition or consolidation.

10.2 METHODS

10.2.1 Subjects

Thirty-five right-handed, English-speaking students (mean 24.8 years old; 14 males)

participated using a custom manipulandum apparatus (Fayé, 1983). Participants were screened for history of neurological illness, epilepsy, seizures, head injuries, and neurosurgery. Ethical approval was obtained through the MIT Committee On the Use of Humans as Experimental Subjects. Participants were paid at $10/hour, with a $5 bonus for successful completion of each day of the study. Subjects were asked to ensure they would sleep at least 6 hours the two nights before and during the experiment. The only subject who reported having failed to do so was excluded from the study, as was one subject who arrived too late for the retest epoch. One other participant was excluded for anticipating more than 10% of the trials in the baseline epoch (where "anticipation" occurred whenever a participant's cursor was located outside of the origin when the target appeared). Of the remaining 32 subjects, eight each were randomly assigned to four experimental groups prior to the test epoch. These groups were defined by the combination of uninterrupted forces (i.e. 0% catch trials) in all force epochs and a 5-min interval between the learning and interference epochs (UM, n = 8), uninterrupted forces and a 6-hr interval (UH, n = 8), 20% catch trials and a 5-min interval (CM, n = 8), or 20% catch trials and a 6-hr interval (CH, n = 8).

10.2.2 Paradigm

Task As in Chapter 9.

Intervals The baseline and learning epochs were separated by 5 minutes for all subjects. The two possible intervals between learning and interference epochs were constrained to be within a range of ±1 min (5-min interval subjects) or ±10 min (6-hr interval subjects). Similarly, the 24-hr interval between the interference and retest epochs was observed with a ±10 min range. Intervals were all measured from the end of the previous epoch to the beginning of the next epoch. The epochs themselves required about eight minutes to complete. Subjects sat at the manipulandum during the 5-min breaks, either waiting for the next epoch of trials or talking with the experimenter. We did not control the activities of the subjects in the remaining intervals, except to require that the 24-hr interval include at least 6 hours of sleep (verified by subject report).

Instructions As in Chapter 9.

Forces All subjects experienced a null (0 N·s/m) force field during the baseline epoch, a velocity-dependent clockwise field in the learning and retest epochs, and a counterclockwise field in the interference epoch (Fig. 10-1). The curl forces, of magnitude 10 N·s/m, were calculated on-line as $f = \mathbf{B}\dot{x}$, where $\mathrm{B} = \begin{bmatrix} 0 & 10 \\ -10 & 0 \end{bmatrix}$ (clockwise) or $\mathrm{B} = \begin{bmatrix} 0 & -10 \\ 10 & 0 \end{bmatrix}$ (counterclockwise), and $\dot{x}$ was the movement velocity. On "catch trials," the motors were suddenly, silently, and with no warning to the subject turned off just as the target was presented. These occurred at a rate of 20% in all force epochs performed by the CM and CH subjects. Catch trials

occurred on the same trials for all CM and CH subjects (as in Shadmehr & Brashers-Krug, 1997). They were preprogrammed pseudorandomly such that 2 catch trials occurred among each of the 21 possible movement combinations in each epoch. There was no constraint that they were to occur at a regular rate within each epoch.

Sequence Within each, 216-target epoch, all subjects received the same, pseudorandom sequence of targets. (The one exception was one early subject in the UM condition, who received a 180-target baseline target file and 300-target files in the remaining epochs. As a result of this exception, we consider only the first 180 trials performed by all subjects in the baseline epoch. In the remaining epochs we consider the first 216 trials performed by the subjects.) All subjects completed each movement specified by the target files—trials were not aborted if they failed to reach the target on time.

Targets As in Chapter 9. I used only the pseudorandom, not the sequenced, target files. In addition, my finding that some measures of performance error could vary systematically with movement origin (Chapter 9) prompted me to equalize the frequency of each movement origin/target combination as much as possible, by requiring that each epoch's target file contained at least 7 trials in each of these 21 movement path possibilities.

10.2.3 Recording/Stimulation

Verbal reports As in Chapter 9. Subjects were not asked if catch trials were experienced, but this information was recorded when volunteered.

Performance error For our measure of force field adaptation, we chose to look primarily at the total deviation area swept out by each movement relative to a straight line connecting the beginning and end positions of the trial (Caithness et al., 2004; see also Chapter 9). Several other measures of trajectory deviation (e.g. path distance, peak perpendicular deviation, and deviation angle) yielded qualitatively similar results. All measures were based on the manipulandum joint encoder position signals, translated into endpoint coordinates.

10.2.4 Analysis

Baseline correction Given our anticipated finding that performance error varied with catch trial recency (see Figure 10-4 and Results), and in order to include both catch and force trials in the comparison of UM/UH and CM/CH subjects, we applied a correction for this recency to the results depicted in Figure 10-6. This correction involved equalizing the average, relative performance error each subject displayed in the learning epoch at each catch trial, subsequent force trial, or further force trials (up to five trials following the catch trial; Fig. 10-4), and then subtracting each subject's scores in all force epochs by these factors. The first force trials in each epoch, until the first catch trial, were treated as though they were subsequent to a catch trial. These trials always followed a period in which the subject experienced no forces until they brought the cursor into the central origin in order to start the first trial.

Learning index In order to summarize subjects' internalization of each field using their pattern of errors both on catch trials and "fielded," force trials, we also computed a learning index (*LI*) that expresses performance as a ratio $LI = \frac{area_{catch}}{|area_{fielded}| + |area_{catch}|}$. The measure is like that of Donchin et al. (2002), except that it is based on deviation area rather than perpendicular distance, and we allow the numerator to be signed in order to better distinguish learning of the two curl fields. (We also tried following Donchin et al. [2002] in defining kinematic error to be the perpendicular displacement at 300 ms into each movement, following a reaction time defined as the time point at which subjects reached 15% of their peak speed, with catch and fielded movements averaged within 50- vs. 36-trial bins. The results—despite our concerns that this performance measure may reflect changes in speed profile shape and timing (Chapter 9) as well as changes in movement deviation—were nearly identical to those shown in Figure 10-5.)

Comparisons Trials in which the subject failed to reach the target in the allotted 1-s time limit were still included in the analysis. However, we rejected any trial in which the combined reaction plus movement time was less than 0.5 s or greater than 1.5 s, i.e. outside a ±0.5 range around the allotted time. Trials were binned by 36 trials in each epoch and condition (a duration sufficient to include, across subjects, at least one trial of each movement origin, target and direction, at least among non-catch trials). We did not exclude the first 36-trial bin of each epoch in the analyses. Data within each epoch of Figure 10-6 were fit by single-exponential curves (only constrained in their parameters such that the exponential "growth" or "decay" part of the curve occurred at the beginning and not the end of the epoch). Statistical results were based on the within-bin-averaged trajectory error or learning index. "Aftereffects" of clockwise field learning on counterclockwise performance were estimated by comparing the mean scores of the first two 36-trial bins in the interference epoch with the last two 36-trial bins in the learning epoch. "Transfer of learning" between the two clockwise epochs was estimated similarly, but using the first two bins of the retest epoch instead of the interference epoch. Main and interaction effects of catch trial Frequency (as in Figs. 10-3, 10-5, and 10-6) or Recency (Fig. 10-4), consolidation Interval, and Time (or Bin average, in the case of learning transfer or aftereffects) were assessed using repeated measures ANOVAs. Differences among the "slope" parameter of exponential fits were compared using ANOVAs. All significant effects (at the $p < 0.05$ level) are reported.

10.3 RESULTS

10.3.1 Forces can be inferred from trajectory error

Subjects' trajectories were deviated in the pattern typical of curl force fields. As shown in Figure 10-1 for three reach directions performed by a sample subject who did not experience catch trials, trajectories were initially variable but not systematically skewed in the null-field baseline epoch. Following introduction of a

clockwise force field in the learning epoch, movements from the center to the periphery became deviated in a clockwise direction. Essentially the opposite pattern of errors was evident in the counterclockwise field presented in the interference epoch 6 hours later, but clockwise-deviated movements were again expressed at retest 24 hours later still.

Figure 10-2 presents the trajectory deviation area (our measure of performance error) in the learning epoch for all subjects who experienced catch trials embedded randomly in their force epochs. Catch trials, and subsequent "fielded" trials in which the forces were restored just as suddenly as they were removed, were characterized by opposing deviations. Within this first exposure to the clockwise force field, the magnitude of the "aftereffects" seen on catch trials appeared to grow over time (as quantified below). This increase in aftereffect magnitude may be considered a hallmark of subjects' internalization of a novel dynamical environment (Shadmehr & Mussa-Ivaldi, 1994; Shadmehr & Brashers-Krug, 1997).

10.3.2 Force field acquisition is reflected in catch trial aftereffects

Figure 10-3 depicts the performance of subjects on catch trials. In each force epoch, the catch trial groups (CM and CH) performed with a characteristically high level of error on catch trials. This is confirmed by significant main effects of catch trial Frequency in the three epochs ($F_{(1,31)} = 145.61$, $p < 0.0001$; $F_{(1,31)} = 82.78$, $p < 0.0001$; and $F_{(1,31)} = 236.78$, $p < 0.0001$, respectively). The groups given uninterrupted practice on the forces also changed in their performance on their movement-matched trials (with the same origins and targets). As a result there was also a significant main effect of Time in each force epoch ($F_{(5,31)} = 19.75$, $p < 0.0001$; $F_{(5,31)} = 4.93$, $p < 0.001$; and $F_{(5,31)} = 42.96$, $p < 0.0001$). This effect of Time was reduced in the interference epoch, when the UM and UH subjects plateaued at a higher absolute level of error than they had in the clockwise epochs.

These performance trends were generally consistent between the two clockwise epochs (Fig. 10-3). In the retest epoch, there was an additional, small but significant interaction between catch trial Frequency and Time ($F_{(5,31)} = 2.89$, $p < 0.05$), as well as a nearly-significant interaction between catch trial Frequency, consolidation Interval and Time ($p = 0.05$). These effects might describe the slightly different performance among the CH and CM groups. Overall, though, the subjects' performance on catch trials in the retest epoch was similar to their performance in the learning epoch, suggesting that the clockwise field had to be internalized anew by subjects.

In the interference epoch (Fig. 10-3) there was also a small but significant main effect of consolidation Interval ($F_{(1,31)} = 3.87$, $p < 0.05$). This effect was particularly evident in the CH's group's much more rapid increase in field-consistent aftereffects—i.e. their internalization of the counterclockwise field—as compared to the CM group. There was also a small but significant interaction between catch trial Frequency and Time ($F_{(5,31)} = 3.36$, $p < 0.05$), apparently reflecting the failure of the CM and UM/UH subjects to reach either stable or low levels of absolute error, respectively, on their own catch or matched trials.

10.3.3 Force field acquisition is reflected in fielded trials

Figure 10-4 depicts the groups' mean performance in each force epoch across both catch trials and the subsequent force trials (up to five trials beyond the catch trial). As with catch trials (Fig. 10-3), differences in fielded trial performance within each force epoch were dominated by a distinction between the catch and non-catch groups. Here, the mean level of fielded trial error did not distinguish the groups in any epoch. Instead the differences were validated by significant interaction effects of catch trial Frequency × Recency in each force epoch ($F_{(5,31)} = 73.29$, $p < 0.0001$; $F_{(5,31)} = 55.10$, $p < 0.0001$; and $F_{(5,31)} = 80.49$, $p < 0.0001$, respectively). UM and UH subjects did not experience catch trials, and their error was relatively constant across the seven sets of movement-matched force trials shown for these subjects (these including movements of any origin/target combination). The CH and CM subjects did display catch trial aftereffects counter to the field in each epoch (as in Fig. 10-3), but on fielded trials their errors were initially enhanced in the direction of the field, until after about five trials when their errors were consistent with those of subjects who had not experienced catch trials. The resulting, global trend among these subjects is thus captured by significant main effects of catch trial Recency in each epoch ($F_{(5,31)} = 95.24$, $p < 0.0001$; $F_{(5,31)} = 65.13$, $p < 0.0001$; and $F_{(5,31)} = 106.28$, $p < 0.0001$).

As with catch trial performance, the trajectory errors of CM and CH subjects on fielded trials mainly distinguished these groups in the interference epoch (Fig. 10-4). In this epoch a significant main effect of consolidation Interval once again emerged ($F_{(1,31)} = 5.98$, $p < 0.01$). We interpret this effect as reflecting a generally more rapid acquisition (at Recency = 0) or application (Recency > 0) of the appropriate counterclockwise field learning among subjects given 6 hours instead of 5 minutes to consolidate the previous, anticorrelated field. In the retest epoch there were small, additional effects of consolidation Interval ($F_{(1,31)} = 4.49$, $p < 0.05$) and catch trial Frequency × Interval ($F_{(1,31)} = 3.80$, $p < 0.05$). These effects may reflect a distinctly reduced level of clockwise deviation among UM participants, who thereby appear to be less "prepared" to experience counterclockwise or null-field trials. (Given the trend towards similar trends in the initial learning epoch in Figure 10-4, left, we cannot discount that these differences are a result of baseline variability between subjects.) But overall the retest epoch performance trends appear similar to those observed in the initial clockwise epoch.

A convenient metric to summarize the learning trends evident both in catch trials and fielded movements is the learning index used by Donchin et al. (2002). As shown in Figure 10-5, this measure reproduces the catch trial subjects' shared aftereffect trends within each force epoch, as supported by significant effects of Time ($F_{(5,15)} = 13.70$, $p < 0.0001$; $F_{(5,15)} = 10.08$, $p < 0.0001$; and $F_{(5,15)} = 32.61$, $p < 0.0001$). Although some difference in initial performance within the retest epoch was apparent, it is not statistically significant ($p > 0.05$). The only difference between the CM and CH groups that is distilled by the learning index metric is a small but significant main effect of consolidation Interval on learning in the interference epoch ($F_{(1,15)} = 5.25$, $p < 0.05$). Again, we interpret this effect as indicating a relative difficulty among the CM subjects in acquiring and/or expressing field-appropriate learning.

10.3.4 Force field recall is evident in initial retest performance

The previous results speak to subjects' *acquisition* of each force field, at the level of catch trials as well as subsequent fielded trials (or movement-matched controls of these trials among UM and UH subjects). The ability of participants to *recall* their previous clockwise learning can be assessed by correcting for mean differences in catch vs. fielded vs. control trials (see Methods) and then by directly comparing their average trajectory error in the learning and retest epochs. As shown in Figure 10-6 (and as emphasized by exponential fits), at least some subjects had to re-adapt to the clockwise forces in the retest epoch, just as they had adapted to the basic task in the baseline epoch, and to the clockwise and counterclockwise force fields in the learning and interference epochs. Across groups, there was thus a significant overall adaptation to the task in each of the four epochs, described by main effects of Time ($F_{(4,31)}$ = 37.82, $p < 0.0001$; $F_{(5,31)}$ = 22.43, $p < 0.0001$; $F_{(5,31)}$ = 34.38, $p < 0.0001$; and $F_{(5,31)}$ = 28.16, $p < 0.0001$, respectively).

It is the particular pattern of adaptation or re-adaptation among subjects in the two clockwise epochs that distinguishes the groups. In the learning epoch (Fig. 10-6, left), despite a similar initial level of error the catch trial subjects came to plateau at a higher level of average error compared to the non-catch subjects, as captured by a significant main effect of catch trial Frequency on both the bin-averaged data and the exponential slopes that were fit to those data ($F_{(1,31)}$ = 23.02, $p < 0.0001$; and $F_{(1,31)}$ = 11.79, $p < 0.001$), and by a significant interaction of Frequency × Time ($F_{(5,31)}$ = 4.91, $p < 0.001$).

These patterns of learning are similar to those exhibited in the interference epoch, where there was a significant main effect of catch trial Frequency on performance ($F_{(1,31)}$ = 9.23, $p < 0.01$), and a small but significant Frequency × Time interaction ($F_{(5,31)}$ = 3.12, $p < 0.05$). Comparing participants' initial counterclockwise performance with their error level late in the learning epoch (Fig. 10-6, center), all subjects performed counterclockwise field movements with elevated absolute error levels, as confirmed by a main effect of Time ($F_{(1,31)}$ = 282.25, $p < 0.0001$). But catch trial subjects displayed a distinctly pronounced aftereffect ($F_{(1,31)}$ = 11.34, $p < 0.001$). There also appears to be an effect of consolidation interval, such that subjects both start and plateau at lower level of error if given 6 hours to consolidate the previous field. However, all main and interaction effects of Interval on performance scores, exponential fits, and aftereffects are non-significant ($p > 0.08$).

In the retest epoch—in contrast to the initial clockwise learning—subjects plateaued at a *similar* level of error, but they began the epoch with *different* levels of error (Fig. 10-6, right). In particular, the CM and CH participants have a reduced level of initial error. As such there is no main effect of catch trial Frequency on the retest data, but there is a significant Frequency × Time interaction ($F_{(5,31)}$ = 14.56, $p < 0.0001$) and a significant effect of Frequency on the exponential slopes ($F_{(1,31)}$ = 35.72, $p < 0.0001$). Furthermore, whereas in the learning epoch there was no effect of consolidation interval, in the retest epoch there is a small but significant effect of Interval × Time ($F_{(1,31)}$ = 4.83, $p < 0.05$). Inspection of the data suggests that the UM subjects, and in particular the CM subjects, show particularly little re-adaptation to the clockwise forces.

The effect of catch trials on clockwise field recall can perhaps be summarized most succinctly by comparing subjects' performance at the end of the learning epoch

with their performance at the beginning of the retest epoch (Fig. 10-6, center). The only significant effect among these transfer patterns was again a significant catch trial Frequency × Time interaction ($F_{(1,31)} = 28.17$, $p < 0.0001$). (Effects of Frequency × consolidation Interval, and of Time, both approached but did not reach significance, $p = 0.06$.) Subjects who performed each force epoch with uninterrupted forces showed no recall of the clockwise force field learned earlier, even when 6 hours elapsed before an interfering force field was introduced. Subjects who performed each force epoch with randomly inserted null-field trials showed an almost immediate recall of their earlier clockwise field learning, even if that learning had been followed by the anticorrelated field only five minutes later.

10.3.5 Awareness of force field identity and predictability

As shown in Table 10-1, subjects were generally accurate at recognizing forces when they had occurred, although none were able to describe the structure of the force field (beyond using words such as "resistive," "jerky," "stronger in certain directions," etc.). Most subjects found that the forces were consistent or declined over time. Several participants in each group (between 4 and 6 of the eight subjects) were able to recognize some distinction between the counterclockwise forces and the force fields in one or other of the clockwise epochs (e.g. they were reported to be stronger or weaker, more or less jerky, etc.). Likewise, at least a few subjects in each group (between 3/8 and 6/8) found that the force fields in the learning and retest epochs were either similar to each other (regardless of their relationship to the interference forces) or at least both noticeably different from the interference epoch. These responses were relatively balanced between groups. But of the few participants who were able to report correctly the equality of the two clockwise epochs *and* the inequality of the clockwise and counterclockwise epochs, a disproportionate number (and half of the group, 4/8) were CM subjects.

Subjects' reports of force field predictability were generally as correct as their recollections of force field identity (Table 10-1). Participants given massed practice on forces in each epoch (5/8 UM and 3/8 UH subjects) generally found the forces to be more "predictable" (or more easy to "adapt" or "compensate" to) than did catch trial participants (2/8 each of the CM and CH subjects). But the catch trial participants were the only subjects to volunteer that they had experienced trials when the forces were "off" (2/8 CM participants and, notably, 5/8 CH subjects).

10.4 DISCUSSION

10.4.1 Consolidation interval and motor acquisition

Our results are surprising in at least two ways. First, they suggest that consolidation interval has little effect on the degree of motor recall (Fig. 10-6). Subjects who practiced with uninterrupted forces in each force epoch showed similar patterns of adaptation and retest performance, regardless of the time allowed for learning stabilization. Participants who practiced with randomly-interspersed catch trials in each force epoch also showed similar performance, although this pattern was distinct from the subjects not given catch trials. The near-irrelevance of consolidation

interval on recall was particularly evident in errors made on catch trials (Fig. 10-3)—or control movements in the case of subjects not given catch trials—and in a composite measure reflecting both catch and fielded trials (Fig. 10-5). Only small main and interaction effects of consolidation interval were evident among the retest epoch force trials (Fig. 10-4) and overall performance (Fig. 10-6). Furthermore these trends, while weak, suggested that it was the CM participants who started, and the UM subjects who reached, the lowest level of trajectory error—i.e. the two groups given the least time to consolidate the clockwise field.

Consolidation interval appeared mainly to affect the manner in which subjects were able to internalize the counterclockwise field—as could be uniquely assessed among the catch trial subjects. Catch trial aftereffects are not evident when naïve subjects first practice moving in a force field; they only develop with practice in the field. Like Shadmehr and Brashers-Krug (1997), we have used aftereffect magnitude to depict the differences in force field learning between catch trial participants differing in their consolidation interval. A distinction between catch trial groups in our study was evident only in the interference epoch (Figs. 10-3, 10-5 center; compare Figure 6 in Shadmehr & Brashers-Krug, 1997). In both studies, catch trial subjects all experienced the same sequence of targets and catch trials, and thus the error measure could be averaged across participants and directly compared across groups. In Shadmehr and Brashers-Krug (1997), the critical difference between the groups plotted is their starting error at the first catch trial. Their CM subjects—fresh from clockwise training—appeared to apply a clockwise "internal model," in that they displayed aftereffects in the same direction as those they displayed in the clockwise field. Their CH subjects—having already consolidated their clockwise learning—appeared naïve. The mean aftereffect errors of these subjects pointed in the clockwise direction, suggesting that their longer interval since learning had enabled them to learn anew, with minimal anterograde interference.

Like Shadmehr and Brashers-Krug (1997), we found significant main effects of consolidation interval on error magnitude in catch trials (as well as subsequent force trials) in the interference epoch. However, we also suggest that the time and/or rate by which each of these groups begins to internalize the new force field may better distinguish CM and CH participants (Figs. 10-3, 10-5 center). The superior counterclockwise field acquisition by the CH subjects (and, we might presume, by the UH participants), might have come at a cost, however, given the marginally worse initial or plateau performance these groups exhibited at retest relative to their CM and UM counterparts (Figs. 10-4, 10-6, right).

Consolidation interval may also have had some influence on subjects' awareness of the force fields. In our participants' verbal reports following the experiment (Table 10-1), they were usually able to recognize the presence but not the structure of forces, and to do so regardless of experimental condition. But the ability to recognize: 1) the presence of unpredictable forces and/or catch trials, and 2) the equality of the clockwise force fields and the inequality of these with the counterclockwise force field, appeared to be enhanced among the catch trial subjects. Though difficult to quantify, there also appeared to be a differential tendency of the CM subjects to be more aware of force field contrasts (consistent with their closer juxtaposition of the clockwise and counterclockwise fields), and of the CH subjects to be develop more awareness of catch trial presence (consistent with their demonstrated, superior ability to acquire a second force field).

It might be argued that our subjects' performance at retest merely reflects the anterograde interference from the counterclockwise field (Miall et al., 2004). This is particularly plausible given the inverse relationship apparent between each group's performance late in the interference epoch and early in the retest epoch 24 hr later (Fig. 10-6). That is, participants who retained high levels of error in the counterclockwise field did best when retested in a clockwise field. Such anterograde interference would be consistent with reports that aftereffects of clockwise learning can be observed a day later when subjects return to practice in null field (Shadmehr et al., 1998; Donchin et al., 2002). To be sure, future experiments with our paradigm might try allowing more than 24 hours before retest (Shadmehr & Brashers-Krug, 1997; cf. Goedert & Willingham, 2002; Krakauer et al., 2005), or inserting several null-field trials (Krakauer et al., 1999), rather than a single null-field pre-trial as in our experiment, prior to every force epoch (Shadmehr & Brashers-Krug, 1997; Krakauer et al., 2005). However, our catch trial aftereffect results present an alternative hypothesis: subjects who retain a high level of error in the interference epoch (in particular, the CM subjects) do so because they are unable to internalize it as effectively as other groups (CH, and to an even greater degree the UM and UH), due to their own, lingering anterograde interference from the clockwise practice (Figs. 10-3, 10-5, 10-6). Their failure to adapt to the interfering condition then allows them to retain and express a superior memory of the clockwise field, as is evident at retest (Fig. 10-6).

10.4.2 Catch trials and motor consolidation

Our second surprising finding was that the pattern of learning was strongly related to participants' catch trial frequency. Indeed, the dominant factor affecting subjects' performance during initial learning, in the interfering field, or at retest (Fig. 10-6) was not consolidation interval but rather the frequency of catch trials that they experienced in each force epoch. The participants who appeared able to retain their initial clockwise learning despite interference (and regardless of consolidation interval) were those subjects who had practiced non-monotonous forces.

These catch trial subjects were also distinguished by their relatively high level of error in each epoch relative to the subjects given uninterrupted forces. This under-compensating error level (as shown by Donchin & Shadmehr, 2004) appears to reflect these subjects' response to each catch trial, following which they displayed enhanced deviations in the direction of the field for several subsequent fielded trials (Fig. 10-4). Thoroughman and Shadmehr (2000) followed not only trajectory deviations following catch trials but also the preferred directions of movement-initiating arm and shoulder muscles. They showed that transient muscular overcompensation, predicted by their formalization of internal model formation, was washed out by about three trials following a catch trial. In the retest epoch the UH group may too have acquired a moderately elevated clockwise error relative to the UM group (Figs. 10-4, 10-6), perhaps following their own experience with non-clockwise forces. But as catch trials are both unannounced and only discovered after their movement has begun, CM and CH participants in particular may have been attempting to mitigate the effect of force field removal by directing their movements in the same direction as the force field.

Although we did not explore catch trial frequencies beyond 0% and 20% in this

study (as modeled by Thoroughman & Shadmehr, 2000), it is further plausible that the level of field-consistent error the CH and CM subjects adopted was chosen to balance the large error they displayed in the opposite direction on occasional catch trials (Fig. 10-4). It is also possible that the number of fielded trials in which subjects displayed enhanced field-consistent error following a catch trial was a function of catch trial frequency. Indeed, enhanced trajectory error on fielded trials persisted for approximately four or five movements following catch trials (Fig. 10-4), calling to mind the 4:1 frequency of fielded:catch trials. Given these observations, the errors on fielded trials thus appear to reflect an adaptive preparation for catch trials, and not a reflexive, kinematic task switch cost (Logan, 1985) following the removal or addition of forces.

The presence of these "adaptive errors" could explain why the catch trial subjects' overall performance in the retest epoch—reflecting both catch and fielded trials—appears stable even while their catch trial deviations become enhanced. The learning model of Shadmehr and Mussa-Ivaldi (1994) posits an increase in learning index (Fig. 10-5) with both increased aftereffect magnitudes and decreased deviations on fielded trials. In contrast, we suggest that consolidated memories in our paradigm may be characterized by an equilibrium of opposing trajectory errors on catch trials and fielded trials (Fig. 10-4), and that subjects repeatedly recalibrate their reference level of kinematic error when changing between fields (Bock et al., 2003). But whatever the interpretation of our catch trial subjects' retest learning indices, they do appear to have uniquely transferred their earlier clockwise experience to this epoch, even with only 5 min of consolidation time after practice.

Experiments by Krakauer et al. (2005), Caithness et al. (2004), and Goedert and Willingham (2002) have all challenged the notion that motor memories are protected against interference once a "consolidation window" of several hours has passed. Others have challenged the notion of such a window by finding that under certain conditions subjects can develop a memory resistant to retrograde interference after only 5 min. In particular, Krakauer et al. (2005) showed that prolonged practice at reaching with a visuomotor rotation (i.e. 66 "cycles" each of 8 trials, instead of 33 cycles) appears to protect participants from interference by a counter-rotation even if it is presented only 5 min after initial learning.

It may appear that we too show that subjects can develop a relatively stable, protected memory after only 5 min, thus challenging the traditional view of motor consolidation. But alternatively our results in Figures 10-3 and 10-5 may be interpreted as showing that the 5-min catch trial participants failed to be affected by the counterclockwise interference because of their strong, lingering aftereffects from their clockwise learning. Only the subjects given catch trials and six hours to consolidate demonstrated *both* internalization of the counterclockwise field *and* resistance to this retrograde interference, as measured by their retest performance (Fig. 10-6).

10.4.3 Catch-trial vs. uninterrupted experience

The rapid resistance of catch trial subjects to retrograde interference is particularly surprising given that the two force fields experienced by these subjects were in a sense more similar than those experienced by the non-catch subjects: 20% of the trials in both force fields were catch trials. Given the suggestion (and partial

evidence) that retention of multiple motor memories is impaired by their competition in working memory (Bays et al., 2005; cf. Bock et al., 2001), the catch trial subjects should have been worse at expressing their clockwise field learning at retest. In addition, the catch trial subjects should have been disadvantaged because they essentially had to juxtapose three rather than two force fields, including the null field.

While the route by which catch trials appear to enable these powerful reductions in retrograde interference is unclear, our results are consistent with extensive literature showing long-term benefits of distributed rather than massed practice (see Schmidt & Lee, 1999). While monotonous repetition of a motor behavior is known to lead to superior immediate performance, practice with some degree of randomness facilitates long-term retention (Shea & Morgan, 1979; Proteau et al., 1994). Even at the cellular level, it has been shown that visual activity-induced synaptic modifications are afforded resistance against subsequent interference from white-noise stimuli by distributed presentation of the initial stimuli (Zhou et al., 2003).

Behaviorally, we may interpret this effect as follows: practice of a motor skill on a relatively random schedule, as in our experiment, may be more difficult but also more *effortful*, thereby both causing and allowing subjects to repeatedly re-solve a motor learning problem. Research into saccadic adaptation by primates with either a block of catch trials or an equivalent period of rest without visual inputs suggests that practice under null conditions is required in order to cause active unlearning and relearning of the novel condition (Kojima et al., 2004).

An additional benefit of catch trials in our study is that they may have provided distinct error cues aiding memory recall (see Shadmehr & Brashers-Krug, 1997) or disambiguating novel and null-field environments. Consistent with this supposition, researchers have shown that subjects can separately internalize two opposing viscous force fields if the fields are presented randomly with audiovisual cues (e.g. background color) prior to movement (Osu et al., 2004; Wada et al., 2003). If the fields were simply alternated each trial, participants learned poorly, suggesting that their cue-based switching was only triggered when the subsequent field were not known until the beginning of the trial (as was the case in our experiment as well).

Catch trials may also have influenced learning by causing our subjects to consciously attend to the perturbations they experienced. The importance of conscious attention is relevant given the recent findings of Malfait and Ostry (2004) that the degree of interlimb generalization of force field adaptation depends on the subject's awareness of the force field (which awareness can be eliminated entirely by gradually ramping up the force field magnitude). Among our subjects, awareness of force field unpredictability (among CH subjects) and in particular the recognition of force field differences (among CM subjects) was associated with superior initial recall at retest.

Yet another possibility is that motor adaptation without catch trials is simply coactivation learning—a possibility that cannot be disproved without using null-field trials. Far from interfering with dynamic motor learning (Milner & Franklin, 2005), catch trials might in this scenario create it. Paradoxically, the very learning feature that catch trials were designed to measure, consolidation, may only exist experimentally when people practice with such random interruptions.

Table 10-1 Catch trial study subjects' awareness of the forces they experienced. Participants were all able to recognize that they had felt forces during the epoch, and were usually accurate in placing these experiences in the epochs in which they actually appeared. (B_1, B_1': clockwise learning and retest; B_2: counterclockwise interference epochs) rather than the null-field baseline epoch (N). When participants were asked to describe the relationships between forces, regardless of their experimental group they were generally able to recognize at least that the counterclockwise forces were somehow different from the force fields in one or other of the clockwise epochs, and that the force fields in the two clockwise epochs were similar to each other, or at least both different from the counterclockwise field. Almost half of participants who recognized both that the clockwise forces were consistent between epochs, and distinct from the counterclockwise force field, were CM subjects. Subjects were generally accurate in labeling forces as predictable when they had *not* experienced catch trials (UM and UH), but of those participants who volunteered an experience of catch trials, most were CH subjects. (Numbers in bold correspond to relatively complete, correct answers within each category of question. Responses for each group and report do not sum to eight because participants could give multiple, single, or no answers.)

groups	*force field awarenes*								
	forces in epoch...?				*relations between forces?*			*predictable?*	*catch trials?*
	N	*B1*	*B2*	*B1'*	*B1=B1'*	*(B1,B1')~B2*	*(B1=B1')~B2*		
UM (*n* = 8)	1	**8**	**8**	**7**	5	5	**2**	**5**	0
UH (*n* = 8)	1	**8**	**7**	**7**	4	4	**1**	**3**	0
CM (*n* = 8)	2	**8**	**8**	**8**	6	6	**4**	2	**2**
CH (*n* = 8)	0	7	**8**	7	6	3	2	2	**5**

Figure 10-1 Sample trajectories in each epoch. Shown are all center-out reaching trajectories in the first half of each epoch performed by a subject (group UH) experiencing no catch trials but a 6-hr interval between the learning and interference epochs. Darker circles (•) represent trials early in the epoch; lighter circles (•), trials near the middle of the epoch. Movements in the baseline epoch are shown superimposed on a grid with arrowheads denoting, for all epochs, the possible combinations of the seven origins/targets. Like all participants, this subject experienced four epochs with null, clockwise, counterclockwise, or clockwise viscous force fields (shown schematically) in the baseline, learning, interference, and retest epochs, respectively. Despite the 6-hr interval following clockwise field learning, the participant's trajectories appear as curved in the retest epoch as they did in the learning epoch, suggesting that the original learning did not consolidate and so was interfered with by the opposing field.

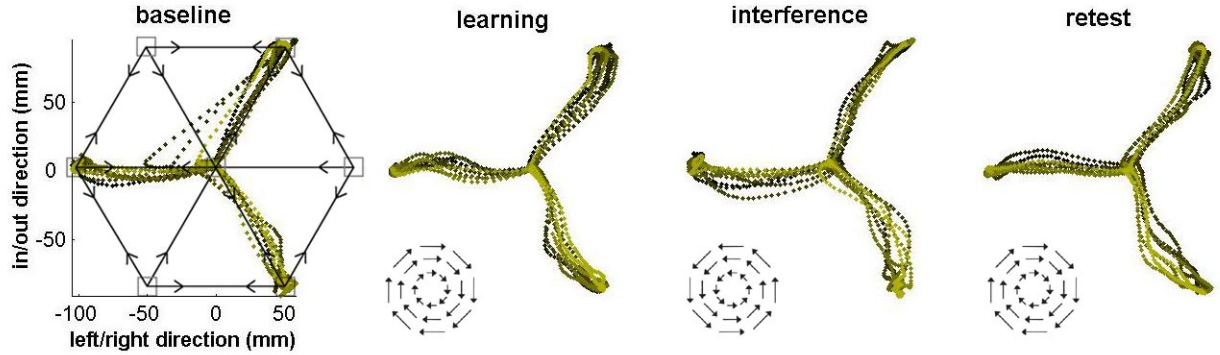

Figure 10-2 Subject errors on catch trials and subsequent force trials have characteristic magnitude. Shown for all subjects who experienced catch trials (n = 16) are the trajectory deviation areas on each trial in the learning epoch. Catch trials, in which the force field was unexpectedly removed, are characterized by deviations in the direction counter to the viscous field otherwise experience by the participant, i.e. in the counterclockwise direction in this epoch. The trajectories are pointed in the opposite direction when the force field is restored. These patterns are less evident at the beginning of the epoch, when subjects are learning to reach in the field.

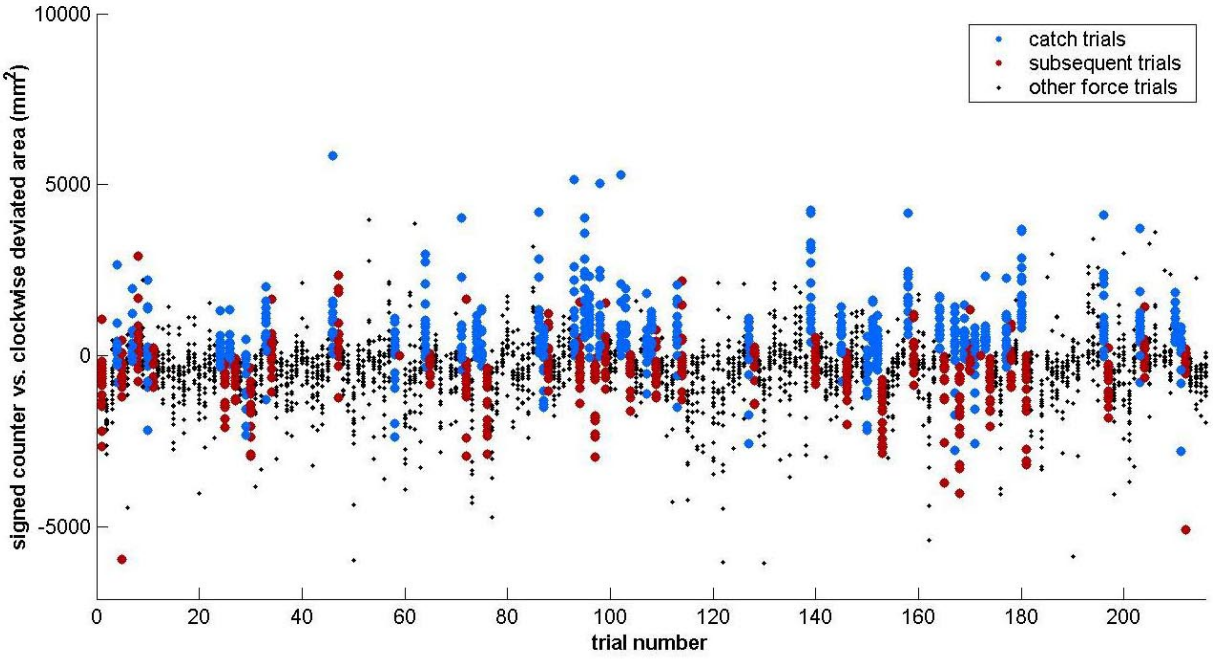

Figure 10-3 Subjects' performance on catch trials reflects their internalization of each field. Participants learning the clockwise field with interrupted forces (left; CM and CH) develop an elevated level of counterclockwise error on catch trials (as shown in Fig. 10-2 at the individual-trial level). The parallel changes in trajectory deviation on the movement-matched clockwise force trials experienced by the UM and UH subjects instead reflect their general adaptation to the forces. These trends are generally recapitulated in the retest epoch (right), despite the different intervening experience of the participants. In the interference epoch (center), however, the passage of time between initial learning and interference has an effect, particularly on the performance of the catch trial subjects. While CM subjects initially display evidence of clockwise-appropriate catch trial errors, CH subjects seem relatively unhampered by their prior clockwise field experience, and instead internalize the counterclockwise field with aftereffects that appear to mirror those they displayed during initial, clockwise field learning. (Data are averaged within each 36-trial bin and plotted ±S.E.M., as in the following figures.)

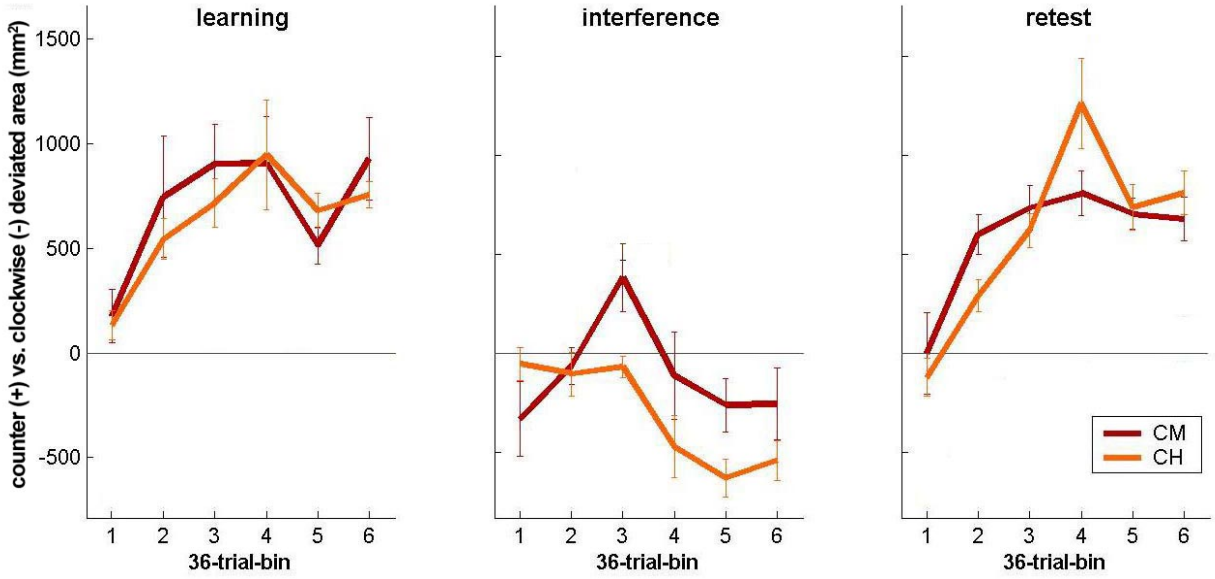

Figure 10-4 Subjects' performance on fielded trials reflects their internalization of each field. On force trials subsequent to catch trials, CH and CM subjects display an elevated clockwise level of kinematic error relative to the corresponding clockwise-force trials UH and UM subjects. This is evident both in the learning epoch (left) and the retest epoch (right), with error summed across all catch trials and subsequent force trials (up to six trials following the catch trial, and lumping further force trials into the last data point in each plot). As in Figure 10-3, the CH and CM groups are distinguished by "consolidation interval" mainly in their performance on the interfering, counterclockwise field. Here it is again evident that the pattern of error in CH subjects, but not CM subjects, more closely mirrors their level of error when learning the clockwise field. Their aftereffects are counter to the field, and their error on subsequent trials gradually converges down to the level exhibited by UH and UM participants, who perform with uninterrupted forces.

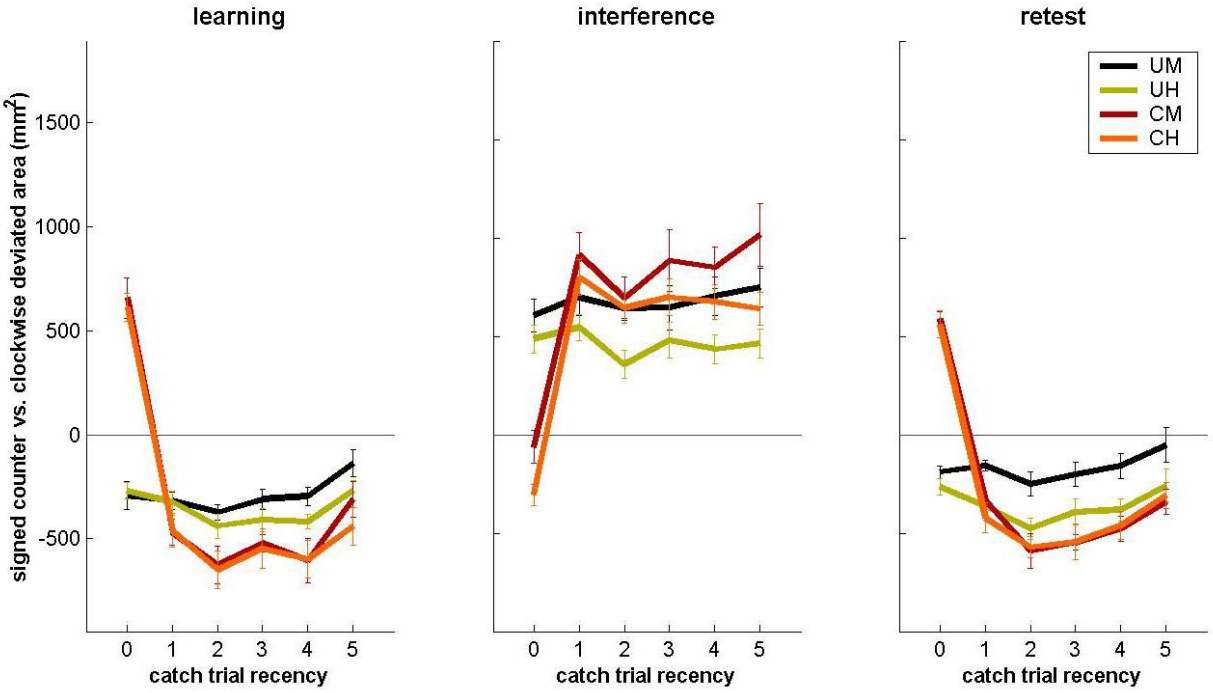

Figure 10-5 Subjects' internalization of each field can be summarized by a learning index. The trends reported above for the CM and CH groups are distilled when their performance is assessed by a learning index (Donchin et al., 2002; see Materials and Methods)—a measure that grows both as catch trial aftereffect magnitudes increase, and errors on fielded trials decrease. CM and CH subjects learn similarly in the learning epoch (left)—and re-learn similarly in the retest epoch (right). But the longer consolidation interval experienced by the CH group appears to let them internalize the counterclockwise field more rapidly in the interference epoch (center), as suggested by the catch and fielded movement errors alone in Figures 10-3 and 10-4.

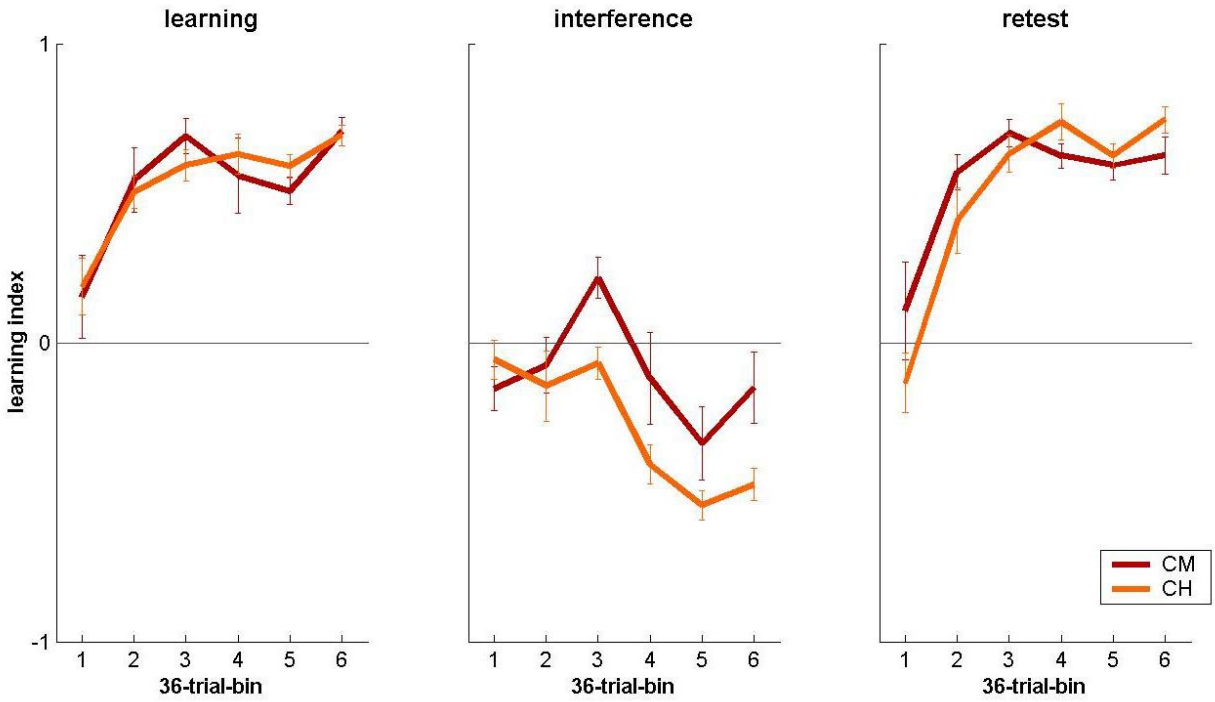

Figure 10-6 Subjects' performance in each force epoch depends on their experience of catch trials. CM and CH participants, who experienced the catch trials on 20% of their clockwise force field trials, plateaued at a higher level of error in the learning epoch (left), as compared to subjects who performed with uninterrupted forces (UM and UH). A similar pattern is repeated in the interference epoch when participants all experienced a counterclockwise field. In the retest epoch (right), the groups soon converged to a similar level of error but the CM and CH groups begin the epoch with a lower level of error than the UM and UH subjects. Data in these plots are overlaid with single-exponential fits. The central panel depicts the transfer of learning from the end of the learning epoch to the beginning of the retest epoch (wider bars), again demonstrating evidence of motor recall among the CM and CH subjects. For comparison, the panel also depicts the aftereffects displayed by subjects when they experience counterclockwise forces rather than the clockwise field they earlier trained on (narrower bars).

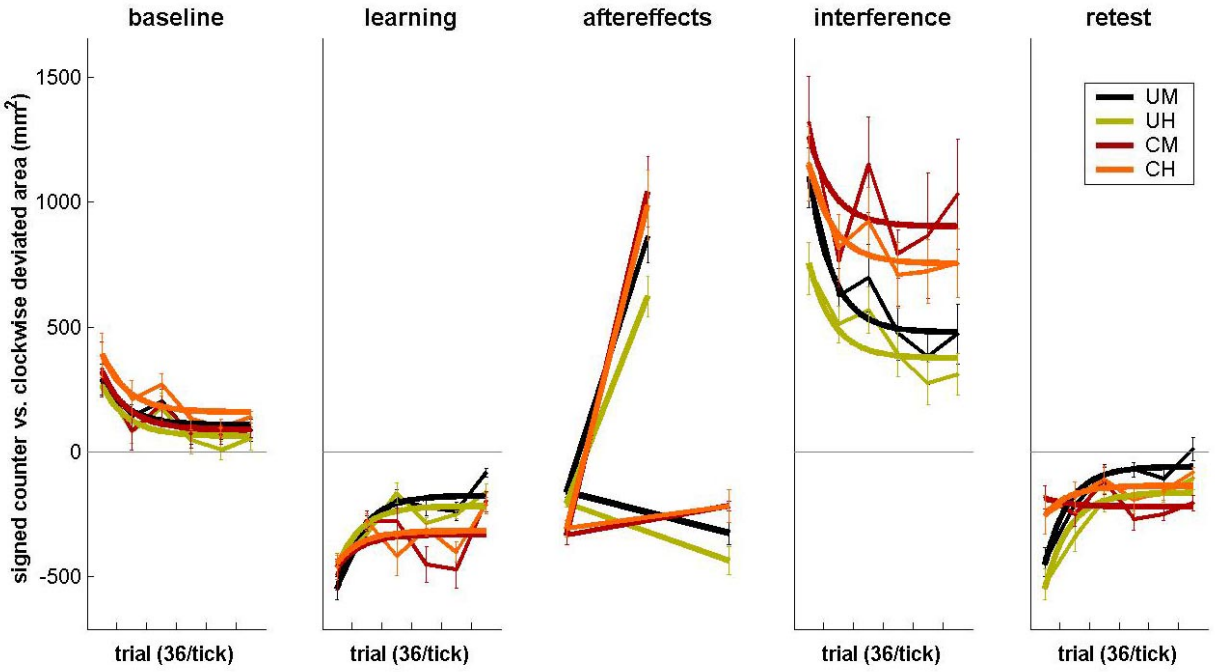

11 Distributed Digit Somatotopy in Somatosensory Cortex

We obtained high-resolution somatotopic maps of the human digits using 4.0 T functional magnetic resonance imaging (fMRI). In separate experiments, the volar surface of either the right thumb, index or ring finger was stimulated in a sliding-window fashion in both distal-to-proximal and proximal-to-distal directions using a custom-built pneumatic apparatus. Analysis of the functional images was restricted to Brodmann's areas 3b and 1 and areas 4 and 3a, as well as a randomized simulation of the functional data in each of these areas. Using in-house algorithms, we detected discrete regions of cortical activation showing phase reversal coinciding with alternation in stimulation direction. Most stimulation-related phase maps of the digits were obtained in areas 3b and 1, rather than "control" areas 3a or 4, despite the somatic input to the latter two areas. The area 3b and 1 representations thus appear to be relatively discrete and somatotopic compared to other somatic processing regions. Our results within areas 3b and 1 confirm the nonlinear mapping of the body surface suggested by recordings in nonhuman primates in terms of phase band topography, scaling, and frequency relative to the actual digit surfaces. The scaling and frequency nonlinearities were more evident within area 3b than 1, suggesting a functional differentiation of these regions that has previously been observed only in more invasive recordings. Specifically, the area 1 representations were larger overall than those observed in area 3b, and the frequencies of area 3b phase bands and voxels were related disproportionately to thumb and index finger stimulation and to particular areas on the digit surface, suggesting a weighting based in part on receptor distribution.

11.1 INTRODUCTION

High-resolution studies of cortical response to cutaneous stimulation in the human have come from preoperative exploration in brain surgery patients. Such studies are restricted to superficial cortex (Gelnar et al., 1998) and may further be limited by deviant cortical organization (Maldjian et al., 1996; Weiller et al., 1993; Maegaki et al., 1995). While the advent of fMRI (functional magnetic resonance imaging; Ogawa et al., 1992) has enabled comparably high-resolution mapping of somatosensory responses (Maldjian et al., 1999), few investigators have examined the precise spatial organization of this activity in humans, even for a body surface as small and accessible as the digits. Researchers have been limited by magnetic field strength (Gelnar et al., 1998; Kurth et al., 1998; Blankenburg et al., 2003), or by restricting their stimulation to two digits (Kurth et al., 1998; Francis et al., 2000; McGlone et al., 2002) or just the tips of the digits (Gelnar et al., 1998; Maldjian et al., 1999; McGlone et al., 2002). Investigators then typically delineate a somatosensory organization on the basis of distinct activation hotspots in response to cutaneous stimulation (Gelnar et al., 1998; Kurth et al., 1998; Maldjian et al., 1999; Francis et al., 2000; McGlone et al., 2002). Even when multiple areas are stimulated on the same finger (Blankenburg et al., 2003), the sites are stimulated in separate experiments, thus making it difficult to compare neighboring somatosensory responses.

Here we present results of high-resolution somatotopic mapping, achieved by

using a high-field (4.0 T) magnet and by stimulating the entire surface of three digits: the thumb, index and ring fingers. While higher-resolution scanning limits the signal-to-noise ratio in individual voxels (Bandettini, 2001), this effect is countervailed by an analysis based on the temporal relation of BOLD (blood-oxygenation level dependent) activity to the stimulation time course. To study this relation we used the sliding-window stimulation technique that Servos et al. (1998) developed to map out the somatotopic representations of the human arm. This method is based on the phase-analysis technique that was originally employed to yield precise retinotopic maps of visual cortex (Engel et al., 1994; Sereno et al., 1995). While our basic pattern of stimulation is a square wave of stimulation interspersed with non-stimulation periods, the skin surface experiences the stimulation in a moving window that cycles over the surface repeatedly during the course of the experiment. In the case of digit stimulation, the general direction of stimulation is always the same, either from the base of the digit to the fingertip (the proximal-to-distal condition) or from the tip to the base (distal-to-proximal). One such cycle is depicted in Figure 11-1, with six channels of stimulation available over the course of the experiment, but only three stimulation locations active at any one time. The two directions of stimulation act as control experiments for one another, with only the temporal pattern of stimulation across the digit acting to distinguish the conditions. Within a somatotopic map of a given digit, the hemodynamic activity should approximate the on/off stimulation pattern, with characteristic delays in each voxel depending on the voxel's receptive area along the digit. Furthermore, such a somatotopic map would necessarily have an early response to tip relative to base stimulation in a distal-to-proximal experiment, but relatively late phase of tip response in proximal-to-distal stimulation.

We individually tested each of the three digits (thumb, index and ring finger) of the right hand of right-handed subjects. Scanning focused on the contralateral sensorimotor region, where the somatotopic representation of the hand is known to occupy a particularly large surface area (Penfield & Boldrey, 1937). Analysis focused on Brodmann's areas 1 and 3b, as well as area 3a (all in primary somatosensory cortex, SI) and, further rostrally, area 4 (corresponding to primary motor cortex, MI). Each of these areas has been suggested to contain a parallel somatotopic sensory representation of the body surface among primates (Strick & Preston, 1978a; 1978b; Wong et al., 1978; Kaas et al., 1979; Nelson et al., 1980). Areas 3a and 4, however, are involved in motor production (Huffman & Krubitzer, 2001) and are typically responsive to kinesthetic afferents rather than cutaneous inputs (Kaas et al., 1979; Mountcastle, 1998). We therefore treated them as controls for areas 3b and 1, which are responsive to more superficial stimuli (Mountcastle, 1998). Area 2, though also in SI, was not included in the analysis both because it is thought to be secondary to area 3 processing (Vogt & Pandya, 1977; Künzle, 1978) and because the somatotopy here was expected to be obscured by overlapped, multifingered representation of the digits (Iwamura et al., 1980; Darian-Smith et al., 1984; Iwamura et al., 1985).

We also investigated whether the digit representations in these areas reflected several details evident from electrophysiological results, including nonlinearities in the multiplicity, scaling, and arrangement of the maps. More precisely, we located maps of the digits that showed phase reversal coinciding with reversal in stimulation direction, and compared: 1) the frequency of these representations in SI and its controls (areas 4/3a and a simulation of the data described in the Methods) as well as

within SI areas; 2) the differential representation of the three digits (and the surface within each digit) in terms of map volume and voxel populations within each map; and 3) the topography of the digit responses.

11.2 METHODS

We obtained high precision maps of the neural response to hand stimulation by using 4.0 T fMR imaging and a custom-built pneumatic device with a grid of closely spaced stimulation sites. We tested each of three digits (the thumb, index and ring fingers) twice, in opposite directions of stimulation. In data analysis, we paid particular attention to the delineation of Brodmann's areas 4, 3a, 3b, and 1. Functional analysis was applied to these regions, but was not restricted to the knob region usually associated with hand sensation and control in humans. We used in-house algorithms to detect discrete regions of cortex showing phase reversal coinciding with stimulation reversal.

11.2.1 Subjects

Six right-handed subjects (three males; average age 25 years) participated in this study. An additional subject was run but his data were discarded because of a suboptimal choice of functional slice planes. The subjects were neurologically intact and in good health. Ethical approval was obtained through the University of Western Ontario.

11.2.2 Paradigm

Stimulation apparatus A custom-built arc-shaped clear Plexiglas frame conveyed pulses of air to the surface of the hand. An array of 1152 fixed tubes (3 cm long, 1 mm aperture) opened into shallow depressions (0.5 cm wide) along the frame surface. The array was constructed such that air could flow back into each opening after striking the hand surface and be conducted away through the frame, in order to minimize the spread of air to adjacent regions of the digit. The device was modified for each subject to optimize the distribution of the jets under their digit surfaces, by selecting 16 particular tubes from among the 1152 available on the frame. The chosen jets were spaced regularly and in a straight line under each digit, extending from the base of each to within 1 cm of its distal end. Six jets were used for both the index and ring fingers, and four jets for the thumb, allowing for two jets per phalanx. The approximate spacing between jets was thus either one-sixth or one-quarter the length of the digit, generally about 1.5 cm. The hand frame rested on a Plexiglas table above the torso of the subject.

Pneumatic stimulation A Power PC Macintosh computer with an A/D board (National Instruments NI PCI-DIO-96) was used to control a series of 16 manifold-mounted air valves located directly outside of the magnet chamber. The valves received air through plastic tubing (6 mm aperture) from an air compressor (Campbell Hausfeld) located outside the magnet room. Sixteen flexible tubes (aperture constricting gradually from 6 mm to 1 mm) led from the air valves and

passed through a waveguide in the wall of the room before connecting to the 16 selected fixed tubes embedded in the stimulus frame under the subject's hand. The length of all tubing was constant across the sixteen channels. The air was supplied at a steady-state pressure of 240 to 275 kPa (35 to 40 p.s.i.) as measured at the air compressor outlet. This pressure was chosen empirically to maximize the strength of the stimulation while minimizing the spread of air. Pilot tests prior to the experiments indicated that puffed air would not elevate the digit above the Plexiglas frame or spread detectably along the length of the digit. A program written in MATLAB (MathWorks Inc.) specified the pseudorandom sequence of air puffs to be delivered to a digit in a given experiment.

Stimulation calibration Prior to entering the bore of the magnet, the distribution of air jets across the hand surface was optimized for each participant, and subjects' arms were positioned such that they reported feeling comfortable with their hand resting on the air delivery apparatus. Subjects were instructed to keep their eyes closed and their body, including both hands, as still as possible during each experiment. Each subject's head was also stabilized with a bite bar. Each experiment was preceded by the sagittal scout, and then a sequence of air puffs delivered over the surface of a digit. Subjects were instructed to make any adjustments in the position of that digit so as to cover all the active jets. At this time other digits could be moved slightly to keep the digit being stimulated in a "natural" position, as long as the digits were not in contact with each other. These adjustments, along with the curvature of the hand frame, were designed to keep the hand comfortable and unstretched, and thus to stimulate the digit under investigation without excessive spread of air to the other regions of the hand. This was followed by a 1-2 min pause before the experiment proper.

Stimulation protocol Subjects each participated in six experiments, i.e. two experiments on each digit, corresponding to the contrasted distal-to-proximal and proximal-to-distal directions of stimulation. The experiments were pseudo-randomly ordered such that no two successive experiments would stimulate the same digit, and to preclude order effects across subjects. Each experiment consisted of 6 cycles of 36 s each. During the experiments, jets were on for 40 ms per "puff". The minimum interval between puffs was 60 ms, giving a frequency of stimulation of 10 Hz. To reduce the predictability of the stimulus, the jets were activated in "bursts" of between 5 and 10 puffs, each separated by 60 ms. These bursts were themselves separated by random interburst intervals equal in duration to between 10 and 20 empty stimulation cycles of 100 ms each; hence the frequency of bursts varied between 0.33 and 0.67 Hz. Finally, the jets within each window were activated in a random sequence. As depicted in Figure 11-1, within each stimulation cycle the window of stimulation (equal to half of the available jets) would cycle through all 4 or 6 jets, depending on the digit stimulated. Each burst of 5-10 air puffs was confined to a single jet, but could be followed by another burst of 5-10 puffs at the same or another jet within the window.

11.2.3 Recording/Stimulation

Functional recording parameters Scanning was performed using the 4.0 T

magnetic resonance imager (Varian, Palo Alto, California, USA; Siemens, Erlangen, Germany) at the Robarts Research Institute (London, Ontario, Canada). Functional and anatomical images were acquired with a custom-built 14-cm quadrature surface coil centered around the left frontoparietal region. In addition to these scans, a full-brain volume was collected in a separate scanning session using a custom-built transmit-receive cylindrical birdcage coil. Functional images (TR = 750 ms, 4 shots, TE = 15 ms, FA = 40°, FOV = 19.2 × 19.2 cm) were acquired using a T2*-weighted gradient echo-echo planar imaging (EPI) pulse sequence. We sampled nine contiguous pseudocoronal 5-mm thick functional slice planes (1.5 × 1.5 mm in-plane resolution). Seventy-two functional volumes were acquired over the course of the 216 s long experiment.

Anatomical recording parameters During the same scanning session we also acquired 64 T1-weighted contiguous pseudocoronal 1-mm thick slice planes (0.75 × 0.75 mm in-plane resolution; TR = 12 ms, TI = 500 ms, TE = 6 ms, FA = 11°, FOV = 19.2 × 19.2 cm). In a separate scanning session 256 T1-weighted contiguous axial 0.94-mm thick anatomical slices were collected (TR = 12 ms, TI = 500 ms, TE = 6 ms, FA = 11°, FOV = 24.0 × 24.0 cm). The orientation of the pseudocoronal images approximated the angle of each subject's central sulcus. The scanning volume encompassed most of the pre- and postcentral gyrus, but clipped the most posterior extent of the postcentral gyrus in five subjects (S1-S5).

12.2.4 Analysis

Anatomical landmarks We initially analyzed the data with BrainVoyager (Brain Innovation, 2000). We defined the cortical region of interest (ROI) based on anatomical landmarks delineating Brodmann's areas 4, 3a, 3b, and 1, as illustrated by the colored regions in Figure 11-2. The borders approximately followed previous macroanatomical (Allison et al., 1989; Gelnar et al., 1998; Francis et al., 2000; Moore et al., 2000a; Blankenburg et al., 2003) and cytoarchitectonic (Geyer et al., 1999; Rademacher et al., 2001) divisions, insofar as these are correlated (Rademacher et al., 1993; White et al., 1997). Fortunately the central gyrus anatomy is relatively consistent between subjects (Ono et al., 1990; Rademacher et al., 2001) and reliably identifiable in MR images (Sobel et al., 1993), in contrast to the more variable anatomy of the primary auditory (Penhune et al., 1996) and visual (Amunts et al., 2000) cortices. We were also able to identify an omega-shaped "knob" region in coronal views from each subject, following previous anatomical characterizations (Yousry et al., 1997; Moore et al., 2000b). Note, however, that even expert judgments of anatomy are less reliable in identifying a functional "hand" sensation region here (as validated by direct cortical recording and stimulation) than are noninvasive responses measured with fMRI or somatosensory-evoked potential dipole localization (Towle et al., 2003). Hence the ROI included primary sensorimotor cortex medial and lateral to this structural landmark.

Anatomical delineation Our ROI selection was performed manually for each subject based on careful inspection of three-dimensional cortical anatomy in the subject's full-brain volume. The high resolution images in this volume allowed us to clearly delineate the precentral and postcentral gyri. In general, area 3a was defined as

the gray matter flanking the fundus of the central sulcus; area 4 was symmetrical and anterior to both area 3b (the posterior wall of the central sulcus) and area 1 (the crown of the postcentral gyrus, extending posteriorly to the rostral lip of the postcentral sulcus). More medially, areas 4 and 3b converged directly at the paracentral lobule. These ROI borders were used to localize functional activation on a within-subject basis, but for comparison purposes each subject's brain volume was also standardized according to the Talairach and Tournoux (1988) atlas. Also, an averaged brain volume was processed and rendered for display of functional points of interest.

Functional data preprocessing We corrected for linear trends in the vascular activity of each slice by preprocessing the functional images within the frequency domain. A significant motion artifact excluded the experiments involving digit 4 stimulation of subject S2. The remaining data were not spatially averaged but functional images were generated with minimal spatial clustering. A reference time course determined by the stimulation protocol (18-s on/off half-cycles) was blurred and systematically shifted by a 5-s hemodynamic response lag. We selected this lag both on the basis of other published results (e.g. Glover, 1999) and on our own empirical optimization of the correlation between the hemodynamic reference sinusoid and the BOLD changes in each fMR image voxel. The reference time course was then correlated with the functional data after being shifted iteratively by 3 s increments, i.e. phase delays. (As such, the 5-s hemodynamic lag was not the only lag allowed in correlating the response function to the BOLD signal in each voxel.) As described in the Introduction, the phase delay of a given voxel can be related to the delay in stimulation of a particular region on the digit surface. As shown in Figure 11-3, voxels were color-coded according to the phase delay of maximal correlation to the reference time course. The twelve such colors included phase values for which the maximal correlation was found with a reference time course interpolated between the actual sliding-window positions. Thus, in the case of the index or ring finger, six of the twelve values would refer to positions between the six actual stimulation jets. For all digits, the smallest phase delay is depicted as orange to yellow, the longest as violet to red, and intermediate phase shifts run through the color spectrum between these extremes.

Functional phase analysis The functional slice planes were coregistered with the full-brain volume of each subject using BrainVoyager. This was accomplished by iterative translation and rotation of the trilinearly-interpolated anatomical volume. Images of ROI-masked, phase-coded activity above an initially low, $r^2 = 0.10$ correlation value cutoff were then exported to MATLAB. We applied in-house algorithms to detect bands of at least 20 laterally connected anatomical voxels (i.e. a cortical volume of at least 56 mm^3) that exhibited phase reversal coinciding with stimulation direction reversal. (This minimum number of voxels, enough to allow for at least five independent functional phase values, was chosen after an initial qualitative inspection of the data.) The phase bands were also required, following gyral/sulcal anatomy, to be relatively straight (having no turns equal to or exceeding 90° in physical space), to be relatively continuous in phase space (having no neighboring voxels separated by more than a 90° phase shift in either stimulation direction), and to span at least one quarter (90°) of the phase spectrum. This two-

dimensional analysis was also repeated in simulations of each experiment. These simulations used randomly generated phase lags, taken from a uniform distribution of 12 values ranging from 0° to 330° in 30° bins. These values were overlaid on all voxels which, in the real dataset, showed hemodynamic activity significantly correlated to the stimulation waveform (at $r^2 > 0.10$). The simulated dataset may be considered as an additional control (besides the paired distal-to-proximal and proximal-to-distal experiments) which define the frequency of phasic relations that would be expected by chance.

11.3 RESULTS

We located continuous bands of functional voxels showing a reversed ordering of phase delays associated with directions of stimulation inverted between experiments on the same digit and subject. Although the search algorithms were designed in principle to look for phasic relations in three dimensions, in practice all such phase bands were located within-slice in the original pseudocoronal scan planes. As a result of the individually-applied ROI masks, these within-subject representations were necessarily limited to gray matter in the central gyrus region. As shown in Figure 11-4, the same digit could be represented multiple times in the same subject. In addition, the representations of two digits (observed in separate experiments) would occasionally cluster together (as in Fig. 11-4), though this was not commonly observed.

11.3.1 Frequency of representation across sensorimotor areas

As a criterion for significance, the phase maps were thresholded above a correlation value, averaged across voxels, of $r^2 > 0.22$ (cf. the $r^2 > 0.10$ cutoff originally applied to individual functional voxels). This criterion was the greatest average correlation value achieved among the simulated data; above this cutoff we detected representations across sensorimotor cortex but none in the simulated dataset. (Recall that the simulated dataset was a randomization of functional voxel phase values overlaid on the observed signal correlation values, and was intended to act as an additional control to gauge the number of phase bands expected purely by chance.) Among the real digit representations, we observed a relative predominance of bands in primary somatosensory areas over those in the "control" areas 4 and 3a (Fig. 11-5). This disproportionate representation in areas 3b and 1 appeared despite greater combined cortical territory in areas 4 and 3a. On average, and for each subject, area 4/3a occupied more volume (15.3 ± 1.6 cm^3) than area 3b/1 (13.3 ± 2.2 cm^3). Most of this volume can be attributed to area 4: as in Geyer et al. (2000) and insofar as areas 3a and 3b can be distinguished (Geyer et al., 1999), we found that area 3a (unlike area 4) occupied a particularly small area relative to both areas 3b and 1.

11.3.2 Somatotopic variation by digit identity

Within SI, the phase bands distinguished between the digits in both frequency and in size. Among the bands sampled in Figure 11-5, a majority (11/13) were

associated with thumb or index digit stimulation. Similarly, there was a significant difference between the average volume of the digit representations, with thumb representations occupying the most volume (94 ± 9 mm^3), index finger maps less (81 ± 12 mm^3), and ring finger bands the least (67.5 ± 0 mm^3). A two-way (area 3b/1 × digit 1/2/4) ANOVA found a significant effect on map size of digit ($F_{(2,8)} = 10.30$, $p < 0.01$). A Tamhane post hoc pairwise comparison—a conservative test assuming heterogeneity of variance as well as unequal sample sizes (Toothaker, 1991)—found the digit 1 vs. 4 difference significant, $p < 0.01$.

11.3.3 Somatotopic variation by SI area

The two-way (area 3b/1 × digit 1/2/4) ANOVA revealed a moderately significant effect of area on map size ($F_{(1,8)} = 6.25$, $p < 0.05$), with area 1 maps possessing slightly larger volume. The area × digit interaction was non-significant ($p > 0.05$). As a whole, area 3b occupied an average of 6.3 ± 0.9 cm^3, while area 1 occupied 7.1 ± 1.6 cm^3. Geyer et al.'s (2000) cytoarchitectonic mapping results (in which area 3b occupies 27% more volume than area 1 within subjects) thus suggest that we may have delineated area 3b conservatively relative to area 1. Nevertheless most of the phase bands in SI (8/13) were in area 3b. All of these represented the thumb (4/8) and index finger (4/8), while a smaller fraction (2/5 and 1/5) of the area 1 bands represented these digits.

11.3.4 Representational bias in area 3b

Not only between digits but *within* the area 3b digit representations there was heterogeneous representation. That is, the distributions of phase values making up each digit map were less uniform in this area. Collapsing voxel populations across digits, the functional voxel distributions in area 3b were significantly non-uniform in both directions of stimulation. Using Rayleigh's statistic for circular data (Fisher, 1993) we found $Z = 14.37$, $p < 10^{-6}$ (distal-to-proximal) and $Z = 12.57$, $p < 10^{-5}$ (proximal-to-distal). In area 1 the proximal-to-distal voxel distribution was non-uniform, but less significantly so ($Z = 3.44$, $p < 0.05$). Figure 11-6 displays the area 3b voxel distributions as a function of phase, and makes clear both the non-uniformity and the symmetry of the two direction-specific distributions. For example, there is a representational peak for both stimulation directions at phase delays of 210°—the phase lag associated with stimulation at the very tip of the digit in both directions of stimulation—and frequency dropoff in the adjacent bins.

11.3.5 Distribution of digit representations

While most phase bands were localized to the somatosensory region in the posterior part of the ROI (Fig. 11-5), the digit maps appeared to be much more distributed in the lateromedial and dorsoventral dimensions. As shown in Figure 11-7, the average locations of the digits were proximal and slightly lateral to the "knob" area. In Talairach coordinates, the average coronal extent of the knob region was -37.7 ± 5.4 to -23.2 ± 5.0 (lateromedial) and 43.5 ± 3.3 to 65.3 ± 3.6 (dorsoventral). However, the spread in digit map locations, particularly in the lateromedial

dimension, was substantial compared to the relatively consistent knob-area borders. Insofar as the locus of each digit representation could be distinguished, the average thumb map location was on average more lateral, anterior and ventral (Talairach -45 ± 18, -21 ± 11, 42 ±17) than the index finger representation (-35 ± 18, -32 ± 9, 52 ± 17). The average ring finger representation appeared to be more dorsal and otherwise intermediate between these two (-41 ± 9, -26 ± 8, 54 ± 6). However, one-way ANOVAs showed no significant difference between the within-slice locations of these averaged digit representations at ($p > 0.05$), either lateromedially or dorsoventrally. The distributed pattern of representation is visible in Figure 11-8, which projects the locations of those phase bands meeting the more stringent significance criterion on a rendered view of the average subject brain volume.

11.4 DISCUSSION

Three patterns of results deserve further discussion. First, the presence of stimulation-related phase reversing bands in areas 3b and 1 but not in areas 3a or 4 suggests that the input organization of the former areas is relatively discrete and somatotopic. Second, our results in SI confirm those obtained by more invasive recordings as to the nonlinear representation of the body surface in terms of phase band arrangement, scaling, and frequency compared to the digit surfaces stimulated. Finally, within SI the area 3b and 1 representations were differentially nonlinear in their topographical weighting (both across and within digits), size, and multiplicity—consistent with functional and afferent differences between the two areas.

11.4.1 Nonlinearities in somatosensory mapping of the digits

A remarkable characteristic of SI is its somatotopic patterning after the body's own conformation in the form of a contralateral somatosensory homunculus. Several striking nonlinearities may be noted in this homunculus. First, the body parts represented are not all attached in their real-world configuration. Farah (1998) suggests that the somatotopic proximity between, for instance, the hands and face is a result of their repeated, synchronous stimulation in the womb. Second, disproportionate representation is given to the tongue, lips, and hands, especially the digits (Penfield & Boldrey, 1937). These parts of the body are also among the most receptor-dense and sensitive, as measured by the two-point discrimination task (Weinstein, 1968). Third, multiple somatotopic maps exist in SI. Detailed studies of somatotopic organization in monkeys (e.g. Kaas et al., 1979) have revealed that parallel homunculi are present within each of the four Brodmann areas (1, 2, 3a, and 3b) of SI (Kaas et al., 1979; Nelson et al., 1980). Each somatotopic strip appears to be primarily responsive to a given receptor type (Kaas et al., 1981). Definitive evidence of multiple SI maps coding for different mechanoreceptors within the human brain is still lacking, despite the results of Moore et al. (2000a) and Gelnar et al. (1998).

The structure of the area 3b/1 somatotopy we observed is generally consistent with previous reports. The average location of the digits is slightly lateral to, but

otherwise within the anteroposterior and dorsoventral bounds of the knob region (Fig. 11-7). This localization was not a result of a lateromedial ROI restriction (cf. Blankenburg et al., 2003), since our ROI included nearly all of areas 4, 3a, 3b, and 1. The observed somatotopy was also in agreement with the previously discussed nonlinearities of the sensory homunculus. The differential representation of the three digits sampled in this study is consistent with the relative sensitivity of the three digits, as recorded directly by Penfield and Boldrey (1937) in somatosensory cortex. In particular, the differential number of phase bands (Fig. 11-5) attributed to the three digits may reflect a greater representation of the thumb and index finger, both of which are involved in precision grip and other opposition behaviors (Napier, 1956). The significantly greater average volume associated with cortical maps of the thumb testifies further to the size and sensitivity of the thumb pad.

In addition to frequency and scaling nonlinearities, the arrangement of digit maps was at odds with the actual ordering of the digits. In agreement with previous reports from evoked potential recording in animals (Woolsey et al., 1942) and direct stimulation and recording in humans (Penfield & Boldrey, 1937; Woolsey et al., 1979), we find that the locus of representation for the thumb lies laterally to that of the index finger. A relatively anterior and ventral average location for the thumb representation compared to the index finger locus is also consistent with the fMRI findings of Maldjian et al. (1999). However, the average ring finger map location does not follow a regular somatic ordering of the digits, being more dorsal but otherwise intermediate between the thumb and index representations. In other fMRI research, Kurth et al. (1998) also report some variability in the lateromedial arrangement of the second and fifth fingertip representations. In contrast, McGlone et al. (2002) and Gelnar et al. (1998) find no regular lateromedial progression of the maps. An anteroposterior arrangement is even more controversial (McGlone et al., 2002). We suggest that the neuronal firing response of areas 3b and 1, as measured electrophysiologically, may be more discretely and consistently organized than the metabolic activity thought to underlie the BOLD response (Logothetis et al., 2001).

11.4.2 Caudal restriction of somatotopic maps

The digit representations we observed were necessarily localized to primary sensorimotor areas given our a priori ROI definition. However, some form of somatotopic organization exists in areas outside of SI (Kaas & Pons, 1988) such as secondary somatosensory cortex (SII) as well as Brodmann's areas 4, 5 and 7. For instance, although its function is not well understood, in primates area 3a has been implicated in providing motor cortex (Huffman & Krubitzer, 2001) and area 1 (Jones & Friedman, 1982) with somatosensory input. McGlone et al (2002) report fMRI evidence that this area responds to vibrotactile stimulation in humans (cf. Moore et al., 2000a).

As for motor cortex, while cutaneous inputs to MI (in particular the cutaneous inputs to Brodmann's area 4p) are generally neglected, they have been observed in single-unit recordings from squirrel monkeys (Strick & Preston, 1978a; 1978b) and macaques (Wong et al., 1978). In humans, fMRI evidence suggests that MI also passively receives at least kinesthetic input from the muscle spindles (Naito et al., 2002), and positron emission tomography (PET) shows that MI is activated by passive limb movements in humans (Weiller et al., 1996) as it is in monkeys

(Colebatch et al., 1990). Such cutaneous and kinesthetic activity is observed even when stimulation is passive, as it was in the present experiment.

Somatotopic organization is a feature of areas 3a and 4, as it is for the more posterior areas 3b and 1. Furthermore, the overall somatotopy of the area 4 map (Penfield & Rasmussen, 1950; Woolsey et al., 1952) and possibly the area 3a map (Kaas et al., 1979) appears to be nonlinear in the arrangement of somatotopic features (Woolsey et al., 1952; Huffman & Krubitzer, 2001). The representations in these areas are also scaled nonlinearly like those in somatosensory cortex, with disproportionately large areas devoted to the hand, digits, and face (Woolsey et al., 1952; Krubitzer & Kaas, 1990). Finally, as in somatosensory cortex, in primates there appears to be multiple somatosensory representation in areas 4 and 3a, based on parallel sensory input. In squirrel monkeys, Strick and Preston (1978a; 1978b) found two separate motor representations of the hand and wrist in MI, one responsive to cutaneous receptor input and the other to joint receptors. In area 3a, besides a somatotopic representation based on muscle spindle input (Kaas et al., 1979), work by Huffman and Krubitzer (2001) revealed responses to cutaneous stimulation in the marmoset monkey.

Areas 4 and 3a thus appeared to be suitable anatomical controls for areas 3b and 1, since all these areas handle cutaneous afferents but the latter are better known for discrete somatotopic patterning. Indeed, we found that both control areas had a much lower concentration of discrete, continuous digit representations than did areas 3b and 1 (Fig. 11-5), despite a greater combined cortical territory in areas 4 and 3a. The only other fMRI study known to us to directly compare somatotopic digit-related activation in motor and somatosensory cortex (McGlone et al., 2002; cf. Gelnar et al., 1998) also found precentral activation in most subjects in response to stimulation of digits 2 and 5, but the activation was not spatially distinct for the two fingers.

11.4.3 Functional differentiation of area 3b and 1 representations

The degree of positional variability we measured between subjects' digit representations, and the infrequency of clustering among different maps within subjects, suggest caution in identifying a precise "hand" area in SI. Previous studies have attempted to describe such a hand area based on average locations of digit-related activation hotspots (e.g. Maldjian et al., 1999), thus overlooking the likelihood that the digits are represented multiple times even within SI, as suggested by single-unit recording work of Kaas et al. (1979) in areas 3a, 3b, 1 and 2 of New World monkeys. Conversely, a "multiple-representation view" (McGlone et al., 2002) has been invoked when additional activation centers are observed outside of SI (e.g. Gelnar et al., 1998; Kurth et al., 1998).

We believe that the multiplicity of representation in areas 3b and 1 observed in our results (Fig. 11-5) may be specifically related to receptor type. The class of superficial cutaneous receptors includes Meissner's corpuscles and Merkel's disks; these cells differ in several respects including response adaptivity and optimal stimulation frequency. The rapidly-adapting Meissner's corpuscles (associated with motion perception) respond best to stimuli with a 3-40 Hz frequency, while the optimal stimulation range for the slowly-adapting Merkel's disks (suited for fine detail discrimination) is 0.3-3 Hz (Bolanowski et al., 1988). Within SI, areas 3b and

1 are themselves specialized for certain receptor types (Mountcastle, 1998), though few human studies have looked for receptor-specific representation here. Anatomically, area 3b is a sensory distribution center that represents the cutaneous receptors associated with both slowly- and rapidly-adapting fibers (Mountcastle, 1998), including both Merkel's disks and Meissner's corpuscles. Area 1 is more restricted to the input of rapidly adapting fibers from deep as well as cutaneous receptors (Kaas et al., 1979).

Given the frequency dependence of Meissner's corpuscles and Merkel's disks, both types of receptors were likely activated by our stimulation protocol (which included both 0.33-0.67 Hz bursts of 10 Hz puffs of air). In our study we observed digit representations in both areas 3b and 1, and furthermore a functional differentiation between the two areas. Area 3b had a greater fraction of the observed SI phase bands, a result consistent with the notion that it receives input from two receptor types rather than one—and may thus have even more functional maps of the digits (Iwamura et al., 1985) than estimated by Kaas et al. (1979). A relatively greater (Gelnar et al., 1998) or more balanced (Kurth et al., 1998) number of digit response hotspots in area 1 relative to area 3b can similarly be explained by the use of higher (50 Hz) or intermediate (8.1 Hz) stimulation frequencies, respectively, leading to greater activation of rapidly-adapting fiber inputs.

We observed these multiple representations in area 3b despite a conservative delineation of area 3b relative to that of area 1 (cf. Geyer et al., 2000), and the partial voluming that might be expected more in area 3b than area 1, the latter being generally orthogonal to our pseudocoronal slice planes. Note, however, that we were limited to detecting phase bands that happened to lie coplanar to our slice planes. Although the phase reversal search algorithms operated in three dimensions it would have been difficult to track phase maps that stretched even 5 mm between successive functional slice planes. Such an anisotropic bias may have contributed to the fewer phase maps observed in area 1, whose surface was frequently normal to the slice planes. Our sampling of digit representations was also limited by the relatively stringent correlation threshold applied to the aggregate of voxels included within each phase band.

All of the area 3b digit maps represented the thumb or index finger, in contrast to the relatively equal representation of the three digits in area 1. A similar bias exists at the sensory periphery, where the surface area of glabrous skin is greater for the thumb and index finger than for the ring finger. This bias holds for the entire digits as well as the fingertips (Johansson & Vallbo, 1979). The discrepancy we measured between areas 3b and 1 may reflect a greater bias of this receptor density earlier in the somatosensory processing stream, as anatomical evidence suggests that area 3b (as well as 3a) sends projections to area 1 (Jones & Friedman, 1982).

The more heterogeneous representation of digits observed in area 3b (Fig. 11-6) is mirrored by the non-uniform distribution of phase values within the digit maps of this area. The heterogeneity of phase values in area 3b that we observed may reflect the non-uniformity of Meissner and Merkel receptor distribution across the digits themselves (Johansson & Vallbo, 1979; Stark et al., 1998). For instance, there is a local maximum of voxel responses associated with fingertip stimulation in both stimulation conditions (Fig. 11-6). Besides this distal-to-proximal variation in response we did not further investigate within-digit somatotopy. Despite our use of high-resolution fMRI, such fine patterning within phase band maps would be

difficult to interpret given our anisotropic and frequently non-parallel sampling of the cortical surface.

While area 3b maps were small and possibly localized to a particular digit segment (Iwamura et al., 1983), the area 1 digit representations were larger in size. This finding appears to contradict electrophysiological results from monkeys. Specifically, relative to other SI subregions area 3b has been shown to have the largest cortical area devoted to representation of the body, including the digits (Kaas et al., 1979; Sur et al., 1980), and smaller (i.e. more sensitive) receptive fields (Hyvärinin & Poranen, 1978). Yet insofar as fMRI measures aggregate subthreshold dendritic activity (Logothetis et al., 2001), the cortical activation seen in area 1 supports the existence of larger receptive fields here (Kurth et al., 1998). In particular, greater activation volume in area 1 may enable multifingered representation (and the concomitant need for overlap of the different digit maps), as observed in primates (Iwamura et al., 1985). Our results are thus consistent with a functional differentiation of areas 3b and 1 in terms of digit representation, with area 3b maps more discrete and biased by receptor distribution.

Figure 11-1 Sliding-window paradigm. In this example a digit (here the index or ring finger) is stimulated at any of six jet locations distributed over the glabrous surface of the finger. Three jets define a "window" of potential stimulation that moves along the surface of the digit in one direction, and completes one stimulation cycle over the digit surface in 36 s. In this example the stimulation direction is distal-to-proximal, or from the tip to the base of the digit. At any given time one of the three jets within the sliding-window may be active. In the case of a thumb experiment there are only four jets and so the stimulation window is limited to two jets.

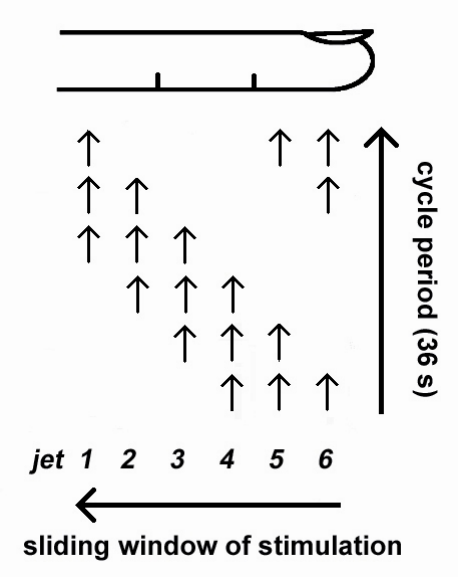

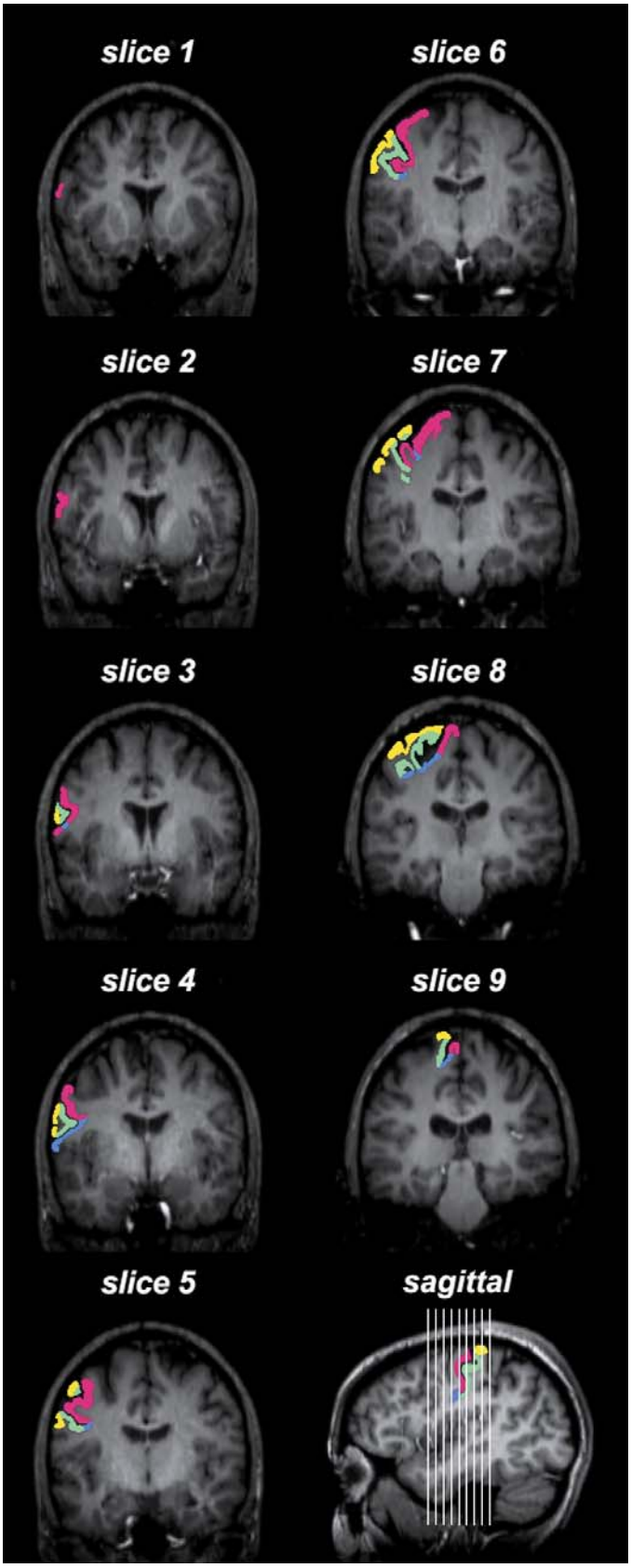

Figure 11-2 Regions of interest. The nine functional slice planes in pseudocoronal orientation from one subject, spanning the primary sensorimotor areas (Brodmann's area 4 in red, area 3a in blue, area 3b in green, area 1 in yellow). The anatomical slices representing each plane are 0.5 cm apart, with slice 1 most anterior and slice 9 most posterior. The bottom right image shows a sagittal image taken from the left hemisphere of the same subject, oriented so that the nine slice planes (shown in cross-section) are vertical. Areas 4, 3a, 3b, and 1 are color-labeled as in the pseudocoronal slices.

Figure 11-3 Phase reversal. The direction of stimulation leads to different phase values being associated with the same location on the digit. Phase values are coded by color, and represent the temporal shift required to achieve maximal correlation between the reference time course and the measured hemodynamic activity in a voxel. The reference time course is shown prior to hemodynamic convolution. Stimulation occurs with a phase lag of 0° near the middle of the digit, because the first stimulation windows in the first half of each stimulation cycle include the jet in this location. In distal-to-proximal experiments, areas on the tip of the digit are stimulated with an earlier phase with respect to areas nearer the base of the digit; the converse is true for proximal-to-distal experiments. Thus across the voxels representing a digit, the colors associated with different phase shifts of the reference time course should show a reversed ordering when the direction of stimulation is reversed.

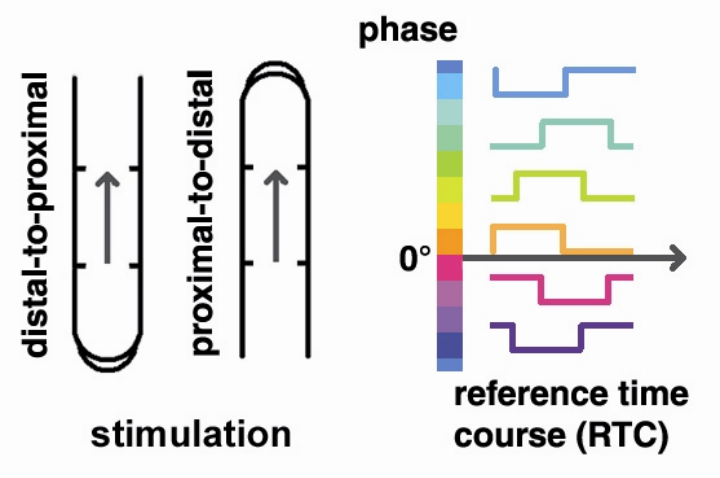

Figure 11-4 Sample digit maps, showing phase reversal, conjunction and multiple representation. Phase bands representing the thumb (D1) and index finger (D2) are shown with heavy and light outlines for one subject (S2). Two maps in area 3b (Talairach -56, -16, 30) are seen to lie adjacent to one another and show phase reversal between **a**) distal-to-proximal stimulation, and **b**) proximal-to-distal stimulation of the digits. The digits are also represented multiple times in this subject, as shown by overlapping phase bands in another location in area 3b (-46, -28, 48), again showing phase reversal between **c**) distal-to-proximal and **d**) proximal-to-distal stimulation directions. Note that the digit maps shown here are atypical in that their phase values appear to reflect stimulation of more basal regions of the thumb and index finger.

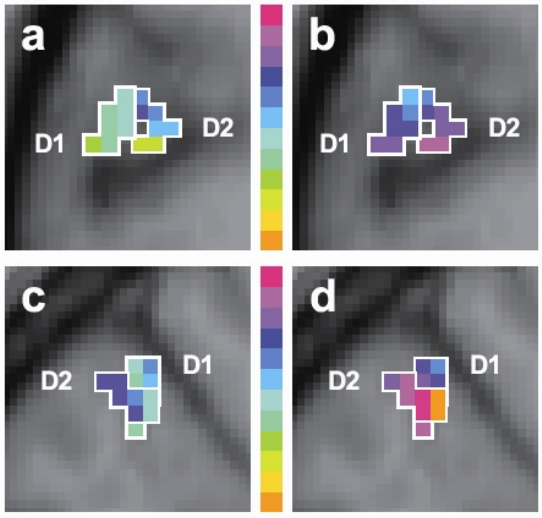

Figure 11-5 Total frequency of digit representations across subjects. Most bands of functional voxels showing phase reversal coinciding with a reversal of stimulation direction lay in Brodmann's areas 3b and 1, despite a greater cortical territory in area 4. The phase bands in areas 3b/1 depicted a greater frequency of representation for the thumb, followed by the index and then ring fingers. Few phase bands were detected in randomized functional data across the aggregate of areas 4, 3a, 3b, and 1; real digit maps are thresholded above the maximal correlation achieved by these simulated phase bands.

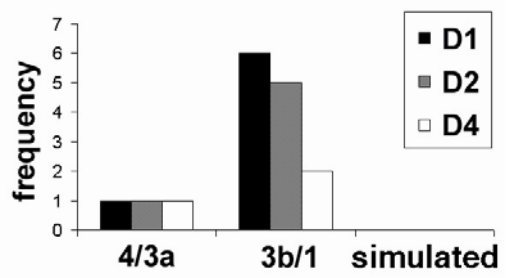

Figure 11-6 Area 3b representations as a function of phase value. Both the distal-to-proximal and proximal-to-distal voxel distributions are displayed, superimposed over the color-coded phase spectrum. The radial scale (shown on the horizontal axis) indicates voxel frequency per phase value. The voxels are derived from the area 3b phase bands thresholded as in Fig. 11-5, collapsed across all digits stimulated in each of the two directions. Significantly, the two distributions appear to be symmetrical around the axis defining phase reversal (i.e. the phase values at which the same location on the digits is stimulated in either direction of stimulation). The two distributions also reflect a non-uniform clustering of voxels around particular phase values. The two arcs represent the phase of distal fingertip stimulation (solid, distal-to-proximal; hollow, proximal-to-distal). The symmetrical pattern of the two distributions, while complex, suggests that they both reflect the structure of the afferent inputs from the digit surface, with more voxels representative of more sensitive digit locations.

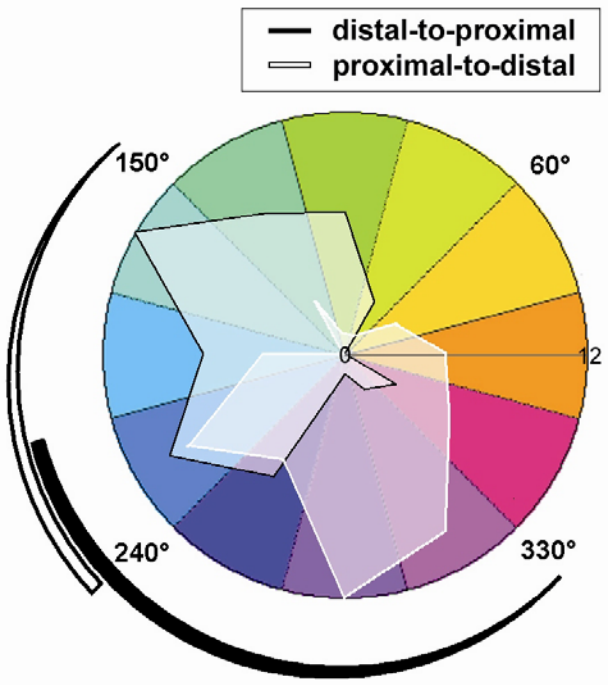

Figure 11-7 Average location of area 3b/1 phase maps in coronal view. The loci of the representations exhibit a lateral to medial progression from thumb (D1) to index finger (D2), with an intermediate location of the ring finger (D4) representation, but there is substantial variability in the positions across subjects. Phase bands are thresholded as in Fig. 11-5. The coronal projection of the knob region borders are also shown for the six subjects (S1-S6).

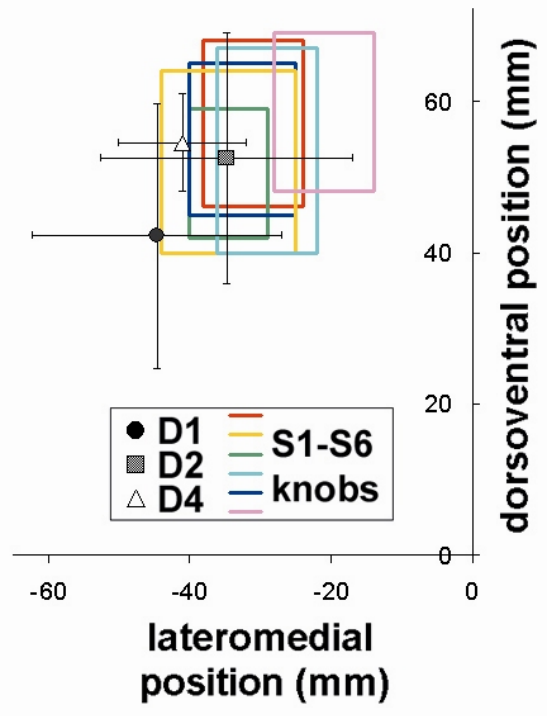

Figure 11-8 Area 3b and 1 phase maps projected onto rendered, averaged brain. The central sulcus (CS) and postcentral gyrus (PoCG) are seen from the front. Brain and skull matter anterior to CS have been removed, as well as skull matter overlying the left postcentral sulcus (PoCS) and more caudal cortex. Despite Talairach standardization of the brains the brain surface appears smoothed due to averaging. Digit map locations are indicated by superimposed colored icons. The lateromedial segregation of the thumb and index finger representations is again evident, as are the preponderance of area 3b phase bands, the occasional clustering between maps, and the substantial variability between subjects. Phase bands are thresholded as in Fig. 11-5.

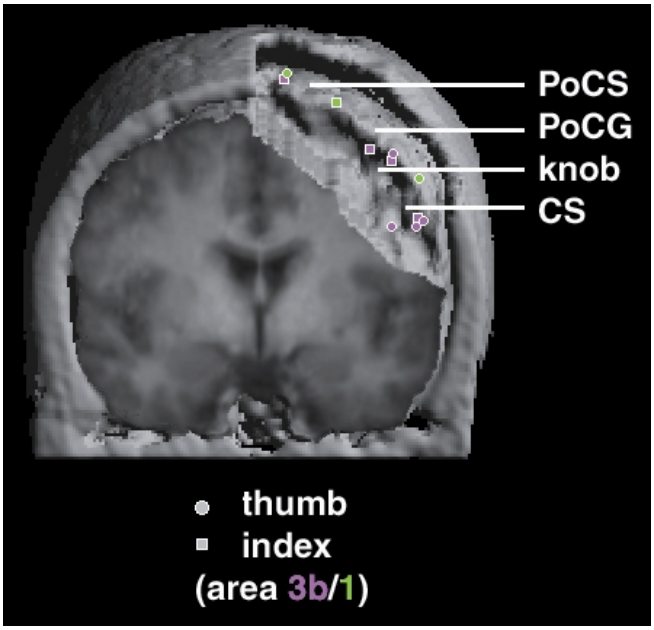

12 Symmetric Sensorimotor Somatotopy

Receptors in the skin provide cutaneous information to the primary somatosensory cortex. Detailed studies of cortical somatosensory responses have traditionally been based on electrophysiological recordings from monkeys. Investigations of somatosensory organization in human cortex have either relied on superficial recordings from epileptic patients, or more recently from fMR (functional magnetic resonance) imaging. The latter has been limited not only by scanning resolution but by the assumption that fMRI can reveal discrete activation "hotspots" in response to cutaneous stimulation, like those measured electrophysiologically as the firing output of cells (particularly under anesthesia). Here we instead accept that fMRI largely reflects the metabolic demands of dendritic input to cells. Using high-resolution functional magnetic resonance imaging in human subjects, we find a widely distributed cortical response upon pneumatic stimulation of the hairless surface of three digits: the thumb, index and ring fingers. Areas of primary somatosensory and motor cortex were both extensively active during stimulation of the thumb and index finger. Though not organized in a discrete somatotopic fashion, the thumb/index population activity indicates a disproportionate response to fingertip stimulation that is modulated by stimulation direction. Qualitatively, the activation appears to be structured with a line of symmetry through the central sulcus reflecting inputs both to primary somatosensory cortex and, precentrally, to primary motor cortex. These findings suggest a striking functional mirroring of areas conventionally ascribed either an input or an output somatotopic function.

12.1 INTRODUCTION

Receptors in the skin provide cutaneous information to the primary somatosensory (SI) cortex. Following detailed electrophysiological studies of cortical somatosensory responses in monkeys, investigations of somatosensory organization in human cortex have either relied on superficial recordings from epileptic patients (Penfield and Boldrey, 1937), or more recently from fMRI (Blankenburg et al., 2003; Dechent and Frahm, 2003; Gelnar et al., 1998; Kurth et al., 1998). Previous human somatotopy studies using fMRI have been limited not only by scanning resolution (Blankenburg et al., 2003; Gelnar et al., 1998) but by an underlying premise that fMRI reveals discrete activation "hotspots" in response to cutaneous stimulation (Dechent and Frahm, 2003; Kurth et al., 1998), like those measured electrophysiologically as the firing output of cells—particularly under anesthesia (Tommerdahl and Whitsel, 1996). Recent evidence suggests instead that fMRI may reflect more the metabolic demands of dendritic input to cells (Logothetis et al., 2001). Here we applied this tentative interpretation to our methodology, and used high-resolution (4T) fMRI to seek cortical somatosensory responses.

Our experimental paradigm adapted the phase analysis method used previously to identify retinotopic maps in visual cortex (Engel et al., 1994) to instead map the cortical representations of the human digits. The approach validates observed activation on the basis of spatiotemporal relations between voxels comprising the cortical response to stimulation across each digit. In our sliding window stimulation technique (Servos et al., 1998; Chapter 11), a reference time course is made up of periods of stimulation interspersed with non-stimulation intervals, but in contrast to conventional block designs, different points on the digit receive stimulation at

staggered points in time. That is, the stimulated digit experiences a moving window of stimulation which cycles repeatedly over the surface. For a finger spanned by six air jets, this window consists of three jets potentially active within any given stimulation half-cycle (Fig. 12-1a). Correlated cortical activity is therefore driven by an on/off stimulation time course shifted by a particular time delay unique to a location on the digit surface (Fig. 12-1b). As a within-digit control, we vary the general direction of stimulation (Fig. 12-1c), from the base of the finger to the fingertip, or from the tip to the base.

For this investigation we passively stimulated the glabrous (hairless) surface of the thumb (D1), index (D2) and ring finger (D4) of seven subjects using puffs of air delivered through a custom-built apparatus (see Methods). Each subject participated in all six experiments (three digits × two directions) in a pseudorandom sequence such that no two successive experiments would involve the same digit. While stimulating the digits we measured the blood-oxygenation level dependent (BOLD) response of left-hemisphere cortex using fMRI. The functional voxels were assigned phase lags of maximal correlation to the reference time course (Fig. 12-1c). The phase lag associated with each significantly correlated voxel was taken to reflect its activation delay (including a 5-s hemodynamic lag) following stimulation at a particular location on the digit surface.

12.2 METHODS

12.1 Subjects

We scanned seven healthy right-handed human subjects (four males; average age 26 years), at the Robarts Research Institute (London, ON) using a 4T magnetic resonance imager (Varian, Palo Alto, CA; Siemens, Erlangen, Germany). Ethical approval was obtained through the University of Western Ontario. A significant motion artifact excluded the D4 experiments of subject 1.

12.2 Paradigm

Stimulation apparatus As in Chapter 11.
Pneumatic stimulation As in Chapter 11.
Stimulation calibration As in Chapter 11.
Stimulation protocol As in Chapter 11.

12.3 Recording/Stimulation

Anatomical recording parameters As in Chapter 11.
Functional recording parameters As in Chapter 11.

12.4 Analysis

Anatomical landmarks As in Chapter 11.
Anatomical delineation As in Chapter 11.
Functional data preprocessing As in Chapter 11.

Functional phase analysis As in Chapter 11, functional voxels were color-coded according to the phase delay of maximal correlation (Fig. 12-1). Because there were either four (thumb) or six (index/ring finger) jets per digit, but twelve possible phase delays, for some of the phase values the maximal correlation was achieved with a reference time course interpolated between the actual sliding-window positions. For all digits, the largest phase shift is depicted as violet to red, the smallest as orange to yellow, and intermediate phase delays span the color spectrum between these extremes. After coregistering the functional and full-brain anatomical slice planes of each subject, phase-coded functional data were assigned to one of the regions of interest and tested for uniformity. The same analysis was applied to Monte Carlo simulations of each subject × digit × direction experiment. In these simulations, the voxels retained their measured degree of correlation to the reference time course, but the optimal phase lag of each voxel's correlation was substituted by a random value taken from a uniform distribution of the possible phase delays.

12.3 RESULTS

Our fMR imaging and subsequent analysis were directed at primary sensorimotor cortex contralateral to the right hand. Using the full-brain anatomical volume from each subject we highlighted the lateromedial extent of several cortical regions, including Brodmann's areas 1, 3b, and 3a in SI as well as area 4, i.e. MI. For visualization purposes, the cortex of the left hemisphere of each subject was further delineated by white-matter segmentation, and inflated using an iterative morphing algorithm (BrainVoyager). Area borders were estimated on these inflated maps based on point-to-point correspondence with the anatomical volume.

12.3.1 Nonuniformity of phase representation

We found in most experiments that the entire region of interest was dominated by voxels having only a few of the possible phase delay values. In particular, the distributions of all D1 and D2 (but not D4) voxels that were correlated to the reference time course in each digit × direction stimulation condition were significantly nonuniform ($p < 0.01$, using Rayleigh's statistic (Fisher, 1993) for the circular distribution of $r^2 > 0.25$ voxels). Remarkably, this trend of nonuniform phase response was true not only in SI areas 3b and 1 but also in MI and area 3a in between (Fig. 12-2). These polar plots depict the distribution of all voxels significantly correlated to the reference time course, with color and degree equivalently representing the phase delay of maximal correlation. In cortex outside of areas 4, 3a, 3b, and 1, the populations of $r^2 > 0.25$ voxels in both of these experiments were not significantly tuned ($p > 0.05$). In a simulated data set in which the active region-of-interest voxels were substituted by random values taken from a uniform distribution of the possible phase delays (see Materials and Methods), the distributions were also uniform ($p > 0.05$). Hence the occurrence of significant nonuniformity within the D1 and D2 experiments exceeded the frequency either observed in cortex neighboring MI and SI, or expected on the basis of randomized simulations.

12.3.2 Fingertip predominance in digit-related activation

This significant tuning of the D1/D2 phase value distributions corresponded to the stimulation delay at which the surface of the fingertip was being stimulated. That is, during the time window when the tip was being stimulated, in most area × direction experiments a disproportionate number of voxels in these SI and MI areas were maximally correlated with the stimulation time course (Fig. 12-3, summed over subjects and over D1 and D2).

Moreover, while the mean directions in the two cumulative distributions were both within the phase delay range corresponding to fingertip stimulation, they were also significantly different ($p < 0.01$). The peak of the underlying response distribution appeared to have shifted to a more proximal phase lag in the base-to-tip experiments. This suggests in both stimulation conditions that there was an enhanced population BOLD response to the part of the fingertip initially contacted in each cycle of stimulation. The cutaneous response we observed was therefore not discretized into activation hotspots but did reflect fingertip sensitivity, in MI as well as in SI.

12.3.3 Sensorimotor distribution of fingertip-related activity

The digit-related activation in both motor and somatosensory cortices was not only extensive and biased towards fingertip representation, but was also markedly symmetric with respect to the central fundus. To better visualize the topographical layout of sensorimotor activation in our experiment, we displayed our functional data on inflated views of the pre- and postcentral gyri (Fig. 12-4). While the BOLD response may have been globally tuned to fingertip phase lags, at a more local level a mosaic of activation was visible on both sides of the central sulcus. Within each mosaic, a reversal of phase lag order could frequently be seen in overlapped activity between the tip-to-base and base-to-tip experiments. The symmetrical pattern of the activation was clear in inflated views in each of our subjects, but could also be reconstructed from the original pseudocoronal slice planes (not shown), and was thus not an artifact of volume coregistration or segmentation.

12.4 DISCUSSION

12.4.1 Non-somatotopic, digit-related activity is distributed throughout SI

Our experimental methodology has previously allowed us to describe discrete somatotopic maps of the digits as regions of connected voxels displaying a strong correlation to the pattern of stimulation across the digit surface, and a reversed pattern of peak correlations when the stimulation direction is reversed. While we have found evidence for such somatotopic patterning in areas 3b and 1 in response to digit stimulation (see Chapter 11), the digit maps are widely distributed outside of the "knob" region (Yousry et al., 1997) often associated with hand somatotopy in human studies.

Indeed, we demonstrate here that it is the overall pattern of functional activation in the region of the central sulcus—not limited to SI areas showing phase reversal—that is of most interest. While in identifying areas 1, 3b, 3a, and 4 we have had to

rely on macroanatomical landmarks rather than more precise cytoarchitectonic divisions (e.g. Young et al., 2003), the similarity in population-level BOLD waveforms across these independent areas (Fig. 12-2) suggests a common response. Our analysis allows for non-somatotopic but nevertheless significantly correlated activation, and in doing so has revealed widely distributed activation that appears weighted towards fingertip stimulation of the thumb and index finger (Fig. 12-3), in accordance with the high sensitivity of the distal finger pad. That we observe no consistent tuning of the D4 activation in the region of interest is compatible with the relative importance of D1 and D2 in precision grips and other behaviors (Napier, 1956).

12.4.2 Non-somatotopic, digit-related activity spans SI and MI

Furthermore, we have considered digit-related activation not only in Brodmann's areas 1 and 3b—sensory receiving centers for the afferents from Merkel's disks and Meissner corpuscles[1]—but also in area 3a (also in SI) and area 4 (MI). The latter two areas are conventionally thought to be involved principally in motor output and to receive kinesthetic rather than cutaneous afferents (Mountcastle, 1998). Studies of sensorimotor organization in human cortex have frequently neglected the possibility of somatosensory processing in motor cortex, and simultaneously of motor functions in somatosensory cortex—despite old but extensive neurophysiological and anatomical evidence for such sensorimotor overlap.

Indeed, the origin of corticospinal projections (which include direct corticomotoneuronal projections, allowing voluntary movement) is not limited to primary motor areas. In rhesus monkey (Russell & DeMeyer, 1961) and cat (Crevel & Verhaart, 1963b), about 40% of pyramidal tract fibers are derived from parietal areas including the postcentral gyrus, as opposed to the relatively thicker (Crevel & Verhaart, 1963a; Lassek, 1962) fibers from areas 6 and 4 precentrally. In humans this postcentral fraction is still significant but probably closer to 20% (Jane *et al.*, 1967), and pyramidal fiber projections from postcentral areas 3b, 1, 2, and 5, which in primates generally terminate in the spinal dorsal horn (Coulter & Jones, 1977), are relatively sparse (Schoen, 1964). Area 3a pyramidal fibers are also significant, although the relative contribution of area 3a and 4 fibers, projecting mainly to motoneurons of the intermediate zone of the spinal cord, is inconclusive (Coulter & Jones, 1977; Asanuma *et al.*, 1979; Jankowska *et al.*, 1976; Kuypers, 1960; Kuypers & Brinkman, 1970). Latent motor function within somatosensory areas presumably underlies the plasticity of these areas following motor impairment (McKenzie et al., 2003), and the widespread activation across MI and SI areas observed as normal subjects flex and extend their digits (Moore et al., 2000a).

Conversely, cutaneous inputs to MI have been observed in single-unit recordings from awake macaques (Murphy *et al.*, 1978) and squirrel monkeys (Strick & Preston, 1978c), and these cutaneous receptive fields have been shown to associate with intracortical microstimulation effects at the nearest joint. As in SI, these sensory inputs to area 4 appear to segregate in modality-specific maps, with neighboring representations of the hand and wrist differentially responsive to cutaneous and joint receptor input (Strick & Preston, 1978b,c). Straddling MI and SI, area 3a is thought to play a role in providing both motor cortex (Huffman and Krubitzer, 2001) and area 1 (Jones and Friedman, 1982) with kinesthetic input. But in addition to muscle spindle input to this area (Kaas et al., 1979), cutaneous responses can emerge with

training in owl monkeys (Recanzone et al., 1992) and in the marmoset monkey may physically parallel those in primary somatosensory cortex (Huffman and Krubitzer, 2001).

There is also evidence that the sensorimotor maps in areas 4 and 3a are physically parallel to those in primary somatosensory cortex. For instance, the area 3a marmoset simiunculus has disproportionately large hand, digit, and face representations (Krubitzer & Kaas, 1990), and a lateromedial representation of the digits like that in neighboring area 3b (Huffman & Krubitzer, 2001). Within humans, a somatosensory homunculus has not been defined precentrally, although the motor output of MI is known to be somatotopically organized as shown by electrical stimulation in epileptic patients prior to surgery (Penfield and Boldrey, 1937; Woolsey et al., 1979). Indeed, despite fMRI evidence that a vibrotactile stimulus can elicit precentral gyrus activity (Moore et al., 2000a; McGlone et al., 2002), few researchers have tried to localize cutaneous even kinesthetic function (Naito et al., 2002) to the frontal lobe in humans.

12.4.3 Non-somatotopic, digit-related activity is mirrored by the central sulcus

Qualitatively, this coactivation of SI and MI appears to have a symmetric character. There are no statistical tools known to us to quantify this multidimensional phase symmetry, particularly across two-dimensional slices where it can be observed to follow the central sulcus along its mediolateral, rostrocaudal, and inferior-superior contortions. The symmetry we observe across these areas exists despite less orderly somatotopic organization in precentral relative to postcentral areas in the primate. For instance, relative to the SI representations the area 4 and 3a maps in monkeys appear to be more fractured (Huffman and Krubitzer, 2001; Recanzone et al., 1992), perhaps consistent with the involvement of these areas in coordinated muscle recruitment. Less discrete representation may underlie investigators' inability to resolve precentral activation hotspots in response to human digit stimulation (McGlone et al., 2002; see Chapter 11) or indeed to digit motor output (Dechent and Frahm, 2003; Indovina and Sanes, 2001).

In contrast to the spiking-defined somatotopy found with electrophysiological mapping of motor cortex, fMRI, like optical imaging (Tommerdahl and Whitsel, 1996), appears to reflect a more distributed, dendritic-level processing (Logothetis et al., 2001) of both sensory signals and motor commands. Under this interpretation the relative absence of activity we observe within the fundus of the central sulcus (Fig. 12-4)—despite the interposition of this region between MI and SI—may reflect area 3a's integration of diffuse, converging inputs from areas 4, 3b and 1 (Huffman and Krubitzer, 2001). The observed fanning of activity away from the central sulcus may also reflect a diffusion of the hyperoxic response (Malonek and Grinvald, 1996) in the vasculature on either side of the Rolandic artery. However, Young et al. (2003) found that in the human left hemisphere, the resting regional blood flow in the area 3b classical "hand" area was correlated to blood flow in both anterior MI and area 3a.

The mosaical yet symmetrical nature of somatosensory inputs that we find in sensorimotor cortex is the first evidence known to us of activation symmetry across function-defined modalities. Within-modality mirror symmetry has recently been reported within tonotopic maps of primary auditory cortex (Formisano et al., 2003) and object representations within occipito-temporal cortex (Hasson et al., 2003). Within SI, researchers have found mirrored area 3b/1 responses to stimulation of the

third finger and palm (Blankenburg et al., 2003). Such somatotopic regionalization may reflect a natural tendency for functionally related neural networks to segregate with each other, under the two-dimensional constraint imposed by the cortical sheet (Kaas, 1987).

Figure 12-1 Sliding window paradigm. **a**) Pneumatic stimulation was delivered to D1, D2, or D4, via a restricted set of jets within a sliding window of stimulation. **b**) Voxels correlated to the reference waveform were assigned one of 12 colors, according to the discrete delay of maximal correlation within a stimulation cycle. Because the number of jet positions was only four (D1) or six (D2/D4), the color values included interpolated phase lags. **c**) The colors corresponded to locations on the digit surface, although the mapping from phase delay to location differed depending on stimulation direction (tip-to-base, black, or base-to-tip, grey).

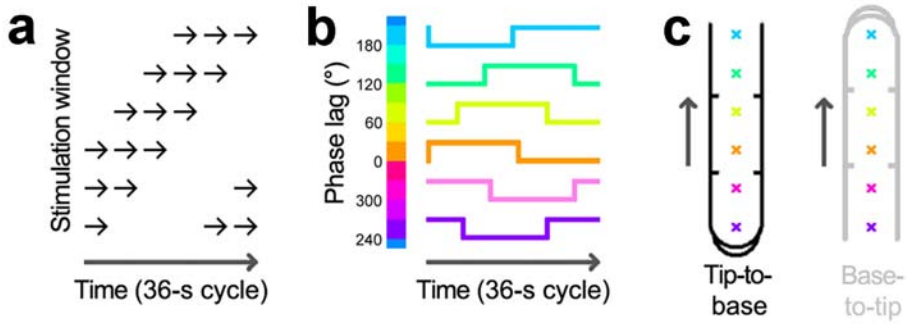

Figure 12-2 Phase value distributions are nonuniform across areas 4, 3a, 3b, and 1. Shown here for D2 (summed over subjects), the distributions are nonuniform for voxels in all areas of interest. Each histogram is a cumulative sum of voxels having a correlation to stimulus waveform of $r^2 > 0.18$, 0.25, or 0.33, these populations depicted by successively thicker outlines. Black or grey coloring of the distribution borders denotes stimulation direction as in Fig. 12-1. Mean direction is represented by a thick black or gray radial line; the radial axis represents voxel frequency (with range 0 to 400 voxels).

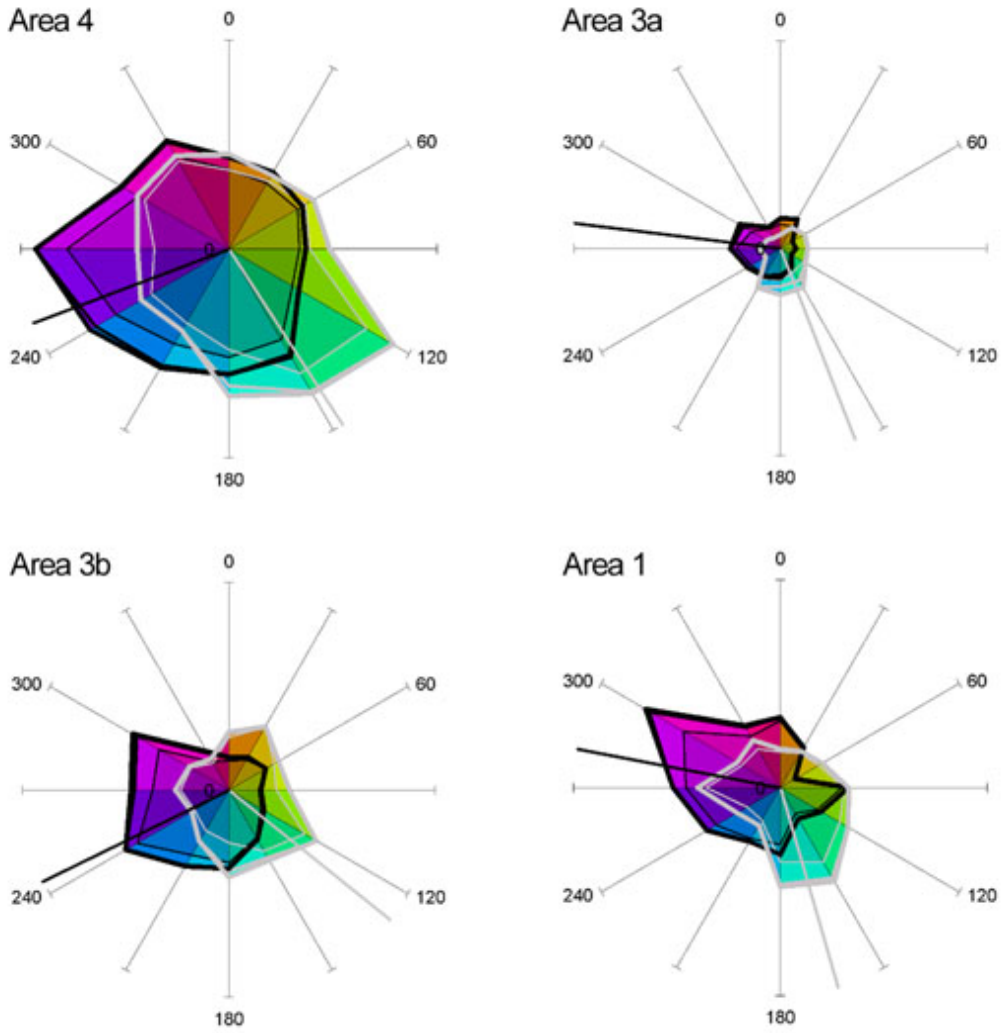

Figure 12-3 Responses are tuned to fingertip stimulation. Distributions of $r^2 > 0.33$ voxels are summed across digits (D1 and D2) and subjects, and are shown cumulatively for areas 4, 3a, 3b, and 1 along a linearized axis (cf. polar plots of Fig. 12-2) aligned with the digit surface. In the distributions for both tip-to-base (top; ordinate flipped) and base-to-tip (bottom) stimulation directions (shown as arrows next to schematic digit), there is a strong response coincident with stimulation across the fingertip jets. The peak of this response appears to shift in phase as a function of stimulation direction.

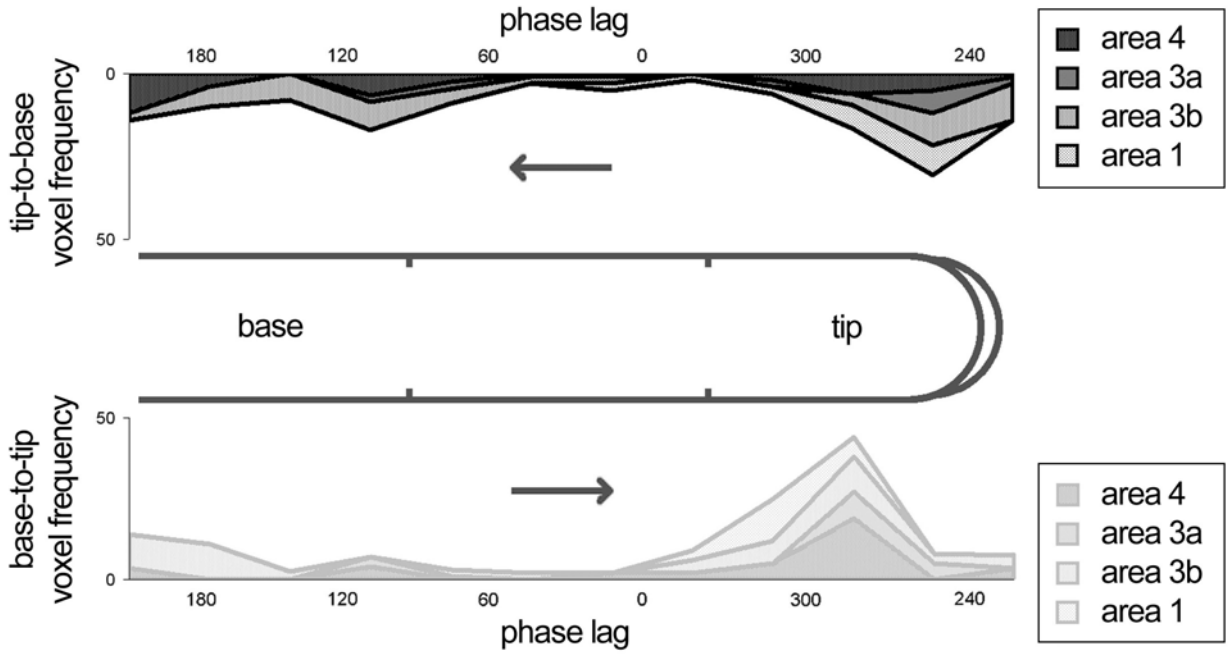

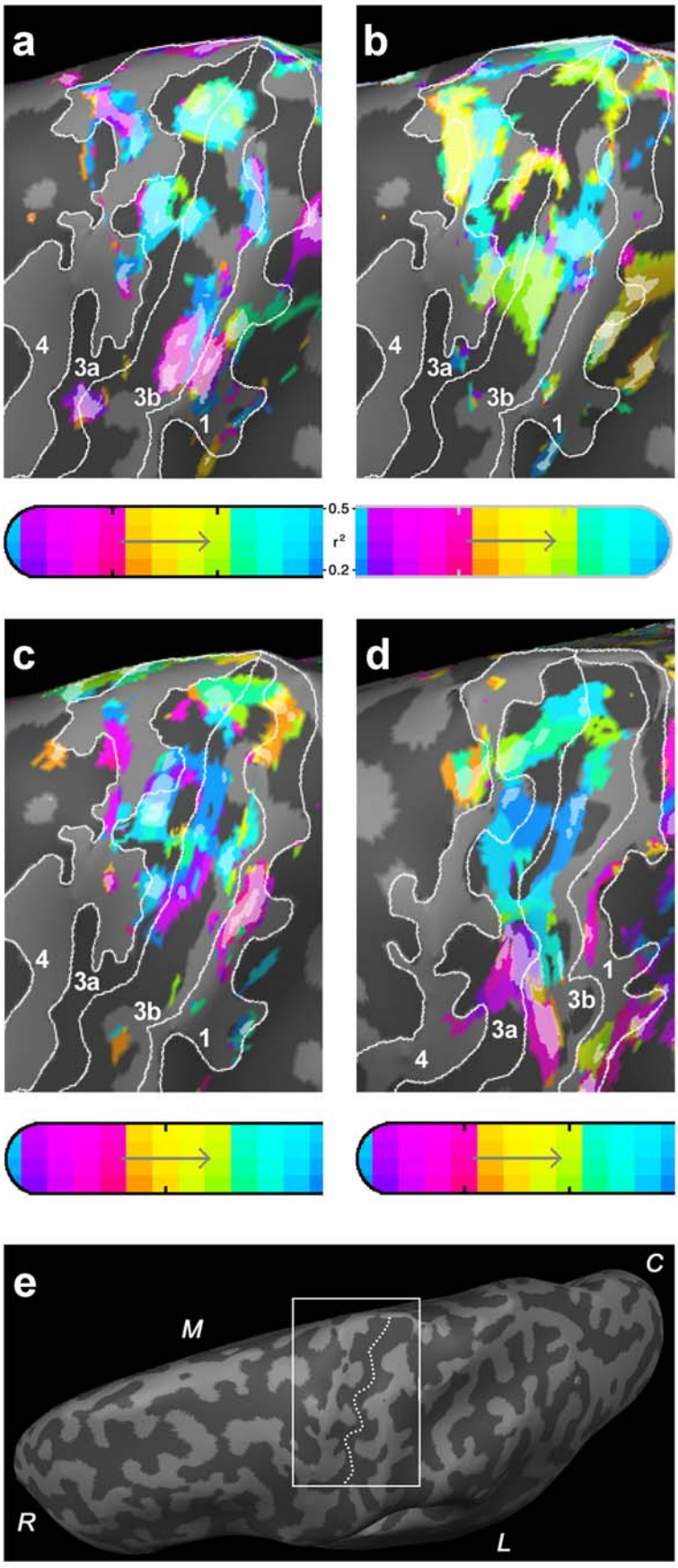

Figure 12-4 Mosaical responses are mirrored across the central sulcus. Sample anatomical images **a**) through **c**) (subject 1) and **d**) (subject 3) depict the region of interest on the inflated left hemisphere from a viewpoint above the central sulcus. The region is shown within an expanded view for subject 3 in **e**), with a dotted line indicating the approximate fundus of the central sulcus. White borders in panels a) through d) approximate areas 4, 3a, 3b, and 1; the "knob" area is in the bottom half of each image. Functional data are superimposed on panels a) through d) with color coding for phase lag and brightness indicating correlation, as schematized in the digits drawn below each image. Experiments with tip-to-base (a) and base-to-tip (b) D2 stimulation of subject 1 depict partially-overlapping voxel distributions weighted in each case towards fingertip representation. Panel c) shows the activation associated with tip-to-base D1 stimulation of the same subject, while panel d) depicts the response found for tip-to-base D2 stimulation in subject 3. Again, the activations have a complex mediolateral distribution but are relatively symmetric with respect to the central sulcus. R, rostral; C, caudal; M, medial; L, lateral.

CONCLUSIONS

In this thesis I have addressed three particular questions: What are the organizational principles subserving the control of the forelimb? How do such principles facilitate learning of new movements? And, how is this control implemented physiologically? Among these principles, I have focused on three independent candidates: 1) muscular coordination patterns, 2) motor cortical excitability, and 3) sensorimotor interactions.

In regards to muscular patterns, I recorded electromyographic activity from a large number of chronically-implanted muscles in the left or right forelimbs of awake macaques as they performed behaviors including grasping and reaching. I then reconstructed the recorded patterns of muscle activity underlying such behaviors as combinations of a small number of time-varying muscle primitives. Such synergies provided a description of the motor output that is compact, in that they only require specification of independent, scalar activation and timing coefficients for a group of muscles, rather than individual time courses of activation for each muscle. Such synergies were also able to explain a substantial amount of the variance present within the muscle data, and to be informative of some of the behavioral variables experienced by the monkey. In addition to their facilitation of motor control, such muscle primitives furthermore appeared able to simplify the process of motor learning, insofar as such learning could be described parsimoniously as a recombination of existing muscle synergies, both in amplitude and time. Three to four synergies appeared to be an appropriate number to capture the bulk of the EMG variance in these tasks. Additional evidence that this number was appropriate came from these synergies' relative dissimilarity, and their ability to span the spatial (and temporal) workspace relevant to the task. In general only limited spatiotemporal or functional similarities could be identified between synergies extracted from different monkeys performing the same task. I also found relatively little evidence for the hypothesis that these muscle synergies are non-malleable. For instance, the synergies did not appear to generalize well to behavioral conditions, unless these conditions differed parametrically (e.g. according to a range of object masses) rather than categorically (e.g. the task performed with the object). Also, at least one monkey exposed to a velocity-dependent force field appeared to develop progressively more dissimilar synergy structures particular for that task. When one monkey was exposed to a force field that scaled with the activity of an individual muscle sampled in real-time, it was frequently able to adapt to these forces; furthermore, this process may have been subserved by a relative attenuation of descending motor drive to this muscle, as suggested by suppression of the target muscle following cortical microstimulation in primary motor cortex (MI).

To study cortical excitability, I analyzed the results of MI microstimulation in the context of the reaching task in more detail. I confirmed recent reports that long-train microstimulation of MI is able to evoke complex and multijoint movements that typically drive the monkey's limb to a particular, invariant configuration, even when its arm is restricted to the planar workspace of a hand-held manipulandum. Extraction of functional, "musculokinematic synergies" from the monkey's performance on the reach task similarly suggested that the invariant dimensions underlying its motor control are heavily weighted towards kinematic variables including displacement. In further experiments I investigated the role of MI in enabling motor adaptation as well as in organizing movements. In one pilot study, I applied tissue plasminogen activator (tPA) to MI over several days while the monkey was practicing reaching movements under a relatively novel clockwise force field. The tPA did not appear to disrupt motor performance per se, given the monkey's stable level of kinematic error during null-field baseline trials each day. If anything, the tPA application may have been associated with a temporary decrease in the monkey's ability to perform under force field condition—or perhaps to recall its recent internalization of the clockwise field. In a manipulation

that in some respects mirrored the tPA application, in a human study I applied 1-Hz repetitive transcranial magnetic stimulation (rTMS) to MI of human subjects just prior to their acquisition of the clockwise force field. While the rTMS, like tPA, did not appear to disrupt basal performance, in the human subjects it also spared performance on the clockwise force field. Only at retest a day later did the rTMS subjects perform differently than controls, the latter having developed off-line improvements in performance during the intervening time. Although tPA and rTMS are thought to have opposite effects on cortical excitability and cellular learning mechanisms, both appeared to have disrupted the subjects' ability to retain, improve, or recall recent motor adaptations.

Finally, I conducted several additional human studies to look at the importance of sensorimotor interaction in motor learning and control. In one study, I investigated the interaction of force field adaptation and sequence learning, two modes of motor learning that have previously been investigated as wholly independent phenomena. By modifying the reach task to allow for implicit sequencing of the targets, I showed that simultaneous acquisition of a force field and a sequence does not impair performance on either, as measured by kinematic error and reaction time. Instead, subjects given both conditions appeared to have become attuned to their enhanced kinematic errors and thereby to have developed a chunking strategy to organize their movements. In a second study, I showed that motor consolidation—a gradual resistance of recent learning to retrograde interference from a second motor program—is critically dependent on the manner of learning. In particular, clockwise force field learning in human subjects appeared to be more stable if subjects had been given random null-field trials interspersed in their force trials, rather than monotonous performance with the forces. Catch trials may both have made motor learning more effortful, and allowed more effective cue disambiguation of the fields. Lastly, I investigated in more detail the importance of sensory cueing in motor performance that was hinted at by the previous studies. Using a passive, cutaneous stimulation procedure, I performed functional magnetic resonance imaging (fMRI) of human subjects in order to localize cortical activation associated with finger stimulation. I initially treated MI as a control area, and confirmed that relatively somatotopic representations of the finger are restricted to primary somatosensory cortex (SI) However, when I examined non-somatotopic patterning of the activity, I found that it was widely distributed throughout sensorimotor cortex, while still biased according to receptor concentration on the fingers. This distributed sensory input was consistent with the correlation of fMRI with synaptic inputs, and anatomical evidence for a continuum of input and output functions in MI and SI.

REFERENCES

Abeele S, Bock O (2003) Transfer of sensorimotor adaptation between different movement categories. Exp Brain Res 148:128–132.

Adamovich SV, Levin MF, Feldman AG (1997) Central modifications of reflex parameters may underlie the fastest arm movements. J Neurophysiol 77:1460–1469.

Ajemian R, Bullock D, Grossberg S (2001) A model of movement coordinates in the motor cortex: posture-dependent changes in the gain and direction of single cell tuning curves. Cereb Cortex 11:1124–1135.

Alexander GE, Crutcher MD (1990) Preparation for movement: Neural representations of intended direction in three motor areas of the monkey. J Neurophysiol 64:133–150.

Allison T, McCarthy G, Wood CC, Darcey TM, Spencer DD, Williamson PD (1989) Human cortical potentials evoked b y stimulation of the median nerve. I. Cytoarchitectonic areas generating short-latency activity. J Neurophysiol 62:694–710.

Amunts K, Malikovic A, Mohlberg H, Schormann T, Zilles K (2000) Brodmann's areas 17 and 18 brought into stereotaxic space—where and how variable? NeuroImage 11:66–84.

Angel RW, Eppler W, Iannone A (1965) Silent period produced by unloading of muscle during voluntary contraction. J Physiol 180:864–870.

Asanuma H, Rosén I (1972) Topographical organization of cortical efferent zones projecting to distal forelimb muscles in the monkey. Exp Brain Res 14:243–256.

Asanuma H, Zarzecki P, Jankowska E, Hongo T, Marcus S (1979) Projections of individual pyramidal tract neurons to lumbar motor nuclei of the monkey. Exp Brain Res 34:73–89.

Asatryan DG, Feldman AG (1965) Functional tuning of the nervous system with control of movement sor maintenance of a steady posture: I. Mechanographic analysis of the work of the joint on execution of a postural tasks. Biophysics 10:925–935.

Ashe J, Georgopoulos AP (1994) Movement parameters and neural activity in motor cortex and area 5. Cereb Cortex 4:590–600.

Baker SN, Olivier E, Lemon RN (1998) An investigation of the intrinsic circuitry of the motor cortex of the monkey using intra-cortical microstimulation. Exp Brain Res 123:397–411.

Balasubramanian M, Schwartz EL (2002) The isomap algorithm and topological stability. Science 295:7.

Bandettini PA (2001) Selection of the optimal pulse sequence for functional MRI. In: Functional MRI: An Introduction to Methods (Jezzard P, Matthews PM, Smith SM, eds), pp123–143. New York, NY: Oxford UP.

Baraduc P, Lang N, Rothwell JC, Wolpert DM (2004) Consolidation of dynamic motor learning is not disrupted by rTMS of primary motor cortex. Curr Biol 14:252–256.

Baranes D, Lederfein D, Huang YY, Chen M, Bailey CH, Kandel ER (1998) Tissue plasminogen activator contributes to the late phase of LTP and to synaptic growth in the hippocampal mossy fiber pathway. Neuron 21:813–825.

Bays PM, Flanagan JR, Wolpert DM (2005) Interference between velocity-dependent and position-dependent force-fields indicates that tasks depending on different kinematic parameters compete for motor working memory. Exp Brain Res 163:400–405.

Bell AJ, Sejnowski TJ (1995) An information-maximization approach to blind separation and blind deconvolution. Neural Compu 7:1129–1159.

Bennett KMB, Lemon RN (1994) The influence of single monkey corticomotoneuronal cells at different levels of activity in target muscles. J Physiol (Lond) 477:291–307.

Berardelli A, Inghilleri M, Rothwell JC, Romeo S, Curra A, Gilio F, Modugno N, Manfredi M (1998) Facilitation of muscle evoked responses after repetitive cortical stimulation in man. Exp Brain Res 122:79–84.

Berniker M (2005) Linearity, motor primitives and low-dimensionality in the spinal organization of motor behavior. Ph.D. thesis (in press). Cambridge, MA: MIT Press.
Bernstein N (1967) The coordination and regulation of movements. New York, NY: Pergamon Press.
Bestmann S, Baudewig J, Siebner HR, Rothwell JC, Frahm J (2004) Functional MRI of the immediate impact of transcranial magnetic stimulation on cortical and subcortical motor circuits. Eur J Neurosci 19:1950–1962.
Bizzi E, Giszter SF, Loeb E, Mussa-Ivaldi FA, Saltiel P (1995) Modular organization of motor behavior in the frog's spinal cord. Trends Neurosci 18:442–446.
Bizzi E, Hogan N, Mussa-Ivaldi FA, Giszter S (1992) Does the nervous system use equilibrium-point control to guide single and multiple joint movements? Behav Brain Sci 15:603–613.
Bizzi E, Mussa-Ivaldi FA, Giszter S (1991) Computations underlying the execution of movement: a biological perspective. Science 253:287–291.
Blankenburg F, Ruben J, Meyer R, Schwiemann J, Villringer A (2003) Evidence for a rostral-to-caudal somatotopic organization in human primary somatosensory cortex with mirror-reversal in areas 3b and 1. Cereb Cortex 13:987–993.
Bock O, Abeele S, Eversheim U (2003) Human adaptation to rotated vision: interplay of a continuous and a discrete process. Exp Brain Res 152:528–532.
Bock O, Schneider S, Bloomberg J (2001) Conditions for interference versus facilitation during sequential sensorimotor adaptation. Exp Brain Res 138:359–365.
Bolanowski SJ, Gescheider GA, Verrillo RT, Checkosky CM (1988) Four channels mediate the mechanical aspects of touch. J Acoust Soc Am 84:1680–1694.
Brashers-Krug T, Shadmehr R, Bizzi E (1996) Consolidation in human motor memory. Nature 382:252–255.
Brochier T, Spinks RL, Umilta MA, Lemon RN (2004) Patterns of muscle activity underlying object-specific grasp by the macaque monkey. J Neurophys 92:1770–1782.
Bruce CJ, Goldberg ME, Bushnell MC, Stanton GB (1985) Primate frontal eye fields. II. Physiological and anatomical correlates of electrically evoked eye movements. J Neurophysiol 54:714–734.
Burdet E, Osu R, Franklin DW, Milner TE, Kawato M (2001) The central nervous system stabilizes unstable dynamics by learning optimal impedance. Nature 414:446–449.
Caithness G, Osu R, Bays P, Chase H, Klassen J, Kawato M, Wolpert DM, Flanagan JR (2004) Failure to consolidate the consolidation theory of learning for sensorimotor adaptation tasks. J Neurosci 24:8662–8671.
Cajochen C, Knoblauch V, Wirz-Justice A, Krauchi K, Graw P, Wallach D (2004) Circadian modulation of sequence learning under high and low sleep pressure conditions. Behav Brain Res 151:167–176.
Chen R, Classen J, Gerloff C, Celnik P, Wassermann EM, Hallett M, Cohen LG (1997) Depression of motor cortex excitability by low-frequency transcranial magnetic stimulation. Neurology 48:1398–1403.
Cheney PD, Fetz EE (1985) Comparable patterns of muscle facilitation evoked by individual corticomotoneuronal (CM) cells and by single intracortical microstimuli in primates: Evidence for functional groups of CM cells. J Neurophys 53:786–804.
Cheney PD, Fetz EE, Palmer SS (1985) Patterns of facilitation and suppression of antagonist forelimb muscles from motor cortex sites in the awake monkey. J Neurophys 53:805–820.
Cheng EJ, Schott SH (2000) Morphometry of *Macaca mulatta* forelimb. I. Shoulder and elbow muscles and segment inertial parameters. J Morphol 245:206–224.
Cheung VC, d'Avella A, Tresch MC, Bizzi E (2005) Central and sensory contributions to the activation and organization of muscle synergies during natural motor behaviors. J Neurosci

25:6419-6434.
Chouinard PA, Van Der Werf YD, Leonard G, Paus T (2003) Modulating neural networks with transcranial magnetic stimulation applied over the dorsal premotor and primary motor cortices. J Neurophysiol 90:1071–1083.
Clark SL, Ward JW (1937) Responses elicitable from electrical stimulation of the cortex cerebri of cats in chronic experiments through implanted electrodes. Arch Neurol Psychiat (Chicago) 38:927–943.
Clower DM, Hoffman JM, Votaw JR, Faber TL, Woods RP, Alexander GE (1996) Role of posterior parietal cortex in the recalibration of visually guided reaching. Nature 383:618–621.
Colebatch JG, Sayer RJ, Porter R, White OB (1990) Responses of monkey precentral neurons to passive movements and phasic muscle stretch: Relevance to man. Electroencephalogr Clin Neurophysiol 75:44–55.
Corballis MC (1989) Laterality and human evolution. Psychol Rev 96:492–505.
Coulter JD, Jones EG (1977) Differential distribution of corticospinal projections from individual cytoarchitectonic fields in the monkey. Brain Res 129:335–340.
Cox TF, Cox MAA (1994). Multidimensional scaling: Monographs on statistics and applied probability (2nd ed). London: Chapman & Hall.
Crevel H, Verhaart WJC (1963a) The "exact origin" of the pyramidal tract. A quantitative study in the cat. J Anat 97:495–515.
Crevel H, Verhaart WJC (1963b) The rate of secondary degeneration in the central nervous system. 1. Pyramidal tract of the cat. J Anat 97:429–464.
Criscimagna-Hemminger SE, Donchin O, Gazzaniga MS, Shadmehr R (2003) Learned dynamics of reaching movements generalize from dominant to nondominant arm. J Neurophysiol 1:168–176.
Crutcher MD, Alexander GE (1990) Movement-related neuronal activity selectively coding either direction of muscle pattern in three motor areas of the monkey. J Neurophysiol 64:151–163.
Cutkosky MR (1989) On grasp choice, grasp models and the design of hands for manufacturing tasks. IEEE T Robotic Autom 5:269–279.
Cutkosky MR, Howe RD (1990) Human grasp choice and robotic grasp analysis. In: Dextrous robot hands (Venkataraman ST, Iberall T, eds), pp5–31. New York, NY: Springer-Verlag.
d'Avella A, Bizzi E (2005) Shared and specific muscle synergies in natural motor behaviors. Proc Natl Acad Sci U S A 102:3076–3081.
d'Avella A, Lacquaniti F (2004) Spatiotemporal characteristics of the muscle patterns for reaching explained by synergy combinations. Society for the Neural Control of Movement poster.
d'Avella A, Saltiel P, Bizzi E (2003) Combinations of muscle synergies in the construction of a natural motor behavior. Nat Neurosci 6930:300–308.
d'Avella A, Tresch MC (2001) Modularity in the motor system: Decomposition of muscle patterns as combinations of time-varying synergies. In: Advances in Neural Information Processing Systems 14 (Dietterich TG, Becker S, Ghahramani Z, eds). Cambridge, MA: MIT Press.
Darian-Smith I, Goodwin AW, Sugitani M, Heywood J (1984) The tangible features of textured surfaces: Their representation in the monkey's somatosensory cortex. In: Dynamic Aspects of Neocortical Function (Edelman GM, Cowan WM, Gall WE, eds), pp475–500. New York, NY: Wiley.
deCharms RC, Christoff K, Glover GH, Pauly JM, Whitfield S, Gabrieli JD (2004) Learned regulation of spatially localized brain activation using real-time fMRI. Neuroimage 21(1):436–43.
Dechent P, Frahm J (2003) Functional somatotopy of finger representations in human primary motor cortex. Hum Brain Mapp 18:272–283.
Della-Maggiore V, Malfait N, Ostry DJ, Paus T (2004) Stimulation of the posterior parietal cortex

interferes with arm trajectory adjustments during the learning of new dynamics. J Neurosci 24:9971–9976.
Desmedt JE, Godaux E (1977) Ballistic contractions in man: characteristic recruitment pattern of single motor units of the tibialis anterior muscle in man. J Physiol 264:673–693.
Deuel RK, Dunlop NL (1980) Hand preference in the rhesus monkey: Implications for the study of cerebral dominance. Arch Neurol 37:217–221.
Deuel RK, Schaffer SP (1987) Patterns of hand preference in monkeys. Behav Brain Sci 10:270–271.
Dhall U, Singh I (1977) Anatomical evidence of one-sided forelimb dominance in the rhesus monkey. Anat Anzeiger 141:420–425.
Donchin O, Sawaki L, Madupu G, Cohen LG, Shadmehr R (2002) Mechanisms influencing acquisition and recall of motor memories. J Neurophysiol 88:2114–2123.
Donchin O, Shadmehr R (2004) Change of desired trajectory caused by training in a novel motor task. P IEEE EMBS:4495–4498.
Donoghue JP, Leibovic S, Sanes JN (1992) Organization of the forelimb area in squirrel monkey motor cortex: Representation of digit, wrist, and elbow muscles. Exp Brain Res 89:1–19.
Doyon J, Penhune V, Ungerleider LG (2003) Distinct contribution of the cortico-striatal and cortico-cerebellar systems to motor skill learning. Neuropsychologia 41:252–262.
Engel SA, Rumelhart DE, Wandell BA, Lee AT, Glover GH, Chichilniski EJ (1994): FMRI of human visual cortex. Nature 369:525.
Evarts E.V. (1969) Activity of pyramidal tract neurons during postural fixation. J Neurophysiol 32:375–385.
Evarts EV (1968) Relation of pyramidal tract activity to force exerted during voluntary movement. J Neurophysiol 31:14–27.
Exner C, Koschack J, Irle E (2002) The differential role of premotor frontal cortex and basal ganglia in motor sequence learning: evidence from focal basal ganglia lesions. Learn Mem 9:376–386.
Eysenk H (1965) A three-factor theory of reminiscence. Br J Psychol 56:163–181.
Falk D, Pyne L, Helmkamp RC, DeRousseau CJ (1988) Directional asymmetry in the forelimb of Macaca mulatta. Am J Phys Anthropol 77:1–6.
Farah MJ (1998) Why does the somatosensory homunculus have hands next to face and feet next to genitals? A hypothesis. Neural Comput 10:1983–1985.
Fayé IC (1983) An impedance controlled manipulandum for human movement studies. M.S. thesis. Cambridge, MA: MIT Press.
Feldman AG, Latash ML (2005) Testing hypotheses and the advancement of science: recent attempts to falsify the equilibrium point hypothesis. Exp Brain Res 161:91–103.
Fetz EE (1969) Operant conditioning of cortical unit activity. Science 163:955–958.
Fetz EE, Finocchio DV (1971) Operant conditioning of specific patterns of neural and muscular activity. Science 174:431–435.
Fischer S, Hallschmid M, Elsner AL, Born J (2002) Sleep forms memory for finger skills. Proc Natl Acad Sci U S A 99:11987–11991.
Fischl B, Sereno I, Dale AM (1999) Cortical surface-based analysis. II: Inflation, flattening, and a surface-based coordinate system. NeuroImage 9:195–207.
Fisher NI (1993) Statistical analysis of circular data. Cambridge, UK: Cambridge UP.
Flanagan JR, Beltzner MA (2000) Independence of perceptual and sensorimotor predictions in the size-weight illusion. Nat Neurosci 3:737–741.
Formisano E, Kim DS, Di Salle F, van de Moortele PF, Ugurbil K, Goebel R (2003) Mirror-symmetric tonotopic maps in human primary auditory cortex. Neuron 40:859–869.
Fox P, Ingham R, George MS, Mayberg H, Ingham J, Roby J, Martin C, Jerabek P (1997) Imaging human intra-cerebral connectivity by PET during TMS. NeuroReport 8 2787–2791.

Francis ST, Kelly EF, Bowtell R, Dunseath WJ, Folger SE, McGlone F (2000) fMRI of the responses to vibratory stimulation of digit tips. NeuroImage 11:188–202.
Freedman EG, Stanford TR, Sparks DL (1996) Combined eye-head gaze shifts produced by electrical stimulation of the superior colliculus in rhesus monkeys. J Neurophysiol 76:927–952.
Frensch PA, Miner CS (1994) Effects of presentation rate and individual differences in short-term memory capacity on an indirect measure of serial learning. Mem Cognit 22:95–110.
Friedman GC, Seeds NW (1994) Tissue plasminogen activator expression in the embryonic nervous system. Brain Res Dev Brain Res 81:41–49.
Gandolfo F, Li C-SR, Benda BJ, Padoa Schioppa C, Bizzi E (2000) Cortical correlates of learning in monkeys adapting to a new dynamical environment. Proc Natl Acad Sci U S A 97:2259–2263.
Gangitano M, Valero-Cabre A, Tormos JM, Mottaghy FM, Romero JR, Pascual-Leone A (2002) Modulation of input-output curves by low and high frequency repetitive transcranial magnetic stimulation of the motor cortex. Clin Neurophysiol 113:1249–1257.
Gelnar PA, Krauss BR, Szeverenyi NM, Apkarian AV (1998) Fingertip representation in the human somatosensory cortex: An fMRI study. NeuroImage 7:261–283.
Georgopoulos AP, Kalaska JF, Caminiti R (1985) Relations between two-dimensional arm movements and single-cell discharge in motor cortex and area 5: Movement direction versus movement end point. Exp Brain Res, Suppl 10:175–183.
Georgopoulos AP, Kalaska JF, Caminiti R, Massey JT (1982) On the relations between the direction of two-dimensional arm movements and cell discharge in primate motor cortex. J Neurosci 2:1527–1537.
Georgopoulos AP, Schwartz AB, Kettner RE (1986) Neuronal population coding of movement direction. Science 233:1416–1419.
Geyer S, Schleicher A, Zilles K (1999) Areas 3a, 3b, and 1 of human primary somatosensory cortex. 1. Microstructural organization and interindividual variability. NeuroImage 10:63–83.
Geyer S, Schormann T, Mohlberg H, Zilles K (2000) Areas 3a, 3b, and 1 of human primary somatosensory cortex. NeuroImage 11:684–696.
Ghilardi M, Ghez C, Dhawan V, Moeller J, Mentis M, Nakamura T, Antonini A, Eidelberg D (2000) Patterns of regional brain activation associated with different forms of motor learning. Brain Res 871:127–145.
Gibson JJ (1979) The ecological approach to visual perception. Boston, MA: Houghton Mifflin.
Giszter SF, Mussa-Ivaldi FA, Bizzi E (1993) Convergent force fields organized in the frog's spinal cord. J Neurosci 13:467–491.
Glover GH (1999) Deconvolution of impulse response in event-related BOLD fMRI. NeuroImage 9:416–429.
Goedert KM, Willingham DB (2002) Patterns of interference in sequence learning and prism adaptation inconsistent with the consolidation hypothesis. Learn Memory 9:279–292.
Gottlieb GL, Corcos DM, Agarwal GC (1989) Organizing principles for single-joint movements. I. Speed-insensitive strategy. J Neurophysiol 62:343–357.
Gottlieb JP, Bruce CJ, MacAvoy MG (1993) Smooth eye movements elicited by microstimulation in the primate frontal eye field. J Neurophysiol 69:786–799.
Graziano MS, Aflalo TN, Cooke DF (2005) Arm movements evoked by electrical stimulation in the motor cortex of monkeys. J Neurophysiol 94:4209–4223.
Graziano MS, Cooke DF, Taylor CS, Moore T (2004a) Distribution of hand location in monkeys during spontaneous behavior. Exp Brain Res 155:30–36.
Graziano MS, Patel KT, Taylor CS (2004b) Mapping from motor cortex to biceps and triceps altered by elbow angle. J Neurophysiol 92:395–407.
Graziano MS, Taylor CS, Moore T (2002a) Complex movements evoked by microstimulation of precentral cortex. Neuron. 34:841–851.

Graziano MS, Taylor CS, Moore T, Cooke DF (2002b) The cortical control of movement revisited. Neuron 36:349–362.
Hart CB, Giszter SF (2004) Modular premotor drives and unit bursts as primitives for frog motor behaviors. J Neurosci 24:5269–5282.
Hasson U, Harel M, Levy I, Malach R (2003) Large-scale mirror symmetry organization of human occipito-temporal object areas. Neuron 37:1027–1041.
Hatsopoulos NG, Ojakangas CL, Paninski L, Donoghue JP (1998) Information about movement direction obtained from synchronous activity of motor cortical neurons. Proc Natl Acad Sci USA 95:15706–15711.
Henneman E, Somjen G, Carpenter DO (1965) Functional significance of cell size in spinal motoneurons. J Neurophysiol 28:560–580.
Heuer H, Spijkers W, Kiesswetter E, Schmidtke V (1998) Effects of sleep loss, time of day, and extended mental work on implicit and explicit learning of sequences. J Exp Psychol Appl 4:139–162.
Hikosaka O, Nakahara H, Rand MK, Sakai K, Lu X, Nakamura K, Miyachi S, Doya K (1999) Parallel neural networks for learning sequential procedures. Trends Neurosci 22:464–471.
Hogan N, Bizzi E, Mussa-Ivaldi FA, Flash T (1987) Controlling multijoint motor behavior. Exerc Sport Sci Rev 15:153–190.
Holdefer RN, Miller LE (2002) Primary motor cortical neurons encode functional muscle synergies. Exp Brain Res 146:233–243.
Hopkins WD, Washburn DA, Rumbaugh DM (1989) Note on hand use in the manipulation of joysticks by rhesus monkeys (*Macaca mulatta*). And chimpanzees (Pan troglodytes). J Comp Psychol 193:91–94.
Howell AB, Straus WL Jr (1971) The muscular system. In: The anatomy of the rhesus monkey (*Macaca mulatta*) (Tharman CG, Straus WL Jr, eds), pp89–175. New York, NY: Hafner.
Huffman KJ, Krubitzer L (2001) Area 3a: Topographic organization and cortical connections in marmoset monkeys. Cereb Cortex 11:849–867.
Hyvärinen A, Oja E (2000) Independent component analysis: algorithms and applications. Neural Networks 13:411–430.
Hyvärinin J, Poranen A (1978) Receptive field integration and submodality convergence in the hand area of the post-central gyrus of the alert monkey. J Physiol 283:539–556.
Iberall T, MacKenzie CL (1990) Opposition space and human prehension. In: Dextrous robot hands (Venkataraman ST, Iberall T, eds), pp32–54. New York, NY: Springer-Verlag.
Imamizu H, Miyauchi S, Tamada T, Sasaki Y, Takino R, Putz B, Yoshioka T, Kawato M (2000) Human cerebellar activity reflecting an acquired internal model of a new tool. Nature 403:192–195.
Indovina I, Sanes JN (2001) On somatotopic representation centers for finger movements in human primary motor cortex and supplementary motor area. NeuroImage 13:1027–1034.
Inhoff AW, Diener HC, Rafal RD, Ivry R (1989) The role of cerebellar structures in the execution of serial movements. Brain 112:565–581.
Inoue K, Kawashima R, Satoh K, Kinomura S, Goto R, Sugiura M, Ito M, Fukuda H (1997) Activity in the parietal area during visuomotor learning with optical rotation. Neuroreport 8:3979–3983.
Inoue K, Kawashima R, Satoh K, Kinomura S, Sugiura M, Goto R, Ito M, Fukuda H (2000) A PET study of visuomotor learning under optical rotation. Neuroimage 11:505–516.
Iwamura Y, Tanaka M, Hikosaka O (1980) Overlapping representation of fingers in the somatosensory cortex (area 2) of the conscious monkey. Brain Res 187:516–520.
Iwamura Y, Tanaka M, Sakamoto M, Hikosaka O (1983) Functional subdivisions representing different finger regions in area 3 of the first somatosensory cortex of the conscious monkey. Exp

Brain Res 51:315–326.
Iwamura Y, Tanaka M, Sakamoto M, Hikosaka O (1985) Comparison of the hand and finger representation in areas 3, 1, and 2 of the monkey somatosensory cortex. In: Development, Organization, and Processing in Somatosensory Pathways (Rowe MJ, Willis WD, eds), pp239–245. New York, NY: Alan R. Liss.
Jane JA, Yashon D, DeMeyer W, Bucy PC (1967) The contribution of the precentral gyrus to the pyramidal tract of man. J Neurosurg 26:244–248.
Jankowska E, Padel Y, Tanaka R (1975) The mode of activation of pyramidal tract cells by intracortical stimuli. J Physiol 249:617–636.
Jankowska E, Padel Y, Tanaka R (1976) Disynaptic inhibition of spinal motoneurons from the motor cortex in the monkey. J Physiol (Lond) 258:467–487.
Jenkins IH, Brooks DJ, Nixon PD, Frackowiak RS, Passingham RE (1994) Motor sequence learning: A study with positron emission tomography. J Neurosci 14:3775–3790.
Johansson RS, Vallbo Å (1979) Tactile sensibility in the human hand: Relative and absolute densities of four types of mechanoreceptive units in glabrous skin. J Physiol 286:283–300.
Johnson KO, Phillips JR (1981) Tactile spatial resolution. I. Two-point discrimination, gap detection, grating recognition. J Neurophysiol 46:1177–1191.
Johnson RA, Wichern DW (2002) Applied multivariate statistical analysis. Upper Saddle River, NJ: Prentice Hall.
Johnston JA, Winges SA, Santello M (2005) Periodic modulation of motor unit activity in extrinsic hand muscles during multidigit grasping. J Neurophysiol 94:206–218.
Johnston R, Lee K (1976) Myofeedback: a new method of teaching breathing exercises in emphysematous patients. Phys Ther 56:826–831.
Jones EG, Friedman DP (1982) Projection pattern of functional components of thalamic ventrobasal complex on monkey somatosensory cortex. J Neurophysiol 48:521–544.
Kaas JH (1987) The organization of neocortex in mammals: Implications for a theory of brain function. Annu Rev Psychol 38:124–151.
Kaas JH, Nelson RJ, Sur M, Lin CS, Merzenich MM (1979) Multiple representations of the body within the primary somatosensory cortex of primates. Science 204:521–523.
Kaas JH, Nelson RJ, Sur M, Merzenich MM (1981) Organization of somatosensory cortex in primates. In: The Organization of the Cerebral Cortex (Schmitt FO, Worden FG, Adelman G, Dennis SG, eds), pp237–261. Cambridge, MA: MIT Press.
Kaas JH, Pons TP (1988) The somatosensory system of primates. Comp Primate Biol 4:421–468.
Kakei S, Hoffman DS, Strick PL (1999) Muscle and movement representations in the primary motor cortex. Science 285:2136–2139.
Kakei S, Hoffman DS, Strick PL (2001) Direction of action is represented in the ventral premotor cortex. Nat Neurosci 4:1020–1025.
Kalaska JF, Cohen DAD, Hyde ML, Prud'homme M (1989) A comparison of movement direction-related versus load direction-related activity in primate motor cortex, using a two-dimensional reaching task. J Neurosci 9:2080–2102.
Kargo WJ, Giszter SF (2000) Rapid correction of aimed movements by summation of force-field primitives. J Neurosci 20:409–426.
Kargo WJ, Nitz DA (2003) Early skill learning is expressed through selection and tuning of cortically represented muscle synergies. J Neuroscience 23:1125–1269.
Karni A, Meyer G, Jezzard P, Adams MM, Turner R, Ungerleider LG (1995) Functional MRI evidence for adult motor cortex plasticity during motor skill learning. Nature 377:155–158.
Karni A, Meyer G, Rey-Hipolito C, Jezzard P, Adams MM, Turner R, Ungerleider LG (1998) The acquisition of skilled motor performance: fast and slow experience-driven changes in primary motor cortex. Proc Natl Acad Sci U S A 95:861–868.

Karniel A, Mussa-Ivaldi FA (2002) Does the motor control system use multiple models and context switching to cope with a variable environment? Exp Brain Res 143:520–524.
Karniel A, Mussa-Ivaldi FA (2003) Sequence, time, or state representation: how does the motor control system adapt to variable environments? Biol Cybern 89:10–21.
Kassardjian CD, Tan YF, Chung JY, Heskin R, Peterson MJ, Broussard DM (2005) The site of a motor memory shifts with consolidation. J Neurosci 25:7979–7985.
King JE, Landau VI, Scott AG, Berning AL (1987) Hand preference during capture of live fish by squirrel monkeys. Int J Primatol 8:540.
Klatzky RL, Lederman SJ, Pellegrino JW, Doherty S, McCloskey BP (1990) Procedures for haptic object exploration vs. manipulation. In: Vision and action: The control of grasping (Goodale MA, ed), pp.110–127. Norwood, NJ: Ablex.
Kojima Y, Iwamoto Y, Yoshida K (2004) Memory of learning facilitates saccadic adaptation in the monkey. J Neurosci 25:7531–7539.
Korman M, Raz, N, Flash, T, Karni, A (2003) Multiple shifts in the representation of a motor sequence during the acquisition of skilled performance. Proc Natl Acad Sci USA 100:12492–12497.
Krakauer JW, Ghez C, Ghilardi MF (2005) Adaptation to visuomotor transformations: Consolidation, interference, and forgetting. J Neurosci 25:473–478.
Krakauer JW, Ghilardi MF, Ghez C (1999) Independent learning of internal models for kinematic and dynamic control of reaching. Nat Neurosci 2:1026–1031.
Krubitzer LA, Kaas JH (1990) The organization and connections of somatosensory cortex in marmosets. J Neurosci 10:952–974.
Kuhl P (1988) On handedness in primate and human infants. Behav Brain Sci 11:727–729.
Künzle H (1978) Cortico-cortical efferents of primary motor and somatosensory regions of the cerebral cortex in *Macaca fascicularis*. Neuroscience 3, 25–39.
Kurth R, Villringer K, Mackert BM, Schwiemann J, Braun J, Curio G, Villringer A, Wolf KJ (1998) FMRI assessment of somatotopy in human Brodmann area 3b by electrical finger stimulation. NeuroReport 9:207–212.
Kuypers HGJM (1960) Central cortical projections to motor and somato-sensory cell group. An experimental study in the rhesus monkey. Brain 83:161–184.
Kuypers HGJM, Brinkman J (1970) Precentral projections to different parts of the spinal intermediate zone in the rhesus monkey. Brain Res 24:29–48.
Lackner JR, Dizio P (1994) Rapid adaptation to Coriolis force perturbations of arm trajectory. J Neurophysiol 72:299–313.
Landau WM (1952) Patterns of movement elicited in medullary pyramidal stimulation in the cat. Electroencephalogr Clin Neurophysiol 5:527–545.
Lassek AM (1952) A study of the effect of complete frontal lobe extirpations on the fiber components of the pyramidal tract. J Comp Neurol 96:121–125.
Lawrence DG, Kuypers HGJM (1968) The functional organization of the motor system in the monkey I: The effects of bilateral pyramidal lesions. Brain 91:1–14.
Lederman SJ, Klatzky RL (1987) Hand movements: A window into haptic object recognition. Cognitive Psychol 19:342–368.
Lee DD, Seung HS (1999) Learning the parts of objects by non-negative matrix factorization. Nature 401:788–791.
Lee JA, Lendasse A, Verleysen M (2002) Curvilinear distance analysis versus Isomap. European Symposium on Artificial Neural Networks pp185–192.
Lee KH, Hill E, Johnston R, Smiehorowski T (1976) Myofeedback for muscle retraining in hemiplegic patients. Arch Phys Med Rehabil 57:588–591.
Lee L, Siebner HR, Rowe JB, Rizzo V, Rothwell JC, Frackowiak RS, Friston KJ (2003). Acute

remapping within the motor system induced by low-frequency repetitive transcranial magnetic stimulation. J Neurosci 23:5308–5318.
Lehéricy S, Benali H, Van de Moortele P-F, Pélégrini-Issac M, Waechter T, Ugurbil K, Doyon J (2005) Distinct basal ganglia territories are engaged in early and advanced motor sequence learning. Proc Natl Acad Sci USA 102:12566–12571.
Lemay MA, Grill WM (2004) Modularity of motor output evoked by intraspinal microstimulation in cats. J Neurophysiol 91:502–514.
Lemon RN (1993) Cortical control of the primate hand. Exp Physiol 78:263–301.
Lemon RN, Mantel GWH, Muir RB (1986) Corticospinal facilitation of hand muscles during voluntary movement in the conscious monkey. J Physiol 381:497–527.
Levin MF, Lamarre Y, Feldman AG (1995) Control variables and proprioceptive feedback in fast single-joint movements. Can J Physiol Pharmacol 73:316–330.
Li CS, Padoa-Schioppa C, Bizzi E (2001) Neuronal correlates of motor performance and motor learning in the primary motor cortex of monkeys adapting to an external force field. Neuron 30:593–607.
Loeb EP, Giszter SF, Borghesani P, Bizzi E (1993) Effects of dorsal root cut on the forces evoked by spinal microstimulation in the spinalized frog. Somatosens Mot Res 10:81–95.
Loeb EP, Giszter SF, Saltiel P, Bizzi E, Mussa-Ivaldi FA (2000) Output units of motor behavior: an experimental and modeling study. J Cogn Neurosci 12:78–97.
Loeb G, Gans C (1986) Electromyography for experimentalists. Chicago, IL: University of Chicago Press.
Logan GD (1985) Executive control of thought and action. Acta Psychol 60:193–210.
Logothetis NK, Pauls J, Augath M, Trinath T, Oeltermann A (2001): Neurophysiological investigation of the basis of the fMRI signal. Nature 412:150–157.
MacNeilage PF, Studdert-Kennedy MG, Lindblom B (1987) Primate handedness reconsidered. Behav Brain Sci 10:247–303.
Madani R, Hulo S, Toni N, Madani H, Steimer T, Muller D, Vassalli JD (1999) Enhanced hippocampal long-term potentiation and learning by increased neuronal expression of tissue-type plasminogen activator in transgenic mice. EMBO J 18:3007–3012.
Maeda F, Keenan JP, Tormos JM, Topka H, Pascual-Leone A (2000a) Interindividual variability of the modulatory effects of repetitive transcranial magnetic stimulation on cortical excitability. Exp Brain Res 133:425–430.
Maeda F, Keenan JP, Tormos JM, Topka H, Pascual-Leone A (2000b) Modulation of corticospinal excitability by repetitive transcranial magnetic stimulation. Clin Neurophysiol 111:800–805.
Maeda F, Pascual-Leone A (2003) Transcranial magnetic stimulation: studying motor neurophysiology of psychiatric disorders. Psychopharmacology (Berl)168:359–376.
Maegaki Y, Yamamoto T, Takeshita K (1995) Plasticity of central motor and sensory pathways in a case of unilateral extensive cortical dysplasia: Investigation of magnetic resonance imaging, transcranial magnetic stimulation, and short-latency somatosensory evoked potentials. Neurology 45:2255–2261.
Maier MA, Illert M, Kirkwood PA, Nielsen J, Lemon RN (1998) Does a C3-C4 propriospinal system transmit corticospinal excitation in the primate? An investigation in the macaque monkey. J Physiol 511:191–212.
Maldjian J, Atlas SW, Howard RS II, Greenstein E, Alsop D, Detre J, Listerud J, D'Esposito M, Flamm ES (1996) Functional magnetic resonance imaging of regional brain activity in patients with intracerebral arteriovenous malformations before surgical or endovascular therapy. J Neurosurg 84:477–483.
Maldjian JA, Gottschalk A, Patel RS, Detre JA, Alsop DC (1999) The sensory somatotopic map of the human hand demonstrated at 4 Tesla. NeuroImage 10:55–62.

Malfait N, Gribble PL, Ostry DJ (2005) Generalization of motor learning based on multiple field exposures and local adaptation. J Neurophys 98:3327–3338.
Malfait N, Ostry DJ (2004) Is interlimb transfer of force-field adaptation a cognitive response to the sudden introduction of load? J Neurosci 24:8084–8089.
Malfait N, Shiller DM, Ostry DJ (2002) Transfer of motor learning across arm configurations. J Neurosci 22:9656–9660.
Malonek D, Grinvald A (1996) Interactions between electrical activity and cortical microcirculation revealed by imaging spectroscopy: Implications for functional brain mapping. Science 272:551–554.
Maquet P, Laureys S, Peigneux P, Fuchs S, Petiau C, Phillips C, Aerts J, Del Fiore G, Degueldre C, Meulemans T, Luxen A, Franck G, Van Der Linden M, Smith C, Cleeremans A (2000) Experience-dependent changes in cerebral activation during human REM sleep. Nat Neurosci 3:831–836.
Maquet P, Schwartz S, Passingham R, Frith C (2003) Sleep-related consolidation of a visuomotor skill: brain mechanisms as assessed by functional magnetic resonance imaging. J Neurosci 23:1432–1440.
Marr D (1982) Vision: A computational investigation into the human representation and processing of information. San Francisco, CA: Freeman.
Mason CR, Gomez JE, Ebner TJ (2001) Hand synergies during reach-to-grasp. J Neurophys 86:2896–2910.
Mason CR, Teverapperuma LS, Hendrix CM, Ebner TJ (2004) Monkey hand postural synergies during reach-to-grasp in the absence of vision of the hand and object. J Neurophys 91:2826–2837.
Mataga N, Mizuguchi Y, Hensch TK (2004) Experience-dependent pruning of dendritic spines in visual cortex by tissue plasminogen activator. Neuron 44:1031–1041.
Mataga N, Nagai N, Hensch TK (2002) Permissive proteolytic activity for visual cortical plasticity. Proc Natl Acad Sci U S A 99:7717–7721.
Matsunaga K, Maruyama A, Fujiwara T, Nakanishi R, Tsuji S, Rothwell JC (2005) Increased corticospinal excitability after 5 Hz rTMS over the human supplementary motor area. J Physiol 562:295–306.
McDowall J, Lustig A, Parkin G (1995) Indirect learning of event sequences: the effects of divided attention and stimulus continuity. Can J Exp Psychol 49:415–436.
McGaugh JL (2000) Memory—a century of consolidation. Science 287:248–251.
McGlone F, Kelly EF, Trulsson M, Francis ST, Westling G, Bowtell R (2002) Functional neuroimaging studies of human somatosensory cortex. Behav Brain Res 135:147–158.
McIntyre J, Mussa-Ivaldi FA, Bizzi E (1996) The control of stable postures in the multijoint arm. Exp Brain Res 110:248–264.
McKenzie AL, Nagarajan SS, Roberts TP, Merzenich MM, Byl NN (2003) Somatosensory representation of the digits and clinical performance in patients with focal hand dystonia. Am J Phys Med Rehabil 82:737–749.
McKiernan BJ, Marcario JK, Karrer JH, Cheney PD (1998) Corticomotoneuronal postspike effects in shoulder, elbow, wrist, digit, and intrinsic hand muscles during a reach and prehension task. J Neurophys 80:1961–1980.
McKiernan BJ, Marcario JK, Karrer JH, Cheney PD (2000) Correlations between corticomotoneuronal (CM) cell postspike effects and cell-target muscle covariation. J Neurophys 83:99–115.
Merton PA (1951) The silent period in a muscle of the human hand. J Physiol 114:183–198.
Miall RC, Jenkinson N, Kulkarni K (2004) Adaptation to rotated visual feedback: a re-examination of motor interference. Exp Brain Res 154:201–210.

Miller LE, van Kan PLE, Sinkjaer T, Andersen T, Harris, GD, Houk JC (1993) Correlation of primate red nucleus discharge with muscle activity during free-form arm movements. J Physiol (Lond) 469:212–243.
Milner TE, Franklin DW (2005) Impedance control and internal model use during the initial stage of adaptation to novel dynamics in humans. J Physiol 567:651–664.
Miniussi C, Bonato C, Bignotti S, Gazzoli A, Gennarelli M, Pasqualetti P, Tura GB, Ventriglia M, Rossini PM (2005) Repetitive transcranial magnetic stimulation (rTMS) at high and low frequency: an efficacious therapy for major drug-resistant depression? Clin Neurophysiol 2005 116:1062–1071.
Mistry M, Mohajerian P, Schaal S (2005) An exoskeleton robot for human arm movement study. IEEE/RJS International Conference on Intelligent Robots and Systems. pp3114–3119.
Moore CI, Stern CE, Corkin S, Fischl B, Gray AC, Rosen BR, Dale AM (2000a) Segregation of somatosensory activation in the human rolandic cortex using fMRI. J Neurophysiol 84:558–569.
Moore CI, Stern CE, Dunbar C, Kostyk SK, Gehi A, Corkin S (2000b) Referred phantom sensations and cortical reorganization after spinal cord injury in humans. Proc Natl Acad Sci U S A 97:14703–14708.
Mountcastle VB. 1998. Perceptual neuroscience: The cerebral cortex. Cambridge, MA: Harvard UP.
Muellbacher W, Ziemann U, Wissel J, Dang N, Kofler M, Faccini S, Boroojerdi B, Poewe W, Hallett M (2002) Early consolidation in human primary motor cortex. Nature 415:640–644.
Murata A, Gallese V, Kaseda M, Sakata H (1996) Parietal neurons related to memory-guided hand manipulation. J Neurophys 75:2180–2186.
Murata A, Gallese V, Luppino G, Kaseda M, Sakata H (2000) Selectivity for the shape, size, and orientation of objects for grasping in neurons of monkey parietal area AIP. J Neurophys 83:2580–2601.
Murphy JT, Kwan HC, MacKay WA, Wong YC (1978) Spatial organization of precentral cortex in awake primates. III. Input-output coupling. J Neurophys 41:1132–1139.
Mushiake H, Inase M, Tanji J (1991) Neuronal activity in the primate premotor, supplementary, and precentral motor cortex during visually guided and internally determined sequential movements. J Neurophys 66:705–718.
Mussa-Ivaldi FA, Bizzi E (2000) Motor learning through the combination of primitives. Philos Trans R Soc Lond B Biol Sci 355:1755–1769.
Mussa-Ivaldi FA, Giszter SF (1992) Vector field approximation: a computational paradigm for motor control and learning. Biol Cybern 67:491–500.
Mussa-Ivaldi FA, Giszter SF, Bizzi E (1994) Linear combinations of primitives in vertebrate motor control. Proc Natl Acad Sci U S A 91:7534–7538.
Mussa-Ivaldi FA, Hogan N, Bizzi E (1985) Neural, mechanical, and geometric factors subserving arm posture in humans. J Neurosci 5:2732–2743.
Naito E, Roland PE, Ehrsson HH (2002) I feel my hand moving: A new role of the primary motor cortex in somatic perception of limb movement. Neuron 36:979–988.
Napier J (1956) The prehensile movements of the human hand. J Bone Jt Surg 38B:902–913.
Nelson RJ, Sur M, Felleman DJ, Kaas JH (1980) Representations of the body surface in postcentral parietal cortex of Macaca fasicularis. J Comp Neurol 192:611–643.
Nicole O, Docagne F, Ali I, Margaill I, Carmeliet P, MacKenzie ET, Vivien D, Buisson A (2001) The proteolytic activity of tissue-plasminogen activator enhances NMDA receptor-mediated signaling. Nat Med 7:59–64.
Nissen MJ, Bullemer PT (1987) Attentional requirements for learning: Evidence from performance measures. Cogn Psychol 19:1–32.
Nudo RJ, Milliken GW, Jenkins WM, Merzenich MM (1996) Use-dependent alterations of

movement representations in primary motor cortex of adult squirrel monkeys. J Neurosci16:785–807.
Ogawa S, Tank DW, Menon R, Ellermann JM, Kim S-G, Merkle H, Ugurbil K (1992) Intrinsic signal changes accompanying sensory stimulation: Functional brain mapping with magnetic resonance imaging. Proc Natl Acad Sci USA 89: 5951–5955.
Ono M, Kubik S, Abernathey CD (1990) Thieme, Stuttgart: Atlas of the Cerebral Sulci.
Ostry DJ, Feldman AG (2003) A critical evaluation of the force control hypothesis in motor control. Exp Brain Res 153:275–288.
Osu R, Hirai S, Yoshioka T, Kawato M (2004) Random presentation enables subjects to adapt to two opposing forces on the hand. Nat Neurosci 7:111–112.
Padoa-Schioppa C, Li C-SR, Bizzi E (2002) Neuronal correlates of kinematics-to-dynamics transformation in the supplementary motor area. Neuron 36:751–765.
Pang PT, Teng HK, Zaitsev E, Woo NT, Sakata K, Zhen S, Teng KK, Yung WH, Hempstead BL, Lu B (2004) Cleavage of proBDNF by tPA/plasmin is essential for long-term hippocampal plasticity. Science 306:487–491.
Park MC, Belhaj-Saif A, Cheney PD (2000) Chronic recording of EMG activity from large numbers of forelimb muscles in awake macaque monkeys. J Neurosci Meth 96:153–160.
Park MC, Belhaj-Saif A, Gordon M, Cheney PD (2001) Consistent features in the forelimb representation of primary motor cortex in rhesus macaques. J Neurosci 21:2784–2792.
Pascual-Leone A, Valls-Sole J, Wassermann EM, Hallett M (1994) Responses to rapid-rate transcranial magnetic stimulation of the human motor cortex. Brain 117:847–858.
Penfield W, Boldrey E (1937) Somatic motor and sensory representations in the cerebral cortex of man as studied by electrical stimulation. Brain 60:389–443.
Penfield W, Rasmussen T (1950) The Cerebral Cortex of Man. New York, NY: MacMillan.
Penhune VB, Zatorre RJ, MacDonald JD, Evans AC (1996) Interhemispheric anatomical differences in human primary auditory cortex: Probabilistic mapping and volume measurement from magnetic resonance scans. Cereb Cortex 6:661–672.
Perruchet P, Amorim MA (1992) Conscious knowledge and changes in performance in sequence learning: evidence against dissociation. J Exp Psychol Learn Mem Cogn 18:785–800.
Polit A, Bizzi E (1978) Processes controlling arm movements in monkeys. Science 29:1235–1237.
Polit A, Bizzi E (1979) Characteristics of motor programs underlying arm movements in monkeys. J Neurophysiol 42:183–194.
Povel DJ, Collard R (1982) Structural factors in patterned finger tapping. Acta Psychol (Amst) 52:107–123.
Preilowski B, Reger M, Engele HC (1986) Handedness and cerebral asymmetry in nonhuman primates. In: Current perspectives in primate biology (Taub DM, King FA, eds), pp270–282. New York, NY: Van Nostrand Reinhold.
Press DZ, Casement MD, Pascual-Leone A, Robertson EM (2005) The time course of off-line motor sequence learning. Brain Res Cogn Brain Res 25:375–378.
Proteau L, Blandin Y, Alain C, Dorion A (1994). The effects of the amount and variability of practice on the learning of a multi-segmented motor task. Acta Psychol (Amst) 85:61–74.
Qian Z, Gilbert ME, Colicos MA, Kandel ER, Kuhl D (1993) Tissue-plasminogen activator is induced as an immediate-early gene during seizure, kindling and long-term potentiation. Nature 361:453–457.
Rachman S, Grassi J (1965) Reminiscence, inhibition and consolidation. Br J Psychol 56:157–162.
Rademacher J, Bürgel U, Geyer S, Schormann T, Schleicher A, Freund H-J, Zilles K (2001) Variability and asymmetry in the human precentral motor system. A cytoarchitectonic and myeloarchitectonic brain mapping study. Brain 124:2232–2258.
Rademacher J, Caviness VS Jr, Steinmetz H, Galaburda AM (1993) Topographical variation of the

human primary cortices: Implications for neuroimaging, brain mapping, and neurobiology. Cereb Cortex 3:313–329.
Ranck JB (1981) Extracellular stimulation. In: Electrical stimulation research techniques (Patterson MM, Kesner RP, eds), pp2–34. New York: New York Academic.
Recanzone GH, Merzenich MM, Schriener CE (1992) Frequency discrimination training engaging a restricted skin surface results in an emergence of a cutaneous response zone in cortical area 3a. J Neurophysiol 67:1057–1070.
Reina GA, Moran DW, Schwarz AB (2001) On the relationship between joint angular velocity and motor cortical discharge during reaching. J Neurophysiol 85:2576–2589.
Reinagel P, Reid RC (2000) Temporal coding of visual information in the thalamus. J Neurosci 20:5392–5400.
Rieke F, Bodnar DA, Bialek W (1995) Naturalistic stimuli increase the rate and efficiency of information transmission by primary auditory afferents. P Roy Soc Lond B Bio 262:259–265.
Robertson EM, Pascual-Leone A, Press DZ (2004b) Awareness modifies the skill-learning benefits of sleep. Curr Biol 14:1–20.
Robertson EM, Pascual-Leone, A, Miall RC (2004a) Current concepts in procedural consolidation. Nat Rev Neurosci 5:1–7.
Robertson EM, Press DZ, Pascual-Leone A (2005) Off-line learning and the primary motor cortex. J Neurosci 25:6372–6378.
Robertson EM, Theoret H, Pascual-Leone A (2003) Studies in cognition: the problems solved and created by transcranial magnetic stimulation. J Cogn Neurosci 15:948–960.
Romero JR, Anschel D, Sparing R, Gangitano M, Pascual-Leone A (2002) Subthreshold low frequency repetitive transcranial magnetic stimulation selectively decreases facilitation in the motor cortex. Clin Neurophysiol. 113:101–107.
Romo R, Hernandez A, Zainos A, Salinas E (1998) Somatosensory discrimination based on cortical microstimulation. Nature 392:387–390.
Rosenbaum DA (1980) Human movement initiation: Specification of arm, direction and extent. J Exp Psychol [Gen] 109:444–474.
Rossini D, Lucca A, Zanardi R, Magri L, Smeraldi E (2005) Transcranial magnetic stimulation in treatment-resistant depressed patients: a double-blind, placebo-controlled trial. Psychiatry Res 137:1–10.
Roweis ST, Saul LK (2000) Nonlinear dimensionality reduction by locally linear embedding. Science 290:2323–2326.
Roy AC, Paulignan Y, Meunier M, Boussaoud D (2002) Prehension movements in the macaque monkey: Effects of object size and location. J Neurophys 88:1491–1499.
Russell JR, DeMeyer W (1961) The quantitative cortical origin of pyramidal axons of Macaca rhesus, with some remarks on slow rate of axolysis. Neurology 11:96–108.
Sainburg RL, Ghez C, Kalakanis D (1999) Intersegmental dynamics are controlled by sequential anticipatory, error correction, and postural mechanisms. J Neurophysiol 81:1045–1056.
Sakai K, Kitaguchi K, Hikosaka O (2003) Chunking during human visuomotor sequence learning. Exp Brain Res 152:229–242.
Sakitt B (1980) Visual-motor efficientcy (VME) and the information transmitted in visual-motor tasks. Bull Psychol Soc 16:329–332.
Saltiel P, Tresch MC, Bizzi E (1998) Spinal cord modular organization and rhythm generation: An NMDA iontophoretic study in the frog. J Neurophys 80:2323–2339.
Saltiel P, Wyler-Duda K, d'Avella A, Tresch M.C, Bizzi E (2001) Muscle synergies encoded within the spinal cord: evidence from focal intraspinal NMDA iontophoresis in the frog. J Neurophys 85: 605–619.

Santello M, Flanders M, Soechting JF (1998) Postural hand synergies for tool use. J Neurosci 18:10105–10115.
Santello M, Soechting JF (1997) Matching object size by controlling finger span and hand shape. Somatosens Mot Res 14:203–212.
Santello M, Soechting JF (1998) Gradual molding of the hand to object contours. J Neurophys 79:1307–1320.
Santello M, Soechting JF (2000) Force synergies for multifingered grasping. Exp Brain Res 133:457–467.
Sato KC, Tanji J (1989) Digit-muscle responses evoked from multiple intracortical foci in monkey precentral motor cortex. J Neurophys 62:959–970.
Satow T, Mima T, Hara H, Oga T, Ikeda A, Hashimoto N, Shibasaki H (2002) Nausea as a complication of low-frequency repetitive transcranial magnetic stimulation of the posterior fossa. Clin Neurophysiol 113:1441–1443.
Scheidt RA, Dingwell JB, Mussa-Ivaldi FA (2001) Learning to move amid uncertainty. J Neurophysiol 86:971–985.
Schendan HE, Searl MM, Melrose RJ, Stern CE (2003) An fMRI study of the role of the medial temporal lobe in implicit and explicit sequence learning. Neuron 37:1013–1025.
Schieber MH (1993) Electromyographic evidence of two functional subdivisions in the rhesus monkey's flexor digitorum profundus. Exp Brain Res 95:251–260.
Schieber MH (1995) Muscular production of individuated finger movements: The roles of extrinsic finger muscles. J Neurosci 15:284–297.
Schieber MH (1996) Individuated finger movements: Rejecting the labeled-line hypothesis. In: Hand and brain: The neurophysiology and psychology of hand movements (Wing AM, Haggard P, Flanagan JR, eds) pp81–98. Boston, MA: Academic Press.
Schlesinger G (1919) Betriebswirtschaft und Psychotechnik. Praktische Psychologie 1:3–6. Cited in Cutkosky and Howe (1990).
Schmidt RA, Lee TL (1999). Motor control and learning (3rd ed). Champaign, IL: Human Kinetics.
Scott SH, Kalaska JF (1997) Reaching movements with similar hand paths but different arm orientations. I. Activity of individual cells in motor cortex. J Neurophysiol 77:826–852.
Scott SH, Sergio LE, Kalaska JF (1997) Reaching movements with similar hand paths but different arm orientations. II. Activity of individual cells in dorsal premotor cortex and parietal area 5. J Neurophysiol 78:2413–2426.
Seeds NW, Basham ME, Ferguson JE (2003) Absence of tissue plasminogen activator gene or activity impairs mouse cerebellar motor learning. J Neurosci 23:7368–7375.
Seeds NW, Basham ME, Haffke SP (1999) Neuronal migration is retarded in mice lacking the tissue plasminogen activator gene. Proc Natl Acad Sci U S A 96:14118–14123.
Seidler RD (2004) Multiple motor learning experiences enhance motor adaptability. J Cog Neurosci 16:65–73.
Seidler RD, Purushotham A, Kim SG, Ugurbil K, Willingham D, Ashe J (2002) Cerebellum activation associated with performance change but not motor learning. Science 296:2043–2046.
Sereno MI, Dale AM, Reppas JB, Kwong KK, Belliveau JW, Brady TJ, Rosen BR, Tootell RB (1995) Borders of multiple visual areas in humans revealed by functional magnetic resonance imaging. Science 268:889–893.
Sergio LE, Kalaska JF (1998) Changes in the temporal pattern of primary motor cortex activity in a directional isometric force versus limb movement task. J Neurophysiol 80:1577–1583.
Servos P, Zacks J, Rumelhart DE, Glover GH (1998) Somatotopy of the human arm using fMRI. NeuroReport 9:605–609.
Shadmehr R (1993) Control of equilibrium position and stiffness through postural modules. J Mot Behav 25:228–241.

Shadmehr R, Brandt J, Corkin S (1998) Time-dependent motor memory processes in amnesic subjects. J Neurophysiol 80:1590–1597.
Shadmehr R, Brashers-Krug T (1997) Functional stages in the formation of human long-term motor memory. J Neurosci 17:409–419.
Shadmehr R, Holcomb HH (1997) Neural correlates of motor memory consolidation. Science 277:821–825.
Shadmehr R, Moussavi ZMK (2000) Spatial generalization from learning dynamics of reaching movements. J Neurosci 20:7807–7815.
Shadmehr R, Mussa-Ivaldi FA (1994) Adaptive representation of dynamics during learning of a motor task. J Neurosci 14:3208–3224.
Shadmehr R, Mussa-Ivaldi FA, Bizzi E (1993) Postural force fields of the human arm and their role in generating multijoint movements. J Neurosci 13:45–62.
Shannon CE (1948) The mathematical theory of communication. Bell Syst Technol J 27:379–423.
Shea JB, Morgan RL. 1979. Contextual interference effects on acquisition, retention, and transfer of a motor skill. J Exp Psychol Learn Mem Cogn 5:179–187.
Sherrington CS (1906) The integrative action of the nervous system. New Haven, CT: Yale UP.
Shiavi RG, Champion SA, Freeman FR, Bugel HJ (1979) Efficacy of myofeedback therapy in regaining control of lower extremity musculature following stroke. Am J Phys Med 58:185–194.
Shin JC, Ivry RB (2003) Spatial and temporal sequence learning in patients with Parkinson's disease or cerebellar lesions. J Cogn Neurosci 15:1232–1243.
Siao CJ, Tsirka SE (2002) Extracellular proteases and neuronal cell death. Cell Mol Biol (Noisy-le-grand) 48:151–161.
Smith AM (1981) The coactivation of antagonist muscles. Can J Physiol Pharm 59:733–747.
Sobel DF, Gallen CC, Schwartz BJ, Waltz TA, Copeland B, Yamada S, Hirschkoff EC, Bloom FE (1993) Locating the central sulcus: Comparison of MR anatomic and magnetoencephalographic functional methods. AJNR Am J Neuroradiol 14:915–925.
Stadler MA (1994) Explicit and implicit learning and maps of cortical motor output. Science 265:1600–1601.
Stansfield SA (1988) A robotic perceptual system utilizing passive vision and active touch. Int J Robot Res 7:128–161.
Stark B, Carlstedt T, Hallin RG, Risling M (1998) Distribution of human Pacinian corpuscles in the hand. A cadaver study. J Hand Surg [Br] 23:370–372.
Strick PL (2002) Stimulating research on motor cortex. Nat Neurosci 5:714–715.
Strick PL, Preston JB (1978a) Multiple representation in the primary motor cortex. Brain Res 154:366–370.
Strick PL, Preston JB (1978b) Sorting of somatosensory afferent information in primate motor cortex. Brain Res 156:364–368.
Strick PL, Preston JB (1978c) Two representations of the hand in area 4 of a primate. II. Somatosensory input organization. J Neurophys 48:150–159.
Sur M, Merzenich MM, Kaas JH (1980) Magnification, receptive-field area, and “hypercolumn” size in area 3b and 1 of somatosensory cortex in owl monkeys. J Neurophysiol 44:295–311.
Suzuki M, Shiller DM, Gribble PL, Ostry DJ (2001) Relationship between cocontraction, movement kinematics and phasic muscle activity in single-joint arm movement. Exp Brain Res 140:171–181.
Takahashi CD, Scheidt RA, Reinkensmeyer DJ (2001) Impedance control and internal model formation when reaching in a randomly varying dynamical environment. J Neurophysiol 86:1047–1051.
Talairach J, Tournoux P (1988) Co-planar stereotaxic atlas of the human brain: 3-dimensional proportional system: An approach to cerebral imaging. New York, NY: Thieme Medical.

Tchernichovski O, Mitra PP, Lints T, Nottebohm F (2001) Dynamics of the vocal imitation process: how a zebra finch learns its song. Science 291:2564–2569.
Teesalu T, Kulla A, Simisker A, Siren V, Lawrence DA, Asser T, Vaheri A (2004) Tissue plasminogen activator and neuroserpin are widely expressed in the human central nervous system. Thromb Haemost 92:358–368.
Tegenthoff M, Ragert P, Pleger B, Schwenkreis P, Forster AF, Nicolas V, Dinse HR (2005) Improvement of tactile discrimination performance and enlargement of cortical somatosensory maps after 5 Hz rTMS. PLoS Biol 3:e362.
Tenenbaum JB, de Silva V, Langford JC (2000) A global geometric framework for nonlinear dimensionality reduction. Science 290:2319–2323.
Thoroughman KA, Shadmehr R (1999) Electromyographic correlates of learning an internal model of reaching movements. J Neurosci 19:8573–8588.
Thoroughman KA, Shadmehr R (2000) Learning of action through adaptive combination of motor primitives. Nature 407:742–747.
Ting LH, Macpherson JM (2005) A limited set of muscle synergies for force control during a postural task. J Neurophysiol 93:609–613.
Todorov E (2000) Direct cortical control of muscle activation in voluntary arm movements: A model. Nat Neurosci 3:391–398.
Todorov E (2004) Optimality principles in sensorimotor control. Nat Neurosci 7:907–15.
Todorov E, Ghahramani Z (2003) Unsupervised learning of sensory-motor primitives. P IEEE EMBS 2:1750–1753.
Tommerdahl M, Whitsel BL (1996) Optical imaging of intrinsic signals in somatosensory cortex. In: Somesthesis and the neurobiology of somatosensory cortex (Franzen O, Johansson R, Terenius L, eds), pp369–384. Basel: Birkhauser Verlag.
Toothaker LE (199) Multiple comparisons for researchers. Newbury Park, CA: Sage.
Torres-Oviedo G, Hari TM, Ting LH (2005) Functional muscle synergies controlling balance during one-legged and two-legged postural responses in humans. Society for Neuroscience abstract 868.7.
Towle VL, Khorasani L, Uftring S, Pelizzari C, Erickson RK, Spire JP, Hoffmann K, Chu D, Scherg M (2003) Noninvasive identification of human central sulcus: A comparison of gyral morphology, functional MRI, dipole localization, and direct cortical mapping. NeuroImage 19:684–697.
Tresch MC, Cheung VCK, d'Avella A (2005) Matrix factorization algorithms for the identification of muscle synergies: evaluation on simulated and experimental data sets. Manuscript in submission.
Tresch MC, Saltiel P, Bizzi E (1999) The construction of movement by the spinal cord. Nat Neurosci 2:162–167.
Ungerleider LG, Doyon J, Karni A (2002) Imaging brain plasticity during motor skill learning. Neurobiol Learn Mem 78:553–562.
Valero-Cabré A, Oliveri M, Gangitano M, Pascual-Leone, A (2001) Modulation of spinal cord excitability by subthreshold repetitive transcranial magnetic stimulation of the primary motor cortex in humans. Neuroreport 12:3845–3848.
Valero-Cabre A, Pascual-Leone A (2005) Impact of TMS on the primary motor cortex and associated spinal systems. IEEE Eng Med Biol Mag 24(1):29–35.
Valero-Cabre A, Payne BR, Rushmore J, Lomber SG, Pascual-Leone A (2005) Impact of repetitive transcranial magnetic stimulation of the parietal cortex on metabolic brain activity: a 14C-2DG tracing study in the cat. Exp Brain Res 163:1–12.
Vogt BA, Pandya DN (1977) Cortico-cortical connections of somatic sensory cortex (areas 3, 1 and 2) in the rhesus monkey. J Comp Neurol 177:179–192.

Vollenbroek-Hutten M, Hermens H, Voerman G, Sandsjo L, Kadefors R (2004) Are changes in pain induced by myofeedback training related to changes in muscle activation patterns in patients with work-related myalgia? Eur J Appl Physiol [epub ahead of print].
Von Holst E, Mittelstaedt H (1950/1973) Das Reafferezprincip. Wechselwirkungen zwischen zentralnerven-system und Peripherie. Naturwissenschaften 37:456–476, 1950. The reafference principle. In: The behavioral physiology of animals and man. The collected papers of Erich von Holst. (Martin R, transl), pp139–173. Coral Gables, FL: University of Miami Press. (Cited by Ostry and Feldman, 2003).
Wada Y, Kawabata Y, Kotosaka S, Yamamoto K, Kitazawa S, Kawato M (2003) Acquisition and contextual switching of multiple internal models for different viscous force fields. Neurosci Res 46:319–331.
Wainscott SK, Donchin O, Shadmehr, R (2005) Internal models and contextual cues: Encoding serial order and direction of movement. J Neurophysiol 93:786–800.
Walker MP, Brakefield T, Hobson JA, Stickgold R (2003a) Dissociable stages of human memory consolidation and reconsolidation. Nature 425:616–620.
Walker MP, Brakefield T, Seidman J, Morgan A, Hobson JA, Stickgold R (2003b) Sleep and the time course of motor skill learning. Learn Memory 10:275–284.
Wang H, Wang X, Scheich H (1996) LTD and LTP induced by transcranial magnetic stimulation in auditory cortex. Neuroreport 7:521–525.
Ward JW (1938) The influence of posture on responses elicitable from the cortex cerebri of cats. J Neurophysiol 1:463–475.
Warren JM (1987) Primate handedness: Inadequate analysis, invalid conclusions. Behav Brain Sci 10:288–289.
Wassermann EM, Tormos JM, Pascual-Leone A (1998) Finger movements induced by transcranial magnetic stimulation change with hand posture, but not with coil position. Hum Brain Mapp 6:390–393.
Weiller C, Juptner M, Fellows S, Rijntjes M, Leonhardt G, Kiebel S, Muller S, Diener HC, Thilmann AF (1996) Brain representation of active and passive movements. NeuroImage 4:105–110.
Weiller C, Ramsay SC, Wise RJS, Friston KJ, Frackowiak RSJ (1993) Individual patterns of functional reorganization in the human cerebral cortex after capsular infarction. Ann Neurol 33:181–189.
Weinstein S (1968) Intensive and extensive aspects of tactile sensitivity as a function of body part, sex, and laterality. In: The skin senses (Kenshalo DR, ed), pp195–218. Springfield, IL: Thomas.
Weiss EJ, Flanders M (2004) Muscular and postural synergies of the human hand. J Neurophysiol 92:523–35.
Wessberg J, Stambaugh CR, Kralik JD, Beck PD, Laubach M, Chapin JK, Kim J, Biggs SJ, Srinivasan MA, Nicolelis MAL (2000) Real-time prediction of hand trajectory by ensembles of cortical neurons in primates. Nature 408:361–365.
White LE, Andrews TJ, Hulette C, Richards A, Groelle M, Paydarfar J, Purves D (1997): Structure of the human sensorimotor system. I: Morphology and cytoarchitecture of the central sulcus. Cereb Cortex 7:18–30.
Willingham DB, Goedert-Eschmann K (1999) The relation between implicit and explicit learning: Evidence for parallel development. Psychol Sci 10:531–534.
Willingham DB, Greenberg AR, Thomas RC (1997) Response-to-stimulus interval does not affect implicit motor sequence learning, but does affect performance. Mem Cognit 25:534–542.
Willingham DB, Nissen MJ, Bullemer P (1989) On the development of procedural knowledge. J Exp Psychol Learn Mem Cogn 15:1047–1060.
Willingham DB, Wells LA, Farrell JM, Stemwedel ME (2000) Implicit motor sequence learning is

represented in response locations. Mem Cognit 28:366–375.
Willingham, DB (1999) Implicit motor sequence learning is not purely perceptual. Mem Cognit 27:561–572.
Wong YC, Kwan, HC, MacKay WA, Murphy JT (1978) Spatial organization of precentral cortex in awake primates. I. Somatosensory inputs. J Neurophys 41:1107–1119.
Woolsey CN, Erickson TC, Gilson WE (1979): Localization in somatic sensory and motor area of human cerebral cortex as determined by direct recording of evoked potentials and electrical stimulation. J Neurosurg 51:476–506.
Woolsey CN, Marshall WH, Bard P (1942) Representation of cutaneous tactile sensibility in cerebral cortex of monkey as indicated by evoked potentials. Bull John Hopkins Hosp 70:399–441.
Woolsey CN, Settlage PH, Meyer DR, Sencer W, Pinto Hamuy T, Travis AM (1952) Patterns of localization in precentral and "supplementary" motor areas and their relation to the concept of a premotor area. Res Publ Assoc Res Nerv Mental Dis 30:238–264.
Yeomans JS (1990) Principles of brain stimulation. Oxford: Oxford UP.
Young JP, Geyer S, Grefkes C, Amunts K, Morosan P, Zilles K, Roland PE (2003) Regional cerebral blood flow correlations of somatosensory areas 3a, 3b, 1, and 2 in humans during rest: A PET and cytoarchitectural study. Hum Brain Mapp 19:183–196.
Yousry TA, Schmid UD, Alkadhi H, Schmidt D, Peraud A, Buettner A, Winkler P (1997) Localization of the motor hand area to a knob on the precentral gyrus. A new landmark. Brain 120:141–157.
Zach N, Kanarek N, Inbar D, Grinvald Y, Milestein T, Vaadia E (2005) Segregation between acquisition and long-term memory in sensorimotor learning. Eur J Neurosci 22:2357–2362.
Zhou W, Tao HW, Poo MM (2003) Reversal and stabilization of synaptic modifications in a developing visual system. Science 300:1953–1957.